THE UNIVERSITY OF QUEENSLAND

AUSTRALIA

High Penetration of PV Systems in Low Voltage Distribution Networks: Investigation of Power Quality Challenges and Mitigation

Annapoorna Chidurala

Bachelor of Technology in Electrical and Electronics Engineering

Master of Technology in Electrical Power Engineering

A thesis submitted for the degree of Doctor of Philosophy at

The University of Queensland in 2016

School of Information Technology and Electrical Engineering

Abstract

World electricity demand is continuously increasing and fossil fuel supplies are not sustainable. Solar Photovoltaic (PV) energy is one of the emerging resources around the world, which produces emission free electricity. Nowadays, the advancements in rooftop solar PV technology, government subsidies, decreasing capital cost and feed-in-tariffs have promoted installation in residential and commercial applications. The exponential uptake in widespread integration of PV systems in existing low voltage (LV) distribution networks is raising additional new challenges in terms of power quality, stability and protection. In LV distribution networks, poor power quality (PQ) is the most serious concern.

Characteristically, LV distribution networks are not designed for significant back-feed of power generation to the main grid. Also, these networks are unbalanced in nature due to asymmetry in system impedances and single-phase loads. This together with a large number of small-scale PV system integrations in LV networks can cause poor PQ challenges in terms of voltage quality and harmonics. PV systems can themselves generate harmonics, due to the usage of power electronic inverters. In addition, the augmentation of power electronics based appliances; the loads are becoming voltage sensitive and nonlinear in nature. The proliferation of widespread PV penetrations and a multitude of nonlinear load characteristics can have a stringent impact on the network harmonic levels. Therefore, the main objective of this research is to investigate and understand the impacts of high PV systems penetration on PQ of the distribution network and aim to alleviate them.

In the first part of this thesis, the investigation of voltage quality challenges in the LV distribution network with high PV penetration are discussed. In this research, various voltage quality issues such as voltage rise, unbalance, fluctuations/flicker and sag/swell issues have been explored. Primarily, the analysis of results has been carried out through PSCAD simulations in various case studies. For this purpose, an IEEE-13 bus unbalanced distribution network is considered as a test system. Furthermore, to evaluate the severity of voltage quality issues in real-time grid connected PV systems, field measurement based investigations have been performed. Practical field tests have been conducted at two different sizes of 1.5 MW and 3.3MW PV systems located at the University of Queensland (UQ), St Lucia and Gatton campuses respectively. The impact of dynamic variations in solar irradiation has also been taken into account for the analysis. Further, a data clustering technique is also applied to estimate the probability of voltage flicker severity in the networks. Measurement results show

that voltage quality concerns in the 1.5MW PV system are insignificant compared to the 3.3MW system.

In the second part of this thesis, the characteristics of harmonic emissions from PV inverters and their aggregations during various operating conditions are assessed. The simulation results are validated with the field measurement data collected by various PQ analysers connected at the UQ PV site. Analysis revealed that individual voltage and current harmonic magnitudes are additive in nature due to increased PV system penetration. In addition, a comprehensive analysis has been performed in several different cases studies with high penetration of different PV inverter technologies to evaluate the severity of harmonic propagation and resonance issues on the distribution network. This analysis has also considered the harmonic distortions associated with various power electronic based nonlinear loads. Further, comparative studies have been performed with real-time harmonic measurements, which are obtained using online JAVA programs. The study has highlighted the PV system harmonic contributions on distribution transformer K-factor. Results confirm that the total harmonic distortions (THD) of voltage and current are exceeding the IEEE limits when the number of PV systems increases in the network. Moreover, the impacts of PV controller performance due to solar irradiation variations on the incidence of grid harmonic resonance have been presented.

Furthermore, this research has suggested a novel solution to overcome the above PQ issues. The concept of adopting the PV inverter as a virtual DSTATCOM named as Solar-DSTATCOM has been proposed. Also, a new control strategy for the PV inverter has been developed to provide independent phase voltage regulation and load reactive power and harmonic compensation, which could eliminate issues in the unbalanced distribution network. Initially, the Solar-DSTATCOM controller has been verified in a PSCAD simulation environment. Further, different case studies have been performed on the IEEE-13 bus network for PQ issues compensation. In addition, the proposed Solar-DSTATCOM control system has been tested and verified in controller hardware-in-the-loop simulation environment, which combines the real-time digital simulator and dSPACE DS1103 hardware board. Detailed investigations are carried out for various different case studies, which include daytime, night-time operations, the impact of dynamic load profiles and finally harmonic analysis. The analysis has revealed that Solar-DSTATCOM exceptional performance in the hardware environment has enhanced the grid PQ by providing voltage regulation, reactive power compensation and power factor correction. The harmonic emissions are well within the limits.

Declaration by author

This thesis *is composed of my original work, and contains* no material previously published or written by another person except where due reference has been made in the text. I have clearly stated the contribution by others to jointly-authored works that I have included in my thesis.

I have clearly stated the contribution of others to my thesis as a whole, including statistical assistance, survey design, data analysis, significant technical procedures, professional editorial advice, and any other original research work used or reported in my thesis. The content of my thesis is the result of work I have carried out since the commencement of my research higher degree candidature and does not include a substantial part of work that has been submitted *to qualify for the award of any* other degree or diploma in any university or other tertiary institution. I have clearly stated which parts of my thesis, if any, have been submitted to qualify for another award.

I acknowledge that an electronic copy of my thesis must be lodged with the University Library and, subject to the policy and procedures of The University of Queensland, the thesis be made available for research and study in accordance with the Copyright Act 1968 unless a period of embargo has been approved by the Dean of the Graduate School.

I acknowledge that copyright of all material contained in my thesis resides with the copyright holder(s) of that material. Where appropriate I have obtained copyright permission from the copyright holder to reproduce material in this thesis.

Publications during candidature

Peer-reviewed International Journal Article (1):

1. **Chidurala, Annapoorna**, Kumar Saha, Tapan, Mithulananthan, N.: 'Harmonic impact of high penetration photovoltaic system on unbalanced distribution networks – learning from an urban photovoltaic network', IET Renewable Power Generation, Volume 10, Issue 4, April 2016, pp. 485 – 494 DOI: 10.1049/iet-rpg.2015.0188.

International Journal Articles to be Submitted (2):

1. **Chidurala, Annapoorna**, Tapan Kumar Saha, and Mithulananthan N., "Harmonic Resonance on the Distribution Network with PV Penetration and Field Measurements Validation", in preparation, to be submitted to International Transactions on Electrical Energy Systems Journal by September 2016.
2. **Chidurala, Annapoorna**, Tapan Kumar Saha, and Mithulananthan N., "Real-Time Controller Hardware-in-the-Loop Simulations of Solar-DSTATCOM" in preparation, to be submitted to Electric Power Systems Research Journal by September 2016.

Peer-reviewed Conference Papers (5):

1. **Chidurala, Annapoorna**, Tapan Kumar Saha, and N. Mithulananthan, "Power quality enhancement in unbalanced distribution network using Solar-DSTATCOM," Australasian Universities Power Engineering Conference (AUPEC), Hobart, TASMANIA, Australia, Sept. 29-Oct. 3, 2013, pp. 1-6.
2. **Chidurala, Annapoorna**, Tapan Kumar Saha, N. Mithulananthan, and R. C. Bansal, "Harmonic emissions in grid connected PV systems: A case study on a large scale rooftop PV site," in PES General Meeting Conference & Exposition, 2014 IEEE, National Harbor, MD, 27-31 July 2014, pp. 1-5. USA.
3. **Chidurala, Annapoorna**, Tapan Kumar Saha, and N. Mithulananthan, "Harmonic characterization of grid connected PV systems & validation with field measurements," in Power & Energy Society General Meeting, 2015 IEEE, 2015, pp. 1-5, Denver, USA.
4. **Chidurala, Annapoorna**, Tapan Kumar Saha, and Mithulananthan N., "Field Investigation of Voltage Quality Issues in Distribution Network with PV Penetration", IEEE PES Asia-Pacific Power and Energy Engineering Conference, Brisbane, QLD, Australia, 15-18 Nov. 2015, pp. 1-5.

5. M J E ALAM, R YAN, Tapan Kumar Saha, **Chidurala, Annapoorna**, D EGHBAL, "Learning from a 3.275 MW Utility Scale PV Plant Project", in *CIGRE PARIS Session 2016*, 21, rue d'Artois, F-75008 PARIS 2016.

Publications included in this thesis

1. **Chidurala, Annapoorna**; Kumar Saha, Tapan; Mithulananthan, N.: 'Harmonic impact of high penetration photovoltaic system on unbalanced distribution networks – learning from an urban photovoltaic network', IET Renewable Power Generation, Volume 10, Issue 4, April 2016, pp. 485 – 494 DOI: 10.1049/iet-rpg.2015.0188.

   This paper is incorporated in Chapter 4.

Contributor	Statement of Contribution
Annapoorna Chidurala	Simulation and Modelling (100%) Practical Measurement data collection (100%) Results interpretation and Discussion (75%) Paper Writing (75%)
Tapan K. Saha	Results interpretation and Discussion (20%) Paper Writing and Review (20%)
Mithulananthan N.	Results interpretation and Discussion (5%) Paper Writing and Review (5%)

2. **Chidurala, Annapoorna**, T. K. Saha, and N. Mithulananthan, "Power quality enhancement in unbalanced distribution network using Solar-DSTATCOM," Australasian Universities Power Engineering Conference (AUPEC), Hobart, TASMANIA, Sept. 29-Oct. 3, 2013, pp. 1-6.

   This paper partially incorporated in Chapter 4 and Chapter 7.

Contributor	Statement of Contribution
Annapoorna Chidurala	Simulation and Modelling (100%) Results interpretation and Discussion (75%) Paper Writing (75%)
Tapan K. Saha	Results interpretation and Discussion (15%) Paper Writing and Review (15%)
Mithulananthan N.	Results interpretation and Discussion (10%) Paper Writing and Review (10%)

3. **Chidurala, Annapoorna**, T. K. Saha, N. Mithulananthan, and R. C. Bansal, "Harmonic emissions in grid connected PV systems: A case study on a large scale rooftop PV site," in PES General Meeting Conference & Exposition, 2014 IEEE, National Harbor, MD, USA, 27-31 July 2014, pp. 1-5.

   This paper partially incorporated in Chapter 7.

Contributor	Statement of Contribution
Annapoorna Chidurala	Simulation and Modelling (100%) Results interpretation and Discussion (75%) Paper Writing (75%)
Tapan K. Saha	Results interpretation and Discussion (15%) Paper Writing and Review (15%)
Mithulananthan N.	Results interpretation and Discussion (10%) Paper Writing and Review (5%)
R.C Bansal	Paper Writing and Review (5%)

4. **Chidurala, Annapoorna**, T. K. Saha, and N. Mithulananthan, "Harmonic characterization of grid connected PV systems & validation with field measurements," in Power & Energy Society General Meeting, 2015 IEEE, 2015, pp. 1-5, Denver, USA.

   This paper is incorporated in Chapter 5.

Contributor	Statement of Contribution
Annapoorna Chidurala	Simulation and Modelling (100%) Field Experiments and Data Collection (100%) Results interpretation and Discussion (75%) Paper Writing (75%)
Tapan K. Saha	Results interpretation and Discussion (20%) Paper Writing and Review (20%)
Mithulananthan N.	Results interpretation and Discussion (5%) Paper Writing and Review (5%)

5. **Chidurala, Annapoorna**, T. K. Saha, and N. Mithulananthan, "Field Investigation of Voltage Quality Issues in Distribution Network with PV Penetration", IEEE PES Asia-Pacific Power and Energy Engineering Conference, Brisbane, QLD, Australia, 15-18 Nov. 2015, pp. 1-5.

   This paper is incorporated in Chapter 4.

Contributor	Statement of Contribution
Annapoorna Chidurala	Simulation and Modelling (100%) Field Experiments and Data Collection (100%) Results interpretation and Discussion (75%) Paper Writing (75%)
Tapan K. Saha	Results interpretation and Discussion (20%) Paper Writing and Review (20%)
Mithulananthan N.	Results interpretation and Discussion (5%) Paper Writing and Review (5%)

6. M J E ALAM, R YAN, T K SAHA, **Chidurala, Annapoorna**, D EGHBAL, "Learning from a 3.275 MW Utility Scale PV Plant Project", in *CIGRE PARIS Session 2016*, 21, rue d'Artois, F-75008 PARIS 2016.

   This paper partially incorporated in Chapter 4.

Contributor	Statement of Contribution
M J E ALAM	Field Experiments and Data Collection (100%) Results interpretation and Discussion (75%) Paper Writing (50%)
R YAN	Simulation and Modelling (100%) Results interpretation and Discussion (75%) Paper Writing and Review (15%)
Tapan K. Saha	Results interpretation and Discussion (25%) Paper Writing and Review (20%)
Annapoorna Chidurala	Data Collection (100%) Results interpretation and Discussion (75%) Paper Writing and Review (15%)

Contributions by others to the thesis

"No contributions by others"

Statement of parts of the thesis submitted to qualify for the award of another degree

"None"

Acknowledgement:

First and foremost, I would like to take this opportunity to thank my God “Sri Saibaba” for his presence in my life. His abundance grace, kindness and blessings gave me strength to complete this research successfully.

I would like to offer my sincere thanks and gratitude to all those who helped me in many ways in completing this research work.

I would like to express my gratitude to my principal advisor Prof. Tapan Kumar Saha and Co-advisor Dr. Mithulan Nadarajah for their valuable suggestions, continuous support in every aspect to accomplish my PhD study. Especially, Prof. Tapan Saha for novel association of ideas, encouragement, appreciation and his intellectual zeal have motivated me to endeavor this research successfully. He has been a continuous source of inspiration to me throughout the research. His immense knowledge, creativity and passion always inspired me during the study.

I would like to acknowledge the financial support from the University of Queensland through UQI Scholarship. I am also grateful to Australian Research Council and Industry partner, Ingenero for their financial support towards my living expenses and attending conferences.

I am grateful to all the staff and colleagues of Power and Energy Systems group, who made my stay pleasant and profitable. I would like to thank Dr. Olav Krause and Mr. Shane Goodwin for their assistance in obtaining the field Measurement data for my research work. I would like to thank all my friends from the research group: Mr. Kapila Bandara, Dr. Hung Duong and Mr. Jalil Yaghoobi, who provided me with their help and assistance.

Furthermore, I am grateful to all my family members, especially my husband Aravind Kumar, for his continuous support and encouragement to strive towards my goals. This thesis would not have been possible without his constant love and support. I would like to dedicate this thesis to him.

Keywords

Solar PV system, Power quality, Unbalanced distribution system, Voltage quality, Harmonic impact, Resonance, Solar-DSTATCOM, Controller hardware-in-the-loop simulation, RTDS, dSPACE.

Australian and New Zealand Standard Research Classifications (ANZSRC)

ANZSRC code: 090607, Power and Energy Systems Engineering (excl. Renewable Power), 70%

ANZSRC code: 090608, Renewable Power and Energy Systems Engineering (excl. Solar Cells), 30%

Fields of Research (FoR) Classification

FoR code: 0906, Electrical and Electronic Engineering, 100%

Table of Contents

List of Figures

List of Tables

Abbreviations and Acronyms

PV	Photovoltaic
DG	Distributed Generation
REN	Renewable Energy
AEMO	Australian Energy Market Operator
IEEFA	Institute for Energy Economics and Financial Analysis
NEM	National Electricity Market
LV	Low Voltage
HV	High Voltage
OLTC	On-Load Tap Changer
SVR	Step Voltage Regulator
MPPT	Maximum Power Point Tracking
THD	Total Harmonic Distortion
TDD	Total Demand Distortion
ESS	Energy Storage System
CPD	Custom Power Devices
DSTATCOM	Distributed Static Compensator
DVR	Dynamic Voltage Restorer
IEEE	Institute of Electrical and Electronics Engineering
ANSI	American National Standards Institute
AS	Australian Standard
AS/NZS	Australian/New Zealand Standard
IEC	International Electrotechnical Commission
EN	European
STC	Standard Test Condition
P&O	Perturb and Observe
PWM	Pulse Width Modulation
PLL	Phase Locked Loop
CRCSI	Current Regulated Current Source Inverter
CCVSI	Current Controlled Voltage Source Inverter
PC	Personal Computer
CFL	Compact Fluorescent Lamp

ASD	Adjustable Speed Drive
TV	Television
PSCAD	Power Systems Computer Aided Design
dSPACE	Digital Signal Processing and Control Engineering
RTDS	Real Time Digital Simulator
GTAI	Gigabit Transceiver Analog Input
GTAO	Gigabit Transceiver Analog Output
ADC	Analog to Digital
DAC	Digital to Analog
VU	Voltage Unbalance
PCC	Point of Common Coupling
P.F	Power Factor
SLG	Single Line to Ground
DLG	Double Line to Ground
TPG	Three Phase to Ground
PQ	Power Quality
PI	Proportional Integrator
UQ	University of Queensland
QLD	Queensland

CHAPTER 1

INTRODUCTION

1.1. Background

The world's population is increasing, economies are developing and global energy consumption is increasing faster than ever before, particularly in developing countries. Experts predict that the demand for electricity will have increased by 45% in 2035 [1]. The present energy requirement is mainly supplied by combustion of fossil fuels such as crude oil, coal and natural gas. However, conventional energy sources are inadequate in meeting the rising electricity demand. Moreover, use of fossil fuels in generating electricity creates environmental problems mainly due to emissions of greenhouse gases. Global climate change, substantial rising electricity demand and increasing electricity prices have increased concerns all over the world. Therefore, many nations around the world are pushing towards the deployment of renewable energy sources to ensure a secure, affordable, environmentally clean and sustainable power supply. These resources can help in creating new economic opportunities and providing access to people living without electricity. Renewable energy sources such as solar, wind, hydro and geothermal are expected to supply a considerable percentage of future world electricity requirements. As per REN21-2015 global status report [2], renewable energy provided approximately 19.1% of global energy consumption in 2013. By the end of 2014, the estimated renewable power production has increased to 22.8% of the global power generating capacity and the capacity of total renewable power installation has reached 657GW (excluding hydropower).

During recent decades, renewable energy based distributed generation (DG) has been gaining momentum rapidly due to their feasibility. Among several DG technologies, Solar Photovoltaic (PV) systems are one of the fastest growing resources worldwide due to decreasing capital costs and increasing technological advancements. Out of total renewable power capacity (657GW), the capacity of solar PV installations worldwide had exceeded 177GW by the end of 2014, as shown in Fig. 1.1 [2, 3]. Australia is the ideal location for solar power production because of the high insolation level. The forecasts from Australian Energy Market Operator (AEMO) [4] show that Australia's energy dependence heavily on rooftop solar PV systems in the coming years. In 2030, the cumulative solar PV installed capacity could contribute 21% of the Australia's total electricity needs.

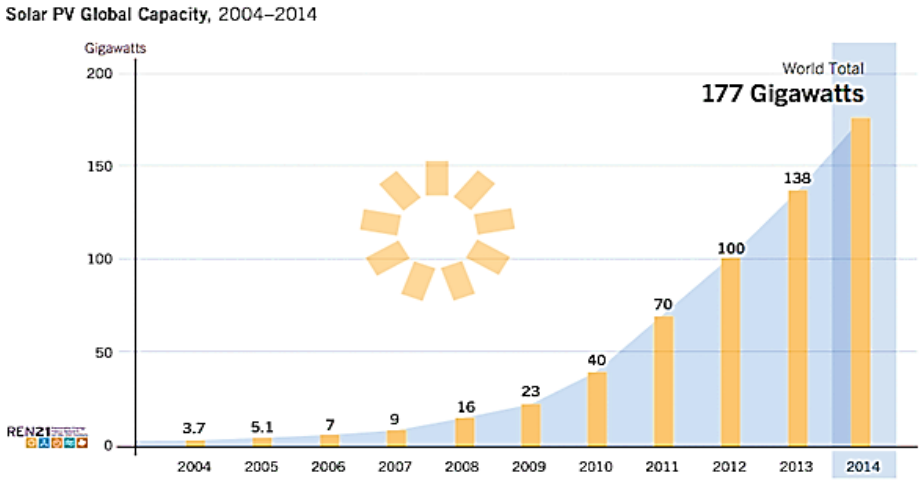

Figure 1.1. Solar PV Global Capacity from 2004 to 2014 [2].

Solar PV systems can be connected to both transmission and distribution networks. The application of solar PV systems in power systems are categorized as grid connected and off-grid. Usually, off-grid PV systems can be used to provide power to remote loads, which do not have access to the power network. Grid-connected solar PV systems can be installed at a location near to the load for power generation, which eliminates the transmission and distribution costs. Recent expansion in rooftop solar PV technology and the potential benefits from government subsidies have promoted installation of systems with capacities ranging from a few kW to 10MW in residential, commercial and industrial applications. In addition, PV system installed prices have gradually been decreasing over recent years, so the average size of installations has been increasing. When compared to other forms of DG generation, solar PV systems are physically small and have lower voltages, which are therefore appropriate to interface with the low voltage distribution network. However, there are several concerns in integrating this technology in low voltage (LV) distribution networks.

Solar PV system integration can have positive aspects on the low voltage distribution network to feed peak energy demands, to reduce the energy losses of distribution feeders and to provide voltage support. However, the exponential uptake in widespread installations of solar PV systems can have negative impacts on the existing distribution network, which can inflict various power quality, stability and protection challenges. Power quality is the major issue of concern in distribution networks, which covers various operational parameters and plays a key role in industrial, commercial and residential power needs. The most frequent power quality issues in existing distribution networks are voltage quality problems such as unbalance, sags and swells.

In fact, existing power dispatch systems are passive networks and are built to distribute power from large generating plants to the end-user in a single direction. Traditionally, low voltage distribution networks possess unbalanced characteristics due to the unbalanced line configurations and phase loadings. Also, these networks are not designed for two-way power flow. Nevertheless, with the distributed integration of solar PV systems into the grid, the networks become active and the customers can export and import power to the grid, which could impact the network voltage profile in terms of voltage rise and unbalance. PV generators are often owned and operated by customers, therefore the location and size of PV system installations is dependent on their financial status and interest. Moreover, this type of resource is intermittent in nature due to seasonal effects and limited predictability results in power imbalance on the utility grid leads to power quality degradation, which has implications on voltage regulation issues. Rapid variations in the solar irradiation due to cloud transients can cause voltage fluctuations/flicker issues and the incidences may exacerbate in the network if PV penetration increases. Furthermore, the solar PV system uses a power electronic based inverter to convert DC electricity from PV panels to AC electricity, which can inject harmonics into the network. Consequently, utility operators with current knowledge will face difficulties in getting control over distribution network performance. Therefore, it is significantly important to investigate and analyse the potential issues with high PV system penetration in the existing distribution networks and to provide a potential solution for improving grid power quality.

1.2. Research Objectives

The main objective of this thesis is to investigate various power quality issues imposed by high penetration of solar PV systems in the utility grid and aiming to alleviate them. Following

are the research objectives, which will be accomplished in this research for enabling high penetration of rooftop PV in low voltage distribution network.

1. To assess voltage related issues in the low voltage unbalanced distribution network with high PV penetration through simulations.
2. To investigate voltage quality problems in real grid connected PV sites through field measurements. Specifically, to study and quantify the impact of short-term solar radiation variations on voltage flicker emissions.
3. To examine the harmonic emission characteristics of solar PV inverters and their aggregation issues for different operating conditions.
4. To investigate and analyse the harmonic impact of high penetration PV systems on an unbalanced distribution network comprehensively.
5. To investigate harmonic resonance issues associated with different PV inverter technologies and their dynamic operational interactions in the network.
6. To propose, develop and validate a new control methodology for solar PV inverters to enhance grid power quality in offline simulation and Real Time Digital Simulation environment.

1.3. Thesis Outline

This thesis is organised as follows:

Chapter 2 reviews the power quality impacts of PV system integration in the literature. Firstly, this chapter introduces the growth of solar PV technology in different countries and provides current and future statistic impacts on the distribution networks. After that, a detailed literature review of various power quality issues and identified research gaps are discussed. Then, traditional solutions for power quality improvement are reviewed. Finally, various regulatory standards and current practices related to power quality criteria are introduced.

Chapter 3 provides the background theory, models and tools used in this research. To simulate real PV system dynamic characteristics, detailed modelling of solar PV sources using a mathematical model, DC-to-DC converter, maximum power point tracking techniques and inverter technologies are introduced first. Following that, the test system and the load modelling requirements are presented. Finally, utilized various software and hardware tools for this research are explained.

Chapter 4 presents a comprehensive investigation of voltage quality issues introduced by PV system integration in the distribution network. Primarily, the assessment on the unbalanced

test system through simulation scenarios is presented. Further, to identify the proliferation of various voltage quality issues in real-time network, field investigations on the real grid connected PV sites have been performed, which are presented at the end.

Chapter 5 assess the characteristics of harmonic emissions from PV inverters and their aggregations during various operating conditions. The analysis of simulation results in different case studies and the validation with field measurement data are presented. Apart from that, a comprehensive analysis has been presented in several different cases studies with high penetration of different PV inverter technologies to evaluate the severity of harmonic propagation on the various nodes of the distribution network. Similarly, comparative studies of simulations and real-time network harmonic measurements are discussed.

Chapter 6 investigate the possibilities of harmonic resonance issues on the distribution network with PV systems. At first, the resonance phenomena associated with PV system is explained. After that, the simulation approach and the results of different case studies are presented. Further, harmonic resonance issues on a real grid connected PV site identified through network harmonic distortion measurements are presented.

Chapter 7 introduces a new solution to prevail the above mentioned power quality issues. The concept of adopting a PV inverter as a Distributed Static Compensator (DSTATCOM) named as Solar-DSTATCOM has been proposed. At first, the proposed new control methodology and the principle of operation are explained. The effect of Solar-DSTATCOM on the unbalanced test network is presented. Finally, validation of the proposed Solar-DSTATCOM control system in a controller hardware-in-the-loop simulation environment is presented.

Chapter 8 concludes the work done for this research and highlights the main findings. The possible future direction of further research is also presented in this chapter.

CHAPTER 2

LITERATURE REVIEW

2.1. Introduction

In this chapter, firstly, an overview of solar PV technology evolution in different countries and their penetration statistics on the distribution networks are reported. After that, a comprehensive literature review on the power quality impacts of solar PV penetration in the distribution networks and the identified gaps are discussed. Further, some countermeasures for power quality improvement in the current literature are provided. In the end, various standards and grid codes of different countries related to the power quality criteria are referred. This chapter partially incorporates some of the literature reviews from the PhD candidate's published and submitted papers [5-11].

2.2. Growth of Solar PV Technology and its Statistics

Solar Photovoltaic (PV) power generation has become a promising technology for integration into distribution networks due to their feasibility and availability of sun compared to other types of renewable energy resources. The installed capacity of small scale and utility scale grid connected PV system installations has grown significantly over the past five years. In the U.S., the solar PV installation capacity has reached a maximum of 7.3 GW in 2015. With this, the total cumulative installation capacity reached over 25GW, which was supplying a total

of 29.5% of all new electricity generation capacity [12]. This trend will continue to grow in the coming years. India has set a target to install 175GW of renewable power generation by 2021-22 [13], which is the highest target in the world. As per the Institute for Energy Economics and Financial Analysis (IEEFA) report, 100GW of power is expected from solar resources. In which, a nearly 40GW target has been set for distributed rooftop solar systems as a way to decrease the nation's grid losses and unpredictable regular power outages [13].

In Australia the importance for solar PV research programs are increasing and are aiming to increase renewable penetration to meet future energy demand. Recently, a new target of renewable power generation of 45,000GWh in 2020 has been set, which represents 25% of total electricity generation in 2020 [14]. This renewable energy target is now encouraging the small-scale renewable energy scheme, which promotes installation of rooftop PV systems and is expected to contribute not less than 12000GWh. According to the Australian PV Institute report, the potential installed PV system capacity has exceeded nearly 4.7GW by the end of 2015, as shown in Fig 2.1 [15].

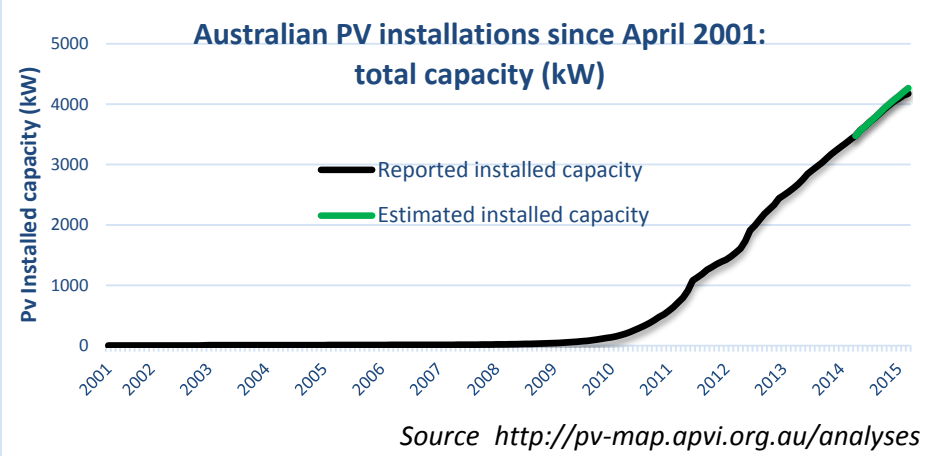

Figure 2.1. Grid Connected PV Uptake in Australia [15].

The forecasts conducted by the Australian Energy Market Operator (AEMO) for each National Electricity Market (NEM) region [4] shows that the rooftop PV system installed capacity in 2031 would increase up to 12 times higher than the present capacity level. Nonetheless, the estimated rooftop PV installed capacity can impose severe impacts on the existing distribution network, which has led to a new set of challenges in power quality, stability and protection. The Energex distribution Annual planning report stated that the current level of rooftop PV penetration (2015) is already causing power quality problems on the network and is expected to exaggerate the issues in the next five years [16]. It is reported that many distribution transformers on low voltage (LV) networks are overloading with higher PV

installed capacity, which in the worst condition, might be at risk of failure and need replacement. This remarkable growth is mainly due to the decreasing PV system costs, incentive programs from federal and state governments and rising electricity prices. Therefore, it is very important to investigate the power quality impacts of PV systems and to take preventive measures to improve the existing network withstand capability to facilitate more PV systems integration.

2.3. Power Quality Issues with Solar PV System Integrations

2.3.1. Voltage Rise

Traditionally, distribution networks are designed as uni-direction power flow systems with a distribution transformer energised from a single source. During normal operation, the current flows through line impedance and to the loads, which results in voltage drops along the feeder line. To compensate voltages on the distribution network, different voltage regulation devices are used, such as on-load tap changing transformers (OLTC), step voltage regulators, switched capacitors, which are designed by considering the primary substation. The objective of the regulators is to regulate the voltage at the output terminals and is then set to boost the voltage along the feeder. Due to the incorporation of PV systems into the grid, the distribution networks are becoming a bi-directional power flow system. The integration of a large number of PV generators in an existing grid causes a significant rise in the local voltage levels due to reverse power flow, which can be seen as a major technical issue. Most importantly, in the case of high PV generation and low load conditions the power injection from PV has a severe impact at the end of the feeder as well as on the neighbourhoods as presented in [17]. In addition, various types of PV inverters until now are typically designed to produce only real power and do not regulate the voltages at the integration point. As a result, there is great difficulty in regulating the voltage due to negative coordination of the unidirectional regulatory equipment and the PV systems [18]. Consequently, in the case of short-term voltage variations due to solar irradiation change, there is a tendency to increase the number of undesirable operations of regulatory devices and therefore, reduce the equipment lifetime.

Reference [19], studied the impact of distributed generation on steady state voltage regulation and also provided the guidelines to mitigate arising issues. In [20], the impact of different penetration levels and sizes of PV systems on steady state voltage has been studied and simulated for Australian Single Wire Earth Return (SWER) networks. It has been shown that this kind of network often experiences voltage rise in large penetrations. In [17, 21], the

voltage rise impacts in an unbalanced distribution network with high PV penetration related to the unbalanced feeder impedance, feeder layout and phase loading have been studied. Conversely, the PV systems are advantageous in reducing line losses and providing voltage support only when the PV generation capacity is lower than the load requirement as presented in [22, 23], however, this is not always possible. This reverse power flow is unpredictable and the management of voltage limits by utility operators at the interconnection point can lead to both voltage rise and voltage drop. Hence, the voltage rise and its regulation issue is likely to be of more concern in LV networks and needs to be investigated in the case of high PV penetration.

2.3.2. Voltage Fluctuations/Flicker

The major problem with solar PV generation is its variable nature due to seasonal effects and limited predictability, which results in intermittent generation, which can lead to power imbalance. It can be noticed [24] that the solar fluctuations can have erratic variations on voltage and power flow. Literature [25, 26], investigated the impacts of voltage variations in unbalanced LV distribution networks due to PV power fluctuations. The study considered a constant PV power profile variation to reflect cloud transient effects but it does not simulate a real-time scenario. The rapid variations in solar irradiation due to cloud transients can cause substantial fluctuations in the PV output power, which in turn could cause voltage fluctuations at the PV integration node [27, 28]. The sudden ramp up/down in PV power can increase the number of undesirable operations of tap changers, which may lead to a hunting effect and can reduce the lifespan of equipment. In addition, sometimes these regulatory devices may react slower than the cloud passage. With high connection densities of PV systems, voltage fluctuations and flicker issues could be the critical constraints in any network. In [29], the PV variability and the extreme ramp rates were examined to analyse the flicker. For this, a realistic solar irradiation profile of only 60sec was applied on the distribution network and simulated for instantaneous power drops. However, this study may be insufficient and not an accurate approach for evaluation of the flicker levels with PV systems. It is important to consider various solar irradiation characteristics and their impacts on network voltage profiles.

2.3.3. Voltage Unbalance Factor

Another significant voltage quality issue in the distribution system with high penetration of PV units is voltage unbalance. Normally, the electric utilities are supplying the loads evenly along the distribution feeder to minimise the voltage unbalance factor. Despite this fact, the

voltage levels at the consumer side are unbalanced due to uneven power consumption by loads. In addition, as the rooftop PV installations are randomly placed along the distribution feeders since the installations depend on customer interest. Therefore, the increment in voltage levels in each phase have different levels with PV power variation, which may further increase the unbalance level [25]. Along with this, the distributed massive integrations of solar PV systems will raise the uncertainties in three phase electric network. In reference [30, 31], the voltage imbalance sensitivity analysis in a residential distribution grid with random rooftop PV penetrations has been carried out, and a stochastic evaluation has been done. This voltage unbalance factor is higher at the end of the feeder than at the beginning of the feeder [32]. In addition, the increase/decrease in voltage unbalance depends on the PV system size and location, and phase loading. An increase in voltage unbalance can result in malfunctioning of regulatory equipment and reduces the lifetime of customer appliances.

2.3.4. Voltage Sag/Swell

Furthermore, voltage sag/swell is recognized as one of the most important power quality issues and is a commonly unavoidable occurrence in utility distribution networks. These are caused by unsymmetrical and symmetrical three phase faults on sensitive loads or starting of large industrial motors, which will trip the three-phase circuit breaker resulting in loss of supply [33]. In practice, faults on the distribution network cause the PV systems to disconnect from the grid [34]. This will create unbalanced voltage sags on highly loaded phases and swells on lightly loaded phases of the network. References [35, 36] highlighted the influence of altering weather patterns and cloud transients on PV power generations. Therefore, depending on the high connection densities of PV systems on the distribution feeder when subjected to sudden deficits in solar irradiation can cause large fluctuations for a few seconds, leading to poor power quality such as voltage sag/swell.

2.3.5. Harmonic Emission Issues from PV Systems and their Impacts

In addition, harmonic problems are common in distribution networks, mainly coming from nonlinear loads, transformers and increased use of power electronic equipment [37-39]. Characteristically, low voltage distribution networks have high R/X ratios and high impedances, which can result in high harmonic voltages. In general, PV systems consist of PV panels, Maximum power point tracking (MPPT) controller, a boost converter, a DC/AC inverter and an interfacing LC filter [40, 41]. With rapid developments in PV technology, a wide range of PV inverter technologies using a variety of control strategies are commercially

available in the market. The harmonics generation from these inverters will be divergent, which depends on the type of control strategy and size of PV systems and on the grid voltage harmonics. The harmonics that are injected into the network should comply with the standard requirements in order to maintain the power quality of the grid. Nevertheless, these PV inverters are negatively interacting in the real network [42].

As mentioned earlier, solar power generation is variable in nature. The active power generation has a linear relation with the solar insolation. However, the current harmonic distortion can possess an inverse trend to varying solar conditions. In addition, a PV inverter with lower switching frequency can generate high harmonic distortion. Therefore, it is important to characterise the harmonics produced from the grid connected PV inverter system for different operating conditions. In the literature [43], the experiments were performed on PV plant to analyse the multifaceted distorted waveform for varied solar conditions. In [42, 44], the investigation was performed to study the power quality characteristics of discrete PV inverter models. In addition, the analysis of current harmonic distortion from different single-phase inverter models was presented and suggested an expression to estimate the average total harmonic distortion. However, these PV inverters need further research to characterise the individual harmonic aggregations in the case of multiple installations. The reason that the harmonic distortions from several identical systems could be different is due to their independent operation. Therefore, the harmonic magnitude and phases are also different for each inverter and the resultant harmonics may suppress or increase because of harmonic superimposition. Furthermore, widespread penetration of several PV systems can affect the harmonic distortion levels of the distribution network [45, 46]. Therefore, accurate PV inverter modelling is essential to estimate the exact harmonic influences in the network.

In reference [47], an approach to model the PV output power generation from a prediction of solar irradiation was proposed. This method considers the input random variables such as clearness index and fraction of diffusion irradiation for prediction. Consequently, the harmonic emissions from PV system are altered by varying solar irradiation conditions. In [48], a probabilistic PV harmonic model has been developed based on the measurement data, which can be used in harmonic load flow studies. The statistical characterization of PV harmonic current emissions at different fundamental frequency output levels was presented. In literature [49], the PV system is modelled as a current source with harmonic frequencies, which eliminates the impact of control strategy. Multiple installations of PV systems in various locations together with the proliferation of nonlinear loads can introduce an issue of increased

harmonics in the distribution system [50]. A harmonic distortion analysis performed on the distribution network with distributed generation and nonlinear loads was given in [51]. Until now, utility network providers maintain the harmonic distortion levels at the customer connection point, which are under the limits according to IEEE 519 standards [52, 53]. However, excessive harmonic currents flowing through the grid can lead to increasing line losses, transformer overheating and premature ageing [54, 55].

The severity of the harmonic issue will depend on the type and rating of the equipment and the loading condition of distribution feeders [56]. In addition, PV systems are usually treated as a negative load in some studies [57, 58]. In the literature, several load models were developed to study the harmonic analysis in the networks [46, 59]. The common approach used to model harmonic producing loads is to include a set of current sources for each frequency. Such modelling ignores the switching harmonics of nonlinear loads and injects a constant harmonic pattern into the grid, which will not give realistic conditions. Dynamic aggregation of different types of domestic and commercial loads that inject harmonics, induce several complexities into the network. In references [38, 39, 60], a few different nonlinear load models namely Compact Fluorescent Lamps (CFL), televisions, computers, variable speed drives, DC drives and other loads have gained attention for harmonic analysis in the distribution network. Therefore, to perform an accurate analysis, the collective impacts of uncertainty in the loading patterns and aggregation of harmonic components need to be considered. Utility companies are familiar with estimating the harmonic levels and their potential effects on the network. However, with the penetration of PV systems on the customer side, it is becoming difficult to estimate the exact harmonic contributions from PV systems and there is a lack of study found in the literature.

2.3.6. Possibility of Harmonic Resonance Incidences

Furthermore, harmonic emission issues related with PV inverters will strongly depend on the type of control scheme and the output filter design, which can configure a resonance circuit with the grid. As a result, the high integration of different varieties of PV systems in the distribution networks, which is already stressed by nonlinear load proliferations, are raising potential concerns of harmonic resonance [50, 61, 62]. In LV distribution networks, harmonic resonance conditions are common, which can cause significant problems in the network. Typically, resonance events occur when the network capacitive reactance and inductive reactance become equal at a particular frequency, called a resonance frequency. In general, the network can have multiple resonance frequencies depending on the system configuration and

characteristics. These resonance frequencies will be a major issue when they are close to any of the individual harmonic frequencies [63]. The type of resonance may be parallel or series in the network. In [45, 64], harmonic resonance problems concerning PV systems integration in a distribution network have been presented. The reported resonance phenomena are based on the assumption that the PV system is modelled as a simple harmonic current source, with capacitor filter and is ignoring the inverter control functions. However, these assumptions are not valid in reality due to the operational and design characteristics of a PV system that leads to inaccurate harmonic analysis. Furthermore, most of the PV inverter filters are designed as LC and LCL types that are also a concern in the grid [65]. In fact, the network impedance changes over time due to operating conditions of loads, the interaction between passive elements and harmonic sources, which can excite the harmonic resonances. Depending on the type of resonance, the network voltage and current harmonics could be amplified to higher than expected [66]. Such resonances can cause overloading of neutral conductors, transformer overheating, nuisance tripping of circuit breakers and capacitor bank overstress [55, 67]. Although the issues associated with PV systems on the distribution grid are widely analysed, the harmonic resonance problems related to PV system penetration and their controller interactions are rarely assessed.

2.3.7. Other Issues

Conventional inverters are designed to operate at unity power factor and produce only active power which may reduce power factor at the distribution transformer as presented in [68]. The active current required by load supplied by PV systems locally while reactive current is drawn from the upstream network results in power factor reduction and increases the reactive power requirement.

2.4. Solutions for Power Quality Improvement

To improve the power quality of low voltage distribution systems, several solutions have been proposed in the literature. Optimal allocation and sizing of solar PV systems can provide voltage support and reduces line losses as presented in [69]. Authors in [70, 71] investigated the voltage quality issues with high PV penetration. Studies revealed that dispersed PV integration could improve the under voltage and voltage unbalance issues as well as sags in the distribution network. Nonetheless, in a utility distribution network this is not always possible because of randomness of PV system installations, which can increase the feeder impedance and overloading of transformers. Consequently, voltage regulation in such a network will

become complicated. As mentioned earlier, traditional Volt-VAr regulatory equipment may operate slowly in the case of power fluctuations with high PV integrations [72].

Authors in [73] proposed a network reconfiguration approach to solve voltage variation problems in an unbalanced distribution network. The sensitivity analysis has been performed by swapping phase sequences, loads, and PV interconnections. However, this network reconfiguration process is complicated in the case of real-time complex distribution networks due to increased random PV installations. Another network solution is upgrading of distribution feeder's cross-section [74], which is very expensive for the utilities to change all the lines. Further in [74, 75], regulation of the distribution transformer between two pre-defined tap settings is proposed, which is based on the feeder loading data. However, most of distribution transformers in the network have fixed tap sets, which require manual adjustments, which is not a reliable process.

Alternatively, Energy Storage System (ESS) plays a vital role in the adoption of renewable energy systems as they can handle the variability issues with renewable energy sources. Battery technology is the most widely used ESS for LV networks. ESSs are designed to store surplus energy during peak generation and low demand periods for later use during high power demand. It has been proposed in [76-78] that distributed ESS can be used for preventing overvoltage and voltage unbalance issues due to high PV penetration in LV residential networks. In references [77, 78], a technique to mitigate the voltage unbalance with single-phase energy storage systems is proposed. Results indicated that the voltage unbalance factor has reduced significantly to less than 2% with ESS operation, which was higher than about 3.5% with high PV penetration in an LV network. In [79], a coordinated control scheme has been proposed for an energy storage system with an on-load tap changing transformer to mitigate voltage rise, which limits the active power injections. The proposed controller sends charging/discharging operation commands to ESS in such a way to minimise the system losses and to shave the peak load. Although OLTC is a promising solution, it practically may not provide continuous voltage support. ESS can also have the capability of reactive power compensation for the grid.

Conversely, reactive power compensators such as shunt capacitors and Custom Power Devices (CPD) have traditionally been used to overcome power quality issues. In [80], various voltage quality issues raised by random rooftop PV installations have been investigated and a comparative analysis has been presented with two custom power devices, namely Distributed Static Compensator (DSTATCOM) and Dynamic Voltage Restorer (DVR). It has been

concluded that DSTATCOM is more efficient for voltage profile improvement and unbalance reduction. In literature [81-83], various functionalities of the DSTATCOM operations in compensating voltage sags and swells in the case of disturbances have been presented. This device is also capable of providing harmonic and dynamic reactive power compensation for the grid. Besides, [84] showed that DVR has the capability to mitigate voltage flickers, unbalance and voltage sags/swells problems. However, the above mentioned solutions are very expensive for the utility operators to install and manage.

Apart from conventional solutions, PV inverters themselves could be used as potential solutions for power quality improvement. Various methods, such as voltage regulation and reactive power injection from PV systems will better manage the LV network. In [85, 86], to minimise the steady state voltage variation and power loss, an adaptive VAr control for PV systems has been proposed. In [87] various VAr control methods for a PV inverter have been discussed. In [88-90], the application of a large-scale solar farm (PV) inverter operating as STATCOM has been proposed for power quality improvement in transmission networks. The proposed control system for a PV inverter with an energy storage system can perform the four-quadrant operation, which provides active and reactive power exchange with the grid.

Nowadays, PV systems with smart inverter technology are commercially available, which have the capability of injecting/absorbing fixed reactive power to address voltage quality issues to some extent [91, 92]. Nonetheless, in the distribution level, small-scale to medium-scale PV inverters can also possess versatile capabilities similar to the DSTATCOM by modifying a few functionalities to the inverter controller. A number of control methods have been proposed for the three-phase inverter topologies in the literature [87, 88, 93] to produce compensation currents for voltage regulation and reactive power compensation. All these methods are well suited for steady state, sinusoidal and balanced conditions of supply. However, in the case of unbalanced supply and non-linear unbalanced load conditions these control techniques are inappropriate. Therefore, an appropriate control strategy should be put in place for the PV inverters to enhance power quality in the unbalanced network. Such transformation of PV inverters as a source of impediment to a viable solution could address several integration issues and offer a cost-effective solution for both utilities and PV customers.

2.5. Overview of Standards

This section introduces several regulatory standards to define the power quality criteria about the distribution networks and PV system interconnection requirements.

2.5.1. Voltage Quality Standards

Voltage magnitude variation is the important constraint in distribution networks with high PV penetration. According to the American standard ANSI C84.1-2006 [94], the preferred operating service voltage range is to be within ±5%, indicated as Range A in the standard. The standard also suggested some countermeasures and required regulatory actions to maintain the voltage range and to protect equipment against increased voltages. In comparison, the equivalent Australian standard AS 60038-2000 [95], does not provide different voltage ranges and regulatory actions. However, it has defined the service voltage limits of a single phase (230V) and three phase supply voltage (400V) with a tolerance of -6% and +10%. The upper voltage range is higher than compared to the ANSI limits. However, in current practice, Ergon Energy and Energex utilities in Queensland, Australia consider the AS 61000.3.100: 2011 [96] standard voltage range. As per the standard, the steady state voltage limits at the customer integration points for the 11kV network should be within ±5% of nominal voltage and for the LV network should be within 415V ±6%. It also indicated the single-phase voltage limit for a 240V range to be ±6%.

Besides, the IEEE 1159-2009 [97] standard describes the various power quality issues caused by electromagnetic phenomena. According to the standard, the drop in RMS voltage by 10% to 90% from rated is defined as voltage Sag. Whereas, the swell is defined as an increase in RMS voltage from 10% to 80% of nominal for the duration of half a cycle to 1 minute. Similarly, according to the AS/NZS 61000.4.30 [98] standard, the thresholds for the voltage dip and swell are 90% and 110% of nominal voltage respectively.

In addition, the various definitions of voltage unbalance (VU) and its calculations are presented in [99]. According to IEEE definition, the percentage of voltage unbalance present in the phase voltages is expressed as given in equation (2.1).

$$\%VU = \frac{\max\left\{\left|V_{avg} - V_a\right|, \left|V_{avg} - V_b\right|, \left|V_{avg} - Vc\right|\right\}}{V_{avg}} \times 100 \qquad (2.1)$$

Where, $V_{avg} = (V_a + V_b + V_c) / 3$

The desirable voltage unbalance limit is specified in IEEE 1159 as 1% for any voltage level and the maximum limit is 2%. In contrast, the Australian standard AS/NZS 61000.4.30 defines voltage unbalance by utilizing the phase to phase voltages as given in equation (2.2). Here V_{ab}, V_{bc} and V_{ca} are the fundamental phase to phase voltages. According to the Australian standard, the limit for the voltage unbalance should not be over 5%.

$$\%\ \mathrm{VU} = \sqrt{\frac{1-\sqrt{3-6\beta}}{1+\sqrt{3-6\beta}}} \times 100 \tag{2.2}$$

Where, $\beta = \frac{V_{ab}^4 + V_{bc}^4 + V_{ca}^4}{\left(V_{ab}^2 + V_{bc}^2 + V_{ca}^2\right)^2}$

Alternatively, the true definition of the voltage unbalance is defined as the ratio of negative sequence voltage magnitude to the positive sequence voltage magnitude as given in equation (2.3).

$$\%\mathrm{V\ U} = \frac{|V_-|}{|V_+|} \times 100 \tag{2.3}$$

Other key issues in the distribution network are voltage fluctuations and flicker caused due to loads. Traditionally, flicker is defined as a rapid objectionable change in the light level often produced by voltage fluctuations [100]. It is usually measured by the quantification of voltage magnitude and the frequency of the fluctuations. Existing IEEE 519 [52] standards for flicker curves are not preferable in the case of PV induced flicker. The ramp rate of voltage variation may be faster or slower depending on the cloud pattern and speed. Therefore, AS 4377 [101] and IEEE 1453 [102] recommended practice suggested two indices for measuring the flicker on a network namely, short-term severity P_{st} (measured over 10 min) and long-term severity P_{lt} (measured over 2 hours). The short-term flicker is calculated every 10 minutes using the cumulative weighted probability values of the flicker sensation levels at 0.1%, 1%, 3%, 10% and 50% of the time interval given in equation (2.4).

$$P_{st} = \sqrt{0.0314P_{0.1} + 0.0525P_1 + 0.0657P_3 + 0.28P_{10} + 0.08P_{50}} \tag{2.4}$$

Where, $P_{0.1}, P_1, P_3, .., \text{etc.}$ indicate the ratio of relative voltage change ($\Delta V = V_{max} - V_{min}$) to the nominal voltage (V_{nom}).

From the standards, the long-term flicker index is determined by an average of P_{st} levels over a 2 hour time period expressed in equation (2.5).

$$P_{lt} = \sqrt[3]{\frac{1}{12}\sum P_{st}^3} \tag{2.5}$$

AS/NZS 61000.3.3: 2012 [103] specifies the limit for voltage fluctuations and flicker produced by devices of input current <16A/phase. According to the standard, the P_{st} and P_{lt} values should be less than 1 and 0.65 respectively. In addition, AS/NZS 61000.3.7:2001 [104] represents the compatibility levels for flicker in both low and medium voltage systems, which are 1 and 0.8 for P_{st} and P_{lt} respectively. Further, the utilities also set the limits depending on

the agreement by the customer, which are indicated as short-term (E_{psti}) and long-term (E_{plti}) flicker emissions in the standard. These levels are restricted to 0.35 (E_{psti}) and 0.25 (E_{plti}).

Moreover, IEEE 1547-2003 [105], IEEE 929-2000 [106] and AS 4777.2 [107] provide the integration requirements of photovoltaic inverter systems in distribution networks. According to IEEE 1547-2003 and 929-2000, currently the PV inverters are not allowed to provide voltage regulation and are required to be disconnect from the grid during the outside operating voltage limits (0.88p.u - 1.10p.u). As per AS 4777.2, these voltage limits are 0.94p.u -1.10p.u. In addition, IEEE 929 specified the power factor requirement of the PV inverter to be higher than 0.85 leading or lagging. The standard also recommended that the grid-connected PV systems are designed precisely to operate at close to unity power factor. It is to be mentioned that the reactive power can be supplied to the grid, but the reactive power compensation and the voltage regulation is not allowed by the IEEE standard. In comparison, the corresponding Australian standard AS4777.2-2005 [107] indicated the PV inverter operating power factor range from 0.95 lagging to 0.8 leading and it allows voltage regulation within this power factor range. However, recent standard AS 4777.2-2015 [108] proposed that the PV inverter is allowed to provide constant reactive power with fixed power factor not exceeding 0.95 leading/lagging. Besides, the standard also stated that if the PV inverter is capable of operating in reactive power mode, the maximum ratio of reactive power to rated apparent power should be up to 100% leading or lagging.

2.5.2. Harmonic Standards

Many standards around the world have presented the limits for harmonic distortion in distribution networks. The most common measure of harmonics is the Total Harmonic Distortion (THD), which is defined as the ratio of the root-sum-square of the harmonic quantity to the fundamental quantity. In addition, the individual harmonic distortion is expressed as the level of harmonics with respect to the percentage of fundamental. IEEE standards 519-1995 [52] and 519-2014 [53] focus on the allowable harmonic distortion levels of the network and IEEE 1547-2003 [105] describes the grid interconnection requirement of the distributed resources. According to the standards, the maximum limit of individual odd current harmonics up to 11^{th} order is 4.0%, followed by up to 17th order is about 2.0%, 1.5% is the limit for up to 23^{rd} order and the orders above 23^{rd} to 35^{th} should be less than 0.6%. Moreover, the current THD should be less than 5%. Recent standard IEEE 519-2014 indicated the individual voltage harmonic should be less than 5% and the total harmonic distortion should be below 8%.

Also, similar limits are specified by AS 4777.2 [107], IEEE 929-2000 and IEC 61000-3-2: 2012 [109] as indicated in Table 2.1. However, the recent standard AS 4777.2-2015 has introduced more strict limits compared to the previous AS4777.2 and IEEE standards. Similarly, as per the EN61727 [110] standard, the voltage THD limit for the photovoltaic interconnection is 2% and individual harmonics should be no more than 1%.

Table 2.1. Harmonic Limits of Grid Connected PV Inverter Requirement

Standards	**Individual Current Odd Harmonic Order**					**THD** $= \frac{\sqrt{\sum_{n=2}^{\infty} I_n^2}}{I_1}$
IEEE 929-200 and AS4777.2-2005	**3^{rd} - 9^{th}**	**11^{th} - 15^{th}**	**17^{th} - 21^{st}**	**23^{rd} - 33^{rd}**	**>33^{rd}**	
(%Fundamental)	<4.0%	<2.0%	<1.5%	<0.6%	<0.3%	**<5%**
AS4777.2-2015	**3^{rd} – 7^{th}**	**9^{th} - 13^{th}**	**15^{th} – 19^{th}**	**21^{st}-33^{rd}**	**>33rd**	
(%Fundamental)	<4.0%	<2.0%	<1.0%	<0.6%	<0.3%	

2.6. Summary

This chapter has provided a clear insight into the problems associated with solar PV system integration into distribution networks. All the studies reviewed so far have demonstrated that power quality is one of the key issues in distribution networks. It has been discussed that voltage quality issues such as overvoltage, voltage fluctuations/flicker, voltage unbalance and sag/swell are critical concerns in the low voltage networks with PV. In addition, due to the involvement of power electronic based inverter technology, there is a potential concern for harmonic injection issues. With the proliferation of a large number of PV inverter systems combined with nonlinear loads, the network harmonic distortion levels could be influenced and excite resonance problems. Therefore, it is important to investigate and quantify how the PV contributes to the network harmonic levels and its operational impacts on network performance. The next chapter presents the background modellings and software tools used for this research.

CHAPTER 3

MODELLING AND SIMULATION TOOLS

3.1. Introduction

To investigate the impact of PV systems on various power quality aspects of the distribution network, an appropriate and accurate modelling of the PV systems, load units and test network is necessary. This chapter presents the background theory and detailed modelling of various components of the grid connected PV systems such as PV source, maximum power point tracking techniques, DC/DC converter and DC/AC inverter control strategies used for this research. Afterwards, the test system and load modelling requirements suitable for different voltage quality and harmonic impact analyses to reflect a real-time scenario have been presented. Finally, the selected various software and hardware tools utilised in this research are explained.

3.2. Grid Connected Solar PV System

Grid connected solar PV systems convert the sunlight into AC electricity. The functional block diagram of a grid connected PV system is shown in Figure 3.1. The system includes solar PV panels connected as arrays, a boost converter, an inverter with interfacing filter and an isolation transformer. In the following sub-sections, background theory and modelling of these components are presented.

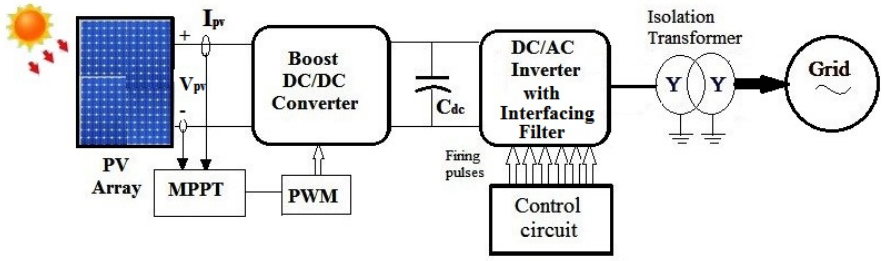

Figure 3.1. Block Diagram of Grid Connected PV System.

3.2.1. Modelling of Solar PV Source

The building block of the PV array is the solar cell, which is basically a P-N semiconductor junction. The solar energy is converted into electricity through photovoltaic effect. In [40], a mathematical modelling of PV arrays was presented. The equivalent circuit of a solar PV cell is shown in Figure 3.2. The current I_d flows through anti-parallel diode producing nonlinear I-V characteristics in the PV cell as shown in Figure 3.3.

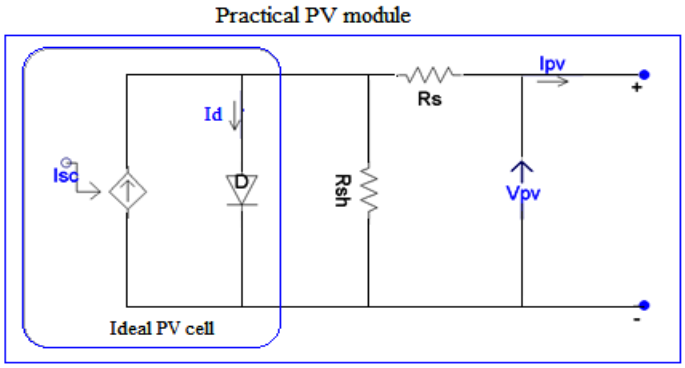

Figure 3.2. Solar PV Cell Equivalent Circuit.

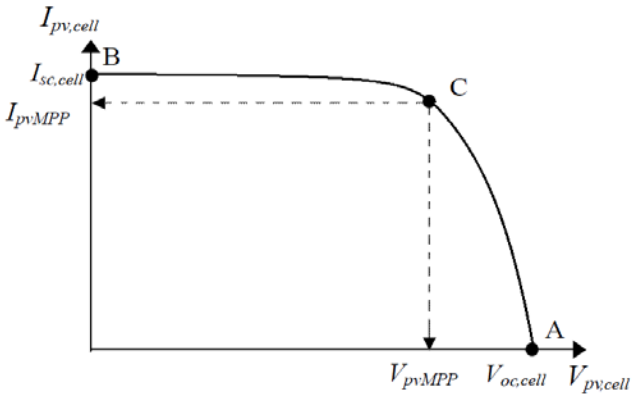

Figure 3.3. I-V Characteristic of Solar PV Cell [111].

The current and voltage relationship of an ideal solar PV cell can be expressed as given in equation (3.1).

$$I_{pv,cell} = I_{sc,cell} - I_d$$

$$= I_{sc,cell} - I_{rs,cell}\left[exp\left(\frac{qV_{pv,cell}}{nkT}\right) - 1\right] \quad (3.1)$$

Where, $I_{sc,cell}$ is the current generated by the incident of sunlight (it is directly proportional to the solar irradiation), I_d is the Shockley diode current, $I_{rs,cell}$ is the reverse saturation or leakage current of the diode, q is the electron charge ($1.60217646 \times 10^{-19}$ C), k is the Boltzmann constant ($1.3806503 \times 10^{-23}$ J/K), T (in Kelvin) is the temperature of the *p–n* junction and n is the diode ideality factor.

A PV module primarily consists of solar cells connected in series and a PV array is composed of series and parallel connected modules. The single PV cell circuit can ideally be scaled up to represent a number of series (N_s) and parallel (N_p) combinations as represented in Figure 3.4.

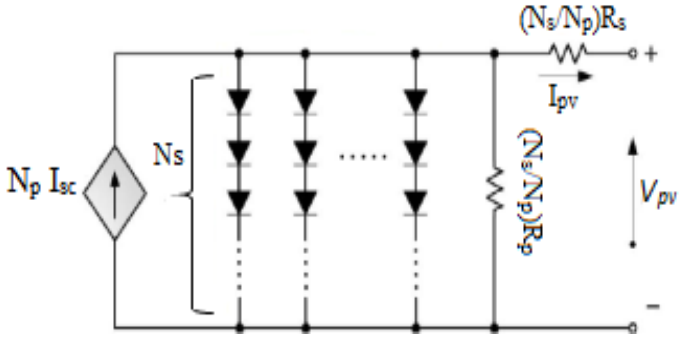

Figure 3.4. Equivalent Circuit of a PV Module/Array [111].

The equation that characterises the current and voltage relationship of a PV array is derived in (3.2). From the equation, it can be seen that the PV output power has a linear relationship with solar irradiation but the temperature has an inverse relationship with PV output power.

$$I_{pv} = N_p I_{sc} - N_p I_{rs}\left\{exp\left[\frac{q}{nkT_c}\left(\frac{V_{pv}}{N_s} + \frac{I_{pv}R_s}{N_p}\right)\right] - 1\right\} - \frac{N_p}{R_p}\left(\frac{V_{pv}}{N_s} + \frac{I_{pv}R_s}{N_p}\right) \quad (3.2)$$

Where I_{pv}: PV array output current (A), V_{pv}: PV array output voltage (V), I_{sc}: Solar cell photocurrent (A), I_{rs}: Solar cell reverse saturation current (A), T_c: Solar cell absolute operating temperature (K), R_S: Cell intrinsic series resistance (Ω), R_P: Cell intrinsic shunt resistance (Ω).

The photocurrent or short circuit current for a given operating condition of the PV array is assumed to be related to the short circuit current at standard test condition (STC).

$$I_{sc(T)} = \left[I_{sc(Tref)} + K_I(T\text{-}T_{ref})\right]\frac{S}{S_{ref}} \quad (3.3)$$

Where $I_{sc(Tref)}$ (A) is the light-generated current at standard test condition (usually at 25°C and 1000 W/m^2), K_I is the temperature coefficient of the current, T and T_{ref} being the actual and reference temperatures [in Kelvin] respectively, S (W/m^2) is the irradiation on the device surface and S_{ref} is the nominal irradiation.

The diode saturation current I_{rs} and its dependence on the temperature for PV model improvement can be expressed as given in equation (3.4). This modified equation could match the open-circuit voltages of the model with real-time data for a very large range of temperatures.

$$I_{rs} = \frac{I_{sc(Tref)} + K_I(T - T_{ref})}{exp\left[\left(\frac{q(V_{oc,(Tref)} + K_V(T - T_{ref}))}{nkT_{ref}}\right)\right] - 1} \tag{3.4}$$

Where, $V_{oc(Tref)}$ is the open circuit voltage at STC, K_V is the temperature coefficient of the voltage. Therefore, the equation (3.4) includes both coefficients K_I and K_V. The saturation current is strongly reliant on the temperature and this equation proposes a different approach to express the dependence of I_{rs} on the temperature.

To develop an absolute PV array system represented in Figure 3.2, the above derived mathematical model has been considered and developed in PSCAD software, which reflects a real-time system as shown in Figure 3.5. The corresponding I-V characteristics of a PV Array at various solar irradiation conditions from 1000W/m^2 to 200W/m^2 is shown in Figure 3.6. Also, the relation between PV output power and open circuit voltage at different solar irradiation conditions is presented in Figure 3.7.

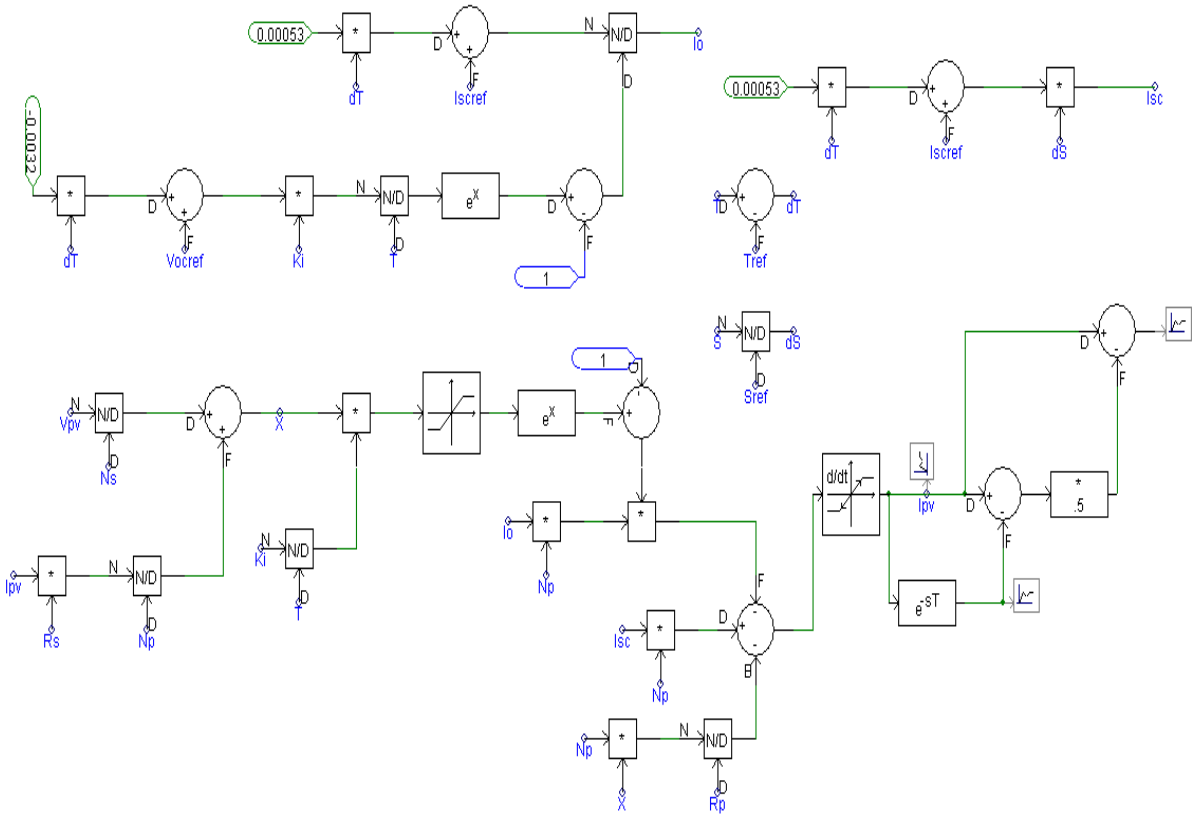

Figure 3.5. Simulation Model of PV Module/Array.

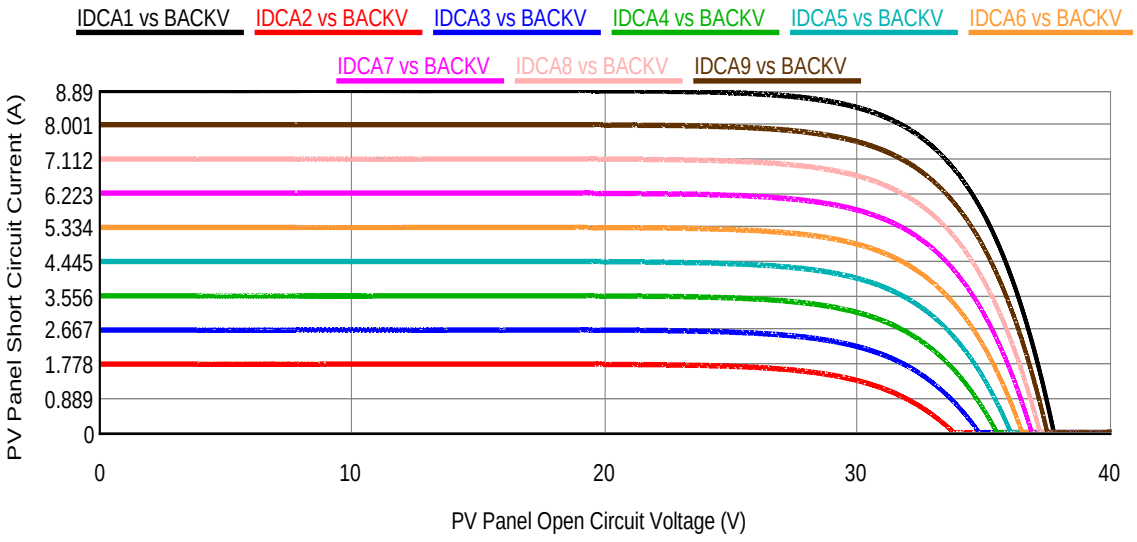

Figure 3.6. I-V Characteristics of PV Array at Various Solar Irradiation Conditions.

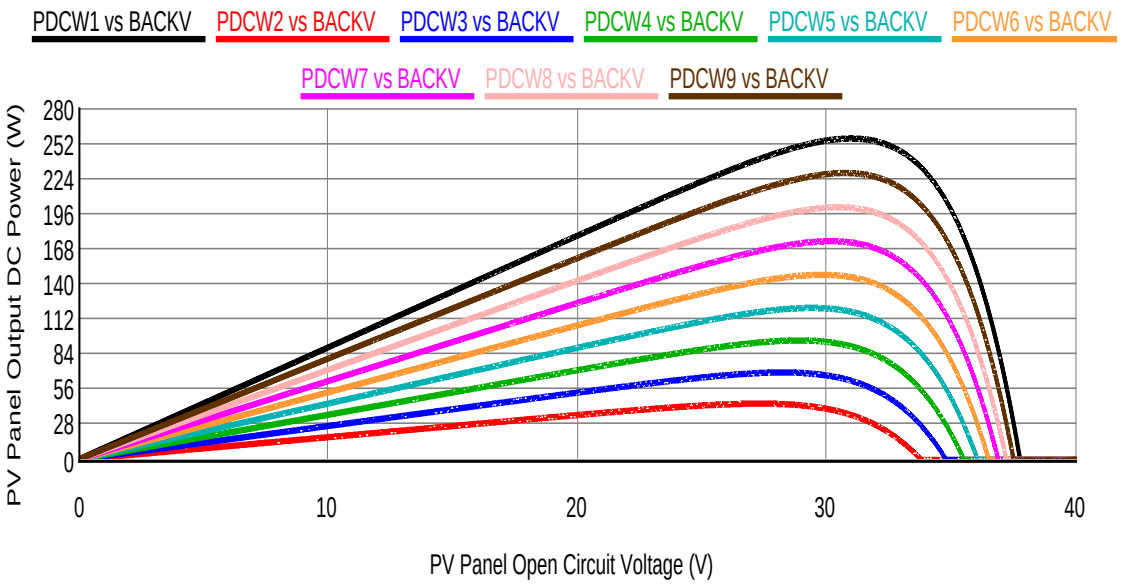

Figure 3.7. P-V Characteristics of PV Array at Various Solar Irradiation Conditions.

3.2.2. DC/DC Converter

Figure 3.8 shows simple DC/DC converter called a Boost converter. This boost converter is used to boost the output voltage of a PV array to achieve the optimum grid voltage level. The duty cycle for the gate switch is obtained from the Maximum Power Point Tracking (MPPT) system. This MPPT controller is essential for increasing the efficiency of the PV arrays.

The equation for boost converter output voltage in terms of input voltage is

$$V_L = \frac{V_{pv}}{1-D} \tag{3.5}$$

Where, *D* is duty cycle of IGBT switch.

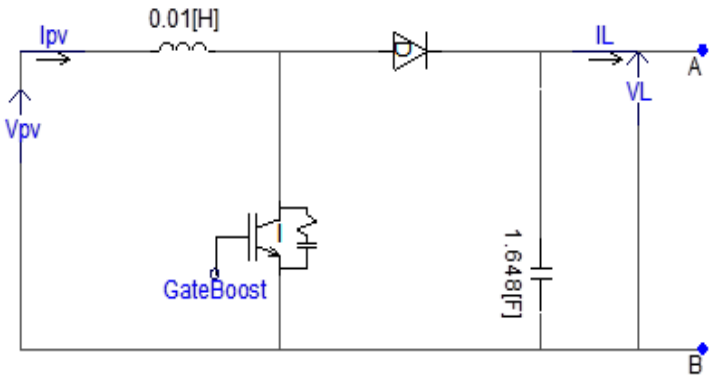

Figure 3.8. Boost Converter Circuit.

3.2.3. Maximum Power Point Tracking Algorithms

MPPT algorithms [41, 112] are necessary for PV applications because the maximum power point of a solar panel varies with the solar irradiation and temperature. Therefore, an MPPT control algorithm is required to extract the maximum power from a solar PV array. In the literature, many methods to find the maximum power point have been developed. These techniques vary in many aspects such as complexity, cost, range of effectiveness, convergence speed and correct tracking when solar irradiation and/or temperature changes. Among them, the Perturb and Observe Algorithm (P&O) and the Incremental Conductance (InCond) algorithms are the most widely used techniques, which have been considered in this research. In both P&O and InCond methods, the tracking of maximum power point depends on the amount of increment in reference voltage.

3.2.3.1. Perturb and Observe (P&O) Algorithm

The P&O method operates periodically by perturbing the terminal voltage or the current of the PV array and comparing the PV power with the preceding cycle. This algorithm continuously examines the sign of the last perturbation and the sign of the last increment or decrement in the PV power to determine and take the decision of what the next perturbation should be. For instance, Figure 3.9 shows the P-V characteristics curve for varying solar irradiation. Initially, starting from point A a perturbation of voltage to increment by ΔV will shift the operating point to B. Then the perturbation will be reversed due to the decrement in the power.

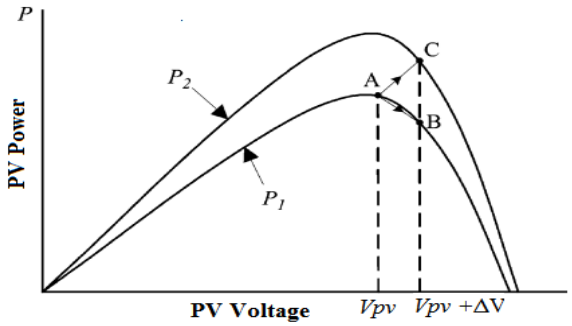

Figure 3.9. PV Panel P-V Characteristic Curve [113].

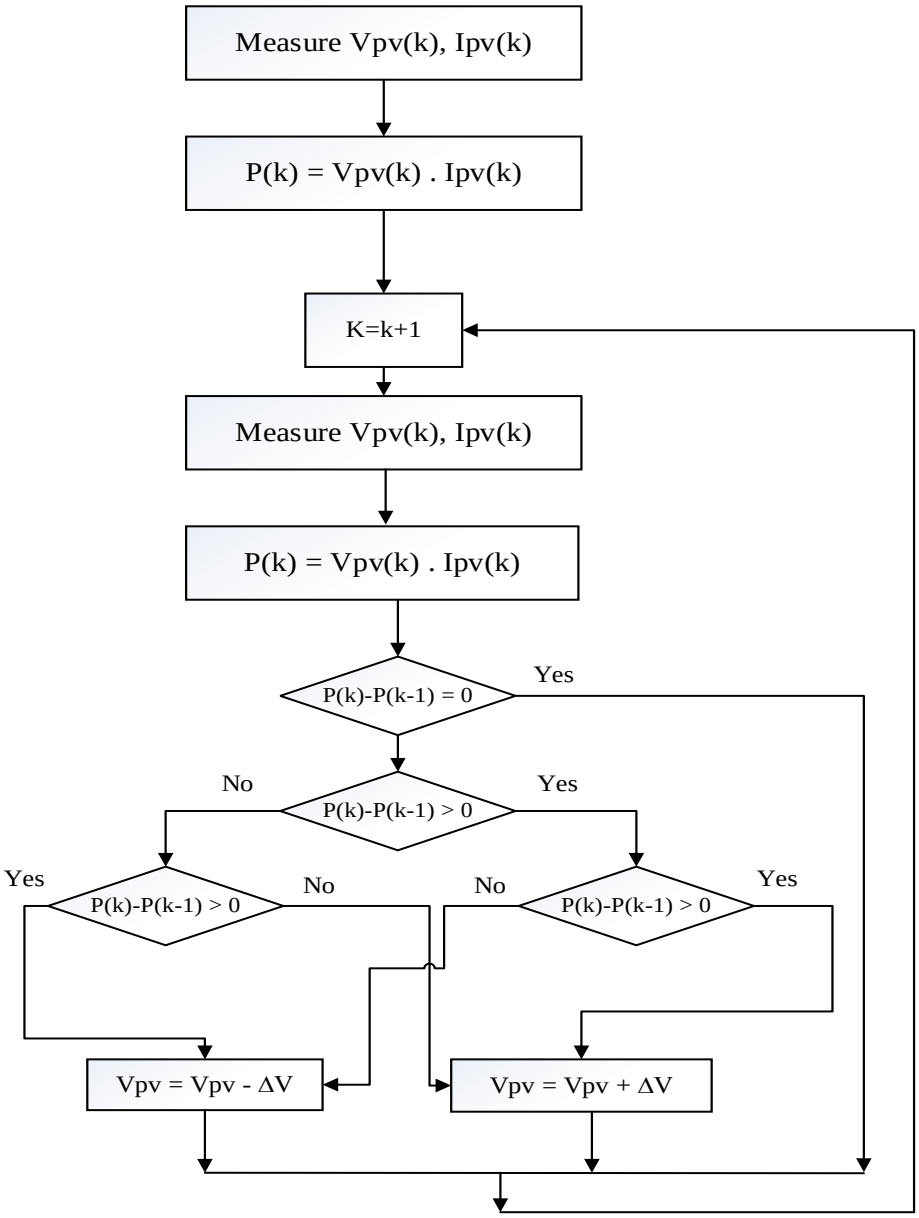

Figure 3.10. The Flow Chart of the P&O Algorithm.

Conversely, if the solar irradiation increases then the P-V power curve shifts from P1 to P2 and the operating point will move from point A to C. Subsequently, if the PV power increases, the perturbation will be in the same direction and if the PV power decreases, then the resulting perturbation should be in the opposite direction. This process is repeated until the MPP is obtained and the operating point oscillates around the MPP. The control algorithm of the P&O method has been implemented based on these facts [4] as shown in Figure 3.10 and the PSCAD model is shown in Figure 3.11.

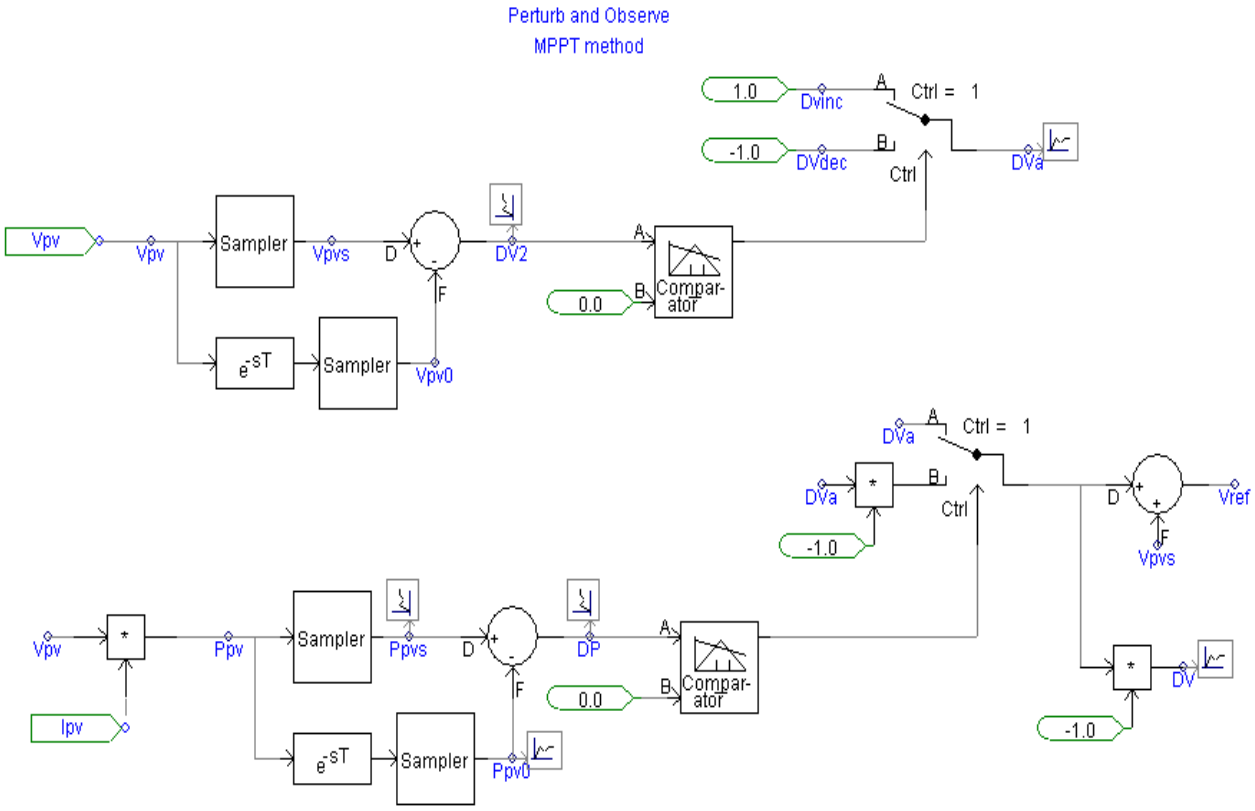

Figure 3.11. PSCAD Model for P&O Algorithm.

3.2.3.2. Incremental Conductance Algorithm

The incremental conductance algorithm [112, 113] is based on the fact that the slope of the curve power Versace voltage of the PV module is zero at the MPP. By comparing the increment of PV power with the increment of voltage between two consecutive samples, the change in MPP voltage can be determined. One millisecond is selected as sampling time. The deviations ΔV and ΔI are calculated from the difference of each sample to the prior one. A flow chart of the Incremental conductance algorithm is shown in Figure 3.12. The following equations (3.6) and (3.7) determine the MPP in this algorithm.

$$\frac{dP}{dV} = \frac{d(VI)}{dV} = I_{pv} + V_{pv}\frac{dI_{pv}}{dV_{pv}} \simeq I_{pv} + V_{pv}\frac{\Delta I_{pv}}{\Delta V_{pv}} \tag{3.6}$$

Further, $\frac{dP}{dV} = 0 \leftrightarrow \frac{\Delta I_{pv}}{\Delta V_{pv}} = -\frac{I_{pv}}{V_{pv}}$ at MPP,

$\frac{dP}{dV} > 0 \leftrightarrow \frac{\Delta I_{pv}}{\Delta V_{pv}} > -\frac{I_{pv}}{V_{pv}}$ left of MPP, (3.7)

$\frac{dP}{dV} < 0 \leftrightarrow \frac{\Delta I_{pv}}{\Delta V_{pv}} < -\frac{I_{pv}}{V_{pv}}$ right of MPP.

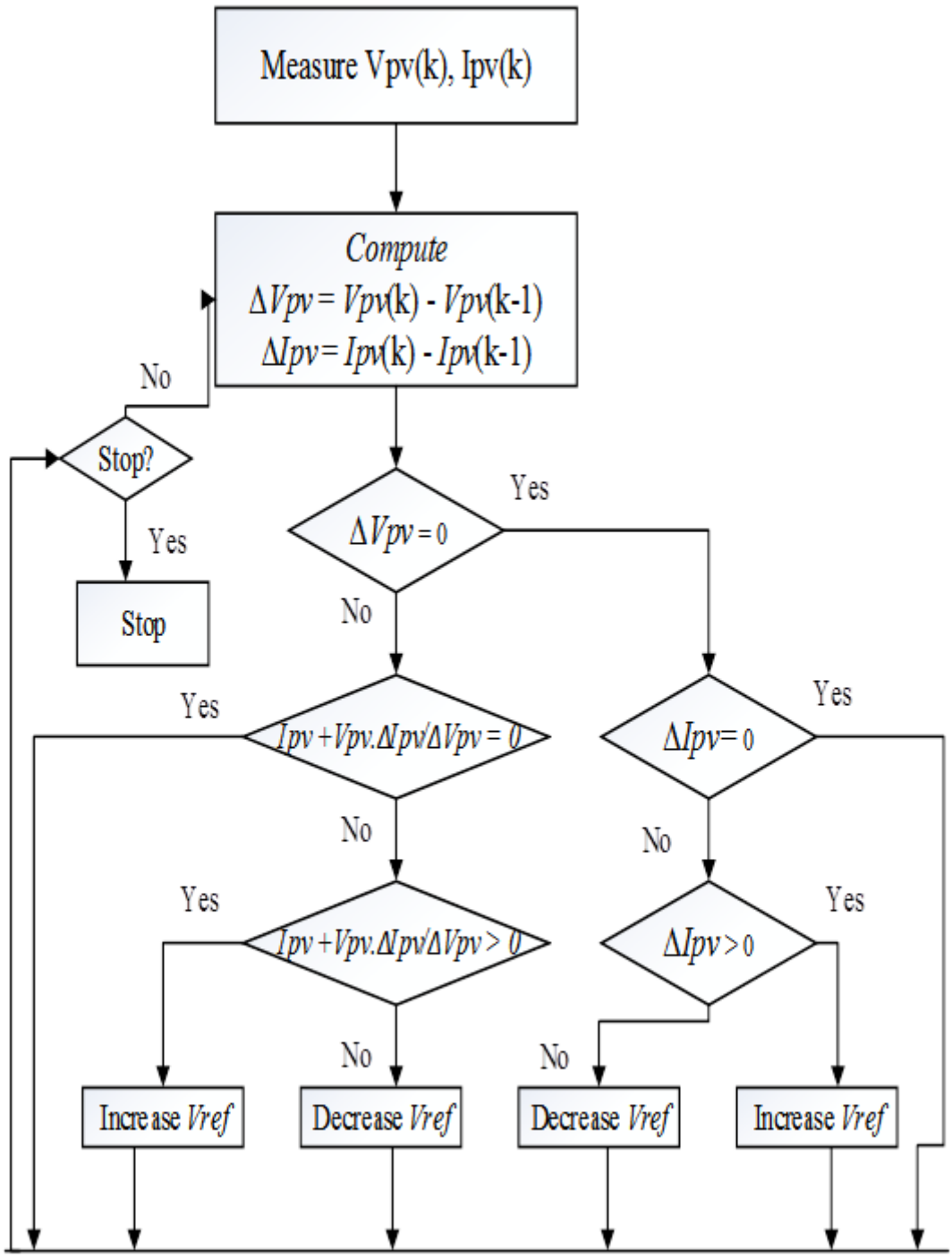

Figure 3.12. Flow Chart of the Incremental Conductance Algorithm.

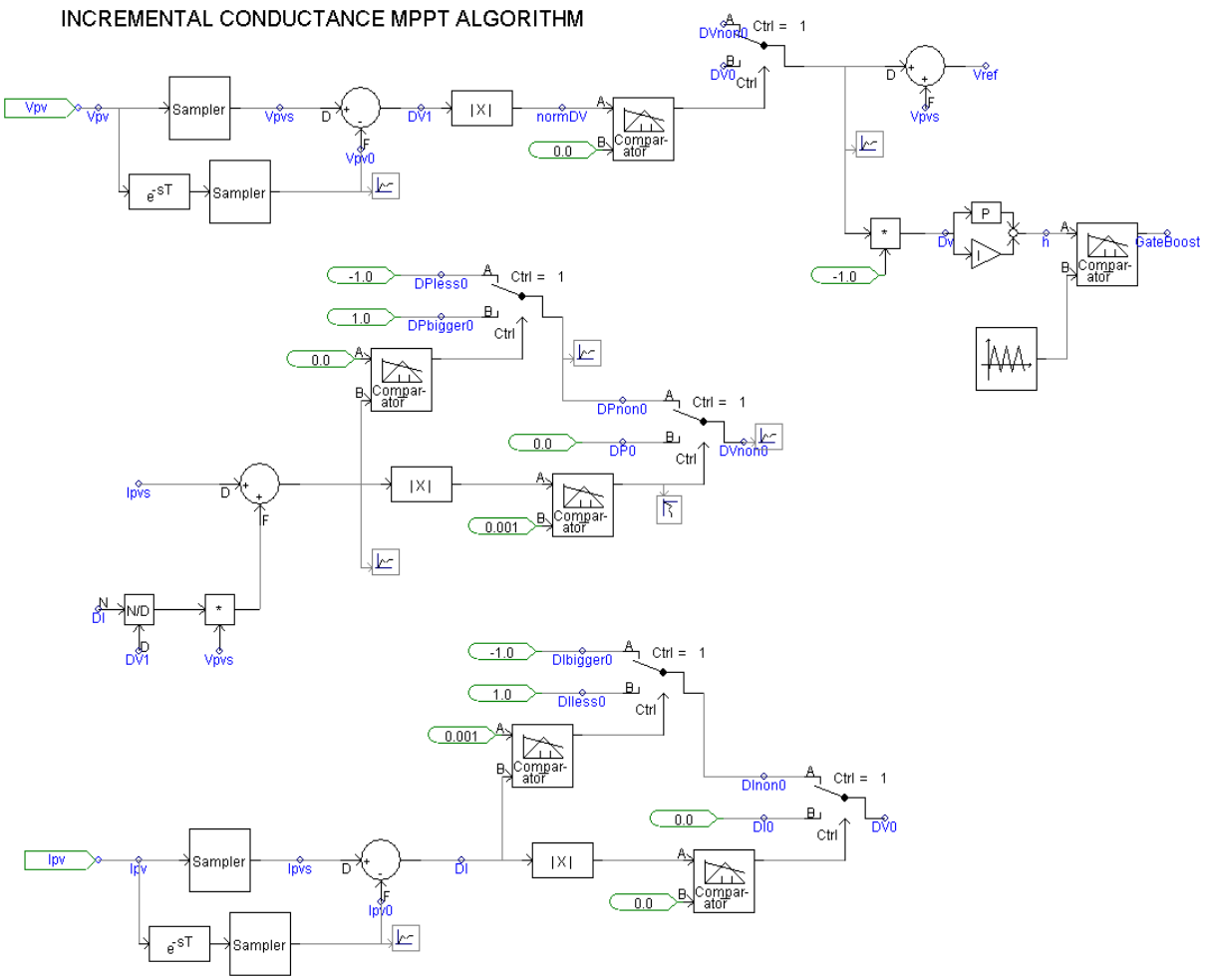

Figure 3.13. PSCAD Model for Incremental Conductance Algorithm.

The PSCAD model of incremental Conductance based MPPT algorithm is shown in Figure 3.13. The command signal Dv is used to increase or decrease the PV voltage by changing the duty cycle. From equation (3.5), the duty cycle is inversely proportional to the output voltage. This PV voltage Dv signal is changed to duty cycle command by multiplying with -1. Then using the PI controller, duty cycle command is applied to PWM generator with switching frequency to create gate pulses.

3.2.4. PV Inverter (DC/AC) Types and Control Topologies

To integrate the Solar PV system into a distribution grid a DC/AC inverter is needed, which converts the DC voltage into AC voltage. The PV inverter is a mature technology consisting of power electronic switches, which are controlled by control topology and switching patterns. Depending on the capacity of the PV system and the application, the inverter has single-phase and three-phase switching configurations. Figure 3.14 shows the grid connected single-phase and three-phase PV inverter configurations along with the filter.

In this research, a bipolar pulse width modulation (PWM) technique is implemented for a single-phase PV inverter switching. The firing pulses were generated by comparing the reference signal with the triangular carrier waveform. For this, the inverter considers the grid voltage as a reference signal used to synchronise the PV output in terms of magnitude and frequency.

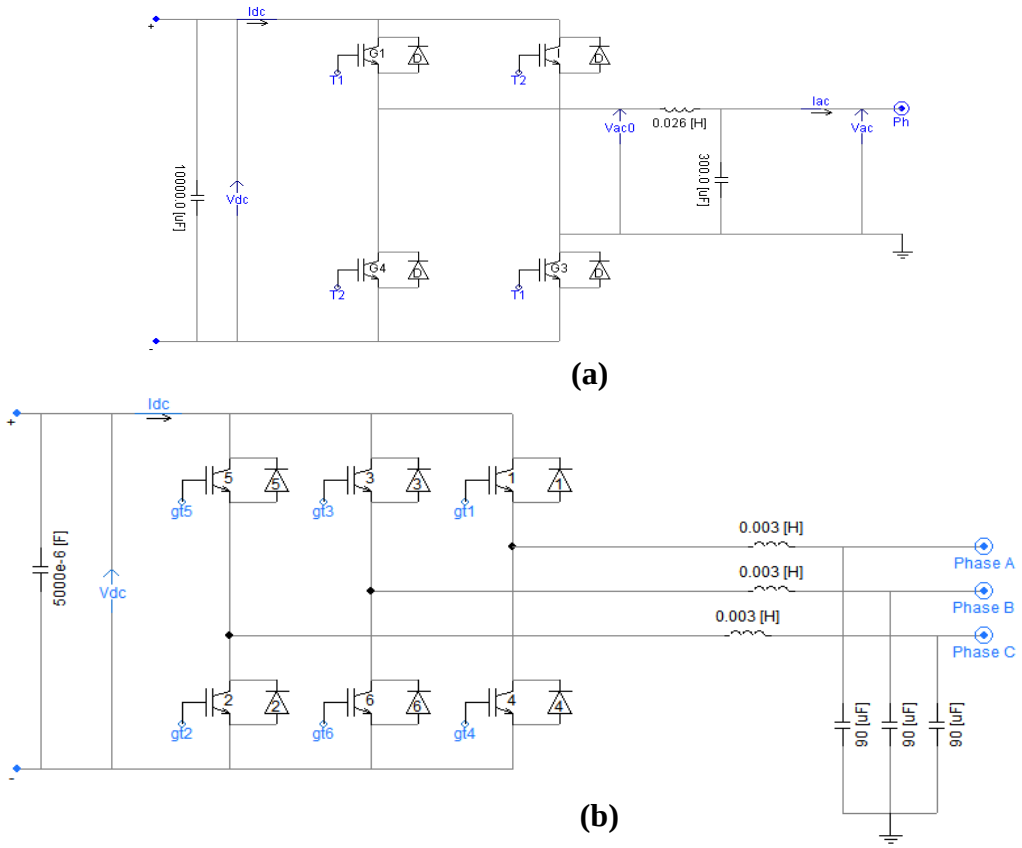

Figure 3.14. (a) Single-phase and (b) Three-phase PV Inverter Systems with Filter.

In order to control three-phase PV inverters, current control techniques are used in most applications. In this thesis, two basic models of the PV inverter with current control capabilities are considered namely Current Regulated Current Source Inverter and Current Controlled Voltage Source Inverter [114]. These PV inverters are capable of controlling real and reactive powers. The topology of the power inverters is modelled with a three phase two-level bridge block as shown in Figure 3.14 (b). The inverter bridge contains six IGBT switches with their respective anti-parallel diodes, which compensate the dead time impacts. Note that the power inverter hardware for the current source inverter and the voltage source inverter are identical.

3.2.4.1. Current Regulated Current Source Inverter (CRCSI)

Figure 3.15 shows the schematic diagram of a control circuit for a PV current source inverter. The current source inverter together with the controller operation synthesizes a current

source connected to the grid. The control circuit utilises the grid voltages to determine the phase angle that is obtained using a three phase PI controlled phase locked loop (PLL). Therefore, the inverter output will be synchronised with the grid voltage in terms of frequency and phase angle. The measured DC output voltage and MPPT controller (V_{mpp}) are compared and the error is given to the PI controller to generate reference active power. In the controller, P_{ref} and Q_{ref} represent the reference real and reactive powers; P_t and Q_t are the measured powers. These real and reactive power reference signals are compared with measured values and the errors are given to the PI controller. The generated real power error (I_{sd_ref}) signifies the real current component, which is in-phase with the voltage in the case of unity power factor (PF) operation and I_{sq_ref} is the reactive current component.

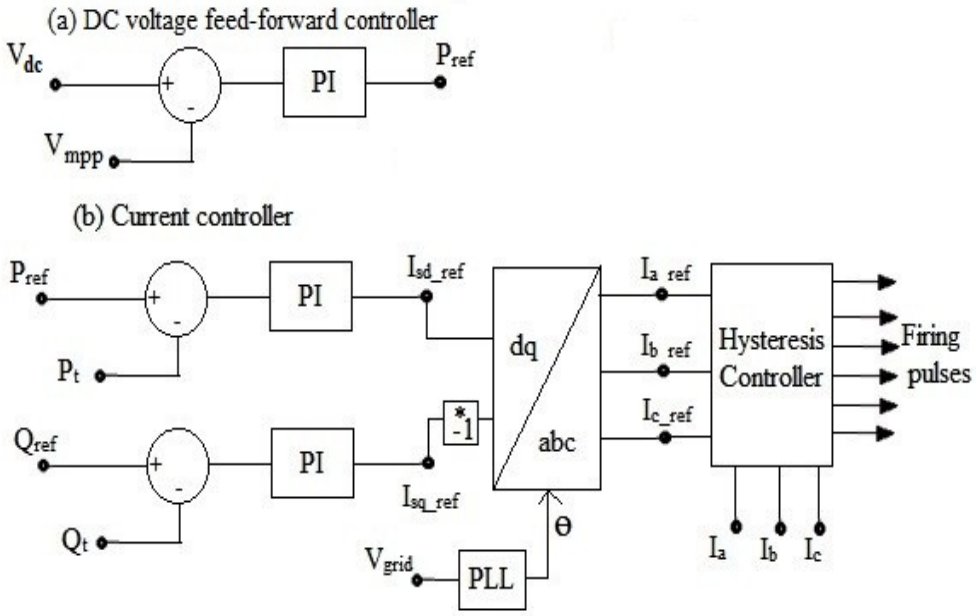

Figure 3.15. Control Circuit of Current Regulated Current Source Inverter.

The generated currents in a dq synchronous rotating frame can be transformed into stationary abc frame (I_{a_ref}, I_{b_ref} and I_{c_ref}) currents through the inverse synchronous frame. The input to the hysteresis controller is the error between the reference currents and the measured PV output currents. If the error surpasses the hysteresis band (HB) limit, a switching instant will be given to the PV inverter switches so that the measured current follows the reference currents. A fixed band type hysteresis controller technique has been considered due to its simplicity and faster dynamic response. Despite of it advantages, this current controller has an issue of variable switching frequency, which may result in injection of high harmonic current components and increased losses. Moreover, the variation in the PV output could change the

inverter reference currents, which in turn could introduce disturbances in the current controller response.

3.2.4.2. Current Controlled Voltage Source Inverter (CCVSI)

Grid connected voltage source inverter generally resembles a voltage source connection in the grid. The detailed control scheme of the current controlled pulse width modulation technique used to control the voltage source inverter is shown in Figure 3.16. This method has several control loops to regulate the PV inverter output current indirectly by controlling the output voltage.

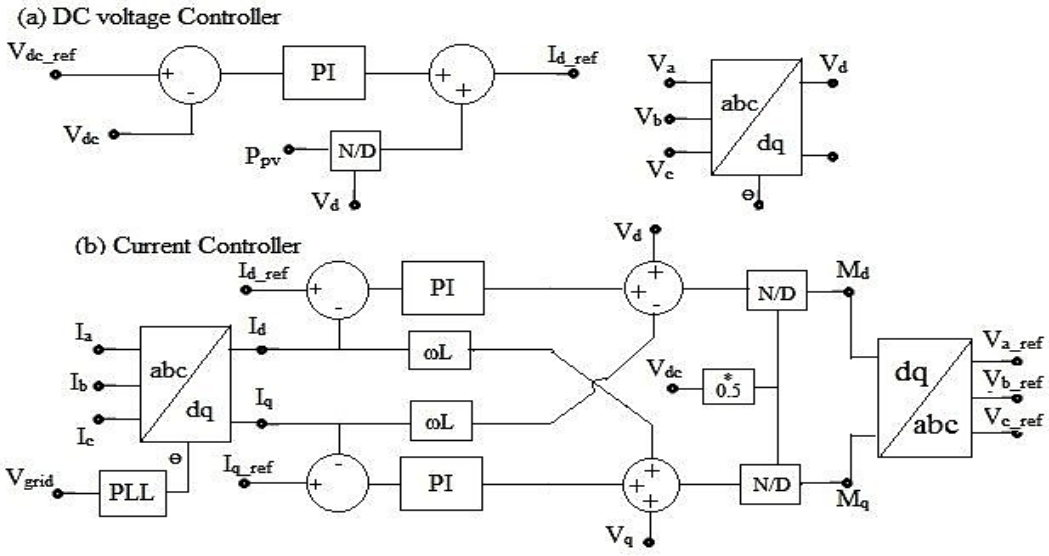

Figure 3.16. Control Circuit of Current Controlled Voltage Source Inverter.

A DC link voltage controller is applied to regulate the DC voltage across the capacitor to a constant value. It can be achieved by controlling the injected active current in the inverter. If the PV output voltage is lower than the reference DC link voltage, the controller decreases the active current so the DC voltage and the capacitor current increases and vice versa [114]. The output of the PI controller is used in the current controller as a reference.

$$I_{d\_ref} = K_{pr}\left(V_{dc\_ref} - V_{dc}\right) + K_{in}\int\left(V_{dcref} - V_{dc}\right)dt + \frac{P_{pv}}{V_d} \tag{3.7}$$

Where, K_{pr} and K_{in} are the proportional and integral constants.

Further, the measured voltages and currents at the grid integration point are used in the controller. A three-phase dq synchronous frame theory is applied to convert the voltage and currents into dc quantities. Here, the phase angle is obtained using three phase PI controlled PLL to synchronise the PV inverter with the grid. The PI controllers are used to track the

reference current with zero steady state error. Then, the grid voltages and the DC voltage are used in the feed-forward loop to get the reference voltages as expressed in the below equation (3.8).

$$\left.\begin{aligned} M_d &= 0.5V_{dc}(2I_{d\_ref} - 2I_d - LwI_q + V_d) \\ M_q &= 0.5V_{dc}(-2I_q + LwI_d + V_q) \end{aligned}\right\} \quad (3.8)$$

For unity PF operation, the q axis component is set to zero so the active and reactive powers can be controlled. Subsequently, the reference signals are then transformed into the stationary frame using the inverse dq transformation. These control signals are compared with the carrier high-frequency signal, which generates the firing pulses for the PV inverter.

3.3. IEEE-13 Bus Unbalanced Distribution Network

As a part of this research, an IEEE-13 bus radial distribution network is selected as the test system [115]. The IEEE-13 bus distribution feeders have interesting characteristics of a real distribution network making it suitable for the analysis. This radial unbalanced industrial distribution network encompasses the following characteristics:

- Three phase four-wire system with a nominal voltage of 4.16 kV.
- This system has three-phase, two-phase and single-phase line configurations.
- Overhead and unground lines with unsymmetrical line geometries possess unbalanced line impedances.
- Substation voltage regulator has three single phase voltage regulators connected in star.
- Single-phase and three-phase shunt capacitor banks.
- In line transformer
- Have balanced and unbalanced spot and distributed loads, which can be modelled as constant kW and kVAr (PQ), constant impedance (Z) or constant current (I) load.

All the loads can be three-phase loads connected in wye or delta and the single-phase loads connected line-to-ground or line-to-line. The test system configurations and the data are given by IEEE PES Distribution Systems Analysis Subcommittee. The line diagram of the IEEE-13 bus test system is shown in Figure 3.17. A simulation model of the IEEE-13 bus network modelled in PSCAD/EMTDC software is shown in Figure 3.18. Simulations have been performed for power flow analysis and the results verified with the available benchmark data sheet.

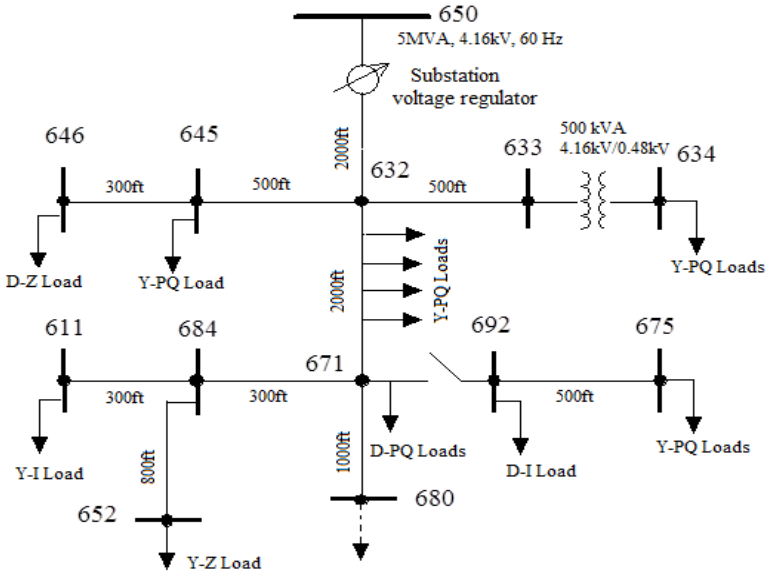

Figure 3.17. IEEE-13 Bus Test System Detailed Line Diagram.

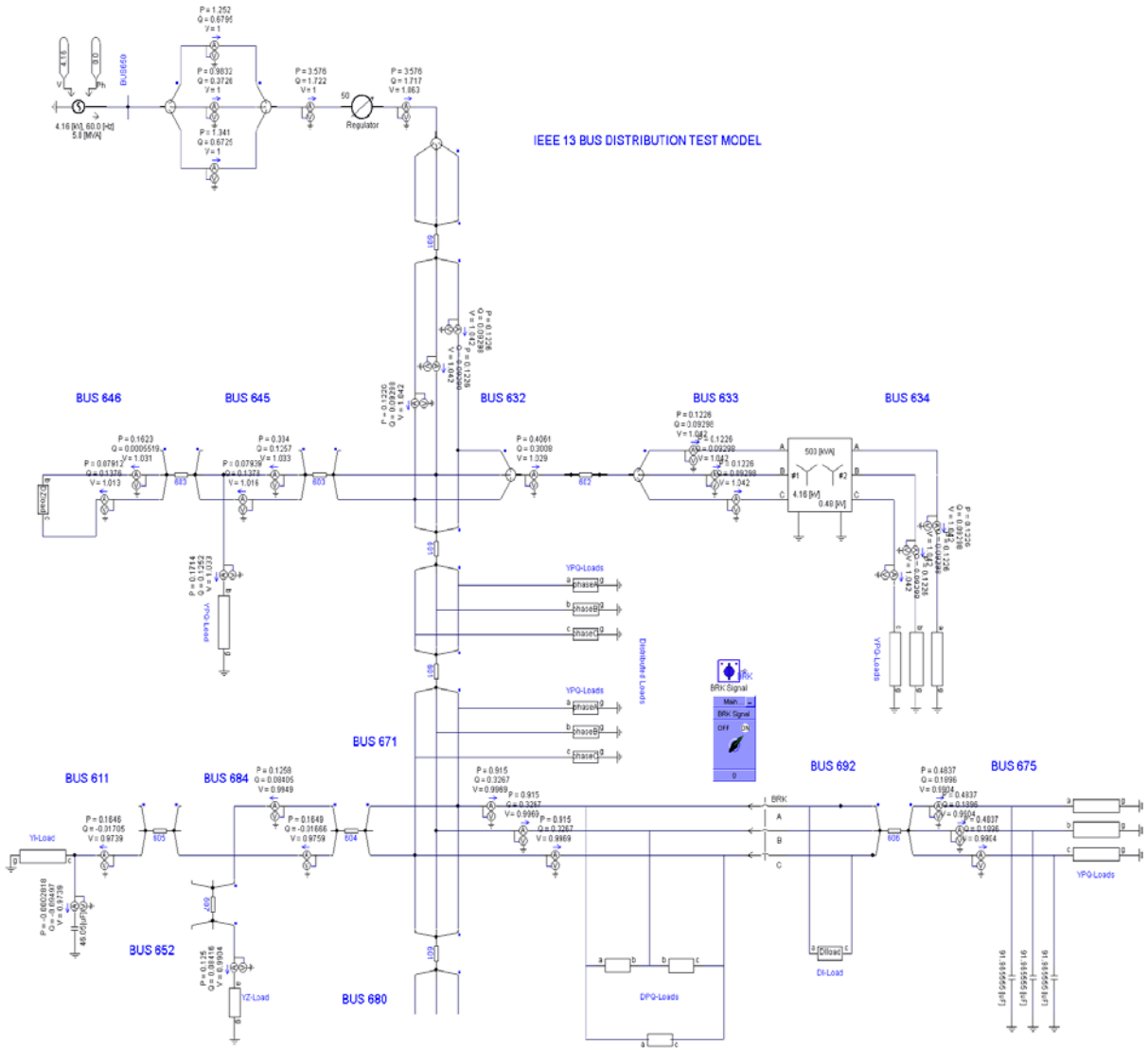

Figure 3.18. Simulation Model of IEEE-13 Bus Distribution System.

3.4. Load Modelling

Various types of static and nonlinear load models have been considered for different power quality analyses. The most widely used static load models are polynomial load model and the exponential load model. In this research, the static load models including constant power, constant impedance and constant current load are considered to study the impact of PV power injection on the voltage quality of the grid.

The constant power loads are connected as a parallel combination of a variable resistor (R) and inductor (L). The respective values are computed using equations (3.7) and (3.8), which are dependent on the grid voltage.

$$R = \frac{{V_{ph}}^2}{P_0} \tag{3.7}$$

$$L = \frac{{V_{ph}}^2}{2\pi f Q_0} \tag{3.8}$$

Where, P_o and Q_o are the constant real and reactive powers of load and V_{ph} is measured RMS voltage across R and L. Figure 3.19 shows the example simulation design of constant power load in PSCAD software.

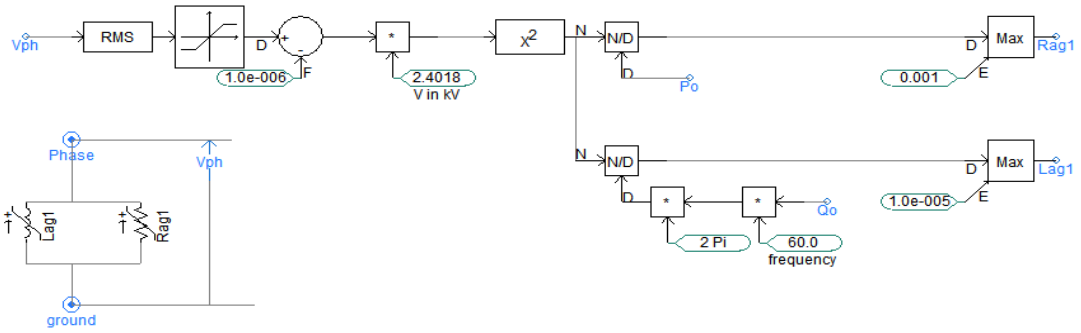

Figure 3.19. Simulation Design of Constant Power (PQ) Load.

Similarly, constant current load model is modelled as a parallel branch of variable resistor and inductor as shown in Figure 3.20 and is calculated using equations (3.9) and (3.10). However, the constant impedance load is not voltage dependent and is modelled as a fixed resistor and inductor values which are measured using the rated grid RMS voltage.

$$R = \frac{V_{ph}}{\left({P_i}/{V_o}\right)} \tag{3.9}$$

$$L = \frac{V_{ph}}{2\pi f\left({Q_i}/{V_o}\right)} \tag{3.10}$$

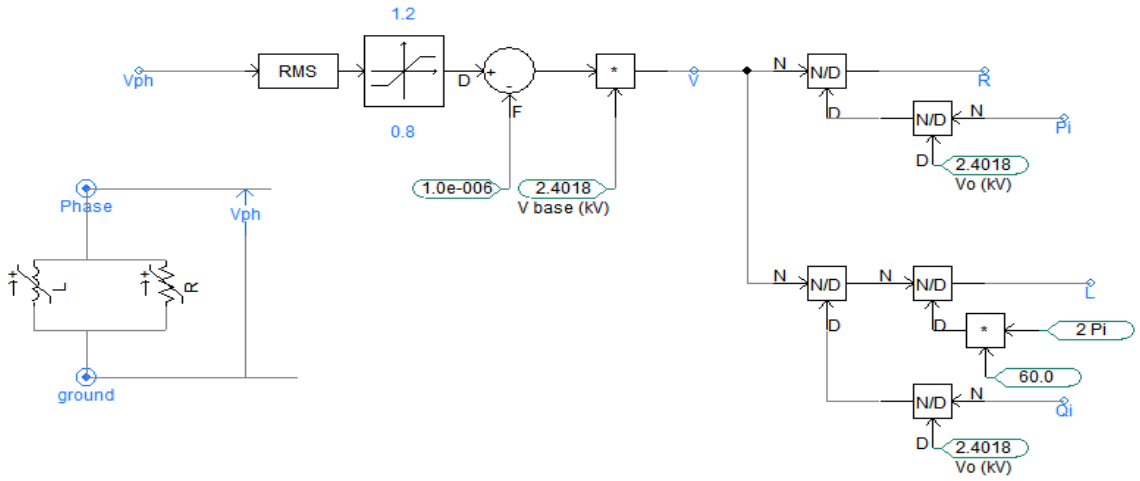

Figure 3.20. Simulation Design of Constant Current Load.

In addition, to study the harmonic impact of PV systems in real-time grid operating scenario, a certain amount of harmonic distortion is injected into the grid through nonlinear load models. These nonlinear load models include single-phase and three-phase power electronic based devices and single-phase motor type loads. Most of the residential and commercial loads have nonlinear loads such as Televisions (TV), Personal Computers (PC), Compact Fluorescent Lamps (CFL), air conditioning appliances with Adjustable speed motor drives (ASD) and other power conversion devices, which are distorting the grid currents and voltage waveforms. The voltage distortion depends on both the system impedance and the amount of harmonic current injected. Consequently, the aggregated impact of a wide variety and different configurations of domestic and industrial loads can influence the network harmonic distortion levels. Accompanied by the proliferation of PV systems and their interaction in the distribution network are the potential issues of harmonics and occurrence of harmonic resonance. Therefore, accurate modelling of these loads should be considered to simulate a real-time network scenario. Regarding that, various types of nonlinear loads and their current harmonic characteristics considered in this research have been discussed.

Loads such as CFL, TV, PC and DC motor drive [38, 39] utilise single-phase diode full bridge converters for their operation, which generate primarily odd harmonics of 3^{rd}, 5^{th}, 7^{th}, 11^{th},..... orders. Simulation models of each of the loads developed in PSCAD software and their respective individual current harmonic spectrum are shown in Figure 3.21. It is seen that these loads are rich in harmonics and generally produce a pulsed waveform, which is due to the extraction of non-sinusoidal currents.

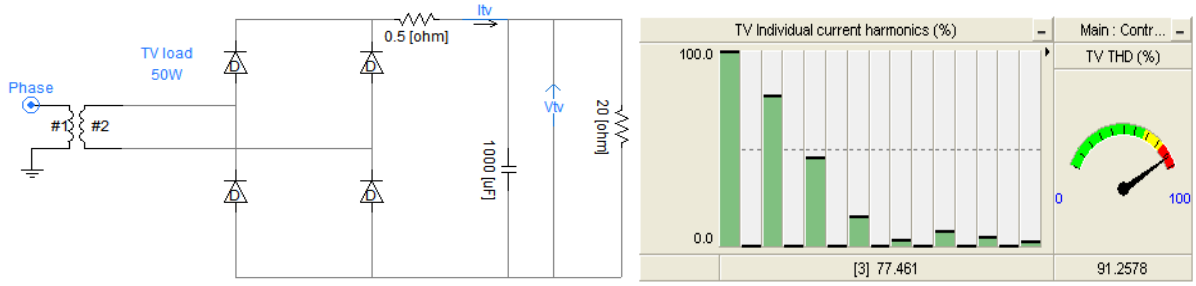

(a) TV or Computer Monitor

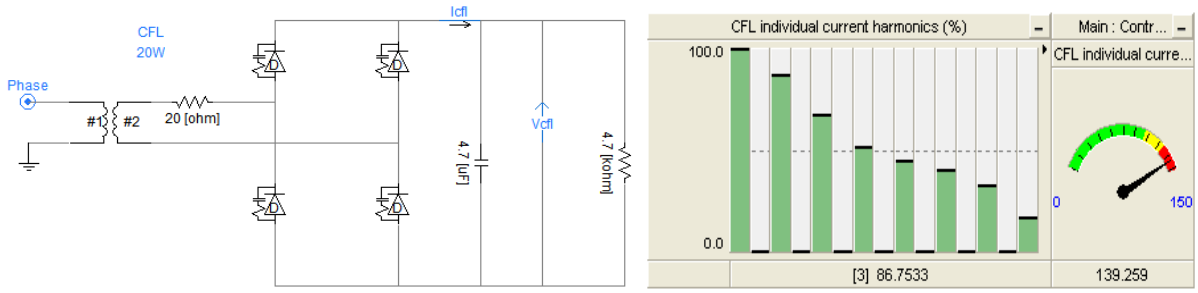

(b) Compact Fluorescent Lamp

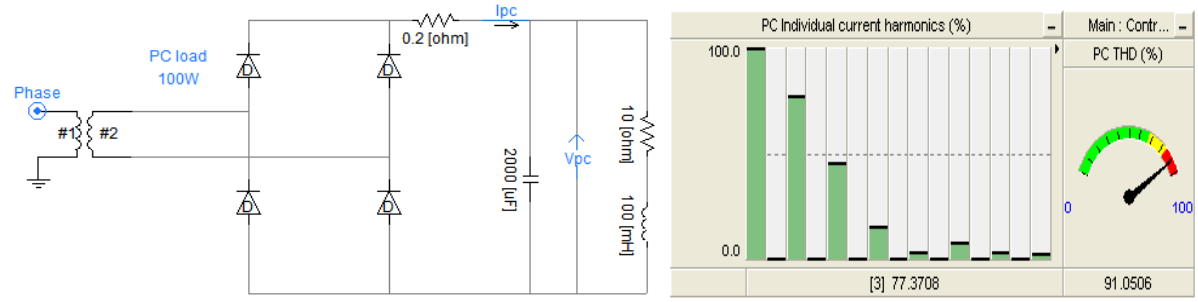

(c) Personal Computer

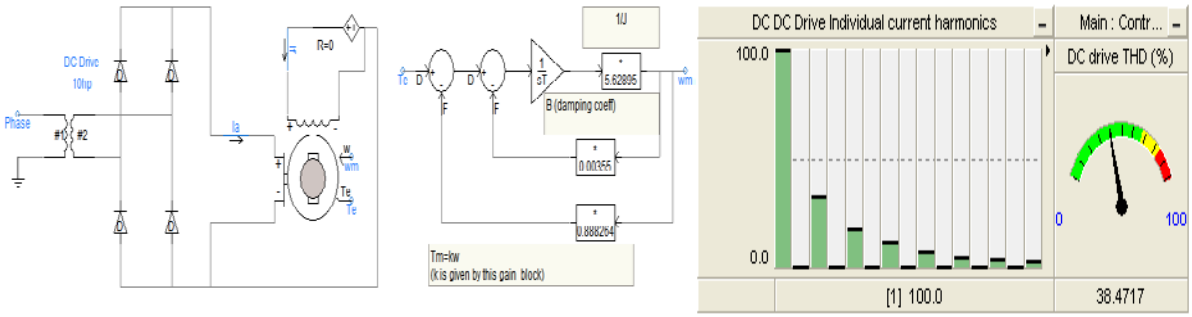

(d) DC Motor Drive

Figure 3.21. Single-phase Power Electronic based Nonlinear Loads.

Also, the PSCAD simulation models of three-phase loads namely lift motors and ASDs with their current harmonic spectrums are shown in Figure 3.22. It is observed that the lift motor utilises a three-phase diode bridge converter circuit with a motor on the DC side, which is modelled as a DC voltage source. However, ASDs are represented as a three-phase thyristor

bridge inverter with a motor on the DC side. This ASD motor is modelled as a direct current source. Figure 3.22(b) also shows the speed control logic for ASD. These types of loads generate current harmonics mainly 5th and 7th order and a small quantity of 11th, 13th and higher orders based on the configuration. The resultant harmonics of several identical devices can be added or subtracted and the collective effect of different kinds of loads could violate the network harmonic distortion levels.

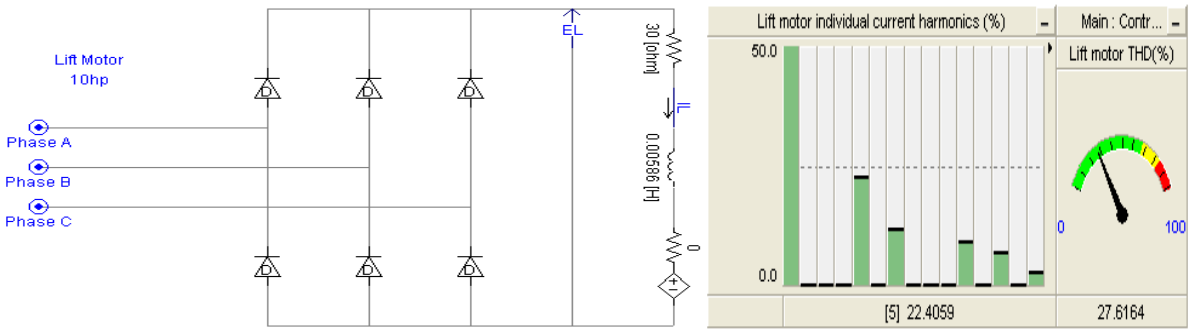

(a) Lift Motor

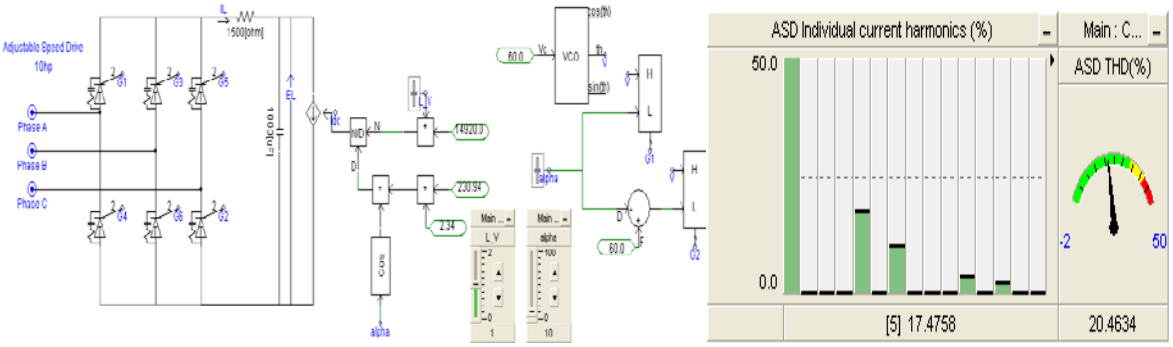

(b) Adjustable Speed Drive

Figure 3.22. Three-Phase Power Electronic based Nonlinear Loads.

Apart from that, in this analysis single-phase induction motor [116] type loads are considered to generate dynamics in the network. Typically, these motors are used in various household appliances such as washing machines, pumps, blowers, refrigerators and fans, which range from 0.5hp to 15hp. Propagation of single-phase induction motor loads are problematic in the network because they increase the unbalance between phase voltages. During the start-up, these motors draw large currents and increase the reactive power requirement. Figure 3.23 shows the simulation model induction motor. It is seen that a three phase induction motor is used to model single phase induction motor, which uses a running capacitor to generate the phase difference required for one phase. Also, this model has a starting capacitor, which can

be used during start-up and stopover to achieve nominal rotating speed. In this figure, tset_2 indicates the torque demand of the mechanical load and *w* is the rotating speed of the motor.

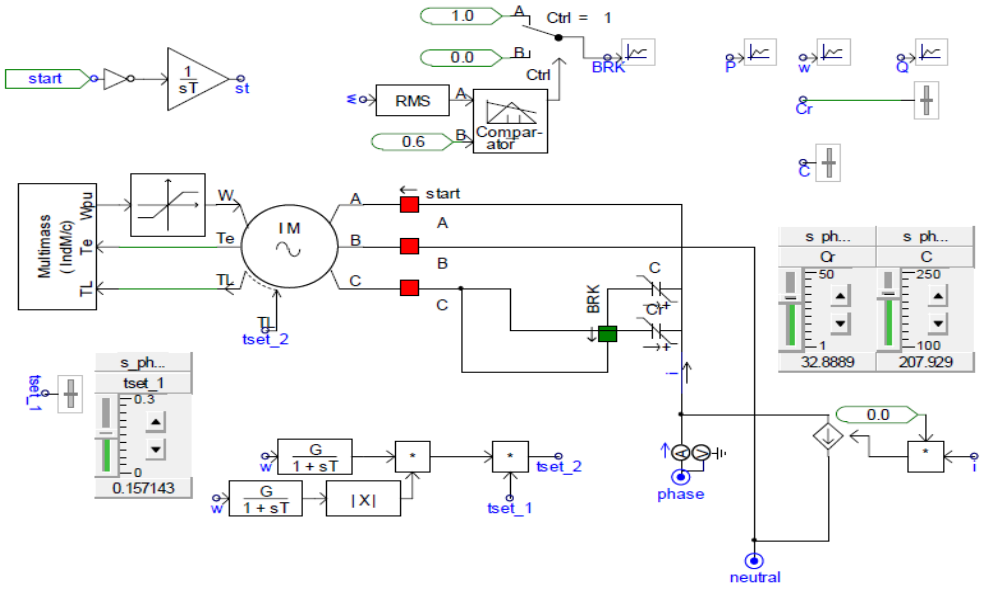

Figure 3.23. Simulation Model of Single-phase Induction Motor Load.

3.5. Software and Hardware Tools

3.5.1. PSCAD [117]

PSCAD stands for Power Systems Computer Aided Design**.** In this project, PSCAD software is selected for simulation purposes. PSCAD software is a professional simulation tool used for electromagnetic transient (EMT) analysis. PSCAD is also known as PSCAD/EMTDC which is more suitable for time domain instantaneous simulations, also known as electromagnetic transient solutions for both power and control systems. PSCAD with its graphical user interface allows the user to design a schematic, run a simulation, analyse the results and manage the data in an integrated graphical environment. Thus, PSCAD is an efficient software for testing and simulation of power quality, especially transients and harmonics. This software is the most preferred EMT program by manufacturers in industry and a popular tool for research and educational purposes. PSCAD provides accurate, effective and reliable solutions.

3.5.2. Real Time Digital Simulator (RTDS) [118]

In the final part of this research, Controller Hardware-in-the-Loop simulations have been performed using an integrated platform of RSCAD/RTDS and dSPACE hardware control board.

RTDS is a digital electromagnetic transient power system simulator, which operates in real-time. The simulator has high speed PB5 and Gigahertz processor cards (GPC) to solve the power system equations and controller system components modelled in RTDS. Also, the simulator contains various analog and digital Gigabit Transceiver Input/output cards namely GTAI, GTAO, GTDI, and GTDO, which interfaces the low power signals exchange from/to external devices [119]. These signals are generally within a range of +/-10V peak and can be easily calibrated with high accuracy. The test system modelling and compilations are performed in RSCAD draft file. The results of simulations and controlling are observed in runtime mode.

3.5.3. dSPACE Control Board Platform [120]

The dSPACE stands for Digital Signal Processing and Control Engineering. The dSPACE control board is specially designed for test and development of control system and for real-time simulations. The hardware contains DS1103 controller card and link boards (DS817 and DS814) to interconnect with the host PC, a PX4 expansion box and the connector panel CLP1103 [120]. The block diagram of dSPACE hardware and the software system is shown in Figure 3.24. This platform depends on the MATLAB/Simulink software, which provides several Simulink libraries and real-time RTI library blocks to design the model. The RTI library has various Analog to Digital (ADC) and DAC channels to interface with the external system. These signals are usually in low power levels. Then, by using the Simulink coder the developed model can be converted to custom C code, which generates a .sdf file suitable for dSPACE controlDesk software. The generated code file can be loaded into the dSPACE controlDesk software for online calibration. The input controlling, output monitoring and recording can be performed during the run-time in controlDesk layout.

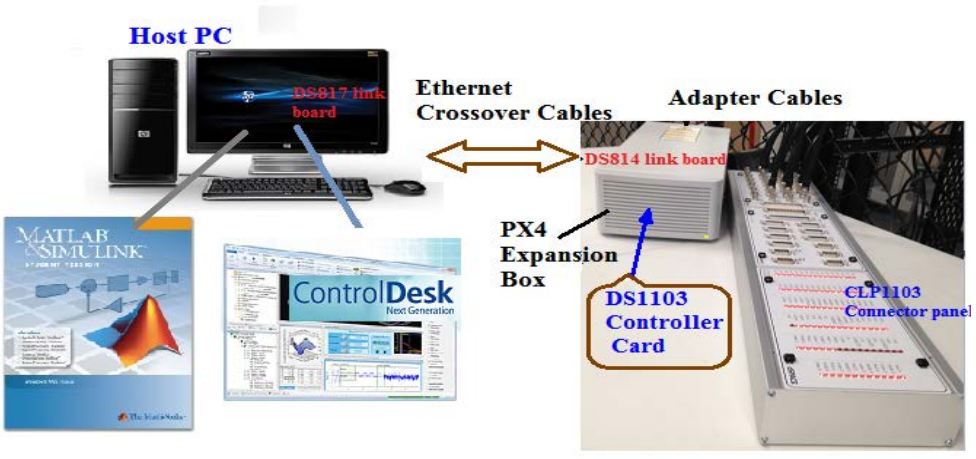

Figure 3.24. Block Diagram of dSPACE Hardware Setup.

3.6. Summary

This chapter has provided background theory and modelling of various components used throughout this research. The PV system components including PV arrays, converters, inverters and their control technologies were explained, and their implementation in PSCAD software were presented. Then, the test system with various types of load models required for the assessment of voltage quality issues and to perform accurate harmonic analysis were simulated and discussed. After that, various software and hardware tools used for this research were introduced. Furthermore, the application of these models and their study approaches will be explained in the contribution Chapters 4, 5, 6 and 7.

CHAPTER 4

INVESTIGATION OF VOLTAGE QUALITY ISSUES

4.1. Introduction[1]

This chapter provides a thorough investigation of voltage quality issues associated with high PV penetration. The evaluation of voltage quality issues such as voltage rise, voltage unbalance, sag/swell issues on the IEEE-13 bus unbalanced distribution network with PV penetration performed through simulations are discussed in the following section. Furthermore, field investigations have been performed on real-time grid connected PV systems located at the University of Queensland St. Lucia and Gatton Campuses, which have installed capacities of 1.5MW and 3.3MW respectively. Finally, the summary of this chapter is presented at the end.

[1]This chapter is incorporated with the following references:

Partially incorporated in Section 4.2:
Annapoorna Chidurala, T. K. Saha, and N. Mithulananthan, "Power quality enhancement in unbalanced distribution network using Solar-DSTATCOM," in *Power Engineering Conference (AUPEC), 2013 Australasian Universities*, Hobart, TASMANIA, Sept. 29-Oct. 3, 2013, pp. 1-6.

Section 4.3 through Subsection 4.3.1:
Annapoorna Chidurala, T. K. Saha, and N. Mithulananthan, "Field investigation of voltage quality issues in distribution network with PV penetration," in Power and Energy Engineering Conference (APPEEC), 2015 IEEE PES Asia-Pacific, Brisbane, QLD, Australia, 15-18 Nov. 2015, pp. 1-5.

Subsection 4.3.2:
M. J. E. Alam, R. Yan, T. K. Saha, Annapoorna Chidurala, D Eghbal, "Learning from a 3.275 MW Utility Scale PV Plant Project," in *CIGRE PARIS Session 2016*, 21, rue d'Artois, F-75008 PARIS 2016.

4.2. Assessment of Voltage Quality Issues in IEEE-13 Bus Unbalanced Distribution Network with High PV Penetration

The IEEE 13-bus test system [115] has been considered in this work as shown in Figure 4.1. This is quite a distinctive unbalanced radial distribution system that reflects the real distribution system. In this study, the developed comprehensive PV model presented in Chapter 3 [40] has been considered as a PV source in order to reflect the real-time system. To investigate the effect of PV penetration on the voltage quality of an unbalanced distribution network, the study has been carried out for two different case studies. In this investigation, emphasis has been given to voltage rise, voltage unbalance and sag/swell issues.

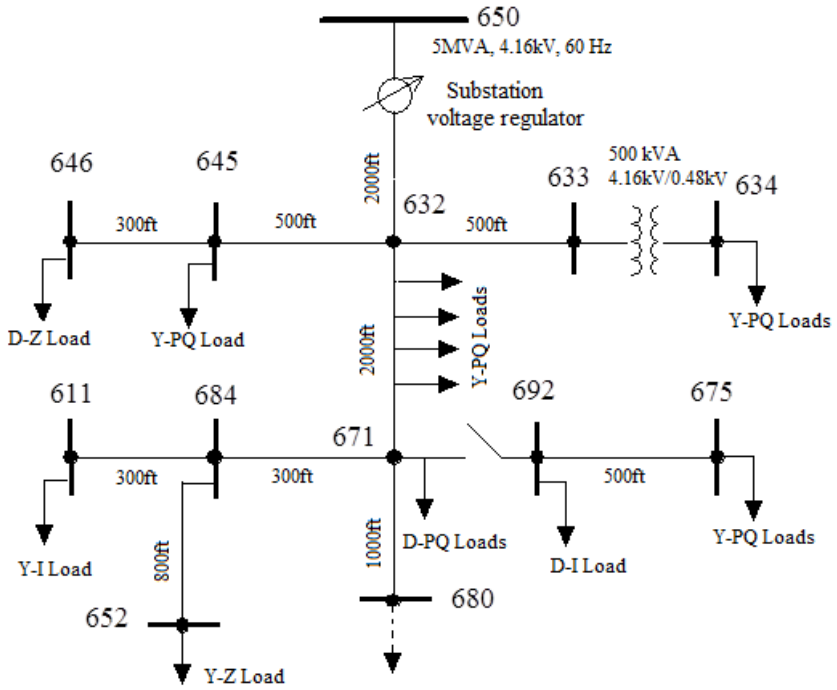

Figure 4.1. IEEE 13 Bus Test System.

4.2.1. Case Study – I: Voltage Rise and Unbalance Assessment

In the first case study, the study has been performed in three different scenarios by considering PV integration at the same bus and multiple buses to investigate their impact on voltage rise and unbalance factor. In the first two scenarios, three-phase PV system integrations are considered at the beginning of the feeder and dispersed PV penetration at the end of the feeder. The total installed capacity of the PV system in these scenarios is 900kWp. Finally, in the last scenario, the penetration capacity has been increased by 250kW with two single-phase PV inverter systems to study the severity of voltage rise and unbalance issues. For this analysis, a typical solar irradiation profile has been applied and the corresponding PV output power is

shown in Figure 4.2. It is shown that PV power generation is reliant on the solar irradiation and has a linear relationship with it.

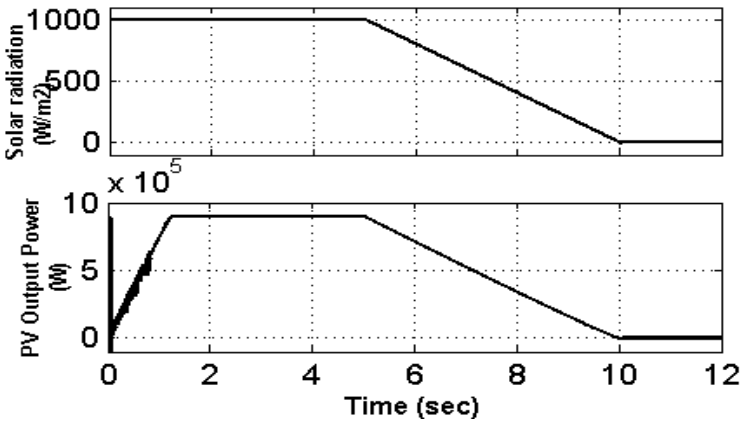

Figure 4.2. Solar Irradiation Pattern and PV Power Output.

In the first scenario, a 900kW PV system has been considered and is only connected to bus 632 in the IEEE 13 bus network. Simulations have been performed and the corresponding RMS voltage magnitudes during day and night times are presented in Table 4.1.

Table 4.1 Scenario-1: RMS Voltage Magnitude Variation due to PV System Integration at Bus 632 during Daytime and Night-time

Node	Phase A RMS Voltage (p.u)			Phase B RMS Voltage (p.u)			Phase C RMS Voltage (p.u)		
	PV at t=4sec	**PV at t=10sec**	**ΔV_A**	**PV at t=4sec**	**PV at t=10sec**	**ΔV_B**	**PV at t=4sec**	**PV at t=10sec**	**ΔV_C**
632	**1.02746**	1.02057	0.00689	1.04296	1.04136	0.00159	1.02148	1.01716	0.00432
633	**1.02433**	1.01717	**0.00716**	**1.04103**	1.03942	0.00161	1.01890	1.01450	0.00440
634	1.00078	0.99347	0.00731	1.02282	1.02102	0.00180	1.00060	0.99563	0.00497
645	-	-	-	1.03388	1.03217	0.00171	1.01958	1.01518	0.00440
646	-	-	-	1.03219	1.03043	0.00177	1.01762	1.01311	0.00451
671	0.99681	0.98943	0.00738	**1.05405**	1.05225	0.00180	0.98260	0.97738	0.00522
675	0.99026	0.98281	0.00746	**1.05645**	1.05460	0.00185	0.98064	0.97538	0.00526
684	0.99486	0.98749	0.00737	-	-	-	0.98057	0.97536	0.00521
611	-	-	-	-	-	-	0.97865	0.97335	0.00530
652	0.98942	0.98191	0.00751	-	-	-	-	-	-

At time t= 4 sec the solar irradiation is 1000 W/m2 (assumed as daytime period or rated PV condition) and at t=10 sec the solar irradiation is 0 W/m2 (assumed as without PV condition or night-time) as indicated in Figure 4.2. It can be seen that the voltage magnitude due to PV power injection in phase A has intensified over phases B and C. The voltage magnitude of

phase A at bus 632 has increased by nearly 0.7% and this increment value is increased towards the end nodes of the feeder. Conversely, the voltage magnitudes of phase B at buses 671, 675 and 634 located at the end of the feeder, have attained higher values, nonetheless the increments in voltages (ΔV_B) are lower. However, it can be observed that the values at buses 675 and 671 have reached 1.05645p.u and 1.05405p.u respectively, which exceeded the ANSI and AS/NZS standard limit of 5%. It can also be seen that PV power injection has provided voltage support in phases A and C of buses located at the end of the feeder.

Table 4.2 Scenario-2: RMS Voltage Magnitude Variation due to PV Systems Integration at Buses 634, 671 and 675 during Daytime and Night-time

Node	Phase A RMS Voltage (p.u)			Phase B RMS Voltage (p.u)			Phase C RMS Voltage (p.u)		
	PV at t=4sec	PV at t=10sec	ΔV_A	PV at t=4sec	PV at t=10sec	ΔV_B	PV at t=4sec	PV at t=10sec	ΔV_C
632	1.02770	1.02057	0.00713	1.04329	1.04136	0.00193	1.02306	1.01716	0.00590
633	1.02567	1.01717	0.00850	1.04263	1.03942	0.00321	1.02170	1.0145	0.00720
634	**1.01032**	0.99347	**0.01685**	**1.03314**	1.02102	**0.01212**	**1.01117**	0.99563	**0.01554**
645	-	-	-	1.03394	1.03217	0.00177	1.02090	1.01518	0.00572
646	-	-	-	1.03219	1.03043	0.00176	1.01886	1.01311	0.00575
671	1.00030	0.98943	**0.01087**	**1.05450**	1.05225	**0.00225**	0.98530	0.97738	0.00791
675	0.99389	0.98281	**0.01108**	**1.05762**	1.05462	**0.00300**	0.98511	0.97538	0.00973
684	0.99726	0.98749	0.00977	-	-	-	0.98401	0.97536	0.00865
611	-	-	-	-	-	-	0.98280	0.97335	0.00945
652	0.99319	0.98191	0.01128	-	-	-	-	-	-

Subsequently, in the second scenario, three-phase PV systems of each 300kWp rated power capacity are considered to connect at buses 634, 671 and 675 in the IEEE 13 bus test system. Simulations have been performed for the duration of 12sec with the solar irradiation profile as indicated in Figure 4.2. The measured voltage magnitudes at various buses of the IEEE network are tabulated in Table 4.2. It is observed that voltage rise due to individual PV systems at the end of the feeders is larger compared to the first scenario. Similar to the first scenario, phase A has been affected more followed by phase C and phase B. Significantly, bus 634 which is a low voltage (480V) bus has experienced higher voltage increments due to PV penetration. Phase B of remote buses 675 and 671 have voltage magnitudes of 1.05450p.u and 1.05762p.u respectively, which are over the limits as per the standards. In comparison with Table 4.1, the voltage variations due to reverse power flow have also increased the magnitudes in the

upstream network. On the other hand, neighbouring buses with higher loads have experienced voltage support from PV power injection.

Table 4.3 Scenario-3: RMS Voltage Magnitude Variation due to the Combination of Three-phase and Single-phase PV Systems Integration at Multiple Locations during Daytime and Night-time

Node	Phase A RMS Voltage (p.u)			Phase B RMS Voltage (p.u)			Phase C RMS Voltage (p.u)		
	PV at t=4sec	PV at t=10sec	ΔV_A	PV at t=4sec	PV at t=10sec	ΔV_B	PV at t=4sec	PV at t=10sec	ΔV_C
632	1.03167	1.02057	0.01110	1.04392	1.04136	0.00256	1.02404	1.01716	0.00688
633	1.02964	1.01717	0.01247	1.04324	1.03942	0.00382	1.02488	1.01450	0.01038
634	1.01330	0.99347	**0.01983**	1.03366	1.02102	0.01264	1.00876	0.99563	0.01313
645	-	-	-	1.03453	1.03217	0.00236	1.02242	1.01518	0.00724
646	-	-	-	1.03281	1.03043	0.00238	1.02033	1.01311	0.00722
671	1.00926	0.98943	**0.01983**	**1.05595**	1.05225	**0.00370**	0.99034	0.97738	0.01296
675	1.00494	0.98281	**0.02213**	**1.06052**	1.05462	**0.00590**	0.98849	0.97538	0.01311
684	1.01019	0.98749	**0.02270**	-	-	-	0.98708	0.97536	0.01172
611	-	-	-	-	-	-	0.98550	0.97335	0.01215
652	1.00476	0.98191	**0.02285**	-	-	-		-	

Finally, in the third scenario, the penetration has been increased by 250kW in addition to the individual PV connections at buses 634, 671 and 675. For this, two single-phase PV systems of rated capacity 150kW and 100kW are connected to phase A of bus 684 and phase B of bus 675 respectively. Simulations have been performed similar to previous scenarios, and the load flow results are presented in Table 4.3. It can be seen that the voltage difference ΔV_A in phase A is almost doubled compared to the second scenario. Even a small increment in PV penetration has a significant effect on the voltage magnitudes. Similarly, the voltage magnitude at bus 675 is increased to above 1.06p.u, which is even higher than the limits specified by standards. Also, the voltage variations with increased PV penetration are reflected on the adjacent buses.

Therefore, it is confirmed that dispersed PV penetration at the end of the feeders can cause significant overvoltage's than if provided at the beginning of the feeder. In addition, the voltage amplitude is more exacerbated with single-phase PV inverter systems.

Furthermore, it is observed that the voltage variation (ΔV) by PV systems in each phase is different due to unbalanced loading on the network. The high density of PV system integration into a distribution grid increases the VU at the PCC and has high values at the end of the feeder.

Therefore, the analysis is performed to verify the impact of PV penetration on network voltage unbalance. Regarding this, the voltage unbalance factor is calculated based on the equation specified by AS/NZS 61000.4.30 standard (see Chapter 2, equation (2.2)), which utilizes phase to phase voltages. The percentage of voltage unbalance at various nodes of the IEEE network for the above mentioned scenarios are plotted in Figure 4.3.

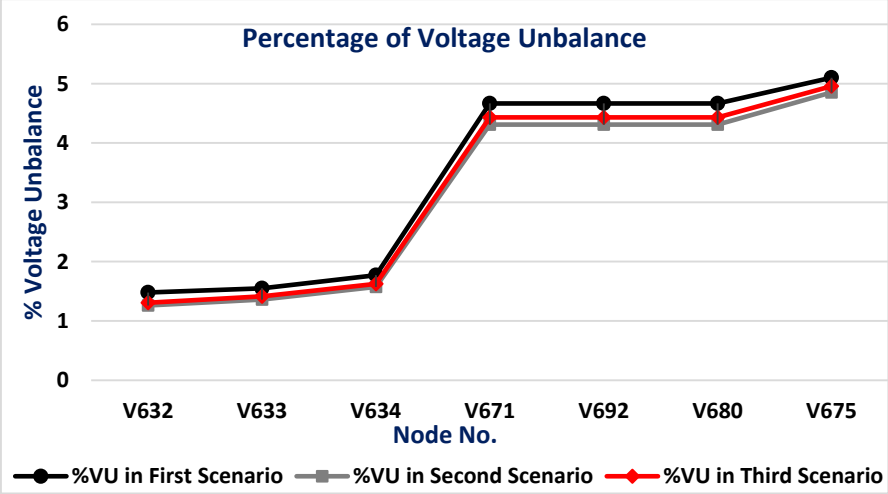

Figure 4.3. %Voltage Unbalance Analysis at Various Buses.

It can be seen that in all scenarios, the active power contribution from PV systems into the grid differed the voltage magnitude and are much higher at buses located at the end of the feeder. The values follow similar trends in all the scenarios. It is observed that the voltage unbalance curve in the first scenario, in which the PV system is integrated at a single location (at bus 632), has higher values compared to the dispersed PV integrations in the second and third scenarios. It was found that the percentage of VU is above 5.1 in the first scenario, which is over the limits according to AS/NZS 61000.4.30. Interestingly, the voltage unbalance is increased in the third scenario compared to the second scenario. The voltage unbalance at bus 675 in the third scenario has reached 4.96%, which is close to the allowable limit of 5%. Further increase in PV penetration can aggravate the voltage unbalance levels in the network. It is estimated that distributed random installation of single phase PV systems can adversely affect the network voltage unbalance level.

4.2.2. Case study-II: Voltage Sag/Swell Assessment by Fault Conditions

The voltage sag/swell issues are common in distribution networks, which are caused by symmetric and unsymmetrical faults on the network. Moreover, PV systems as per the current standards are not allowed to stay connected during fault conditions. However, sudden connections/disconnections of PV systems in response to the faults can also impact the network

voltage levels. Therefore, in this analysis a 900kWp PV system is considered to be connected at bus 632 of the IEEE 13 bus network similar to the first scenario of the above case study.

In this case study, simulations have been carried out for with and without PV inverter penetration in an unbalanced distribution system for each of the three types of faults. In each case the fault is initiated at t = 4.5 sec and the duration of the fault is 100ms. In figures below V_a, V_b, V_c represent the three phase RMS voltages at each bus at before fault condition and V_{af}, V_{bf}, V_{cf} denote the fault magnitudes during a fault. Also, LB and UB indicate the lower and upper band of steady state voltage limits respectively. According to IEEE 1159-2009 [97] and AS/NZS 61000.4.30 [98] standards, the typical voltage sag threshold is 90% of the nominal and the swell threshold is equal to or greater than 110% of nominal.

4.2.2.1. Single Line to Ground Fault (SLG)

SLG fault is considered to occur on phase-A of bus 633. In reality, a fault on the grid causes the PV system to be completely isolated from the grid as considered in the first scenario. At the fault the affected phase voltage drops to zero. Also, due to an unsymmetrical fault unbalanced voltage sag/swells would be created on the other adjacent bus lines and increase system losses. The bar chart in Figure 4.4 shows the RMS voltage magnitude at various buses before and during the fault. It is observed that the voltages of phase A and phase C are dropped by around 15% and 11% of the rated voltages respectively, creating a voltage sag condition. Conversely, a voltage swell of about 10% is observed in phase B.

In the second scenario, a conventional PV inverter (unity P.F) is considered to remain connected during the fault. The PV system injects only active power into the grid that will affect the operation of unidirectional voltage regulators and produce overvoltage on lightly loaded phases. During the unbalanced fault, the PV inverter injects balanced currents into the system due to the balanced controller operation. Figure 4.5 summarizes the simulated results of the RMS voltages at remote buses before and during the fault. By comparing with the first scenario, there is a little improvement in the voltages due to real power injection. As can be observed, phase A voltage was dropped by 12% and there was a swell on phase B of about 11%, which is a lightly loaded phase in the test system. During the fault, it is noticed that the voltage swell is further increased by PV power injection at the PCC, which is violating the limits.

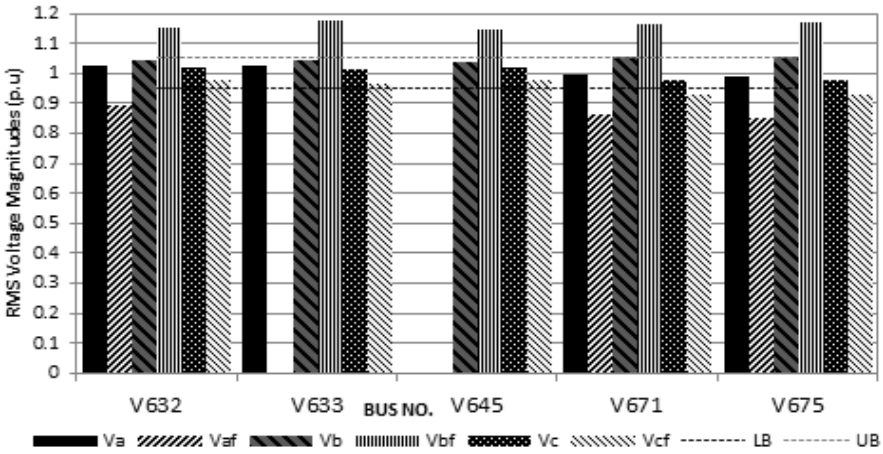

Figure 4.4. RMS Voltages at Prefault and during SLG Fault without PV Inverter.

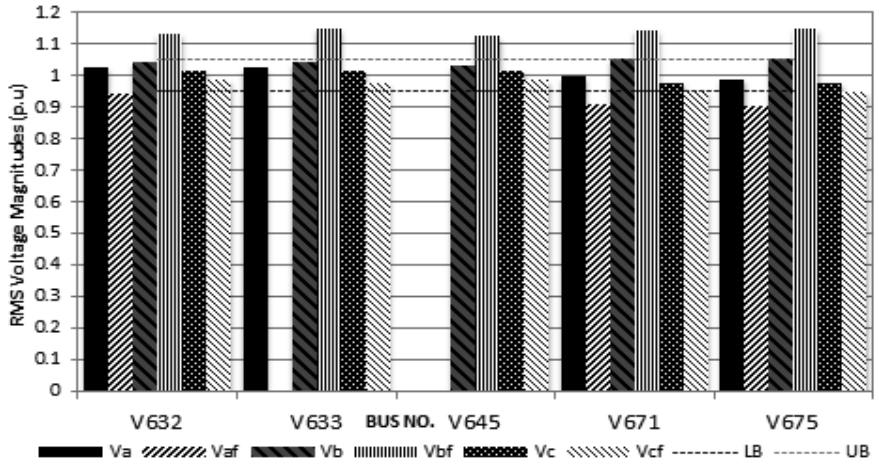

Figure 4.5. RMS Voltages at Prefault and during SLG Fault with PV Inverter.

4.2.2.2. Double Line to Ground Fault (DLG)

In the same way, an unsymmetrical DLG fault is applied on phases A and B of bus 633. The bar charts shown in Figures 4.6 and 4.7 depict the RMS voltages at remote buses for the first and second scenarios as explained above. During the fault, the PV inverter system supplying balanced currents into the grid caused voltage fluctuations at PCC as a result the other buses are also affected. Results show that phase A voltage has experienced a notable sag of around 25% and a swell on phase C of about 10% of the rated voltage almost in both scenarios. It is noticed that due to an unsymmetrical fault, phase C has been much more affected and phase B was only slightly influenced by PV power injection, which is opposite to the case of SLG fault.

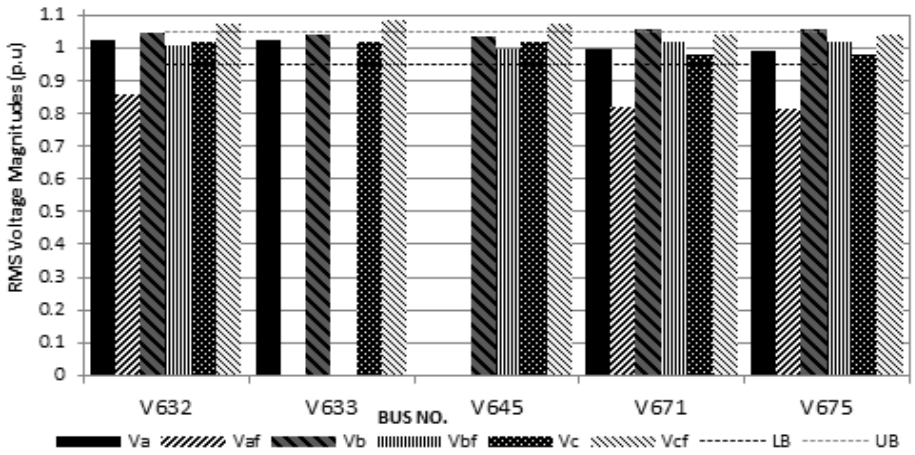

Figure 4.6. RMS Voltages at Prefault and during DLG Fault without PV Inverter.

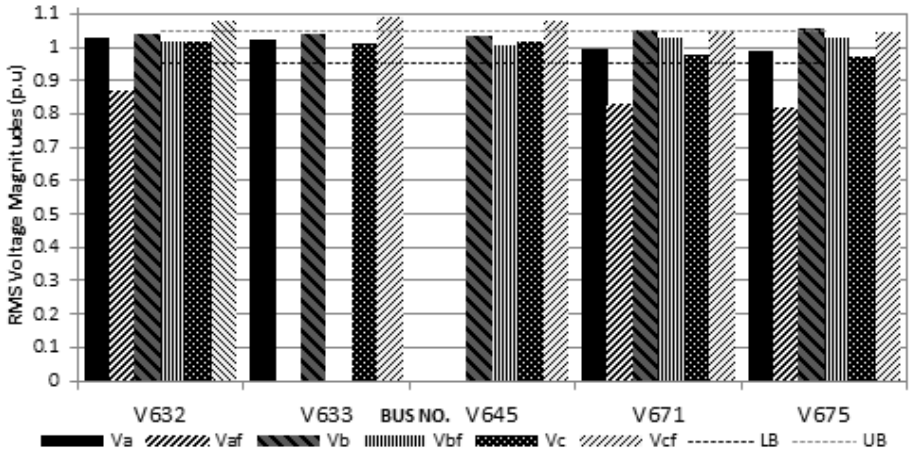

Figure 4.7. RMS Voltages at Prefault and during DLG Fault with PV inverter.

4.2.2.3. Three-phase Symmetrical Fault (TPG)

Finally, the simulations have been carried out for the TPG fault to strike at bus 633, which is often seen as the worst case. Due to the fault, all the bus voltages were affected and resulted in sag on all the phases as presented in Figure 4.8 for the first scenario as mentioned earlier. It is observed that the voltage of phase A plunged to 10% and phase C voltage collapsed to 12% of nominal voltages.

Similarly, in the second scenario when the PV inverter remains connected during the fault, it is noticed from Figure 4.9 that all the phases have experienced a sag in voltage. The phase A and phase C voltages have dropped by around 8% and 7% respectively, but still this drop is characterised as sag and the magnitudes are above the acceptable limits. It is shown that the effect of PV power injection during the fault has slightly improved the voltage levels in adjacent buses. Nevertheless, the voltage swells are negatively affected. Further investigation

will be performed on the real-time grid PV systems through field measurements in order to evaluate the severity of various voltage quality issues.

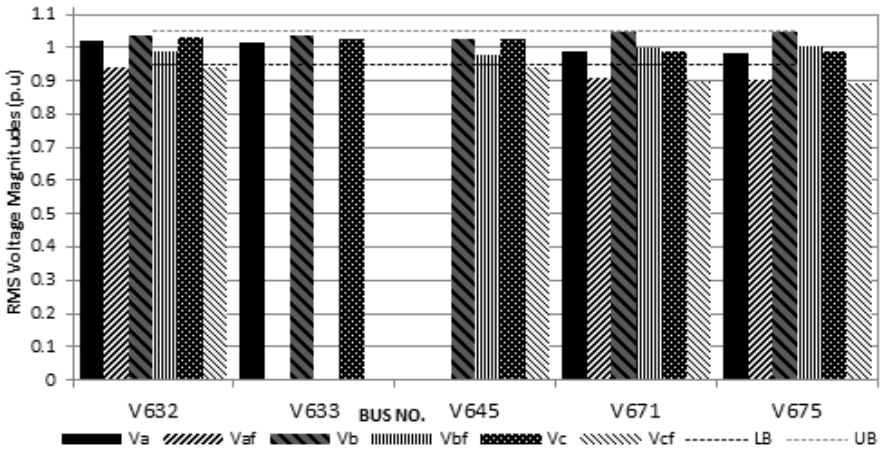

Figure 4.8. RMS Voltages at Prefault and during TPG Fault without PV Inverter.

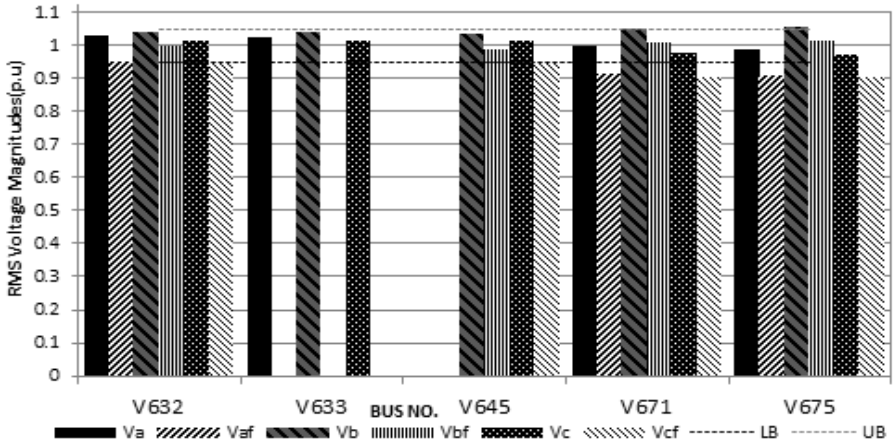

Figure 4.9. RMS Voltages at Prefault and during TPG Fault with PV inverter.

4.3. Field Investigation of Voltage Quality Issues in Distribution Network with PV Penetration

The aim of this research was to investigate the voltage quality issues in a distribution network with high PV system penetration. In this investigation, the power quality field measurements for various PV operating conditions are obtained and analysed for voltage quality issues. The study has focussed on two different scales of PV sites located at the University of Queensland (UQ) St. Lucia Campus and Gatton campuses, which have an installed capacity of 1.5MW and 3.25MW respectively. The description of UQ St. Lucia network and an approach of the measurements are presented in Section 4.3.1. The results and analysis of various voltage issues are discussed in Section 4.3.1.1. Next, the layout of the UQ

Gatton campus PV system is presented in Section 4.3.2. The corresponding results and analysis are explained in subsection 4.3.2.1.

4.3.1. Description of University of Queensland, St. Lucia Campus Network and Measurement Setup

(a) Aerial View of PV Site

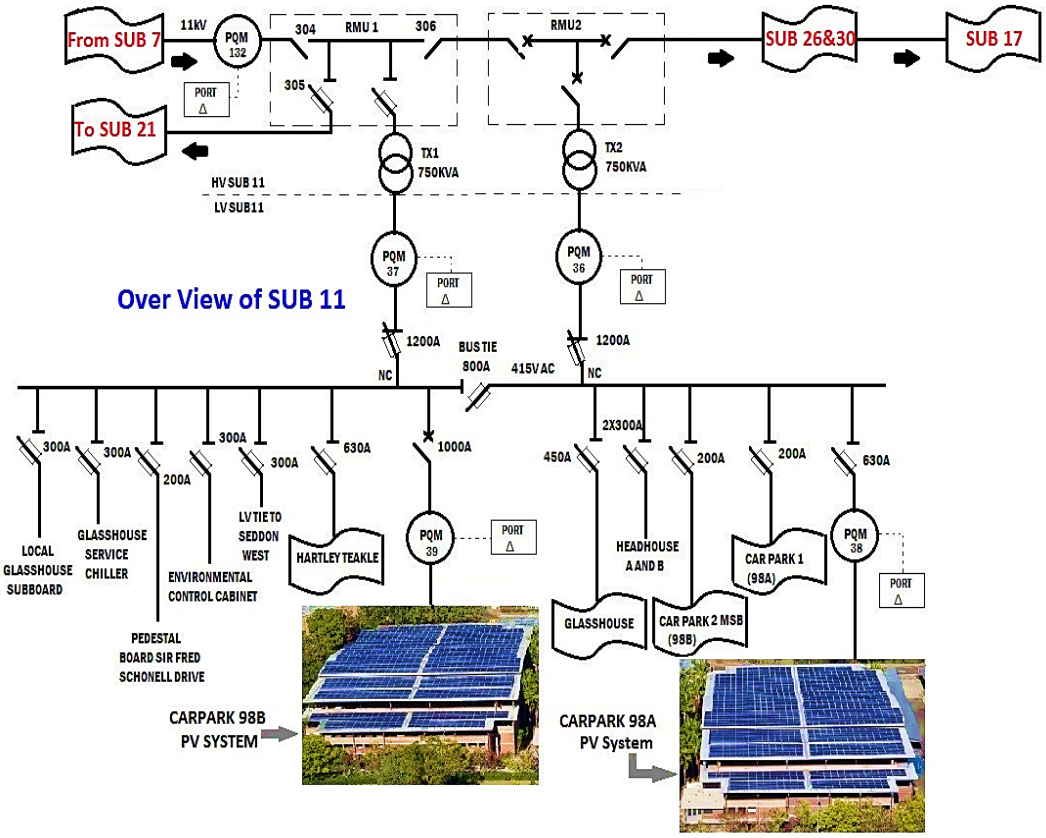

(b) Distribution Feeder of the University Network

Figure 4.10. Overview of the University of Queensland PV Network, St. Lucia Campus.

The University of Queensland (UQ), St. Lucia campus has a large distribution network encircled in a 2km radius. The network receives an 11kV line from the Energex network connected to substation 7. From this substation, there are 8 parallel radial feeders used to feed electricity to the individual buildings, which consist of nearly 40 substations. The university had installed a 1.22MWp PV system in 2011, which is one of the largest rooftop integrated systems in Australia. In 2013, the UQ St. Lucia campus expanded its PV system capacity to 1.5MWp with around 6305 PV panels, which is deployed across eight buildings of the network shown in Figure 4.10(a).

Figure 4.10 (b) shows one of the feeders, where two car park buildings have PV systems, which has been considered for the study. Each car park building has an installed PV system capacity of 339kWp connected to the low voltage side of substation 11. This substation includes two distribution transformers of 750kVA 11kV/415V delta-wye connected as shown in Figure 4.10 (b). From substation 11 the rest of the 11kV line continues to substations 26, 30 and 17. The UQ network is equipped with several online digital power meters and power quality analysers interfaced to the internet for monitoring.

In this research, field measurements were conducted at car park 98A. This building has nearly 26 three-phase PV inverters of 12.5kW capacity each, which are connected directly to the grid. Each inverter has two maximum power point tracking (MPPT) controllers and each MPPT is organized with two arrays of around 30 PV panels of 250W rating. A Fluke power quality (PQ) analyser of 430 series-II type was used for the measurement. This PQ instrument meets the requirements of the standard AS/NZS 61000-4-15:2012 [121] and also certified by the IEC 61000-4-30 Class A standard for flicker and power quality. Figure 4.11 shows the test setup and power board, where the PQ meter is connected at the output of one of those PV inverters.

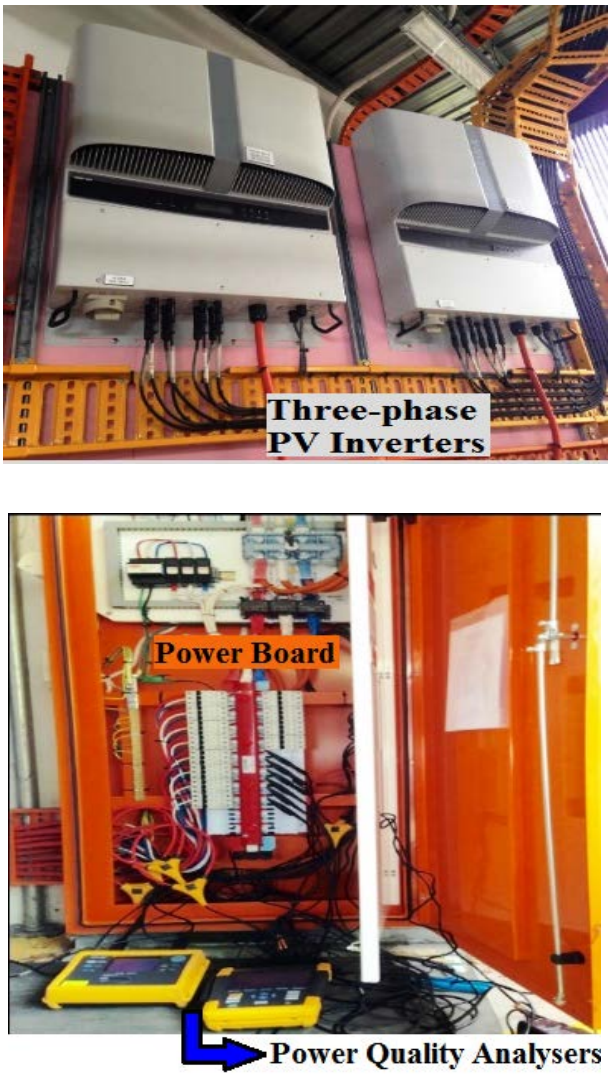

Figure 4.11. Measurement Test Setup.

The PQ analyser recorded a number of parameters, which included power, voltage, current, frequency and flicker data with 5sec resolution. To characterise the voltage variations for various operating days, the measurements were continued for 15 days. The logged data was extracted using Power log software. The PV output power and solar irradiation data were also

captured using weather sensors. In addition, the flicker data of one year at the PV array and the 11kV side was measured for further analysis.

4.3.1.1 Results and Analysis

4.3.1.1.1. Characteristics of Voltage Rise and Fluctuations at 1.5MW PV System

In distribution networks, voltage rise is the most prevalent limiting issue due to reverse power flow with PV power injection. The PV power output strongly depends on the solar irradiation and temperature which can impact the grid voltages. Figure 4.12 shows the time versus PV output power and solar irradiation for the selected different PV operating days.

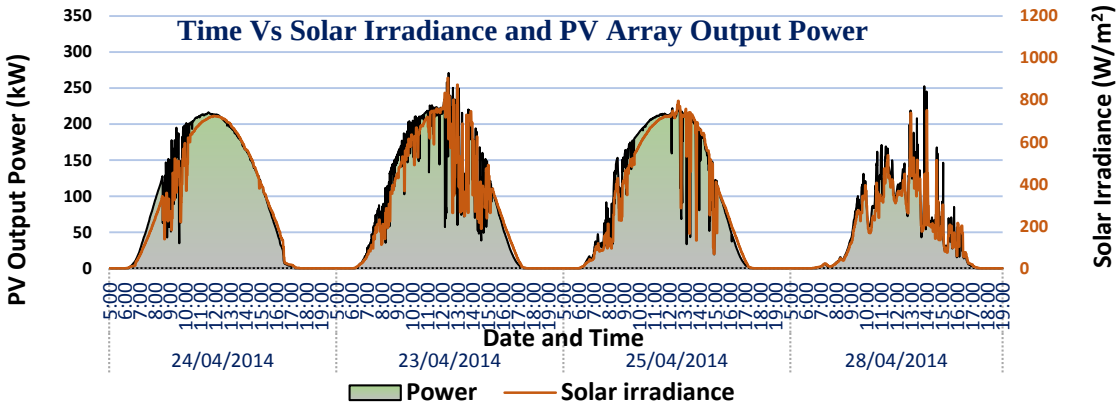

Figure 4.12. Time versus Solar Irradiation and PV Output Power.

The measured per unit three-phase voltage magnitudes at the PV inverter output for the corresponding days are plotted in Figure 4.13. The voltage magnitude at early morning and night times is close to 0.99p.u. It can be seen that the voltage levels have increased with respect to the PV power injection. During the rated PV output, the voltage level reached about 1.02p.u., which is within the limits as per AS/NZS 61000.3.100 [96] standard. The increment in the voltage is appeared to be lower due to the load operation. Since the university peak load demand is from 6 am to 6 pm which is similar to a commercial load pattern, which matches with the PV operational output.

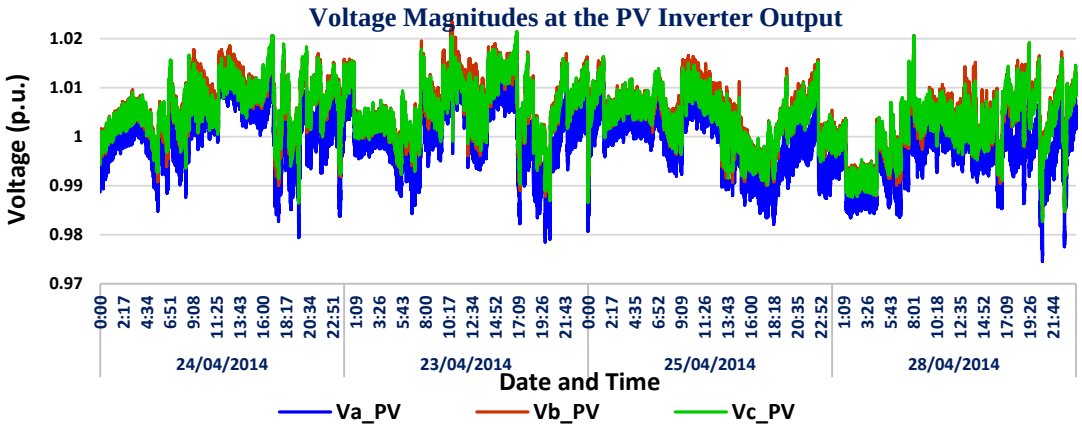

Figure 4.13. Voltage Magnitudes at the PV Inverter Output.

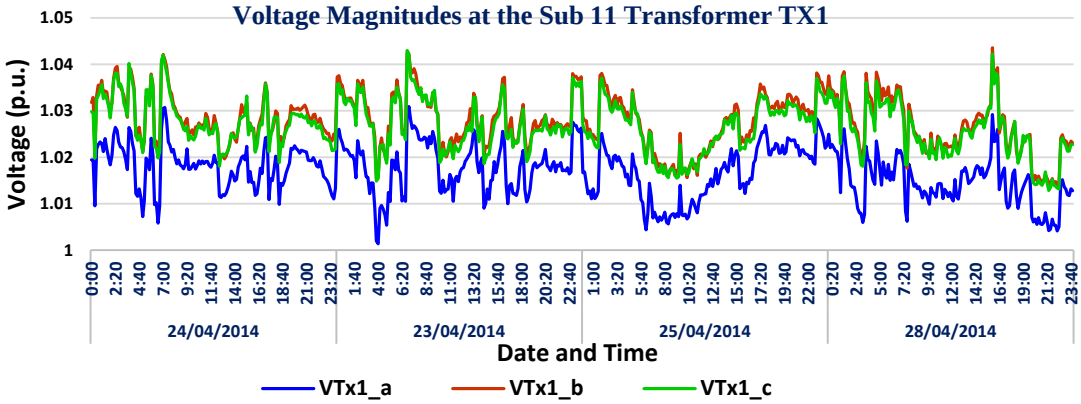

Figure 4.14. Voltage Magnitudes at Substation 11 Transformer TX1.

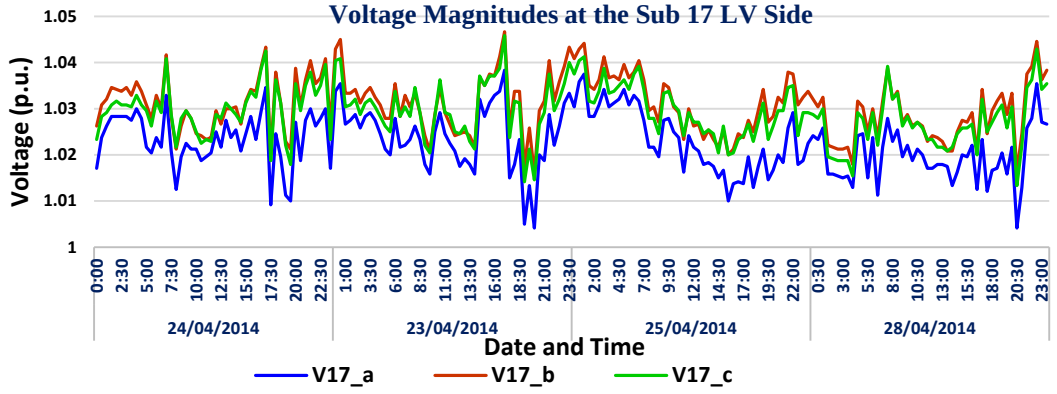

Figure 4.15. Voltage Magnitudes at Substation 17.

In addition, to assess the PV impact on adjacent nodes of the network, the voltage measurements were obtained at the upstream (Sub 11 at TX1) and downstream (Sub 17) nodes as shown in Figures 4.14 and 4.15 respectively. From Figure 4.15, it is observed that the voltage levels on the network have lower values during the day time due to the voltage drop across

loads. The active power injection from PV has actually improved the voltage level. The values are within a range between 1.02-1.035p.u., which are below the upper limits.

From Figure 4.15, it can be seen that the voltages at the downstream nodes during low load period (night-time) have values in the range of 1.03-1.035p.u. It is important to mention that substation 17 comprises of a tap changing transformer, which was set to increase the voltage magnitudes by 5%. As a result, substation 17 has higher voltage levels compared to the voltages at the PV inverter output. During the PV operation period, the voltage levels are in the range of 1.02- 1.03p.u., which are within the limits. However, the load demand pattern in residential networks could be inverse compared to the PV operational profile. In this scenario, the network voltage will rise with high PV penetration.

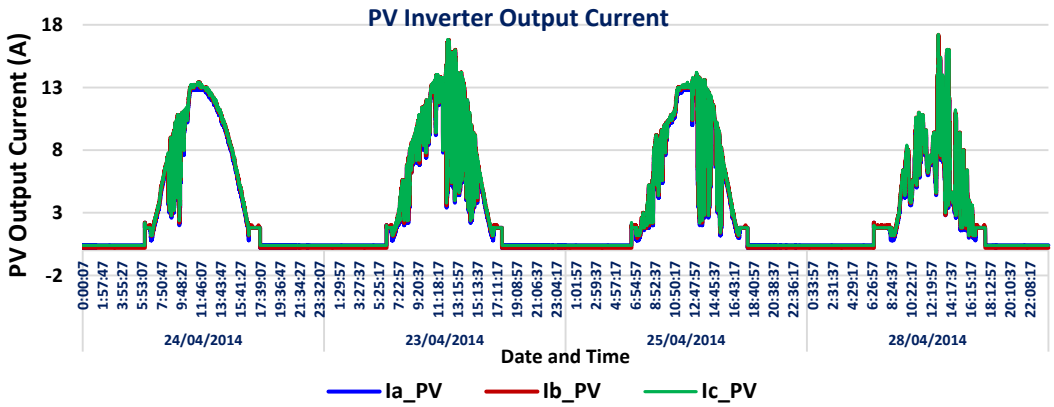

Figure 4.16. Measured PV Inverter Output Currents.

Furthermore, it is noticed that the voltage levels are fluctuating with respect to solar irradiation. Also, the PV inverter output currents have a strong correlation with the solar irradiation transients and are influenced by the voltage magnitudes. Figure 4.16 shows the measured PV inverter output currents for the corresponding days. These rapid and frequent voltage variations due to cloud transients can exceed the standard steady state limits and can cause voltage flicker.

4.3.1.1.2. Voltage Flicker Analysis at 1.5MW PV System

The flicker measurements at the output of the PV inverter for corresponding days have been collected with a Fluke PQ meter and are plotted as shown in Figure 4.17. The severity of voltage flicker is illustrated by the instantaneous flicker index P_{inst}, short-term index P_{st} (over a 10 min period) and the long term index P_{lt} (over a 2 hour period).

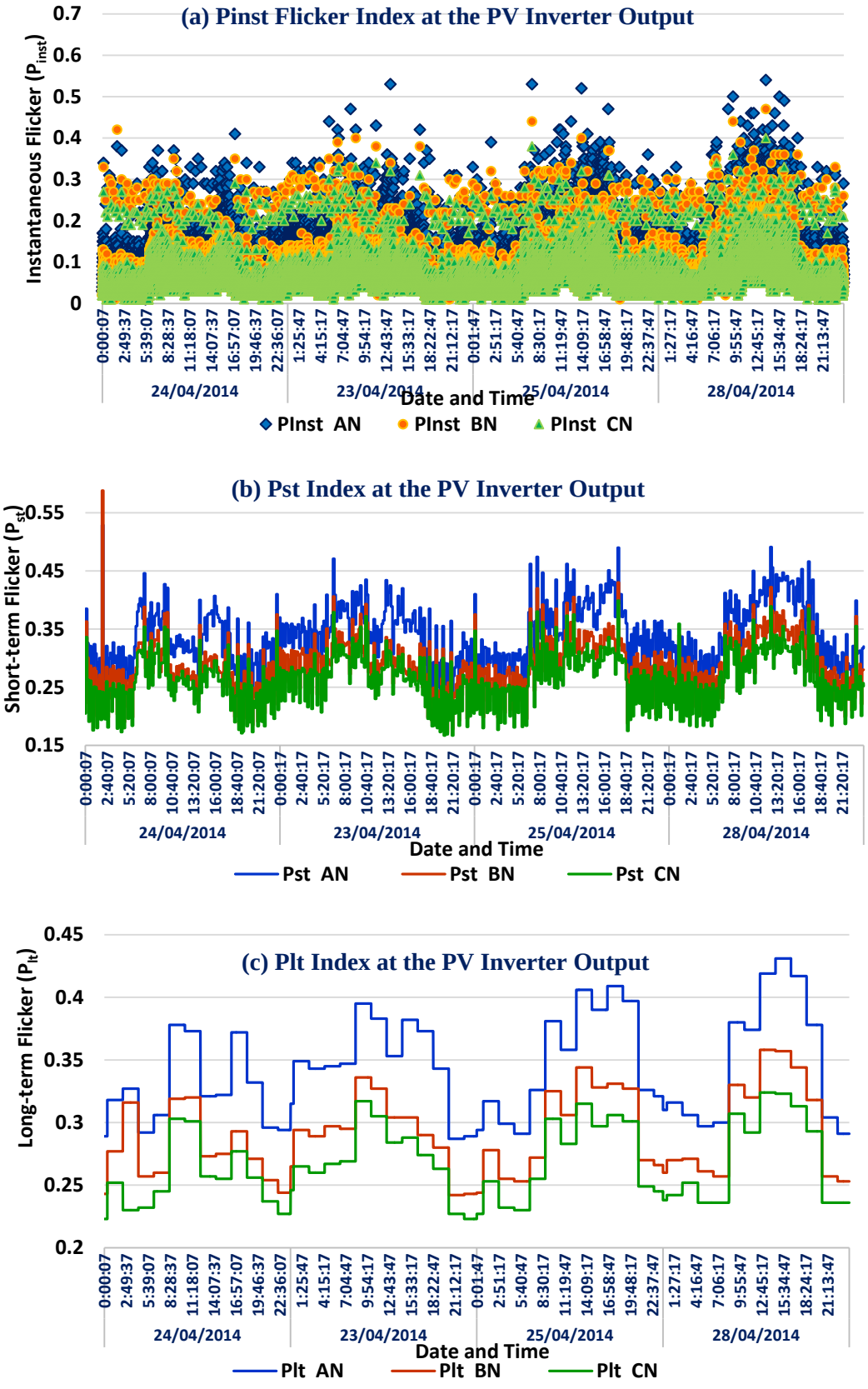

Figure 4.17. Measured Voltage Flicker Indices at the PV Inverter Output.

Results show that the voltage flicker levels during PV operating times are increased and attained higher values during a cloudy day. From Figure 4.17 (a), it is noticed that the

instantaneous flicker index has reached 0.55 due to rapid voltage fluctuations. Nonetheless, the short-term flicker index is within the 0.3 to 0.45 range while the P_{lt} is below 0.43, which are within the limits specified by standard AS/NZS 61000.3.3 [103]. It is also noticed that when there is no PV power, the measured P_{st} and P_{lt} have values lower than 0.3, which can be represented as background flicker. Conversely, the measured flicker levels are violating the utility prescribed flicker emission limits as per AS/NZS 61000.3.7 [104].

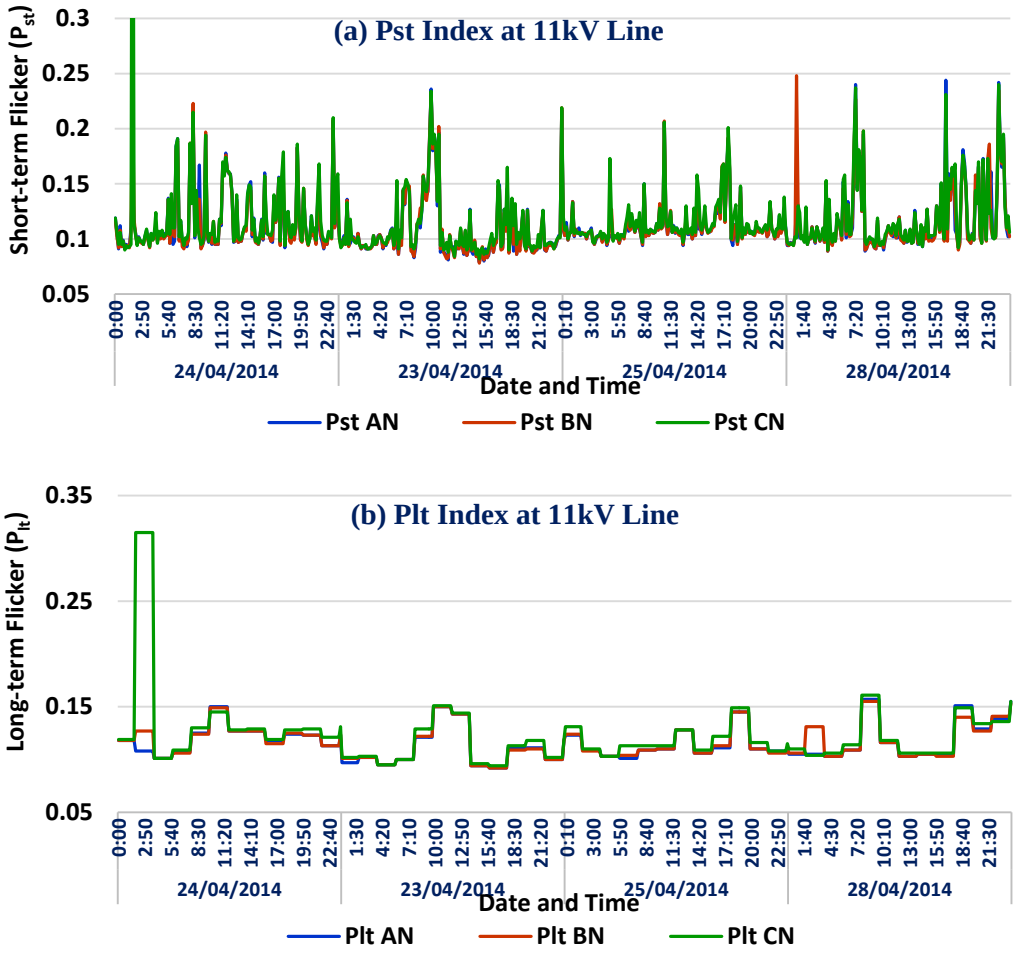

Figure 4.18. Measured Flicker Indices at 11kV Line.

Also, these voltage variations might be propagated towards the upstream network. Therefore, to investigate the flicker level at the HV side of substation 11, the recorded short term and long term flicker data have been extracted from the digital PQ meters. Figure 4.18 shows the measured P_{st} and P_{lt} at the 11kV line for the above mentioned days. It can be seen that both the P_{st} and P_{lt} during the period from 6pm to 7am have values about 0.1. Similarly, these indices are increasing with respect to the PV power variations and are satisfying the limits. Also, the voltage variations in the network are observed to be significant and the P_{st} values are fluctuating between 0.1 to and 0.25.

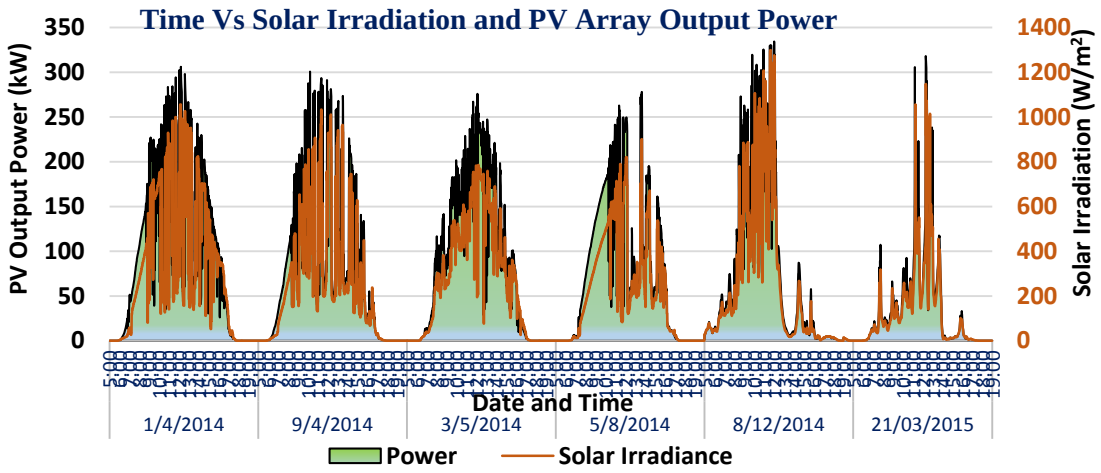

Figure 4.19. Time versus Solar Irradiation and PV Output Power for Typical Days.

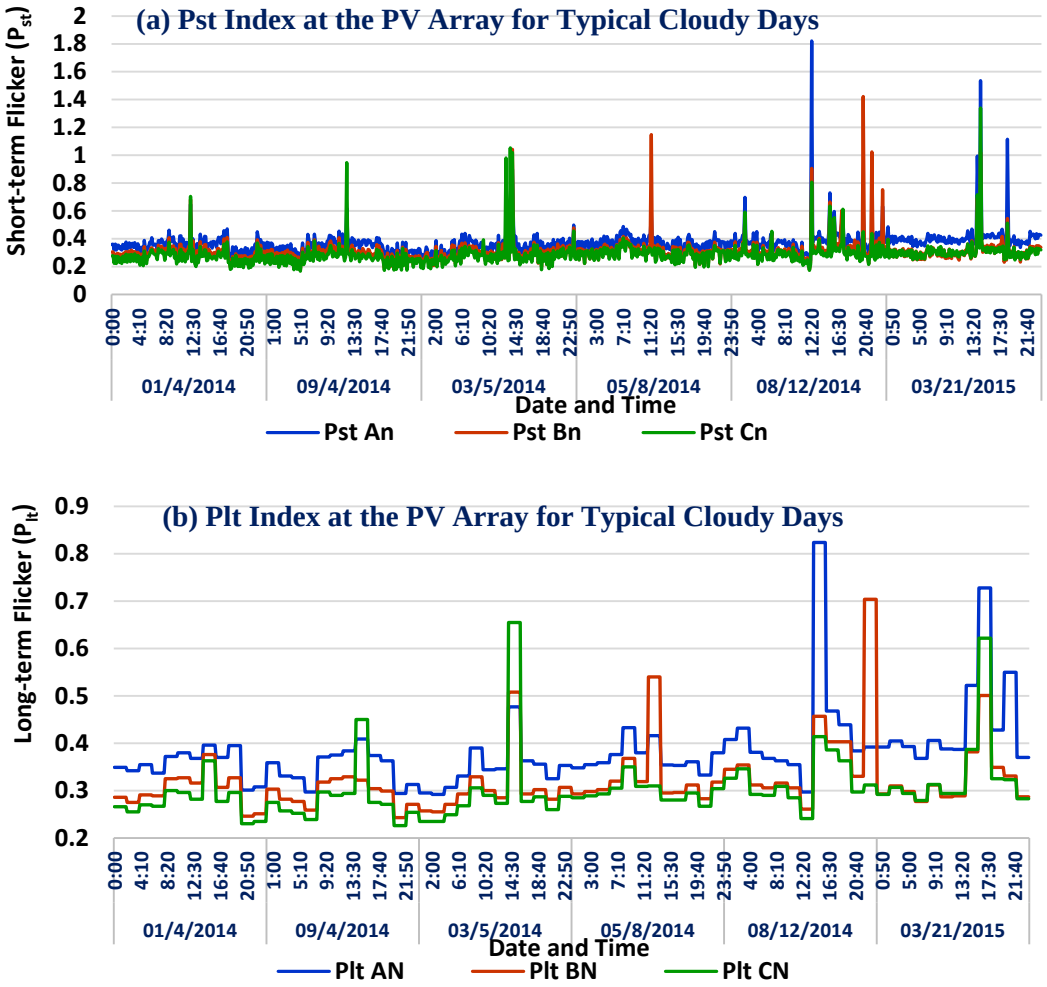

Figure 4.20. Measured Voltage Flicker Indices at the PV Array.

Although flicker levels during the measurement period are appeared to be lower, these values might exceed the standard limits for critical operating conditions. The level of voltage variation depends on the PV system capacity and rate of change in solar irradiation. For this

reason, the voltage flicker data of 1 year measured at the PV array has been analysed. Figure 4.19 shows the critical solar irradiation and PV output power patterns of cloudy days. The P_{st} and P_{lt} indices are plotted in Figure 4.20 for the respective days. Results show that the values of P_{st} were exceeded the standard limit of 1 for several events. Respectively, the P_{lt} was also overlapped the limit of 0.65. Frequent incidence of voltage flicker on the network may lead to hunting of tap changers and degradation of the PQ. Therefore, it is increasingly important to quantify the probability of voltage flicker in the distribution network.

In this regard, a clustering algorithm has been adopted to verify the severity of voltage flicker levels with the time of day. In this analysis, the measured daily flicker data of one year has been utilized and is superimposed on a 24 hour time frame. The stacked data contains every 10 min and 2 hour time interval based groups. Then by using the clustering technique, the short term values at that specific time have been divided into four clusters as follows

Cluster 1 – $0.05<P_{st}\leq0.25$; Cluster 2 – $0.25<P_{st}\leq0.5$;

Cluster 3 – $0.5<P_{st}\leq1$; and Cluster 4 – $P_{st}>1$.

Similarly, the long-term flicker data has been segregated into five clusters as follows

Cluster 1 – $0.05<P_{lt}\leq0.15$; Cluster 2 – $0.15<P_{lt}\leq0.3$;

Cluster 3 – $0.3<P_{lt}\leq0.45$; Cluster 4 – $0.45<P_{lt}\leq0.65$ and Cluster 5 – $P_{lt}>0.65$.

Next, the probability counts for each cluster at that moment are calculated and this process repeated for all time instants. The probability counts of P_{st} and P_{lt} measured at the PV array are plotted in Figures 4.21 (a) and (b) respectively.

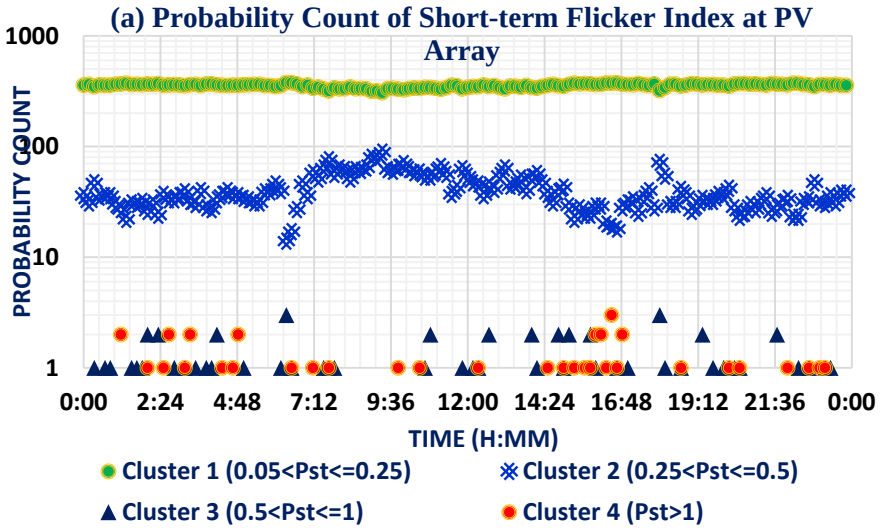

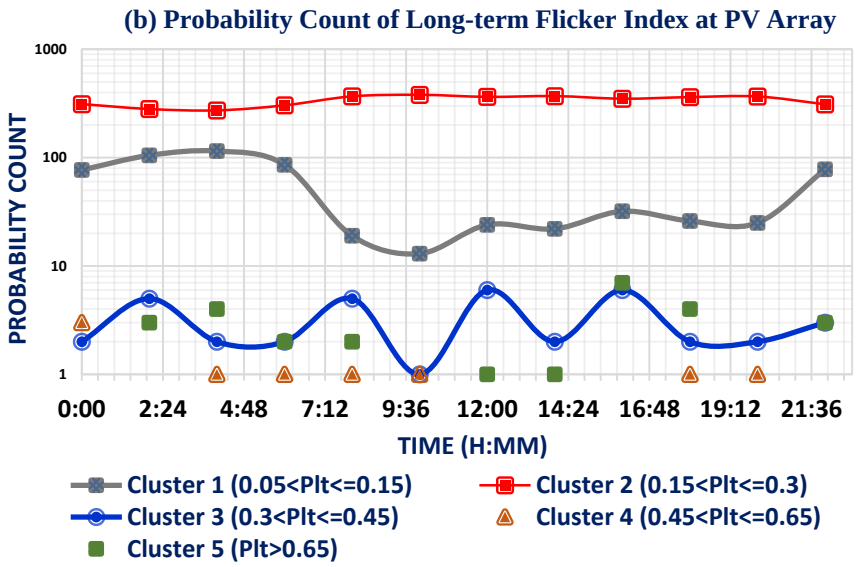

Figure 4.21. Clustered based Probability Count of Flicker Indices at PV Array.

The x-axis is the time period and the y-axis is the probability count shown in logarithmic scale. From Figure 4.21 (a), it can be seen that during PV operation, the probability counts of cluster 2 have increased while those of cluster 1 have decreased. A few number of times the flicker level was within cluster 3. Nonetheless, there were a number of incidents where the flicker level exceeded the limit of 1, which are a total of around 22 times in a year only during 6am to 6pm. In comparison with the flicker emission limits from AS/NZS 61000.3.7 standard, the flicker levels in cluster 2 are violating the limits for nearly 70 to 95 times at every time instant in a year. Similarly, results from Figure 4.21 (b) show that cluster 2 is the probable level of flicker and has a maximum number of counts during PV operation time. In the worst conditions, cluster 5 has accounted for a total of 17 events, which are negligible.

In addition, the inherent flicker levels at the high voltage side are analysed. The clustering process has been repeated and the probability count of P_{st} and P_{lt} are plotted as shown in Figure 4.22 (a) and (b) respectively. It can be observed that the short-term flicker index lies under 0.25 (i.e., cluster 1) for several events, which is within the limits specified by AS/NZS 61000.3.7 standard. Cluster 2 is the next intensified flicker level with less than 10 events per time period. However, these statistics are minor compared with Figure 4.21 (a).

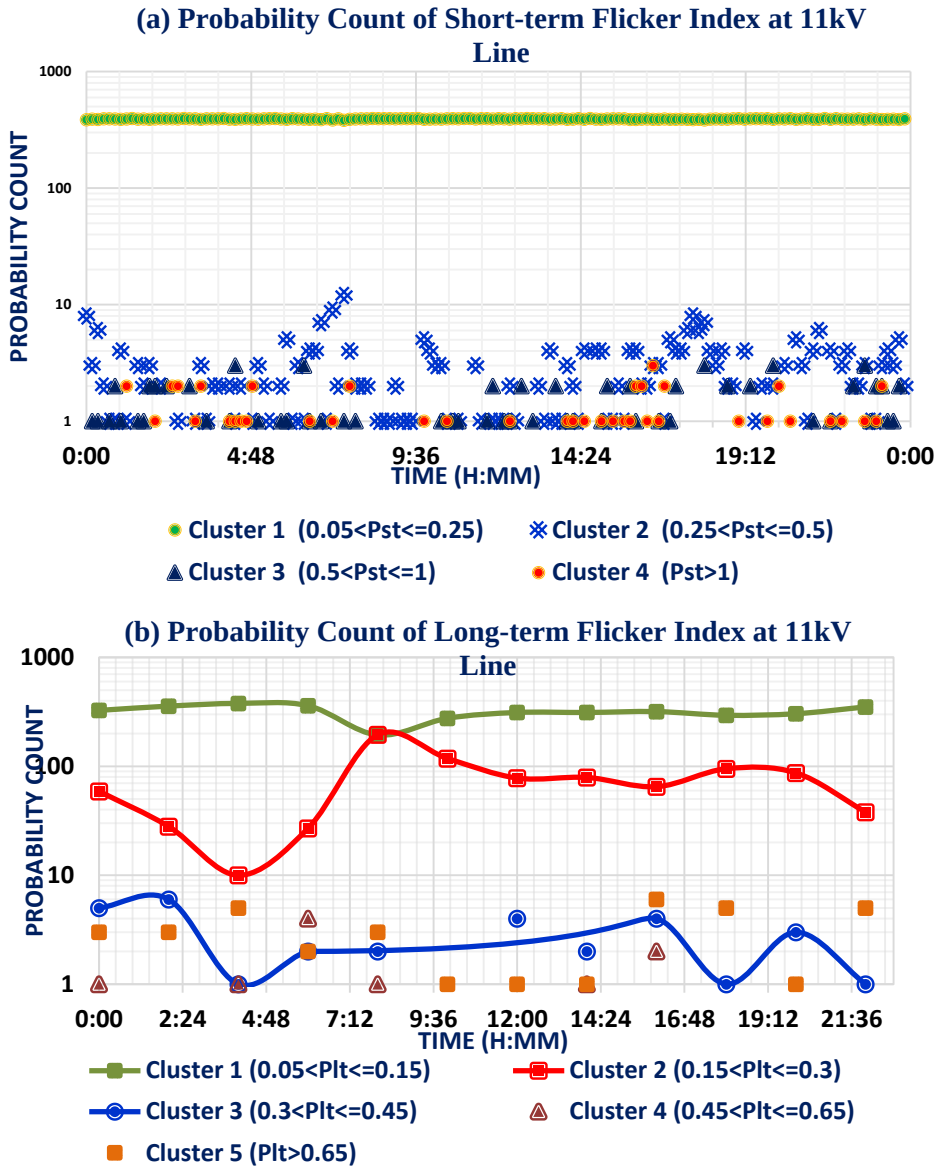

Figure 4.22. Clustered based Probability Count of Flicker Indices at 11kV Line.

From Figure 4.22 (b), it can be noticed that the flicker levels in cluster 2 are increasing with respect to the PV operation time, which are below the limits as per the standards. In contrast to Figure 4.21 (b), cluster 1 has the highest count recorded. So, the impact of PV fluctuations have less influence on the upstream network flicker level. During no PV times, the flicker levels cross over the 0.65 limit (cluster 5) and are calculated to be less than 8 events per time period. This may be due to the voltage drop with load operation.

4.3.2. Field Measurements at the University of Queensland 3.3 MW PV Plant, Gatton Campus

In 2015, the University of Queensland installed a 3.3MW PV system at the Gatton campus, which is one of the largest university PV plants in the world. This PV plant is located in South East Queensland and nearly 82km away from the St. Lucia campus (Brisbane) of UQ. The PV system has advanced PV panel technologies, which include Fixed-Tilt type, Single-Axis, and Dual-Axis tracking types as illustrated in Figure 4.23.

(a) Aerial View of Site

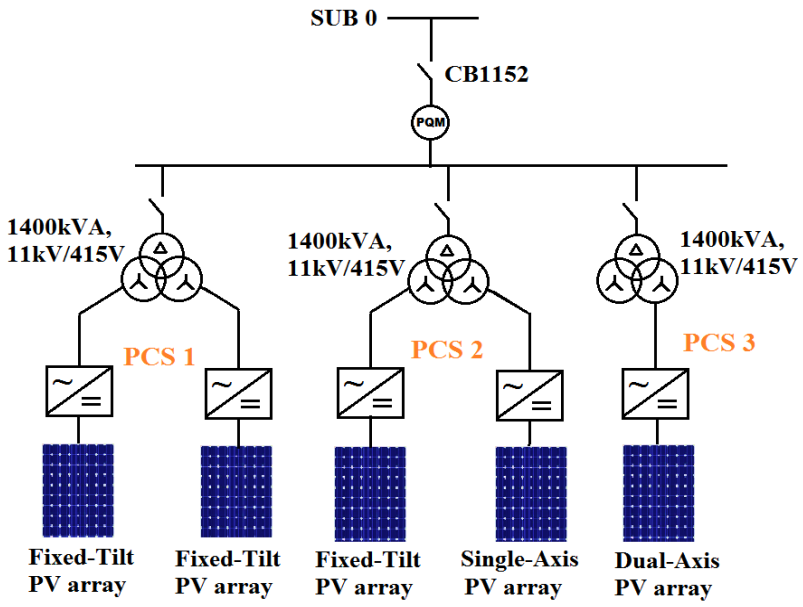

(b) Single-line Electrical Diagram

Figure 4.23. Overview of UQ Gatton PV Plant.

Each PV inverter is connected with 480 strings which contain a total of 7200 panels and provides 684kW of DC power. Each inverter is rated at 725kVA and is allowed to provide reactive power support at full load operation. Currently, the PV inverters are operated to produce only 630kW active power and provide a lagging power factor. The plant contains three distribution transformers of 1400kVA, 11kV/415V delta-wye connected. Each power conversion system (PCS) is fed by two PV inverter systems except the inverter that contains the Dual-Axis tracking system as shown in Figure 4.23 (b). These inverters are connected to the low voltage side of the transformer. This Gatton PV plant is equipped with power quality meters (PQM) at the distribution transformers. Various power quality parameters such as power, RMS voltage, current and flicker data are recorded with second's resolution. For this analysis, the measurements are obtained at one of the PV inverter outputs and the 11kV side of the grid integration point (i.e., at CB1152).

4.3.2.1. Results and Analysis

4.3.2.1.1. Voltage Rise and Fluctuations Assessment at 3.3MW PV System

Characteristically, the amount of voltage rise depends on the PV capacity, connection density and the location. The UQ Gatton campus has lower load demand during the daytime compared to the UQ St. Lucia campus load requirement, and the capacity of PV installation is also higher. Hence, it is expected that there is a possibility of high reverse power flow into the Energex distribution network. Consequently, the utility controls the voltage at the upstream 11kV network by using a step voltage regulator (SVR), which typically regulates the voltages to be in a range of 0.9875p.u +/- 0.0125p.u. Further, according to the connection agreement by the utility, the voltage should not exceed a maximum of 1.01p.u, so that around 3.5% of voltage variation is allowed.

Therefore, to analyse the influence of PV penetration on the LV side of the network, measurements were collected for different operating days with a resolution of 1 second by using power quality analysers. Figure 4.24 shows the time versus output power of one of the PV inverters for typical operating days, which are clear sunny, average cloudy, cloudy, heavy cloudy and low power days. It is noticed that the PV power curve is wider during the daytime compared to the power curves of rooftop PV (see Figure 4. 12), which is due to PV array technology. The corresponding measured per-unit RMS voltage at the LV side of the PV inverter output is plotted as shown in Figure 4.25. It is observed that the trend of voltage variation has followed the trend of PV power injection. During the early morning and evening

periods, the voltages are between 0.98p.u - 0.99p.u, which are within the limits specified by AS/NZS 61000.3.100: 2011 standard. During the daytime, the voltage magnitudes have increased with respect to the PV power injection. The magnitudes are normally lower than the value of 1.01p.u except during the high power production periods (i.e., when the inverter has produced 600kW power, e.g., 5/07/2015), which are within the standard limits. It can also be observed that due to heavy cloud transient periods the voltages are fluctuated between 0.97p.u-1.018p.u, which is nearly 4.5% of the voltage difference.

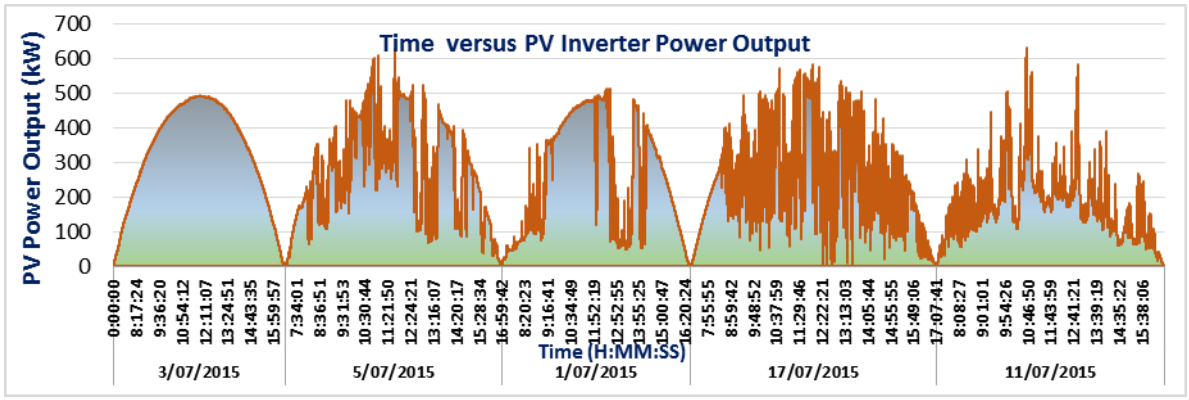

Figure 4.24. Time versus PV Power Output during Various Operating Days.

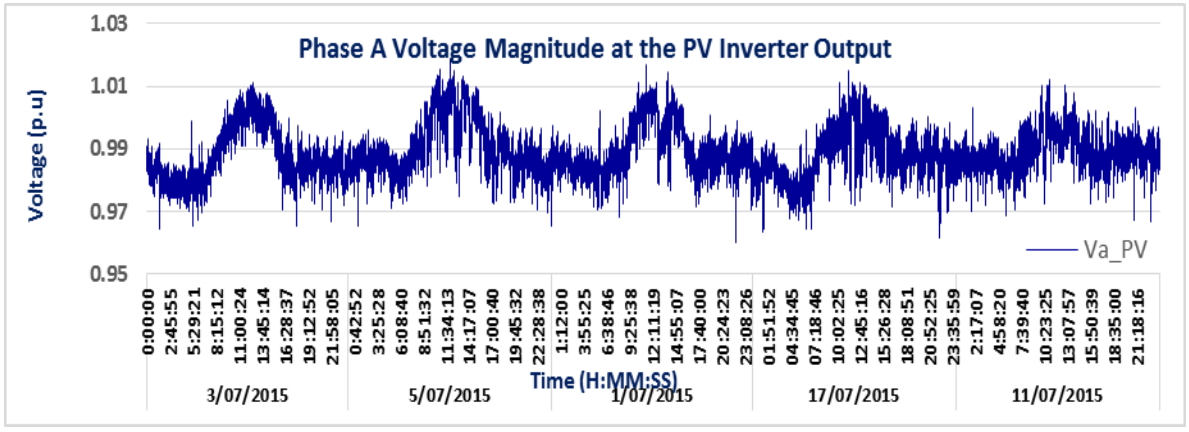

Figure 4.25. Measured Voltage Magnitude Profile at the LV Side of the PV Inverter Output.

Further, the collective impact of all five inverters can affect the upstream HV side of the network voltage levels. Therefore, field measurements at the 11kV connection point for the above indicated days were collected with second's resolution for the analysis as shown in Figure 4.26. Measurements show that the voltages during the early morning and night times are fluctuating between 1.01p.u - 1.02p.u. During the daytime, the voltage rise due to reverse power flow however, is somehow reduced by the SVR operation and the values are lower than 1.02p.u. Nevertheless, the voltage fluctuations are recorded higher, which may be due to the number of regulatory operations. It is observed that these voltage fluctuations are higher during

the heavy cloudy days and the magnitudes oscillated between 0.98 to above 1.03p.u. Also, variations in solar irradiation due to fast moving clouds could be faster than the response of regulators, which may fail to regulate the voltage instantly. Furthermore, these voltage fluctuations could trigger flicker incidence issues on the network with high PV installation capacity, which will be a concern for the utility.

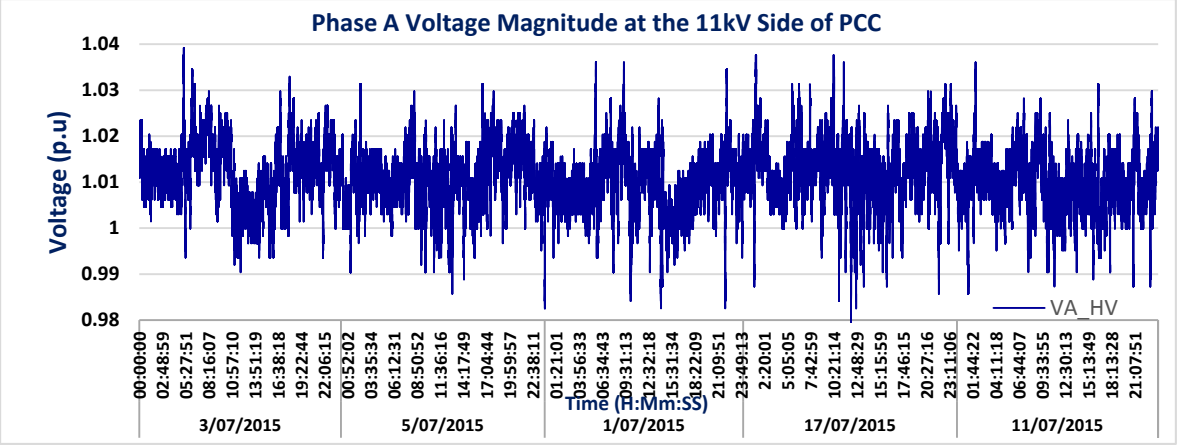

Figure 4.26. Measured Voltage Magnitude Profile at the HV Side of the PV Integration Point.

4.3.2.1.2. Voltage Flicker Analysis at 3.3MW PV System

Flicker is a serious constraint in the network which could impact the operation network voltage regulating equipment and can reduce the equipment life span. The objective of this section is to analyse the flicker sensation levels due to a 3.3 MW PV system at the high-voltage side of the integration point.

As per the interconnection agreement with Energex for the UQ Gatton PV plant, the short term and long term flicker emissions are restricted to 0.35 and 0.25 respectively. According to AS/NZS 61000.3.7: 2001 [104], the short term and long term flicker levels in low and medium voltage networks should not exceed 1 and 0.8 respectively.

To evaluate the probability of the flicker severity on the HV side of the PV integration node, the short term and long term indices are obtained for 3 months which are calculated based on equations (2.4) and (2.5) as presented in Chapter 2. For this, a clustering algorithm has been considered to quantify the flicker sensations during the time of the day. The collected daily data has been overlapped into a 24-hour time frame so that around 90 data points are allocated for every time instant. The flicker data contains every 10 min and 2 hour time intervals. Further, the short-term flicker levels at every time instant are classified into five clusters as indicated in Figure 4.27. The probability counts for each cluster at the specific time instant are calculated and this process is continued for all time instants. It can be observed that cluster 1 has accounted

for the highest number of counts in which the flicker levels are below 0.4 and satisfying the agreed short-term emission limit. Cluster 2 is the next intensified flicker level with a total of 180 counts during the whole 3 months period. It can be noticed that during the no PV power generation periods, the possible level of flicker is in cluster 2 and has a maximum number of counts, which may be due to the load operation. Furthermore, the probability counts of cluster 3 have increased during the PV operation periods, which has accounted for a total of 27 events. Significantly, the flicker levels are between 1 and 5 limits for nearly 41 times during the PV operation time. It can also be seen that the inherent flicker levels also exceed the limit of 5 sometimes during the day, which is due to maximum PV power drop with heavy cloud cover.

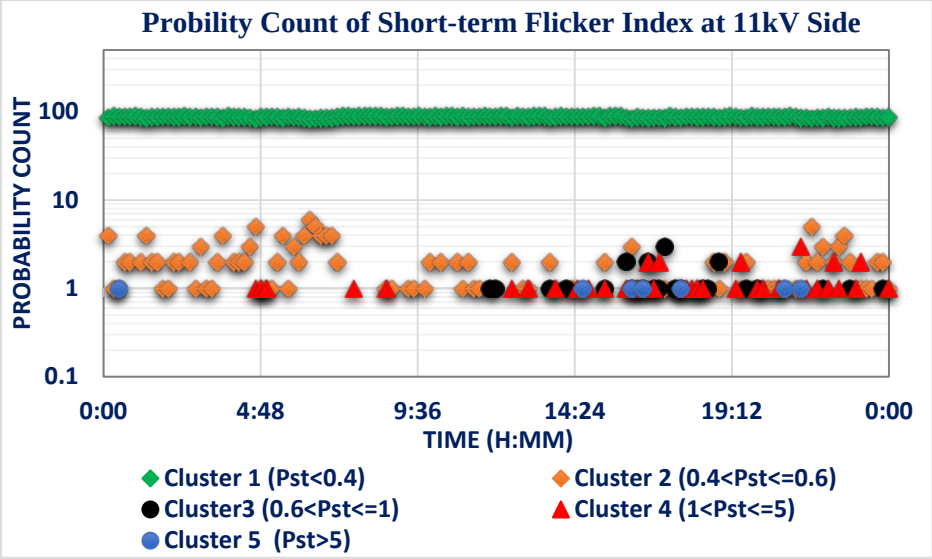

Figure 4.27. Probability Count of Short-term Flicker at the PV Interconnection Node.

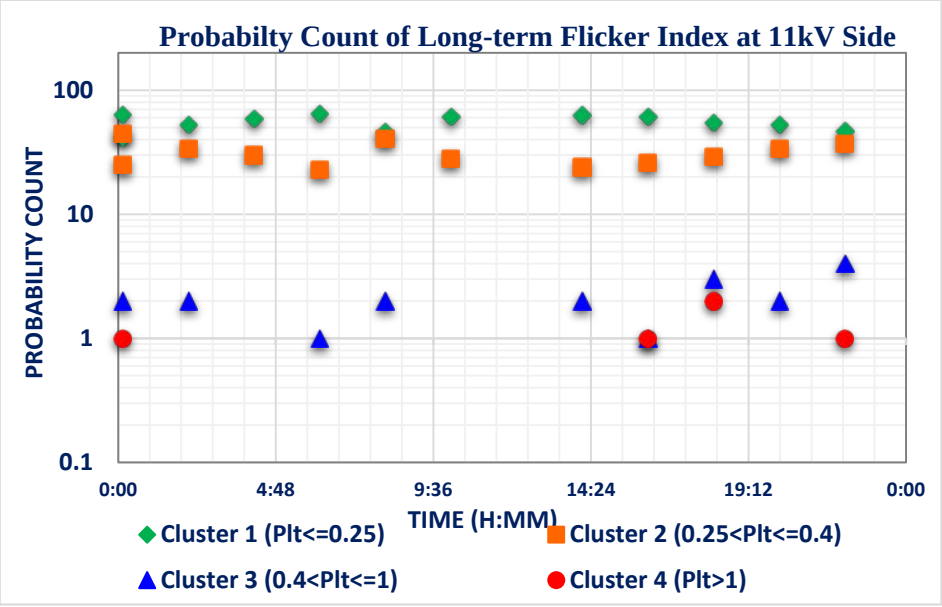

Figure 4.28. Probability Count of Long-term Flicker at the PV Interconnection Node.

Next, the long-term flicker values are segregated into four clusters and can be seen in Figure 4.28. It can be observed that the PV plant has flicker levels below 0.25 for nearly 50 to 65 events at every time instant of the day which satisfies the limits recommended by the plant agreement. Further, cluster 2 is also accounted for about 25 to 30 events at every time instant of the day, which is nearly 30% chance of increased flicker levels. Finally, clusters 3 and 4 have accounted for a lower number of events during the 3 months period. It is confirmed that the voltage flickers are appeared to be under control for most of the time and satisfied the AS/NZS standard limits.

4.4. Summary

This chapter deals with various power quality problems such as voltage rise, unbalance, sag/swells and voltage flicker. Firstly, the investigation through PSCAD simulations in the IEEE 13 bus unbalanced distribution network was presented. In this study, the PV penetration influence on the network voltage performance was assessed in two case studies. In the first case study, the voltage rise and unbalance assessment was carried out in three different scenarios, which included lumped PV system penetration at near to the distribution transformer (at the beginning of the feeder), distributed penetration at multiple locations near to the loads (i.e., at end of the feeder) and also with increased penetration by residential single-phase PV systems. Results show that the voltage rise due to distributed PV integration is higher than compared to the lumped PV penetration at the beginning of the feeder. This impact is even higher with increased PV penetration. In the second case study, fault analysis was carried out for with and without PV system presence during each of the three types of faults on the IEEE network to determine the voltage sag/ swell intensities. Results showed that during the fault condition, the unbalanced voltage sags are slightly compensated by the contribution of PV power. However, the voltage swell is attained higher values compared to without PV scenario.

Furthermore, the influence of PV system penetration and their impacts due to rapid fluctuations in the solar irradiations, on the voltage quality of the distribution network was analysed. The investigation was performed through field measurements on the different PV systems with capacities of 1.5MW and 3.3MW, which are located at the UQ St. Lucia and Gatton Campus respectively. Practical measurements were conducted through the installation of power quality meters in the real PV site. Various power quality measurements at the PV inverter output level to the high voltage and low voltage side of the distribution network level were collected. Further, a clustering method has also been applied to estimate the probability of flicker severity in the network. This analysis identified the long-term and short-term

influence of PV systems on the network voltage levels during different real operating scenarios. Results confirm that the network voltage magnitudes are increasing with respect to the PV power injection. Measurement results demonstrate that voltage quality concerns in the 1.5MW PV system are insignificant compared to the 3.3MW system. The following chapter investigates the harmonic emission issues from PV systems and their penetration impacts, which is another significant power quality issue in the distribution network.

CHAPTER 5

ANALYSIS OF HARMONIC ISSUES WITH PV SYSTEMS

5.1. Introduction[1]

This chapter presents the harmonic impact analysis of high PV systems integration on distribution networks. In the first part of this research, the harmonic emission characteristics of PV systems and their aggregation issues have been analysed. This analysis has been performed on the IEEE 13 bus network through simulations in two different case studies and the results are validated with the experimental measurement data collected at the University of Queensland St. Lucia campus. For this purpose, a Fast Fourier Transform (FFT) algorithm has been utilised for the harmonic analysis.

[1]This chapter is incorporated with the following references:

Section 5.2 and 5.3:
Annapoorna Chidurala, T. K. Saha, and N. Mithulananthan, "Harmonic characterization of grid connected PV systems and validation with field measurements," in Power & Energy Society General Meeting, 2015 IEEE, 2015, pp. 1-5, Denver, USA.

Section 5.2 and 5.4:
Annapoorna Chidurala, T. K. Saha, and N. Mithulananthan, "Harmonic impact of high penetration photovoltaic system on unbalanced distribution networks – learning from an urban photovoltaic network," IET Renewable Power Generation, Volume 10, Issue 4, April 2016, p. 485 – 494
DOI: 10.1049/iet-rpg.2015.0188.

Subsequently, the influence of harmonic emissions from PV systems on unbalanced distribution networks has been assessed. For this purpose, the investigation has been carried out through simulations on three different case studies. Further, an evaluation study has been performed with the online field measurements obtained at the various connection levels of the real-time grid connected PV site, which is located at the UQ St. Lucia campus. The following section presents the test system modelling and an approach for the harmonic analysis.

5.2. Test System Approach for the Harmonic Analysis

In this analysis, the IEEE-13 bus radial distribution network is selected as a test system. The modelling of the IEEE-13 bus distribution system has been presented in Chapter 3, Figure 3.17. This radial unbalanced distribution network is short and has a three-phase four wire system with a nominal voltage of 4.16kV. It has overhead and underground lines of three-phase, two-phase and single-phase line configurations with unbalanced line impedances. The network is equipped with a substation transformer, in-line transformer, single-phase voltage regulators and shunt capacitor banks. The test system contains balanced, unbalanced spot loads and distributed loads, which can be modelled as constant power, impedance (Z) and current (I) loads.

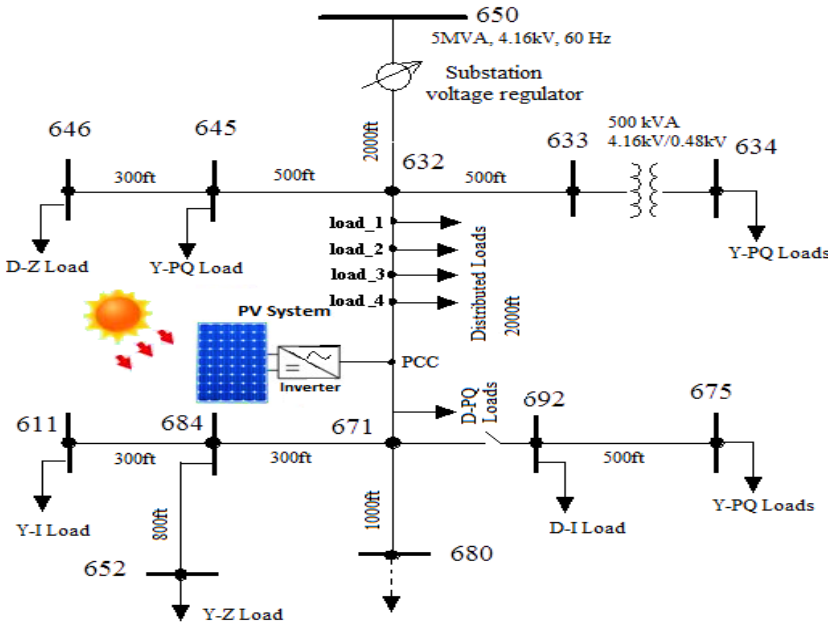

Figure 5.1. IEEE-13 Bus Test System.

Furthermore, in this study, to simulate a real-time residential distribution network the test system has been modified. Regarding this, the total length (2000ft) of the feeder between nodes 632 to 671 is divided into five equal sections and the loads are equally distributed among nodes

load_1 to load_4 as shown in Figure 5.1. In the figure, PCC (point of common coupling) indicates the PV connection node, which is at the middle of the feeder section (load_4 to 671). The investigations have been performed by considering the affect with and without background harmonics applied to the test network.

To simulate the without background distortion case, the network is modelled with constant power, constant current and constant impedance loads considered as presented in Chapter 3. Therefore, the harmonic distortion in the IEEE network is ideally zero. However, in real-time conditions the distribution networks possess harmonic distortions due to residential and commercial loads. Therefore, in order to investigate the impact of PV inverter systems in a real distribution network scenario, some power electronic based nonlinear loads have been introduced to inject necessary background distortion in the network according to the IEEE 519 standards [53]. To achieve a realistic scenario, various single-phase rectifier bridges with RL, RC and motor type load models are connected to the feeder nodes load_1, load_2, load_3 and load_4.

These nonlinear loads comprise numerous power electronic based residential appliances, which include DC drives, computers (PC), television (TV), compact fluorescent lamps (CFL), single-phase induction motors, adjustable speed drives (ASD) and lift motors. The detailed load models were developed in PSCAD and verified for the harmonic levels with the IEEE standard requirement as presented in Chapter 3, Section 3.4. The capacity and the current total harmonic distortion of these loads are as follows: CFL (20W) - 125%; TV (50W) - 91.24%; computer (100W) - 91%; DC drives (10hp) - 56.7% etc. Several combinations of these loads are aggregated in each phase of the feeder nodes (load_1 to load_4) in order to acquire the actual load capacities in the IEEE network. Single-phase loads mainly generate odd order harmonics (i.e. 3^{rd}, 5^{th}, 7^{th}, *etc.*). Moreover, ASDs and lift motors generate primarily 5^{th}, 7^{th}, 11^{th}, 13^{th} and higher order harmonics. Due to the dynamic operation of loads, the generated harmonics from the nonlinear loads can be amplified or suppressed due to harmonic superimposition and can cause distortion in the distribution network. Consequently, increased dispersed PV penetration in existing distribution networks combined with numerous nonlinear loads worsens the PQ of the grid. Therefore, in this chapter, the assessment has been carried out systematically on this IEEE network with PV systems penetrations in different scenarios to estimate the exact harmonic contributions from the PV systems.

5.3. Harmonic Characterisation of Grid Connected PV Systems & Validation with Field Measurements

In the first part of the assessment, the characterisation of harmonics and their interaction issues associated with multiple PV systems interconnection have been studied with simulations and compared with field measurements. Due to the solar irradiation dependency, the power generation is variable. Furthermore, the harmonic emissions from several identical systems could be different due to their independent operation. Hence, the harmonic magnitude and phases are also different for each inverter and the resultant harmonics may suppress or increase because of harmonic superimposition. Therefore, in this research, the harmonic emissions from PV inverter systems have been assessed for various real operating conditions. In addition, harmonics interaction impacts between identical PV inverter integrations have been studied. The simulation approach and the analysis of results are presented in section 5.3.1. Furthermore, the field test approach and measurement results are explained in section 5.3.2. The results from simulations are validated with experimental measurement results in subsection 5.3.2.2.

5.3.1. Simulation Approach and Analysis of Results

To investigate the harmonic characteristics of PV systems, a Current Controlled Current Source Inverter (CRCSI) based PV system has been considered. The operation of a control scheme and the modelling of the grid connected PV system components are discussed in Chapter 3 (refer section 3.2). For this analysis, a dynamic PV system model has been developed in PSCAD, which has all the characteristics similar to a real PV system. The rated capacity of the PV system is about 330kWp and is considered to operate at unity power factor. The switching frequency of the PV system is 2,460Hz (41x60Hz). The PV system is connected to the grid through an LC filter. The value of the filter inductance is chosen as 3mH and the filter corner frequency should be 1/10 of the switching frequency. Therefore, the filter capacitance is calculated as about 90µF. In this study, a static solar irradiation pattern is applied on the PV system as shown in Figure 5.2, realizing this condition as a half-day operation from noontime to night-time. The corresponding active and reactive power outputs of the PV system are shown in Figure 5.2.

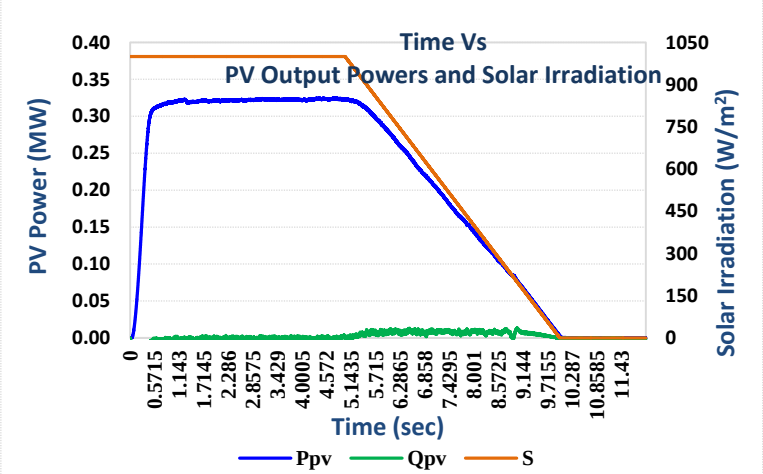

Figure 5.2. Time versus PV Output Active and Reactive Powers and Solar Irradiation.

The analysis has been carried out on two case studies by considering with and without the effect of network background harmonics on the performance of PV systems as described in section 5.2. In each case study, the simulations were performed in five scenarios by integrating identical PV systems consecutively. In the IEEE-13 bus network, PV systems are connected at the PCC node. In the first case study, the IEEE network is modelled with static loads, which produce almost zero harmonic distortion in the network. In each scenario, identical PV systems are connected at the same node for a better understanding. In this case, the harmonics produced by PV inverters are only due to switching harmonics. Therefore, the harmonics that are generated from the input side (also the PV side), due to solar irradiation level, temperature, type and arrangement of PV modules and the inverter current controller are not determined by the supply voltage. Ideally, a three-phase 2-level full bridge PV inverter can generate harmonic orders mainly according to equation (5.1) and do not produce triplen harmonics.

$$h = 6n \pm 1 \qquad \text{Where, n = 1, 2, 3, 4…} \qquad (5.1)$$

The individual harmonics up to 31st order of both voltages and currents were obtained for various solar power generation conditions. The results of voltage and current individual harmonics in percentage of actual magnitudes with respect to the active power generation are plotted as shown in Figures 5.3 and 5.4 respectively. In figures, P/P_n indicates the ratio of actual PV power to the rated power. During simulation, the current and voltage amplitudes change continuously for different power levels. For solar irradiation variations, the hysteresis current controller can inject high frequency harmonics to the current due to its variable switching frequency. From the results, it can be observed that the 5th order harmonic is the most prominent. As expected, the 7th, 11th and 13th order harmonics and the higher order components

29th and 31st are presented in the voltage. It is noticed that the magnitudes of third order harmonics are also exist in both voltage and current. In Figure 5.3, it can be seen that the values of individual harmonics are well within the limits according to the IEEE standards.

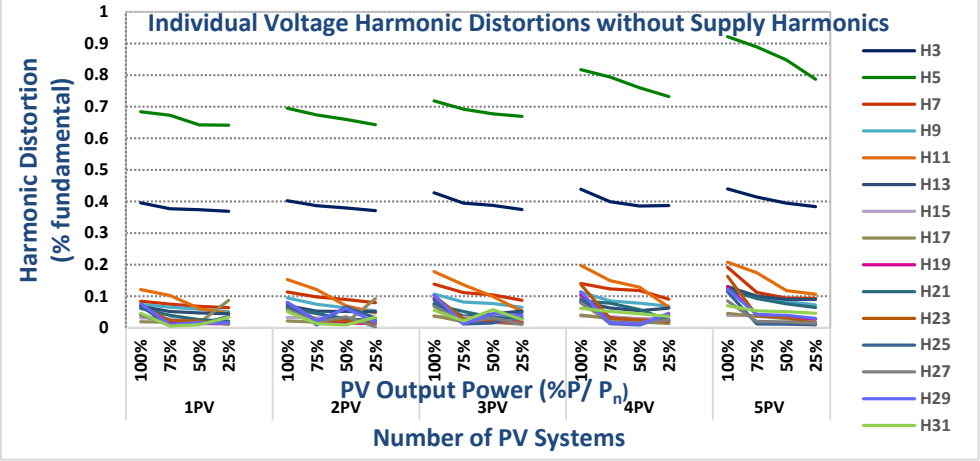

Figure 5.3. Voltage Harmonics at the Output of PV Inverter in Each Scenario.

However, in each scenario the individual harmonics from the identical inverters are increasing with respect to the PV power injection. In addition, the PV power injection into the grid causes an increase in voltage magnitude at the connection point. Furthermore, the individual voltage magnitudes are added up from each inverter integration. As a result, the percentage of distortion showed in the figure is a result of voltage rise and increased individual voltage harmonic magnitudes. During all the power levels, the 5th harmonic is the most intense, having values of about 0.7-0.9%.

In contrast, the current harmonics are following a reverse trend for lower PV power levels and are increasing as shown in Figure 5.4. Besides, the harmonic distortions were appeared to be reduced by each PV inverter penetration. During rated conditions, the generated harmonics have satisfied the standard requirements. The current harmonic magnitudes mainly depend on the active power output and the switching harmonics. However, during low power levels the harmonic distortions have increased to over 5% (5th), 3% (3rd) and 2.8% (7th), which are high. It is noted that the standards only recommend harmonic limits during rated operating condition. The produced higher harmonics with less magnitude may not influence the distribution network. Conversely, the current amplitudes from multiple inverters could be added and those harmonics can affect the grid harmonic levels. In addition, PV inverters operating at low power level, for instance 4 PV inverters operating at 25% PV power can produce a rated current of 1 PV system. Here, increased individual harmonic magnitudes from PV systems with the produced fundamental current also affects the grid harmonic levels. The presence of triple

harmonics flowing through the neutral can cause the overheating and overloading of the neutral conductor. Further, depending on the network configuration, load characteristics and the PV inverter capacity and control strategy can excite a harmonic resonance issue.

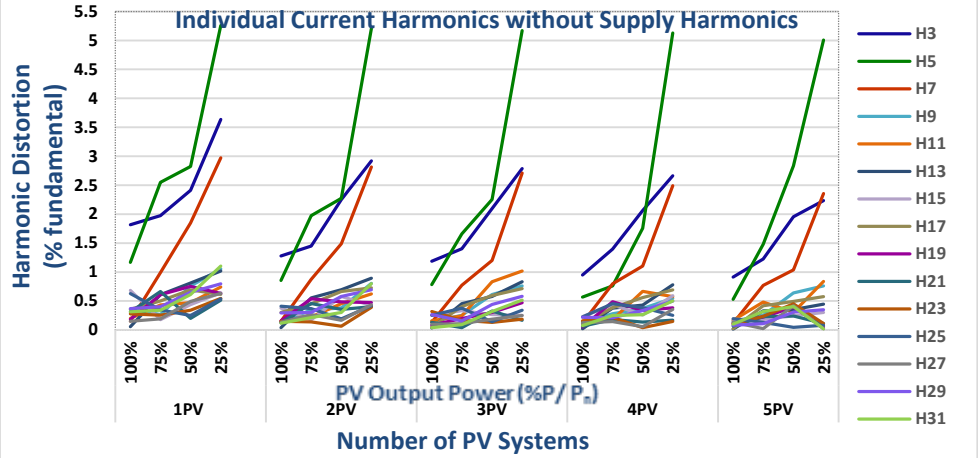

Figure 5.4. Current Harmonics at the Output of PV Inverter in Each Scenario.

In the second case study, the static loads are replaced with nonlinear loads in the IEEE test network. Therefore, due to harmonic producing loads, the voltage THD in the network is about 2-2.5% and the current THD is measured to be 3.5%. Similarly, simulations have been performed for five scenarios. The measured voltage harmonic at the output of the PV system, i.e. at the integration node, is plotted in Figure 5.5. Results show that the contribution of harmonics from the PV inverter has increased the voltage distortion by 1% for the first PV inverter integration. Further, a small increment in voltage distortion is observed with every PV inverter integration. In this case study, the 7th harmonic was the highest, followed by the 5th order harmonic. In comparison with the first case study, the harmonics were amplified. The 3rd harmonics and its odd multiples have values within the 1% range.

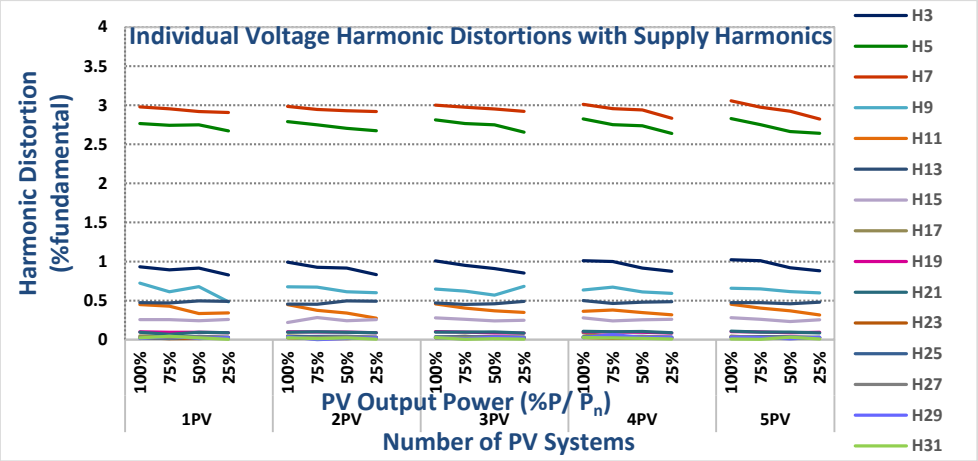

Figure 5.5. Voltage Harmonics at the Output of PV Inverter in Each Scenario with Distortion in the Supply.

Correspondingly, the current harmonics also had the same tendency as with the previous case and the values are almost equal. The emitted current harmonics in this case study contain two causes of distortion; switching harmonics and the harmonics due to distortion in the supply. A comparative plot of current THD during rated power condition in both case studies is shown in Figure 5.6. From the definition, THD refers to the instantaneous measurement of harmonic distortion at individual equipment with respect to the actual fundamental (I_1). It can be seen that the current THD appears to be decreasing due to an increase in fundamental current with PV integration. Even though, background harmonics present in the network, the current harmonics generated from the PV systems are within the limits. Further, the measured inverter current THD with nonlinear loads is slightly reduced compared with the linear loads case, which might be due to harmonic suppression with filters. However, the increased PV penetration can influence the grid by both current and voltage harmonic levels.

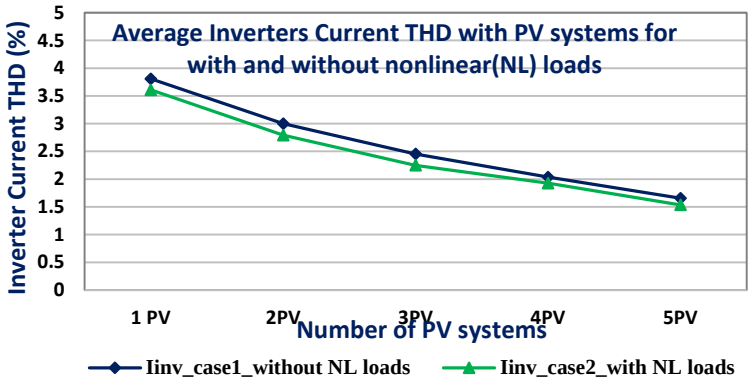

Figure 5.6. Percentage of THDs of PV Inverter Output Currents in Two Case Studies.

Furthermore, field measurements have been conducted at the University of Queensland PV system to evaluate the PV inverter harmonic behaviour in real operating scenarios.

5.3.2. Field Measurement Approach and Analysis of Results

5.3.2.1. Measurement Setup and Data Collection

The University of Queensland has one of the largest rooftop PV systems in Australia with 1.22MWp, which was installed in 2011. The system is scattered on four buildings with around 5000 PV panels. It is equipped with a special type of grid connected three phase PV inverter to synchronize with grid voltages. In this study, field measurements were taken at the multilevel car park (98A), which has an installed DC capacity of 339kWp with nearly 26 inverters. Figure 5.7 shows the 12.5kW transformer less PV inverters that are connected directly to the grid to feed the load demand. Each PV inverter has two MPPT controllers and each MPPT is employed with two strings of PV panels as explained in Chapter 4, section 4.3.1.

Figure 5.7. Grid Connected Three-phase PV Inverters at UQ PV Site.

To assess the harmonic distortion levels at the output of the PV inverter, field measurements have been conducted at two of these PV inverters for different PV operating conditions. For this, two FLUKE power quality analysers of types 434 series-II [122] and 1735 [123], which are certified by IEC 61000-4-30 Class A standard, were used for the measurement. One power quality meter was connected to the output of one PV inverter and the other was connected at the combined output point of two inverters (Inverters 1 and 2). For each meter, four Amp clamps are used to measure the three phase and neutral currents and voltage measurements are conducted to each phase, neutral and ground. Figure 5.8 shows the test set up at the switch board.

Figure 5.8. Measurement Test Setup for Harmonic Analysis.

The power quality parameters include harmonics, voltage, current, frequency and power data, which has been recorded for 15 days. The resolution of each measurement was 5sec and

the sampling time was 50µs. The recorded data was transferred to a computer and extracted using Power Log software. With this software, the measurement data can be exported to spreadsheets for analysis.

5.3.2.2. Measurement Results and Discussion

The university also had installed weather sensors to collect solar irradiation and temperature data. In this study, measurements were collected for various typical operating conditions of the PV system. Figure 5.9 shows some selected days for the harmonic evaluation. The plot illustrates the linear relationship between solar irradiation and PV power with respect to time.

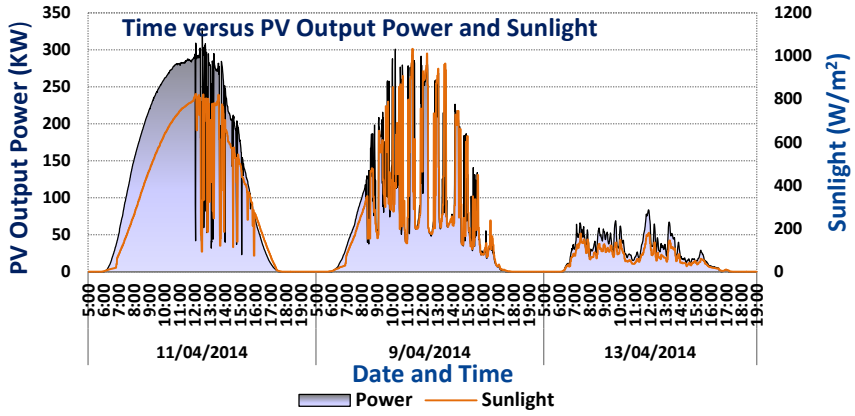

Figure 5.9. Time versus PV output Power and Sunlight.

With the use of two power quality meters, measurements for the corresponding days were obtained. The measured Phase-B individual grid voltage harmonics of PV inverters for up to 31st order and up to 25th order from both Fluke meters are plotted in Figures 5.10 (a) and (b).

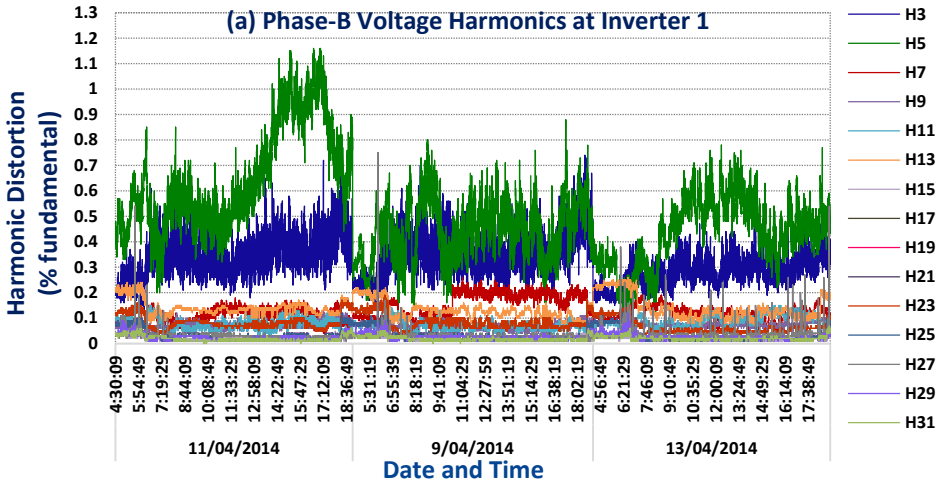

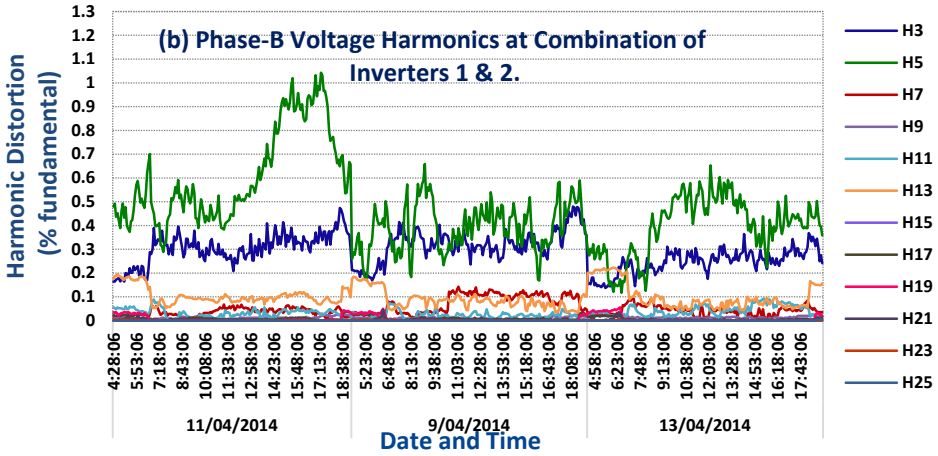

Figure 5.10. Individual Voltage Harmonics of Phase-B at the PV Systems Output.

It can be observed that the voltage harmonics behaviour has a similar tendency compared with the simulation outcomes. In both measurements, 5th and 3rd order harmonics were the highest and were increasing with respect to the PV power output. During rated power level, the 5th order harmonics have values between 1-1.15%, which are within the limits according to the standards. In addition, the 3rd order harmonic is constant throughout the day having values of about 0.4-0.5%. The harmonics orders of 7th to 13th lie in the lower than 0.2% range. It can also be estimated that the level of voltage harmonics was increased by the increased actual voltage amplitude with the addition of PV inverters and the influence of augmentation of individual voltage harmonic magnitudes. The characteristics and the levels of individual harmonics are signifying the first case study of simulation (see Figure 5.3). It is important to mention that the university network had filters and a potential transformer, which reduces the higher frequency harmonics, so the results are appeared to be lower. However, depending on the type of load and the network, voltage harmonic level might influence the individual harmonic magnitudes and that scenario can be seen in the second case study of simulation (see Figure 5.5). Similarly, the measured Phase-B current individual harmonics of one PV inverter (Inverter 1) and the combination of two PV inverters were plotted in Figures 5.11 (a) and (b) respectively.

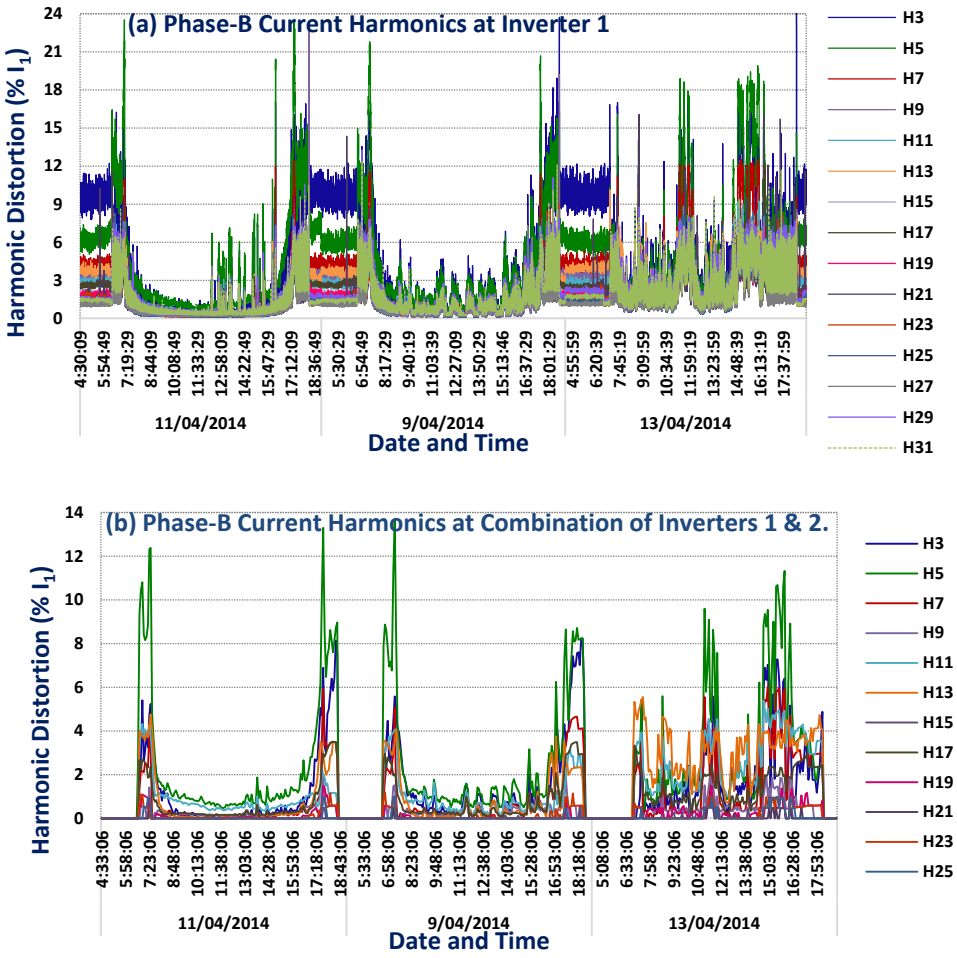

Figure 5.11. Individual Current Harmonics of Phase-B at the PV Systems Output.

It can also be inferred that the measured current harmonics from the inverters have similar trends as with simulated results. During the early hours (low irradiation) of inverter operation, high levels of current harmonics are observed due to decrease in fundamental current. Also in this period, the PV inverters consume a small amount of reactive power for their initial operation depending on their inverter technology, which could also impact the current harmonics. Note that the PV inverters are considered to operate at unity power factor at their rated condition. The triple harmonics, especially 3rd and 9th order harmonics were shown to be higher and were unable to be controlled adequately. These harmonics from each phase can be added up instead of cancelling out, which may overload the neutral conductor.

However, during high power levels, it can be noticed that the 5th order harmonic was the most affected and had values below the 2% limit, which are satisfying the AS 4777.2 standard [107] requirement. Results show that the harmonic magnitudes from 3rd to 27th order were decreased gradually. From Figure 5.11 (a) it can be seen that during rated conditions, the inverter current is also producing higher frequency components (27th to 31st orders) that have

values below 1%, which has slightly exceeded the limits. Furthermore, fluctuation in the solar irradiation can lead to misoperation of the inverter and the controller response may not effectively suppress the harmonic injection. By comparing two current harmonic spectrums, the percentage of harmonics have shown to be reduced, which is with respect to the increase in current magnitudes. However, the individual harmonic magnitudes might be multiplied in nature with identical PV inverters due to harmonic superimposition. Consequently, these current harmonics with higher magnitudes can increase the harmonics in the grid.

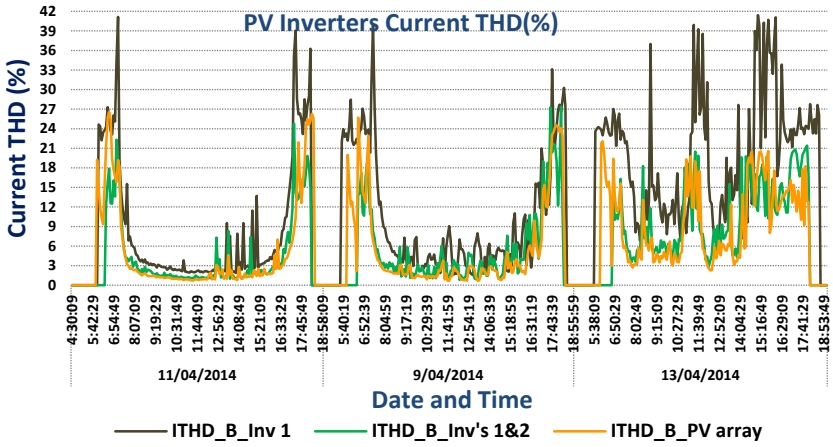

Figure 5.12. Percentage of Current THDs of PV Inverter System.

In addition, the current THD measurements for the above scenarios and at the output of identical PV system arrays were measured and plotted as shown in Figure 5.12. From the results, it can be noticed that the THD is dropping as the number of PV system integrations increase. The current harmonic distortion levels during rated conditions have values below 4%, which are within the limits specified by the data sheet of the inverter and the standards. The measurement results have shown a similar tendency with the simulation results. Further research will assess the harmonic impact issues with high PV system integration in the distribution networks.

5.4. Harmonic Impact of High Penetration PV System on Unbalanced Distribution Networks - Learning from an Urban PV Network

This research has focussed on the harmonic impact of PV system installations in a typical unbalanced distribution network. Harmonic analysis has been performed through simulations of three different case studies, which are considered by with and without the existence of ambient harmonics in the network as mentioned earlier. To consider the effect of a PV inverter control scheme on the network harmonic levels, two types of PV inverter models have been

considered. In this analysis, these two PV inverter system interconnections at a single node and multiple nodes of the network have been taken into account for the characterization of harmonic levels. Further, a harmonic evaluation study has been performed on the University of Queensland (UQ) St. Lucia campus network, which has an installed PV system of 1.5MW. The field measurement data was collected for two months at various levels of the UQ network for different operating conditions of the PV system.

This section is organized as follows: Section 5.4.1 describes the simulation approach and PV system connections for the comprehensive harmonic analysis. In addition, this section presents the results and discussion of different case studies. The description of the university network and an approach to the online field measurements are presented and the results are validated in Section 5.4.2. Finally, the summary of this chapter is presented in Section 5.5.

5.4.1. Simulation Approach and Analysis of Results

To analyse the influence of harmonic distortion levels introduced by the PV systems into the distribution network, two types of PV inverter control topologies have been considered. Since the harmonic generations from PV inverters with different control technology are divergent, their integration impacts may differ. Hence, in this research work two basic models of the PV inverter with current control capability are considered namely Current Regulated Current Source Inverter (CRCSI) and Current Controlled Voltage Source Inverters (CCVSI). The details of these PV inverter control methods are presented in Chapter 3, Section 3.4.

The rated capacity of each PV system is about 330kW and they are operated at close to unity PF. The CRCSI PV topology utilises a hysteresis based current controller for generating the firing pulses as shown in Figure 3.15 (refer Chapter 3). This controller is designed with a switching frequency of 2460Hz (41x60Hz) and HB is limited to 4% of the actual current. The parameters of the PI controller are tuned by using a trial and error method. The DC input voltage is 600V and the AC rated output line-line voltage is 400V. The inductance of the LC filter is 3mH and capacitance is calculated to be about 90µF. A pulse width modulation technique has also been applied to the CCVSI PV topology, which will generate firing pulses for the inverter. The switching frequency is preferred to be about 2460Hz (41x60Hz). The DC output voltage of the boost converter is 1050V and the rated AC output voltage is 400V. The output filter inductance is calculated to be about 1.11mH by considering the 10% ripple at rated output current and the capacitance is about 250µF.

In the simulations, the investigation has been performed on three different case studies. In each case study, these two PV inverter models have been considered in the harmonic analysis and verified to meet standards IEEE 929-2000 [106] and AS4777.2:2015 [108] requirements. It is important to note that in all the simulation case studies, the PV systems are operating at rated output conditions. The total current harmonic distortion from the PV systems is less than 3-3.5%. For simulations, the PSCAD software tool is utilised. These case studies will be helpful for utilities to estimate the grid harmonic distortion levels in the case of high PV penetration.

5.4.1.1. Case Study I: Without Distortion in the Supply with PV Penetration at the Same Bus

In the first case study, the IEEE-13 bus system has been considered and modelled with static loads. Simulations have been performed for two different scenarios with two PV inverter models. In each scenario, identical PV inverter systems are integrated at the same node, which is upstream of bus 671 and treated as a Point of Common Coupling (PCC). With an intention to examine the harmonic effects of each PV system in distribution networks, simulations were carried out for five situations in which PV systems are integrated gradually into the IEEE network.

In the first scenario referring to CRCSI (see Chapter 3.5.1), a 330kW PV system is connected at the PCC. Usually, harmonic distortions are specified in terms of Total Harmonic Distortion (THD) and Total Demand Distortion (TDD), which are used for power quality measurements in the network. THD is the ratio between root-sum-square of harmonic content to the fundamental component whereas TDD is calculated with respect to the load current. According to IEEE 519-2014 standard [53], the voltage THD should be less than 8% and the current TDD should be less than 5%. However, in reality THD is sufficient for analysis because the load current will always be greater than or equal to fundamental current. Due to the technical limitations in PSCAD software, the current and voltage THDs are calculated only up to 31st order, which is lower than the switching frequency considered by the PV systems. In this research work, all the simulations have been carried out at full load condition to eliminate the complexity in calculating the harmonic distortion levels.

Therefore, for every situation simulations have been performed and the measured THD of voltages and currents at different buses are presented in Tables 5.1 and 5.2 respectively. In Tables 5.1 - 5.10, 0PV indicates the scenario without PV systems in the network and the numbers 1PV, 2PV, 3PV, etc., represent the number of PV systems connected to the grid. From

the simulated results it can be seen that the voltage THDs are higher at bus 671 and the PCC compared to the before integration point, which is due to voltage reduction along the feeder. However, the supply side current THDs increased due to a decrease in the current magnitude. Moreover, the THDs are different in each phase and are dependent on the loading level. In the IEEE-13 bus unbalanced system, phase A is an averagely loaded phase, phase B is a lightly loaded phase and phase C is a highly loaded phase. Results show that both voltage and current THDs in phase B have slightly higher harmonic levels compared with the other phases due to the fundamental current differences. Harmonic levels of phase C are almost identical to that of phase A results.

Table 5.1 Percentage of Voltage THDs at Various Buses for Phases A and B with CRCSI

Phase Info	**Node No.**	**Number of PV systems integration at PCC**					
		0PV	1PV	2PV	3PV	4PV	5PV
Phase-A Voltage THD (%)	$V_{632,a}$	0.00	0.0511	0.1019	0.1528	0.2104	0.2829
	$V_{load\_4,a}$	0.00	0.0743	0.1188	0.1911	0.2634	0.3458
	$V_{pcc,a}$	0.00	0.0873	0.2102	0.3041	0.4068	0.4916
	$V_{671,a}$	0.00	**0.1102**	0.2401	0.3276	0.4263	0.5257
Phase-B Voltage THD (%)	$V_{632,b}$	0.00	0.0894	0.1594	0.2154	0.3012	0.3524
	$V_{load\_1,b}$	0.00	0.1230	0.2011	0.2802	0.3516	0.38412
	$V_{pcc,b}$	0.00	0.1964	0.3225	0.4313	0.4936	0.5423
	$V_{671,b}$	0.00	**0.2314**	0.3304	0.4341	0.5299	0.6859

Table 5.2 Percentage of Current THDs at Various Buses for Phases A and B with CRCSI

Phase Info	**Node No.**	**Number of PV systems integration at PCC**					
		0PV	1PV	2PV	3PV	4PV	5PV
Phase-A Current THD (%)	$I_{632,a}$	0.00	0.2621	0.5022	0.8462	1.3389	1.6995
	$I_{load\_4,a}$	0.00	0.2527	0.6061	1.1793	1.6261	1.9678
	$I_{pcc,a}$	0.00	0.2979	0.4064	0.6236	0.8109	0.8476
	$I_{671,a}$	0.00	0.3160	0.4885	0.7271	0.9042	0.9815
Phase-B Current THD (%)	$I_{632,b}$	0.00	0.5177	1.0125	1.4318	2.3640	2.8905
	$I_{load\_4,b}$	0.00	1.2604	2.5168	7.4040	12.9230	**14.8460**
	$I_{pcc,c}$	0.00	0.7887	1.2266	1.9197	2.3261	2.4654
	$I_{671,c}$	0.00	0.6193	1.4699	1.9423	2.1127	2.2800

Table 5.1 shows that with zero harmonic distortion in the network, the penetration of 1PV system contributes a voltage distortion of 0.1% and 0.2% in phases A and B at bus 671 respectively. It can be noticed that the variation in voltage THD at different nodes for each PV

inverter penetration is almost multiplied due to an increase in the individual voltage harmonic magnitudes. It may be observed that the increase in net voltage THD is 'n' times the THD with 1PV system, where 'n' is the number of PV systems. Results show that the supply current THD has an increased trend in each case and reaches a maximum of around 14.84% in phase B with 5 PV systems, which is violating the limit according to IEEE 519 standard.

Table 5.3 Percentage of Voltage THDs at Various Buses for Phases A and B with CCVSI

Phase Info	Node No.	Number of PV systems integration at PCC					
		0PV	1PV	2PV	3PV	4PV	5PV
Phase-A Voltage THD (%)	$V_{632,a}$	0.00	0.0622	0.1275	0.1993	0.2592	0.3003
	$V_{load\_4,a}$	0.00	0.0792	0.1545	0.2472	0.3301	0.4024
	$V_{pcc,a}$	0.00	0.1289	0.2648	0.4012	0.5339	0.6952
	$V_{671,a}$	0.00	0.1343	0.2717	0.4103	0.5409	0.7153
Phase-B Voltage THD (%)	$V_{632,b}$	0.00	0.0927	0.1826	0.2601	0.3781	0.4305
	$V_{load\_4,b}$	0.00	0.1132	0.1983	0.3721	0.4206	0.5808
	$V_{pcc,b}$	0.00	0.2026	0.3886	0.5978	0.7527	0.8503
	$V_{671,b}$	0.00	0.2104	0.4080	0.6122	0.7625	0.9229

Table 5.4 Percentage of Current THDs at Various Buses for Phases A and B with CCVSI

Phase Info	Node No.	Number of PV systems integration at PCC					
		0PV	1PV	2PV	3PV	4PV	5PV
Phase-A Current THD (%)	$I_{632,a}$	0.00	0.4468	0.9920	1.6623	2.6869	3.3257
	$I_{load\_4,a}$	0.00	0.5305	1.1906	2.6748	3.3337	4.6934
	$I_{pcc,a}$	0.00	0.1906	0.3890	0.6115	0.7710	1.0058
	$I_{671,a}$	0.00	0.1715	0.3417	0.6698	0.8605	1.0586
Phase-B Current THD (%)	$I_{632,b}$	0.00	0.6331	1.1906	2.8712	4.0111	5.5531
	$I_{load\_4,b}$	0.00	1.7388	4.5953	11.689	21.9732	**26.7457**
	$I_{pcc,b}$	0.00	0.5249	1.1033	1.8677	2.3928	2.9176
	$I_{671,b}$	0.00	0.4409	1.1544	1.7285	2.1147	2.7717

Similarly, in the second scenario, simulations have been carried out with CCVSI systems and the measured voltage and current THDs for both phases A and B are shown in Tables 5.3 and 5.4 respectively. It can be seen that the voltage and current distortion levels follow similar trends as mentioned earlier. The percentage of voltage and current THDs are slightly greater compared to the first scenario with CRCSI systems. The voltage THDs are increasing from upstream to downstream nodes, which is due to voltage drop along the feeder. Conversely, the current THDs are exhibiting an inverse trend and have increased values at the upstream level

because of PV power injection causing the supply current reduction. Even though PV systems inject balanced harmonics in the network, due to unbalanced loading the current THDs in phases A and B with respect to the fundamental are different. Significantly, phase B is more affected and has a current THD of nearly 27%with respect to the fundamental on the supply side, which is very high.

5.4.1.2. Case Study II: With Distortion in the Supply and Multiple PV Penetration at the Same Bus

In reality, distribution networks are polluted with harmonics, so in order to characterise the harmonic behaviour with PV systems integration in a real power system network, the IEEE-13 bus network is modelled with nonlinear loads in the PSCAD software environment to simulate a realistic scenario as mentioned earlier. In this case study, different power electronic circuit based nonlinear loads are aggregated and connected to the feeder nodes load_1 to load_4 as explained above, which inject harmonics into the distribution network. It is to be mentioned that the load on the IEEE network was increased by 10% and this was considered as a worst case condition. In the same way, simulations have been performed on two scenarios with two PV inverter models. In Tables 5.5 - 5.8, 0PV refers to having no PV and with distortion in the network in which the average voltage THD is around 3.5% and the current THD is about 3-4%.

Table 5.5 Percentage of Voltage THDs at Various Buses for Phases A and B with CRCSI and Distortion in the Network

Phase Info	**Node No.**	**Number of PV systems integration at PCC**					
		0PV	1PV	2PV	3PV	4PV	5PV
Phase-A Voltage THD (%)	$V_{632,a}$	1.6405	2.0643	2.1171	2.1809	2.2519	2.3013
	$V_{load\_1,a}$	1.9993	2.5163	2.5449	2.6228	2.6347	2.6478
	$V_{load\_4,a}$	**3.1243**	**3.8408**	3.8847	3.9270	3.9647	4.1915
	$V_{pcc,a}$	3.1249	4.3427	4.3768	4.4210	4.5375	4.6969
	$V_{671,a}$	**3.5241**	**4.5294**	4.5944	4.6525	4.75316	**4.9868**
Phase-B Voltage THD (%)	$V_{632,b}$	1.4764	1.9810	2.0400	2.0777	2.1384	2.2761
	$V_{load\_1,b}$	1.7999	2.4131	2.4363	2.4925	2.5718	2.6577
	$V_{load\_4,b}$	2.7604	3.6220	3.6798	3.7139	3.8994	4.1378
	$V_{pcc,b}$	2.7612	4.1084	4.1199	4.1652	4.3809	4.5877
	$V_{671,b}$	3.0963	4.2556	4.3783	4.4393	4.6377	**4.8519**

In the first scenario, a CRCSI system is considered in the simulation and connected only at the PCC. The resultant percentage of voltage THD at various buses in the network is presented

in Table 5.5. It can be seen that for the first situation only 1PV integration in the network causes the voltage THD at before PV integration node to increase by 0.5% in phase A and 0.9% in phase B. Subsequently, the voltage THD is amplified by over 1% at node 671 after the PCC node. Results show that the voltage THD has an increased trend as it goes to the end of the feeder compared to the before PV connection point. In addition, the increment in voltage distortion at PCC is about 1.3%. It can be seen that the voltage THD is high in the case of penetration of 5PV systems, the value reaching 5%. If the number of PV systems increases in the distribution network, severe voltage distortion may be caused.

Table 5.6 displays the current THDs in phases A and B from the supply side to the load side. It is observed that the current THD is higher on the supply side due to fundamental current reduction with PV power injection. It is to be noted that the fundamental currents at the supply side nodes will be different with PV systems in this case study compared to the first case study, due to the increased load level of the network. With the integration of 1PV system, the current distortions are raised by around 2% in phase A and 3% in phase B. Moreover, the current THD at the supply side is rising around 1% in each step of PV system integration. Similar to the previous case study, phase B is much more affected compared to other phases and has reached 11% and 7.8% at before and after PV integration node respectively, which is beyond the limit as per IEEE 519 standards.

Table 5.6 Percentage of Current THDs at Various Buses for Phases A and B with CRCSI and Distortion in the Network

Phase Info	**Node No.**	**Number of PV systems integration at PCC**					
		0PV	1PV	2PV	3PV	4PV	5PV
Phase-A Current THD (%)	$I_{632,a}$	2.8213	4.4357	4.7178	5.0265	5.4602	5.9655
	$I_{load\_1,a}$	3.0796	4.8323	5.1884	5.4444	5.8683	6.1089
	$I_{load\_4,a}$	3.1092	**4.9461**	5.2794	5.4458	5.8958	6.1901
	$I_{pcc,a}$	3.1091	4.6945	4.7475	4.7501	4.7565	4.8180
	$I_{671,a}$	3.3046	5.0801	5.1475	5.2026	5.2571	**5.3414**
Phase-B Current THD (%)	$I_{632,b}$	3.1349	5.3518	5.6918	6.0944	6.6003	7.0231
	$I_{load\_1,b}$	4.1897	7.8139	8.4828	9.2361	10.0334	10.5048
	$I_{load\_4,b}$	4.3456	**8.0171**	8.8282	9.4000	10.4277	**10.9493**
	$I_{pcc,b}$	4.3483	7.5153	7.6064	7.6055	7.6943	7.8467
	$I_{671,b}$	4.3495	7.5752	7.6117	7.6738	7.7819	**7.8445**

In the second scenario, a CCVSI type system has been considered and simulations have been carried out similar to the first scenario. Measured voltage and current THDs for different nodes from the supply side to the load side are shown in Tables 5.7 and 5.8 respectively. It can be noticed that the voltage and current THDs have lower values with the CCVSI system compared to the previous scenario, this is because of harmonic suppressions between PV systems and nonlinear loads. It can be seen that the voltage THDs at the downstream nodes have high values of over 4% for phase A and about 4.8% for phase B, which are close to the limit. If the penetration in the network goes high, there will be further increases in harmonic distortion levels, which will violate the limits.

Table 5.7 Percentage of Voltage THDs at Various Buses for Phases A and B with CCVSI and Distortions in the Network

Phase Info	**Node No.**	**Number of PV systems integration at PCC**					
		0PV	1PV	2PV	3PV	4PV	5PV
Phase-A Voltage THD (%)	$V_{632,a}$	1.6405	2.0154	2.0562	2.1275	2.1769	2.3245
	$V_{load\_1,a}$	1.9993	2.4581	2.5206	2.6101	2.7627	2.8470
	$V_{load\_4,a}$	3.1243	3.8012	3.9079	3.9991	4.0271	4.1296
	$V_{pcc,a}$	3.1249	4.2744	4.3798	4.4120	4.4792	4.5487
	$V_{671,a}$	3.5241	4.2524	4.3195	4.3623	4.4245	**4.5525**
Phase-B Voltage THD (%)	$V_{632,b}$	1.4764	1.8817	1.9487	2.0294	2.0856	2.2056
	$V_{load\_1,b}$	1.7999	2.2526	2.2943	2.3256	2.5262	2.6547
	$V_{load\_4,b}$	2.7604	3.4769	3.5442	3.6484	3.7584	3.8411
	$V_{pcc,b}$	2.7612	3.8123	3.9088	4.0838	4.2285	4.5358
	$V_{671,b}$	3.0963	3.8971	4.0188	4.2127	4.4651	**4.7685**

Similarly, the current THDs are following the same trend as in the previous scenario. Results show that phase B has a high current THD value of 9.36% with respect to the fundamental at node load_4 with 5PV systems integration as shown in Table 5.8. Also, it can be observed that there is an increase in current THD of 0.4% for every PV system addition. Moreover, the current THDs in phase B at the PCC and 671 nodes have reached higher values of above 7%. The generated harmonic THDs are exceeding the IEEE standard limits, which will severely affect the network along with connected neighbouring sensitive equipment and loads.

Table 5.8 Percentage of Current THDs at Various Buses for Phases A and B with CCVSI and Distortion in the Network

Phase Info	Node No.	Number of PV systems integration at PCC					
		0PV	1PV	2PV	3PV	4PV	5PV
Phase-A Current THD (%)	$I_{632,a}$	2.8213	4.2981	4.5061	4.8029	4.9837	5.0643
	$I_{load\_1,a}$	3.0796	4.8106	4.9862	5.2701	5.5887	5.8708
	$I_{load\_4,a}$	3.1092	4.8421	5.0988	5.2787	5.6438	6.0260
	$I_{pcc,a}$	3.1091	4.7157	4.7496	4.7608	4.8325	4.8139
	$I_{671,a}$	3.3046	5.1023	5.1382	5.1629	5.2086	5.2238
Phase-B Current THD (%)	$I_{632,b}$	3.1349	5.1389	5.3664	5.6289	5.9077	6.1701
	$I_{load\_1,b}$	4.1897	7.5365	7.9001	8.3363	8.9774	9.1763
	$I_{load\_4,b}$	4.3456	7.8239	8.2055	8.7053	9.1386	**9.3661**
	$I_{pcc,b}$	4.3483	7.4443	7.4508	7.4758	7.4938	7.5197
	$I_{671,b}$	4.3495	7.3798	7.4557	7.4406	7.4353	7.4256

5.4.1.3. Case Study III: With Distortion in the Supply and Multiple PV Penetrations at Multiple Locations

Finally, in the last case analysis has been carried out to study the impact of PV system penetration at different nodes. In this regard, the IEEE-13 bus system is considered with distortions as mentioned above. As for the first scenario, five PV inverter systems of CRCSI have been considered and are integrated along the feeder start from load_1 to the PCC in the test system. Simulations have been performed and the corresponding node voltage and current THDs were measured in each phase as presented in Table 5.9.

Table 5.9 Percentage of Voltage and Current THDs with 5 PV Systems (CRCSI) at Multiple Locations

Node No.	Voltage THD (%)			Current THD (%)		
	Phase-A	Phase-B	Phase-C	Phase-A	Phase-B	Phase-C
632	2.0871	2.0410	1.8765	5.3846	6.9656	7.5568
load_1	2.5311	2.4614	2.2894	5.7285	**9.6245**	**8.8493**
load_2	2.9746	2.8813	2.7036	5.4545	9.1788	8.3642
load_3	3.4253	3.3018	3.1316	5.1854	8.6758	7.8109
load_4	3.8935	3.7628	3.5758	4.9275	8.1494	7.4010
PCC	4.3521	4.1524	4.0363	4.7133	7.6377	6.9158
671	**4.3505**	4.1519	4.0304	5.0980	**7.5822**	**6.5983**

From the results, it is noticed that the harmonic distortion in each phase is different due to unbalance in the network and is higher in phase A, which is an averagely loaded phase. The voltage and current distortions are slightly lower compared to the previous case study, which is due to the harmonic superimposition. The voltage THDs of each node along the feeder line (i.e., from 632 to 671) are increasing and has higher values of nearly 4.4% at bus 671, which are within the limits. Conversely, the current THD profile followed an opposite trend and has values higher at the supply side nodes due to a decrease in current magnitude with PV penetration. Nonetheless, current THDs reached 7-7.6% at bus 671, which are over the limits according to IEEE 519 standards. In addition, these distortions will rise not only dependent on the number and capacity of PV systems but also on the type of control strategy.

Likewise, simulations were carried out with 5PV systems of CCVSI and the measured voltage and current THDs for various nodes are displayed in Table 5.10. In this scenario, the voltage THD in phase A is higher compared to other phases. It is observed that with the harmonic interactions between nonlinear loads and the PV systems, there will be a harmonic cancellation or addition taking place in the network. Results show that the voltage and current THDs have similar values as in the previous case study.

Table 5.10 Percentage of Voltage and Current THDs with 5PV Systems (CCVSI) at Multiple Locations

Node No.	Voltage THD (%)			Current THD (%)		
	Phase-A	Phase-B	Phase-C	Phase-A	Phase-B	Phase-C
632	2.3149	2.1519	2.1778	5.2077	6.1717	6.4699
load_1	2.8289	2.6612	2.5220	5.6163	**8.8829**	**8.2067**
load_2	3.2642	3.1232	2.9914	5.3043	8.5414	7.9292
load_3	3.7075	3.4204	3.3462	5.0652	8.2420	7.6872
load_4	4.1586	3.8586	3.7643	4.9822	7.8055	7.3686
PCC	4.6399	4.2410	4.1982	4.8205	7.4066	6.9575
671	**4.7679**	4.3284	4.1381	5.1520	7.4804	6.6358

It can be concluded that the distortion levels increase with multiple installations at the same node. The voltage distortion depends on both the system impedance and the aggregate of harmonic current injected. The situation may be worse in a real distribution network with a higher number of loads and with more PV inverter systems, which can further increase harmonic levels. Hence, this harmonic analysis has been extended to justify and compare the simulation results with real-time distribution network measurements.

5.4.2. Field Measurements at the University of Queensland - Analysis of Results

The University of Queensland, St Lucia campus is a large university of 2km radius. The university has an extensive power network with a maximum load demand of about 23MW and receives an 11kV supply from the Energex distribution network. The high voltage (HV) lines are supplied around the university and nearly forty substations are employed to step down the voltage to the 415V supply level as shown in Figure 5.13.

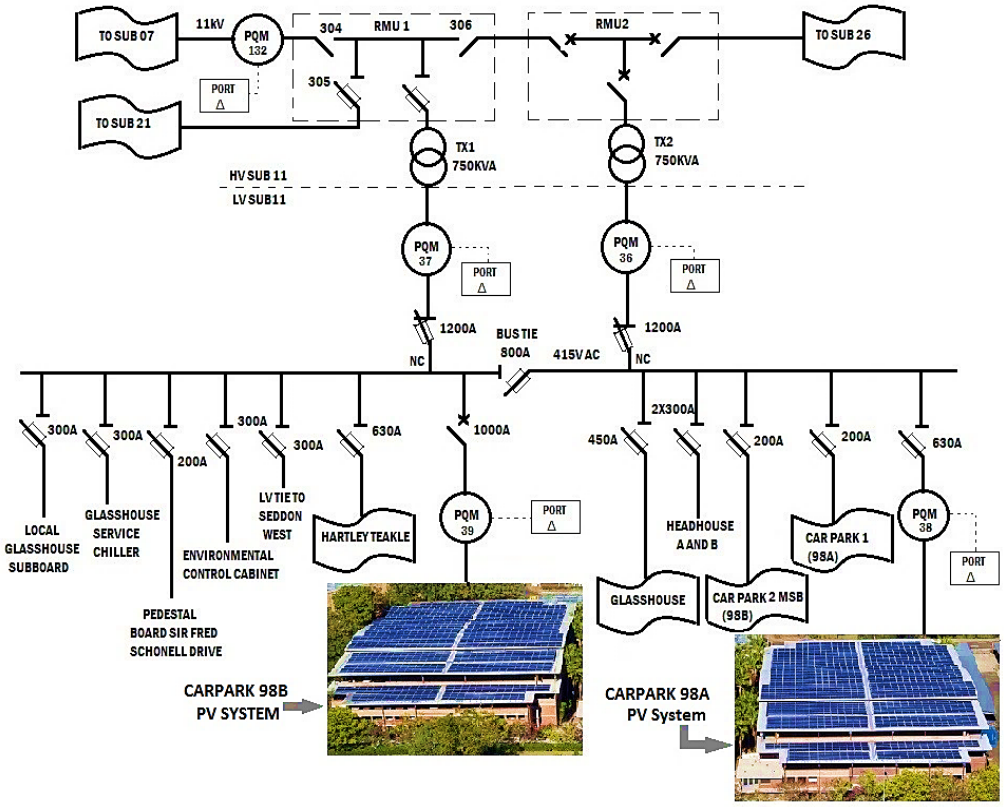

Figure 5.13. Overview of UQ Sub Station 11.

In 2015, the university installed a 1.5MW rooftop solar PV system, which is one of the biggest rooftop PV systems in Australia. This PV system is distributed across eight buildings with more than 6305 PV panels. The network consists of the latest electricity infrastructure including digital power meters and power quality (PQ) analysers connected to the internet for monitoring.

In this study, to assess the effect of PV integration on the harmonic distortion levels of the distribution network, measurements were taken at the multilevel car park buildings. Each building has an installed capacity of 339kWp and uses 26 three-phase inverters. Special types of grid integrated PV inverters are used to synchronise with the grid voltages. The generated

PV power is supplied to other buildings to feed the peak load demand. The car park buildings are interconnected to one of the substations through two 750kVA 11kV/415V distribution transformers. PQ analysers connected at the HV side, transformers and at the output of the PV arrays were used to monitor various PQ parameters.

For this analysis, the harmonic data from various PQ meters in different integration levels were collected for two months. Using JAVA programs, the harmonic measurements were extracted from an online data monitoring system for every 5ms time resolution. The solar irradiation and the temperature data were obtained using weather sensors.

(a) Time versus PV Output Power and Sunlight.

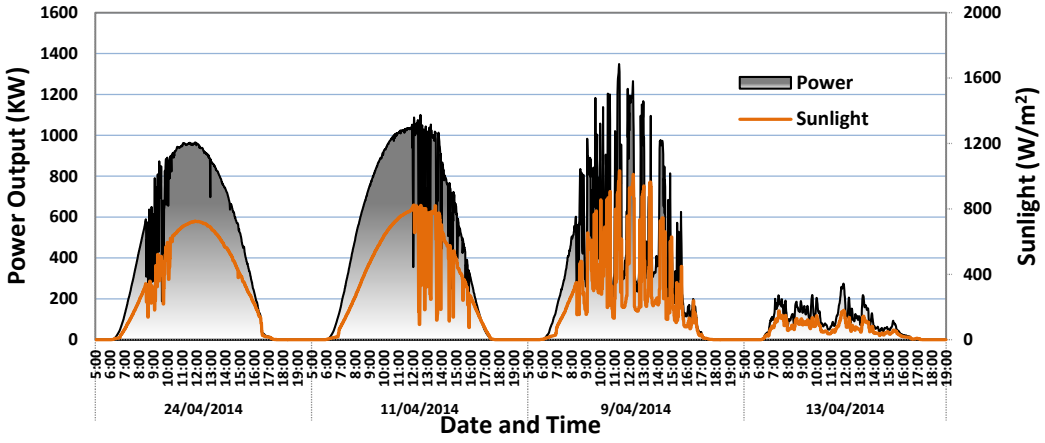

(b) PV Systems Voltage THD (%) at Carpark-98A

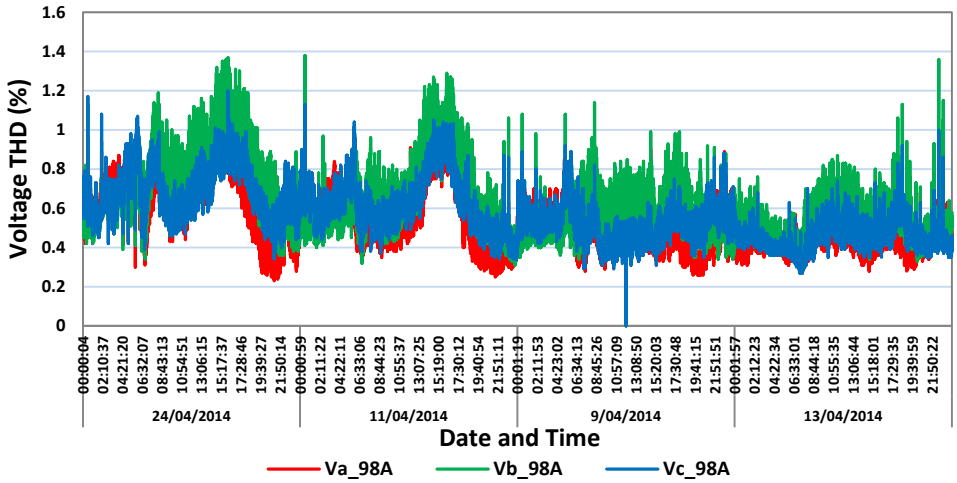

(c) PV Systems Current THD (%) at Carpark-98A

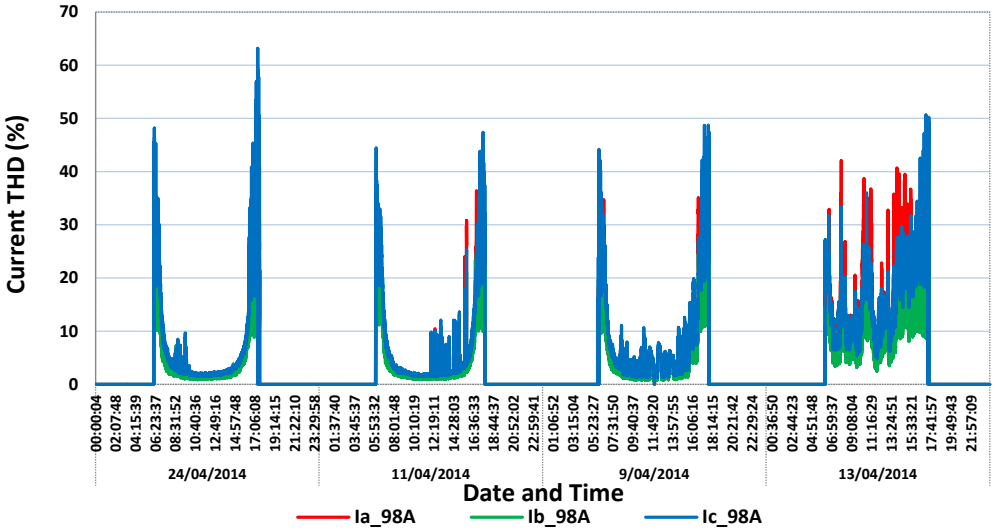

Figure 5.14. Solar PV System Measurements at UQ for Typical Operating Days.

The nature of solar power generation is intermittent because of variation in solar irradiation and it depends on the weather conditions. PV power has a linear relationship with the solar irradiation. Hence, harmonic emissions are varied for generated PV power. Figure 5.14 (a) shows the various operating conditions of the solar PV system and the characteristics of PV power and sunlight with respect to the time. The PV power outputs during a sunny day, average cloudy day, cloudy day and the worst day were shown in Figure 5.14 (a). The corresponding measured THD of PV output voltages and currents at Carpark 98A are shown in Figures 5.14 (b) and (c) respectively. As can be observed, the percentage of voltage THD has higher values during sunny and average mid cloudy days. It can be seen that during the day when PV power is low (especially early morning or evening times) the simulation scenario of without PV and with distortion in supply is replicated. In this period, the voltage THD levels were in the range of about 0.2-0.4%. However, during peak power generation periods (sunny and average cloudy days) the PV system produces voltage harmonics of nearly 1.4%, which satisfies the IEEE 929 [106] standard limit. The increase in voltage THD will depend on the capacity and the number of inverters connected to the network.

Conversely, the current THD has an inverse relationship with generated PV power due to the fundamental current reduction. The measured results show that the current THDs have high values at low output power levels; and lower values around 3% during rated output periods, which are with respect to the fundamental current. However, during rated conditions, the harmonic injections from PV systems will have a negative impact on the distribution

transformer and adjacent distribution network. In addition, the distribution network contains different linear and nonlinear loads, power electronic based loads and heating loads. The proliferation of these types of loads means the distribution networks are already very sensitive in nature and with the integration of PV systems can cause severe impacts. As the generated PV harmonics may be added or subtracted with the network harmonics, they can have a subtle effect on the network.

In addition, field measurements were recorded at the distribution transformer for the same days to analyse the impact of these PV systems at the integration point. The data from the PQ meters provides a K-factor of 1.2, where the K-factor is the sum of the squares of the individual harmonic currents, times the harmonic squared, divided by the rated current as expressed in equation (5.2).

$$K - factor = \sum_{n=1}^{\infty} \left[\frac{I_n}{I_{rated}}\right]^2 n^2 \qquad (5.2)$$

From the standard IEEE C57.110-1998 [124], the distribution transformer is de-rated to 80% of its maximum capacity. The measured voltage and current THDs at the transformer are plotted in Figure 5.15.

(a) Percentage of Voltage THD at the Distribution Transformer TX2

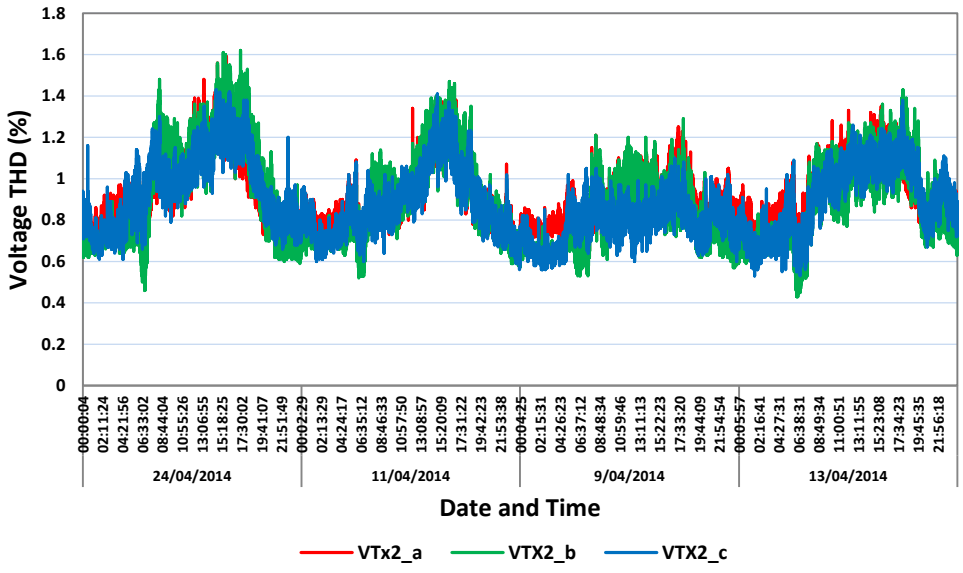

(b) Percentage of Current THD at the Distribution Transformer TX2

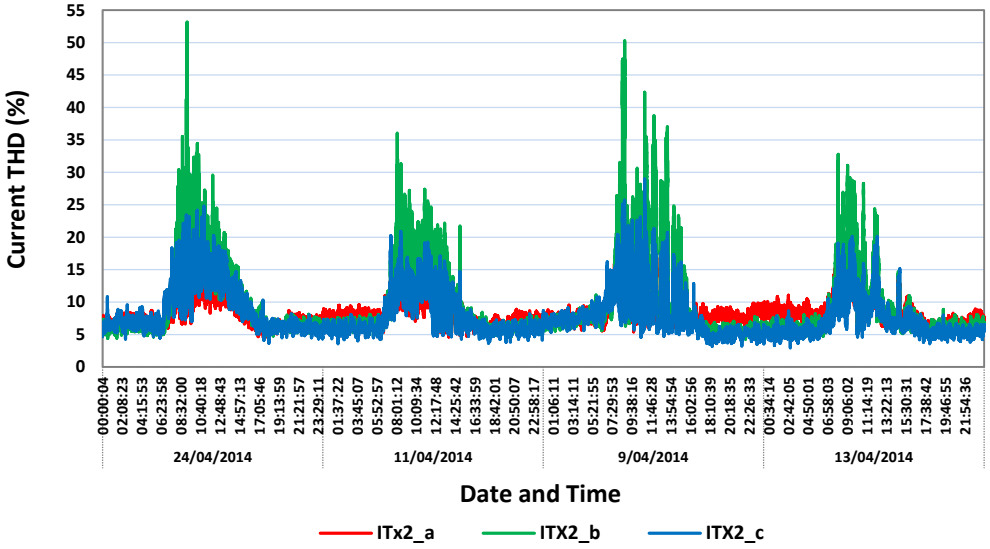

Figure 5.15. Harmonic Measurements at the Distribution Transformer TX2 for the Selected Days.

Results show that the voltage harmonics increased from 0.6% to almost 1.6% during the daytime, which is almost 1% of the variation. Noticeably on the supply side, the impact on the network voltage is less compared to the feeder end node due to voltage reduction. The measured voltage THD levels are shown to be within the limits; however, the network has filters and potential transformers, which eliminate higher harmonic components. It can be estimated that the voltage THDs will be more severe in the network without filters. In addition, the measured current THDs increased from 7% to almost 53% in the case of rated conditions, which is an aggregation of harmonics from the loads and PV systems. However, considering the worst day, the network current THD with a value of about 25% (with only load operation) can be seen as no PV condition in the simulated scenario. Hence, during midday and with PV, the THD is increased to almost 50%. It is observed that the field measurement results follow a similar trend as that of the simulated results.

To study the impact of current harmonics flowing in the transformer, K-factor measurements for the corresponding days have been taken and are shown in Figure 5.16. K-factor is a measure to estimate the influence of harmonics on transformer temperature and to overrate or de-rate the transformer to handle the worst conditions. It is noticed that during low PV power days, the K-factor values are in the range of less than 2. Results show that during the daytime, the K-factor values increase due to PV power injection. During cloudy days, the K-factor value is very high, about 10 when the PV generated maximum power, which

designates the proportion of harmonic content flowing in the network. If the K-factor value is higher, the greater are the heating effects, which indicate the existence of current harmonics in the network.

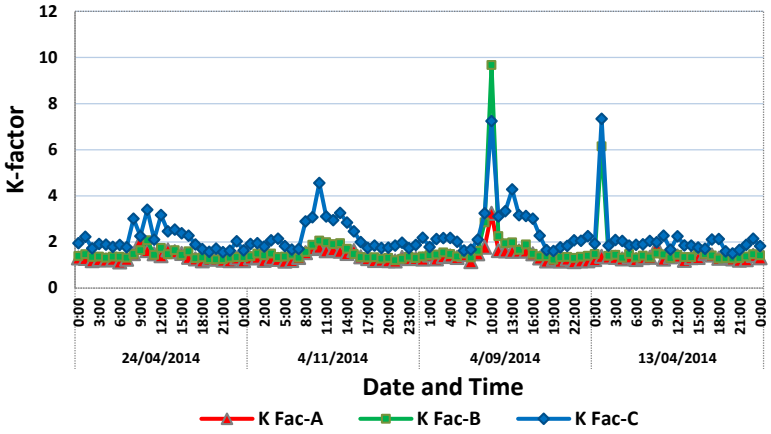

Figure 5.16. K-Factor Measurements for the Corresponding Days at the Transformer.

Highly distorted currents flowing in the grid can cause overheating of distribution transformers, which in turn overheat neutral conductors, tripping the circuit breaker, overstressing of power factor correction capacitors and skin effect [55]. In addition, subtle effects can lead to increased costs due to unnecessary maintenance and equipment replacements. So, focus on this issue and the need to take preventive measures is required. Finally, analysis has been carried out on the 11kV side (HV) and THD measurements for the voltage and currents are plotted in Figure 5.17.

(a) Percentage of Voltage THD at the HV Line

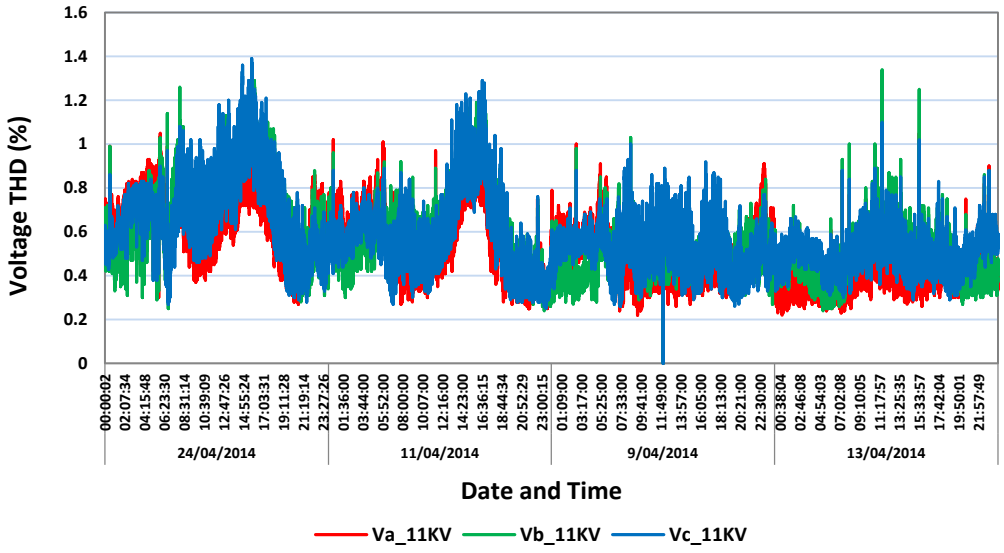

(b) Percentage of Current THD at the HV Line

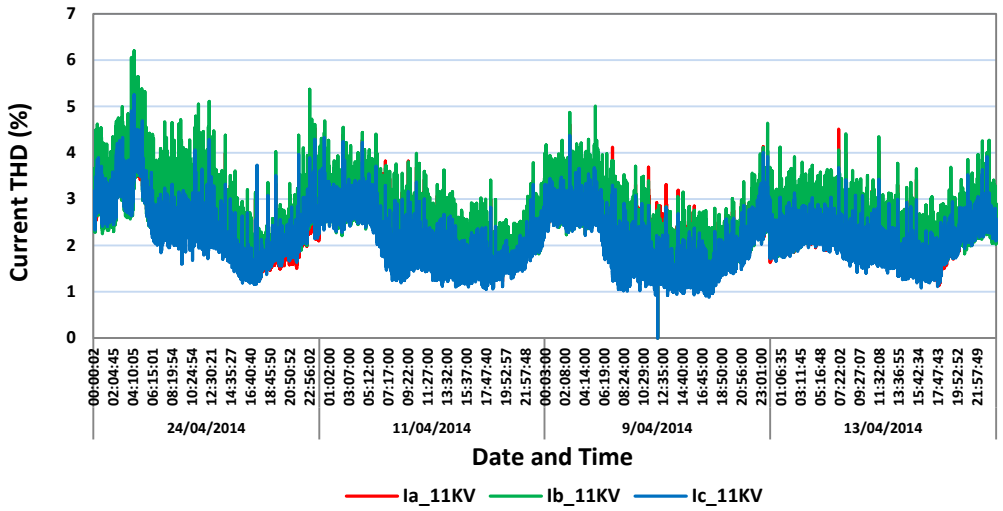

Figure 5.17. Harmonic Measurements at the HV Line.

Results show that the voltage THD has a similar tendency as the transformer voltage THDs. The voltage distortion varies with PV output power and drops during evening times. However, the current harmonic distortions have an inverse trend, for instance during the afternoon, the current THD reduces considerably. It can be seen that the THD values are oscillating from 1% to about 5% during a sunny day. It implies that there is a drastic rise in current THD by 4% that can cause adverse effects in the neighbouring network. In addition, the high integration of PV systems and the network configurations can excite harmonic resonance, which will have severe harmonic distortion levels in both voltages and currents.

5.5. Summary

This chapter has analysed the harmonic characteristics of grid connected PV systems for variations in solar irradiation. In addition, this research has highlighted the individual harmonic emissions and their relative interference associated with PV inverter penetration in various scenarios. The harmonic analysis has been performed through simulations in two case studies by considering with and without the presence of harmonics in the supply network. For this study, the IEEE-13 bus distribution system has been considered. Furthermore, to simulate a real-time network scenario, several types of probabilistic nonlinear loads were incorporated in the network for harmonics injection. Moreover, the analysis has been carried out through field tests conducted at the University of Queensland PV site under real operating conditions. For this purpose, Fluke power quality analysers were connected at the inverter level for measurement purposes. The measurement results were captured and compared with simulation

results. Results show that the harmonic behaviours of voltage and current waveforms are comparable with simulation trends. The individual voltage harmonics had a linear relation to the solar power generation but the current harmonics had an inverse relationship. The individual voltage and current harmonics during rated power levels are within the limits prescribed by the IEEE and AS/NZ standards. Moreover, with multiple PV integrations the current harmonic levels appeared to be minimized due to increase in fundament current, however the harmonic magnitudes incremented with every parallel PV penetration.

Further, a potential issue of increased harmonic distortion levels on a low voltage distribution system with high penetration of PV systems has been assessed. To characterise the effect of PV inverter control strategy on the network harmonic contribution level, two modern PV inverter models were considered. A thorough harmonic impact analysis was carried out through simulations for different case studies with the integration of PV systems in the unbalanced distribution network. This analysis has also considered harmonic distortions associated with various power electronic based nonlinear loads. Furthermore, a field investigation was performed at the University of Queensland PV system. The harmonic field measurements, recorded by various PQ analysers, at the LV and HV sides of the network for different operating conditions and scenarios were collected through online JAVA programs. Moreover, the simulation results were validated with real-time harmonic measurements. Simulation results show that the THDs of voltage and current are exceeding the IEEE limits when the number of PV systems increases in the network. The harmonics generated from PV systems are multiplied in nature due to an increase in individual voltage magnitudes. Simulation case studies revealed that the network harmonic levels increased with multiple installations at the same node compared to the dispersed integration. Measurement results show that the THD trends follow similar trends as with simulation results. Results shows that the current THD has high values at low power levels and lower values at rated condition, which are dependent to the fundamental component. However, during rated condition, the harmonic injections from PV systems have negative impact on the distribution transformer and adjacent distribution network. Further investigation will be continued to understand the impact of PV systems on network harmonic resonance that is presented in Chapter 6.

CHAPTER 6

HARMONIC RESONANCE ISSUES WITH PV PENETRATION

6.1. Introduction[1]

The main objective of this chapter is to investigate the harmonic resonance issues, which can be exacerbated by PV system integration into the LV network. Although issues associated with the PV systems on the distribution grid are widely analysed, the harmonic resonance problems related to PV system penetration and their controller interactions have rarely been assessed and reported. For this purpose, a harmonic analysis has first been performed through simulations in two case studies. Also in this investigation, two types of PV inverter control topologies are considered to study the effect of PV systems dynamic interaction in exciting harmonic resonance conditions in the network. Furthermore, the field measurement data obtained from a real network has been analysed and verified to validate harmonic resonance issues.

[1]This chapter is organised with the following reference:

Annapoorna Chidurala, T. K. Saha, and N. Mithulananthan, "Harmonic Resonance on the Distribution Network with PV Penetration and Field Measurements Validation," in preparation, to be submitted to International Transactions on Electrical Energy Systems Journal by September 2016.

This chapter is organized as follows; Section 6.2 represents the harmonic resonance mechanism accompanied with PV system penetration. Section 6.3 describes the test system and an approach to the simulation analysis. Section 6.4 represents results and discussion with simulations as well as validation by field measurements. The approach for field measurements at the University of Queensland (UQ) PV network is also presented in Section 6.4.2. Finally, the summary of this chapter is presented in Section 6.5.

6.2. Harmonic Resonance Mechanism Associated with PV Systems

Resonance conditions exist in the network when network capacitive reactance and inductive reactance become equal at a particular frequency, known as resonance frequency. In general, the network can have multiple resonance frequencies depending on the system configuration and characteristics. These resonance frequencies will be a major issue when they coincide with any of the induced individual harmonic frequencies in the network. The type of resonance may be series or parallel, which are caused by the series and parallel arrangement of the distribution network passive elements.

Typically, harmonic resonance incidence depends on network configuration, operating conditions, type and capacity of load and PV systems. Series resonance causes the total reactance to be virtually zero at the resonance frequency. Therefore, the network only consists of resistance and provides a low system impedance path, which will result in amplification of harmonic currents for a small distortion in voltage. Parallel resonance makes the equivalent impedance high, which creates to the amplification of harmonic voltages [63], [45]. In a critical case at the resonance frequency, a relatively smaller distortion in the current can create a higher voltage distortion.

The equivalent single-phase harmonic model of a PV connected distribution grid is shown in Figure 6.1. This configuration ignores the impact of a current controller circuit and the PV inverter bridge output voltage (V_x) is represented as a harmonic source, which contains a range of voltage harmonics. In the figure, Z_s represents the total impedance of the transformer and line; Z_L denotes the net impedance of loads. Therefore, the total grid impedance is simplified as Z_g ($Z_s//Z_L$). The injected harmonic current and corresponding voltage at the point of common coupling (PCC) can be expressed as given in equations (6.1) and (6.2). These equations include the effect of V_x, grid voltage and are also influenced by the combined effect of grid and filter impedances.

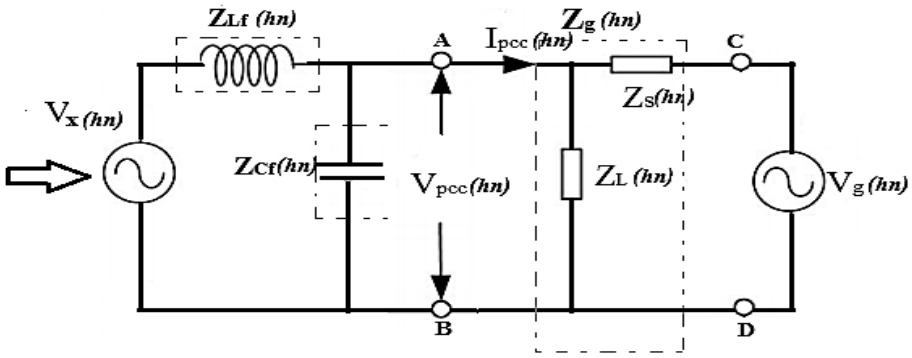

Figure 6.1. Single-phase Equivalent of Grid with PV System Connected at PCC.

$$I_{pcc}(h_n) = \frac{V_x(h_n)Z_{Cf}(h_n) - V_g(h_n)Z_{Lf}(h_n) - V_g(h_n)Z_{Cf}(h_n)}{Z_g(h_n)Z_{Cf}(h_n) + Z_{Lf}(h_n)Z_{Cf}(h_n) + Z_{Lf}(h_n)Z_g(h_n)} \quad (6.1)$$

$$V_{pcc}(h_n) = \frac{V_x(h_n)Z_g(h_n)Z_{Cf}(h_n) - V_g(h_n)Z_{Lf}(h_n)Z_{Cf}(h_n)}{Z_g(h_n)Z_{Cf}(h_n) + Z_{Lf}(h_n)Z_{Cf}(h_n) + Z_{Lf}(h_n)Z_g(h_n)} \quad (6.2)$$

Where, the symbols h_n represent the nth harmonic order.

The resonance phenomenon associated with the PV system in the distribution network is a complex combination of parallel and series resonance. The inverter output impedance for an LC type filter is $Z_{inv} = Z_{Lf}//Z_{Cf}$. Therefore, for the given circuit, the net impedance of the network seen at the PCC is as in equation (6.3). For instance, if the network includes shunt capacitor banks then the Z_{Cf} can be a combination of filter and capacitor banks.

$$Z_{har\_AB} = \frac{Z_{Lf}Z_{Cf}Z_g}{Z_gZ_{Cf} + Z_gZ_{Lf} + Z_{Lf}Z_{Cf}} \quad (6.3)$$

For a parallel resonance condition, the impedance reaches its maximum value when the denominator approaches the minimum value that can be represented as given in (6.4).

$$f_{res} = \frac{1}{2\pi}\sqrt{\frac{L_f + L_g}{C_f L_f L_g}} \quad (6.4)$$

In contrast, the inverter output impedance can also form a series circuit with the associated network impedance. Therefore, in this case the impedance seen at the source side is given in (6.5). For a series resonance condition the impedance becomes minimum when the numerator value approaches the minimum value, which is also expressed as given in equation (6.4).

$$Z_{har\_CD} = \frac{Z_{Lf}Z_{Cf} + Z_gZ_{Cf} + Z_gZ_{Lf}}{Z_{Cf} + Z_{Lf}} \quad (6.5)$$

As the number of parallel PV inverters increases in the distribution network, the resonance frequency might be altered. For identical PV systems, the filter parameters are equivalent to

L_f/n and nC_f. Therefore, the modified resonance frequency can be obtained as given in equation (6.6).

$$f_{res} = \frac{1}{2\pi}\sqrt{\frac{L_f+nL_g}{nC_fL_fL_g}} \tag{6.6}$$

In practice, PV systems consist of PV panels, Maximum Power Point Tracking (MPPT), a boost converter, a DC/AC inverter and an interfacing LC filter as shown in Figure 6.2. The harmonic emission issues related with PV inverters strongly depend on the type of control scheme and the output filter design which can configure a resonance circuit with the grid. Frequent dynamic interactions between multiple PV inverter system control loops and the supply network can also excite the potential resonance conditions in the grid. Moreover, during the resonance, the amplification of voltage and current harmonics might exceed IEEE 519 standard limits [53], even if each PV system satisfies the standards in the network.

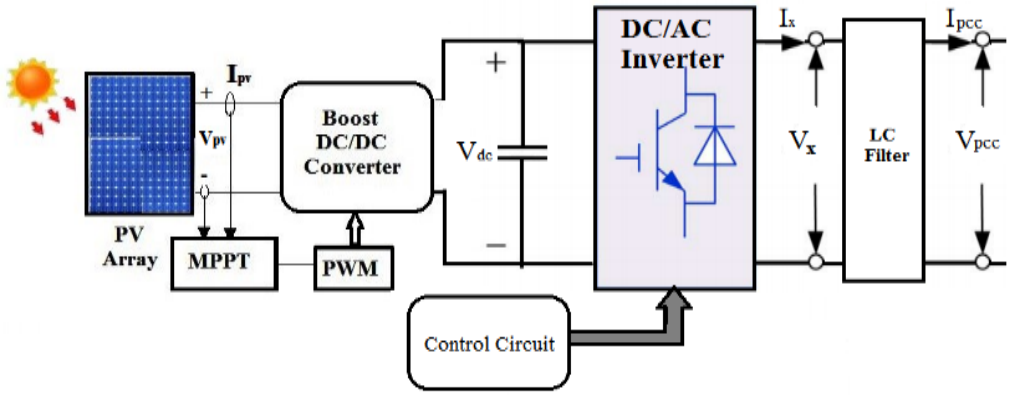

Figure 6.2. Detailed Three-phase PV System Configuration.

6.2.1. Impact of Grid Connected PV Inverter Control Strategies

To analyse the impact of a PV system controller interface on the grid harmonic resonance occurrences, two types of control topologies have been considered. Figures 6.3 and 6.4 show the control block diagrams of the Current Controlled Voltage Source Inverter (CCVSI) and Current Regulated Current Source Inverter (CRCSI) type PV systems respectively [114, 125].

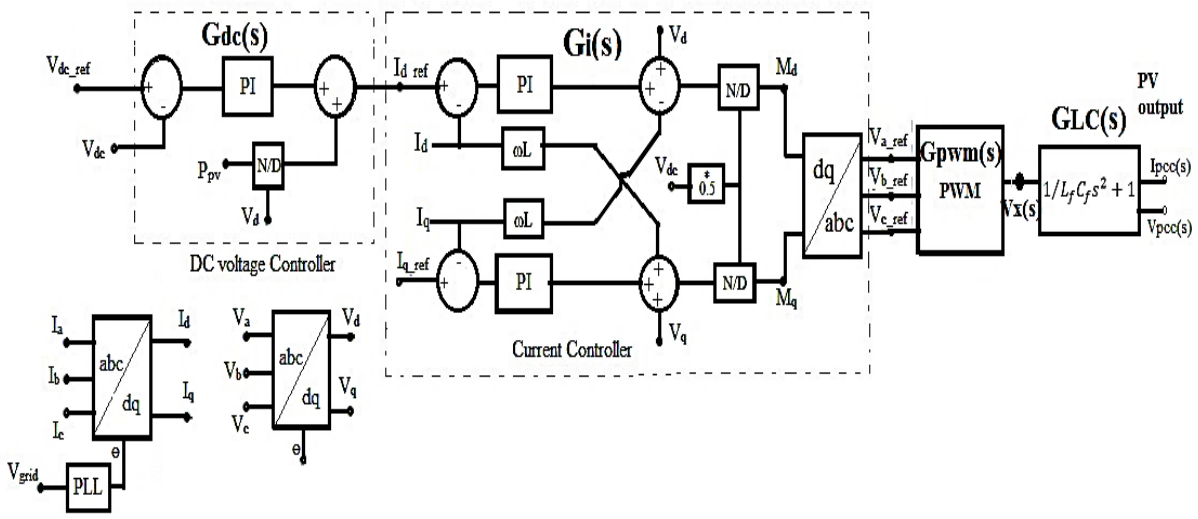

Figure 6.3. Control Circuit of Current Controlled Voltage Source Inverter.

The current regulated PWM control method is applied to operate the voltage source PV inverter. This control topology has two controllers', namely outer DC voltage controller and current controller as shown in Figure 6.3. The DC voltage controller controls the dc capacitor voltage by varying the active current injections. The current controller utilizes the measured inverter output currents and output from the DC controller to generate references for the switching. It then regulates the output current indirectly by regulating the voltage at the PV inverter output. According to the control scheme, the VSI output voltage (V_x) is determined by the control parameters and PV output power. The power flow variations or disturbance caused by PV inverters due to transients in solar irradiation can have an inevitable impact on the controller functions, which can influence the inverter output impedance. The dynamic behaviour of the closed-loop control system can affect the distribution network harmonic levels. The detailed PV inverter model has been considered to study the influence of PV power transients. The resultant PV inverter output impedance involving control system parameters in s-domain is expressed as given in equation (6.7).

$$Z_{inv}(s) = \frac{sL_f + G_{dc}(s)G_i(s)G_{pwm}(s)}{L_f C_f s^2 + C_f G_i(s)G_{pwm}(s)s + G_{dc}(s)G_i(s)G_{pwm}(s)} \qquad (6.7)$$

It is noted that impedance Z_{inv} depends on the control loop gain factors and PWM switching. The interaction of PV output impedance with the grid can modify the total network impedance (i.e., as in equations (6.3) or (6.5)), which in turn shifts the harmonic resonance frequencies in the distribution network. The current and voltage controllers are tuned by a trial and error method to achieve optimum performance with faster response time and minimum overshoot.

Conversely, current regulated CSI PV topology utilizes grid voltages to track the phase angle, which is used to synchronize the PV inverter output with the network voltage. The preferred real and reactive powers are compared with the actual generated powers and the error is processed through PI controllers to produce direct and quadrature components of real and reactive currents. Then by using inverse synchronous reference frame, the stationary reference currents will be generated, which mainly depend on the transients in the PV system output. This control technique uses a hysteresis controller to generate firing pulses. This type of current controller is simple and faster in dynamic response [125]. Similar to the CCVSI control scheme, the inverter output impedance also comprises the gain factors of control loops.

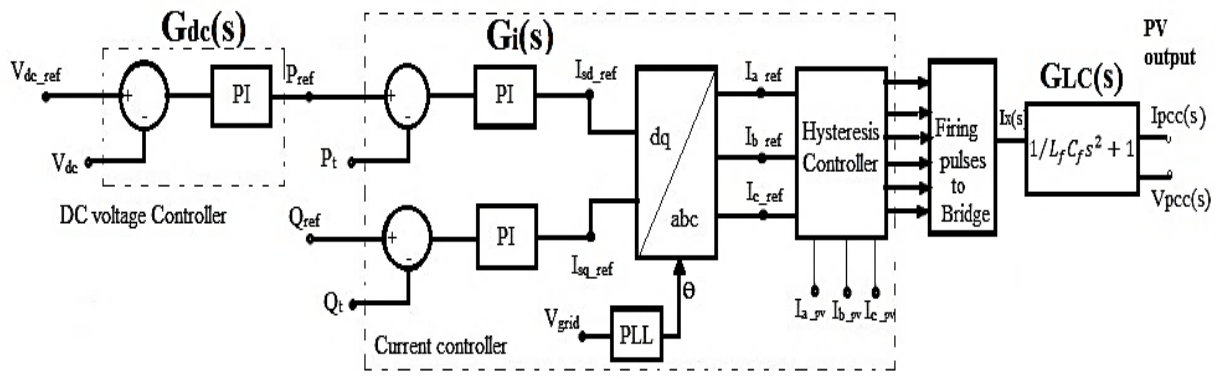

Figure 6.4. Control Circuit of Current Regulated Current Source Inverter.

The analysis has been carried out to investigate the influence of different PV inverter system integrations and their operational interference on the harmonic resonance phenomena. This is developed and tested in PSCAD software to assess the PV inverter output harmonic limits according to the standards IEEE 929-2000 [106] and AS 4777.2:2005 [107].

6.3. Test System Approach and Simulation Study

The IEEE-13 bus distribution network is used for this study, which was shown in Figure 5.1 (refer Chapter 5). The investigation has been carried out on two case studies by considering with and without the presence of background harmonic distortions in the supply network. Loads are modelled as constant power, constant impedance and constant current loads for the first case study as explained in the previous chapter. The simulations have been performed to verify the load flow and harmonic distortions in the network. The parallel connection of these loads can have less influence on the grid impedance, therefore the impedance Z_g (refer Figure 6.1) is approximately equal to Z_s.

In the second case study, the test system loads have been replaced with nonlinear loads for harmonic injection. For this purpose, different types of nonlinear load such as power electronic based single-phase diode bridges with RL, RC loads and motor and heating loads have been considered [39]. These loads include CFL, computer, TV, adjustable speed drives (ASD), DC drives and single-phase induction motor and lift motors as mentioned in Chapter 5. Therefore, the network impedance includes the effect of these loads, which might shift the system resonance frequencies. In the IEEE-13 bus network, the detailed load models are aggregated in each phase and distributed at the feeder nodes from load_1 to load_4. Simulations have been performed to verify the injected harmonic levels in the distribution network to meet IEEE 519 standard. According to IEEE 519:2014 standard, the voltage THD for <1kV voltage level should be less than 8% and for 1kV<V<69kV level the THD should be less than 5%. In addition, the current Total Demand Distortion (TDD) limit should be less than 5%. In this paper, all the simulations have been performed at full load condition to eliminate the complexity in determining the harmonic distortion levels, so TDD is the same as THD.

6.4. Results and Discussion

In this research, harmonic resonance phenomena on the network associated with the PV systems have been assessed through simulations on the IEEE 13 bus network as well as with harmonic field measurements. Here, the harmonic resonance conditions are identified by the amplification of THDs and frequency versus impedance scan plots.

6.4.1. Simulation Study on IEEE-13 Bus Distribution Network

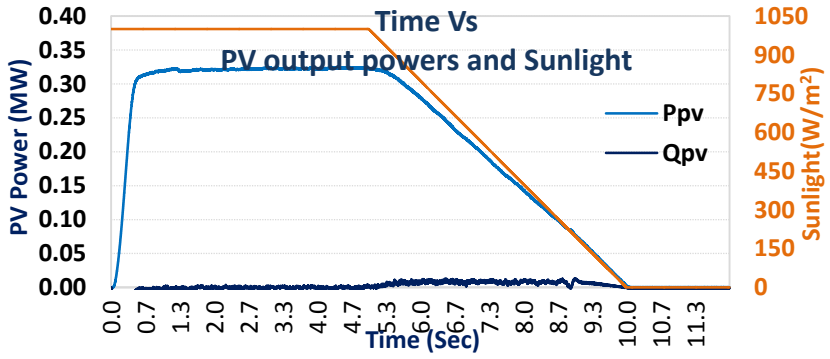

Figure 6.5. Time versus Solar Irradiation and PV Output Pattern.

In this research, the analysis has been performed in two case studies as mentioned earlier. In each case study, CRCSI and CCVSI based PV systems have been analysed. In each case study, the dynamic operation of two PV inverter control topologies for variations in solar irradiation have been considered to characterise the harmonic resonance modes in the network.

Regarding this, a comprehensive model of PV source has been considered. This model has all the dynamic characteristics similar to a real PV system. In this study, a typical solar irradiation profile is applied to the PV system and the corresponding PV active and reactive powers are shown in Figure 6.5. It is noticed that the output of the PV system has a linear correlation with solar irradiation.

6.4.1.1. Case Study-I: Without Background Distortions in the Network and with PV Systems

In the first scenario, a CRCSI PV inverter system of 330kWp capacity is considered, which operates at close to unity power factor. Simulations have been carried out to analyse the harmonic distortion levels in the grid with PV operation at both rated and decreased output power conditions. In every simulation, 5 PV systems of the same capacity are connected consecutively at the PCC to estimate the severity of harmonic contributions in the network.

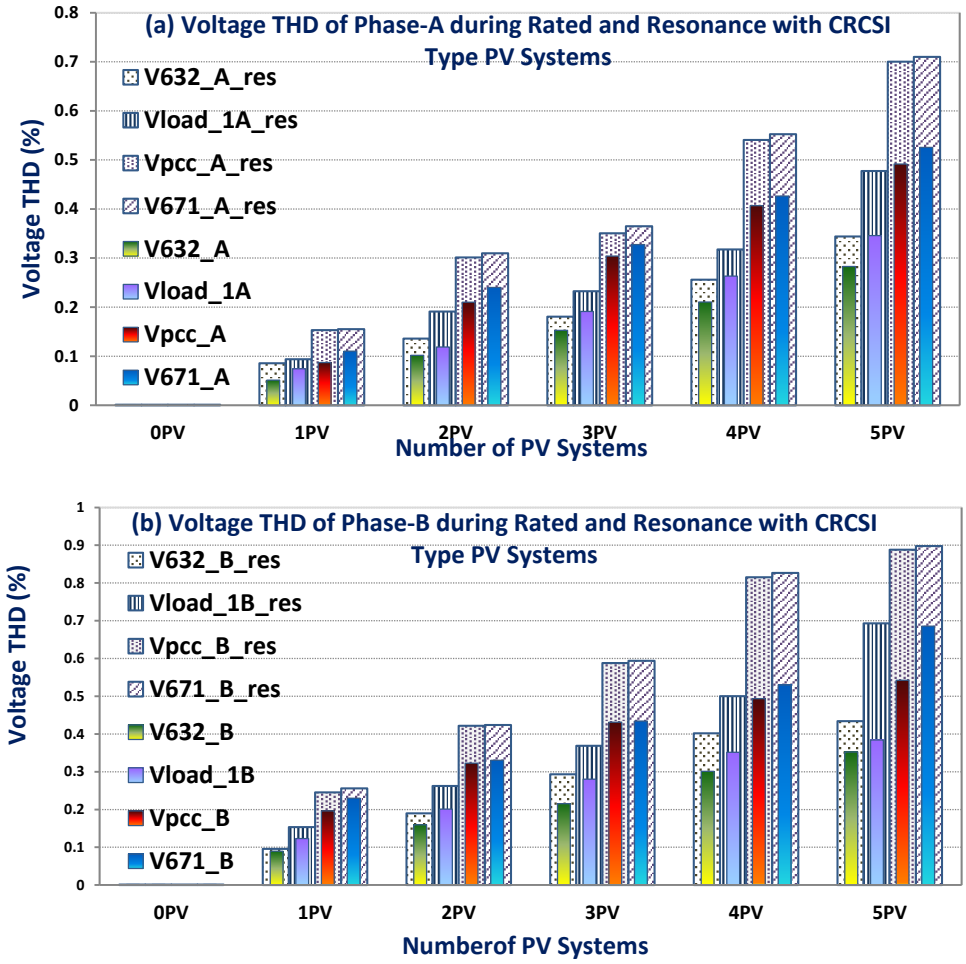

Figure 6.6. Percentage of Voltage THDs at Various Nodes for Phases A and B with CRCSI.

During rated conditions, the measured voltage and current THDs at various buses for both phases A and B are plotted as dark coloured bars shown in Figures 6.6 and 6.7 respectively. The subscripts, for instance, 632_A, load_1A, PCC_A, 671_A represent the corresponding node voltage/current harmonic distortion in the respective phase. Also, 0PV indicates with no PV condition and the numbers 1PV, 2PV, 3PV, etc. denote the number of PV systems integrated into the network. The harmonics produced from the PV inverter systems not only distorts the system voltage but also affects the neighbouring devices due to the harmonic interface. It can be seen that for every PV inverter integration, the voltage THDs at each node have increased and the effect is higher at bus 671 and the PCC compared to the supply side nodes. However, the current THDs at the before integration point is increased due to a reduction in the current magnitude with PV power injection. It is noticed that the harmonics generated by the PV systems are mainly due to active power injection and switching harmonics.

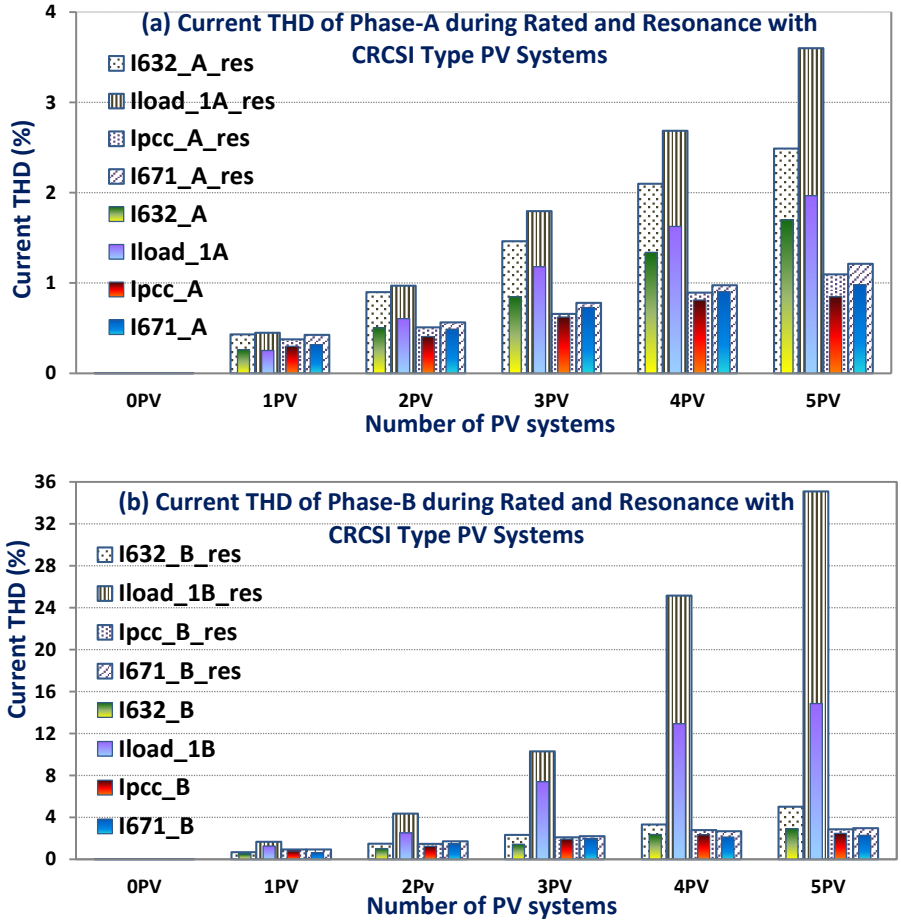

Figure 6.7. Percentage of Current THDs at Various Nodes for Phases A and B with CRCSI.

Subsequently, simulations have been continued for decreasing PV power trends (rest of the time from 5-12 sec) as indicated in Figure 6.5. Remarkably, in all the simulations the THD of voltage and currents in the grid are elevated abruptly during the period of time 5-6.5 sec. At

this instant, the values of voltage and current THDs were also measured and presented as pattern bars in Figures 6.6 and 6.7 respectively. It can be seen that the network current THD is more exaggerated than the voltage THD. In Figure 6.6, the net induced harmonic voltage is increased by nearly 0.2% for each PV system integration. Figure 6.7 shows that the current THDs have remarkably raised at supply side nodes in each step of PV system integration during this period. It can be seen that the current THD at the before connection point was calculated to be high in phase B of around 35% compared to the current THD during rated conditions with 5 PV systems. This value is outside the THD limits according to IEEE 519 standards. Conversely, phases A and C are less affected and have THD values of less than 5%. The level of THD in each phase is different due to unbalanced loading levels and line configurations of the test network. Usually, a decrease in PV power injection causes an increase in supply current magnitude. Therefore, the grid current THD reduces with respect to the increase in fundamental current. Despite this fact, during this period the harmonic THD profile follows the inverse trend.

Even though the PV inverter systems are individually satisfying the harmonic limits during the rated conditions, these PV systems are negatively interacting for variations in PV power generation. Furthermore, it is noted that the harmonic emissions from several identical PV systems connected at the same node could be different due to their independent operation. Also, the harmonic magnitude and phases are different for each inverter and the resultant harmonics may result in harmonic superimposition. Here, the amount of increase in harmonic distortion level is varying with the number of PV inverter systems. As the number of paralleled PV systems increase, then the output current lower order harmonic magnitudes increase [5], [9]. Moreover, the harmonic injection depends on the current controller performance and filtering.

This PV inverter control topology includes a fixed band type hysteresis current controller due to its simplicity and response. Despite its advantages, the hysteresis current controller has an issue of variable switching frequency, which can lead to pollution of the inverter output current. Moreover, the variation in the PV output power changes the inverter reference currents, which in turn introduce disturbances in the current controller response. Therefore, the inverter output currents contain significant harmonics, which are unable to be suppressed by the interfacing filter, injected into the grid lead to the occurrence of harmonic resonance. The level of distortions in the current is found to be higher realizing a series resonance condition at this period of time (i.e., at 5.5 to 6.5sec). Further decrease of PV power injection caused THDs to reduce in the grid that is due to sustain in the controller response. Severe harmonic currents

flowing through the grid can cause transformer overheating and overloading of the neutral conductor.

Consequently, to confirm the system impedance variation due to multiple PV systems integration a frequency scan has been conducted. The positive and zero sequence impedance variations with respect to the frequency at the PCC for before and after PV systems integration are plotted in Figure 6.8. Usually, the positive and negative sequence impedances are similar to each other but the zero sequence may differentiate them. Note that the network shunt capacitor banks are in operation during simulations. It can be seen that the grid positive sequence impedance without PV units has resonance frequencies of 480Hz (8^{th}) and 1440Hz (24^{th}) at peak and lower peak points respectively, which are not harmful harmonics.

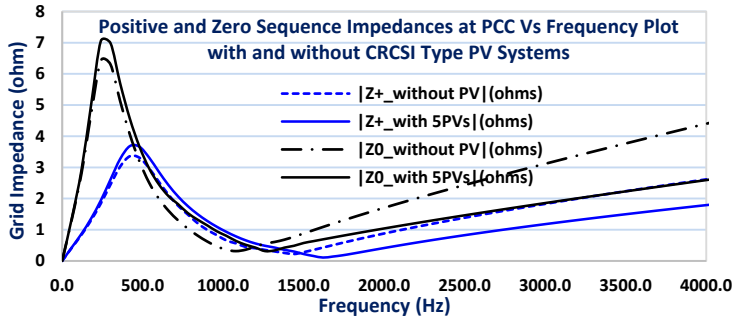

Figure 6.8. Impedance versus Frequency Scan with and without CRCSI PV Systems at PCC.

However, the system impedance with parallel PV systems integration is changed significantly and a frequency shift has occurred. It is to be mentioned that the PV inverter output impedance is a result of the inverter current control and filter components (refer to equation (6.7)). The frequency of the peak impedance moves nearly at 7^{th} harmonic; however, the impact is negligible and the harmonic magnitude of the voltage and current are well within the limits. Conversely, with PV system integration the network lower impedance resonance frequency is shifted to the 27^{th} harmonic, which is close to the harmonic frequency injected by the PV systems. Note that the PV system was the only harmonic source connected to the network. On the other hand, zero sequence impedances with and without PV systems have peak resonance frequencies at fairly close to 240Hz shown in Figure 6.8. However, similar to the positive sequence there is a frequency shift that occurred at the lower impedance peak from 18^{th} to 21^{st} harmonic order, which is close to the harmonic frequency. At these resonance frequencies, the harmonic current emissions from the PV systems are amplified and injected into the grid current, which leads to an excitation of series resonance.

In the second scenario, a CCVSI type PV inverter has been considered for the harmonic analysis. The PV system capacity is 330kWp and the switching frequency is chosen to be 2460Hz (41X60Hz). Similar to the previous scenario, the PV systems were integrated gradually in the test network at node PCC. Simulations have been carried out for rated and reduced PV output power levels. During rated conditions, the THD values possessed similar trends as in the first scenario, which can be observed in Tables 5.3 and 5.4 (refer Chapter 5). The increase in voltage THD with PV system is observed to be less than 1%. Moreover, due to supply current magnitude reduction the current THD is increased to about 25% on the supply side, which is at the before PV integration node. However, this current THD value is quite severe according to IEEE 519 standard. Further, the assessment has been performed for varying solar irradiation conditions. It is observed that the generated harmonics depend on the active power produced from the PV systems. From the results, the net voltage and current harmonic profile at after and before the PCC can be proposed as given in equations (6.8) and (6.9) respectively.

$$THD_{V\ at\ after\ PCC} = THD_{V\_withloads} + i * (\Delta THD) * \left(\% \frac{P_{act}}{P_r}\right) \qquad (6.8)$$

$$THD_{I\ at\ before\ PCC} = THD_{I\_withloads} + i * (\Delta THD) * \left(\% \frac{P_{act}}{P_r}\right) \qquad (6.9)$$

Where, ΔTHD is the voltage or current THD contribution with 1PV system (i.e., $THD_{with2PVs}$ - $THD_{with1PV}$); i = number of PV inverters; P_{act} and P_r refer to the actual and rated PV powers respectively.

Conversely, the network has not been affected by resonance phenomenon as compared with the first scenario. However, the harmonic resonance conditions are likely to change in the network and are influenced by the connected load, type of PV system penetration and their controller interactions.

6.4.1.2. Case Study-II: With Background Distortions in the Network and With PV Systems

In this regard, modern power electronic based nonlinear loads have been connected, which inject harmonics into the test system. Simulations have been performed and the measured voltage THD is in the range 2.5 - 3% and the current THD is calculated to be 4%, which are within the limits as per IEEE 519 standard. In the first scenario, a CRCSI PV system has been considered and simulations have been performed in the same way as the previous case study. Here, the harmonic emissions from the PV system contain switching harmonics and the harmonics due to distortion in the supply. Simulated results show that the voltage THD with

5PV system penetration is increased to 4.5-5.2% at the feeder end node 671 during rated conditions. Also, the current THD values have attained a high value of 9.5% and 7.6% at before and after the PV integration point, these exceed IEEE 519 limits. It is estimated that the harmonic levels in the network are observed as given in equations (6.8) and (6.9), which depend on the number of PV systems and the percentage of produced PV power. The harmonic distortion levels for rated PV operation can also be observed in Tables 5.5 and 5.6 (refer Chapter 5).

As in the second scenario, simulations have been carried out with the integration of CCVSI type PV systems in the same way. During the rated PV power level, the measured voltage and current THDs for phases A and B at various nodes are plotted (coloured bars) as shown in Figures 6.9 and 6.10 respectively. It can be observed that the network voltage and current THDs due to PV systems are increased to nearly 4.8% and 9.5% in phase-B respectively. Subsequently, simulations have been performed for decreasing solar irradiation levels. It can be seen that during the period from 5 to 6.5 sec, the voltage THD is increased from 4.8% to 5.4% with 5 PV systems at 671 node, which is violating the IEEE limits. It can be noticed that the rapid rise in voltage harmonic distortion is simulating a parallel resonance phenomenon. During the resonance, amplification of the 5^{th} and 7^{th} harmonics are more noticeable compared to the 3^{rd} order harmonic.

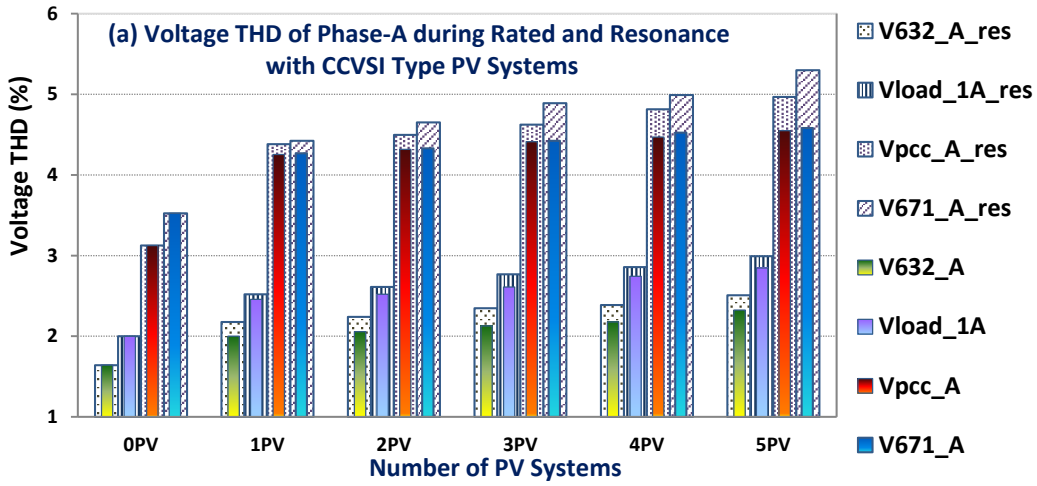

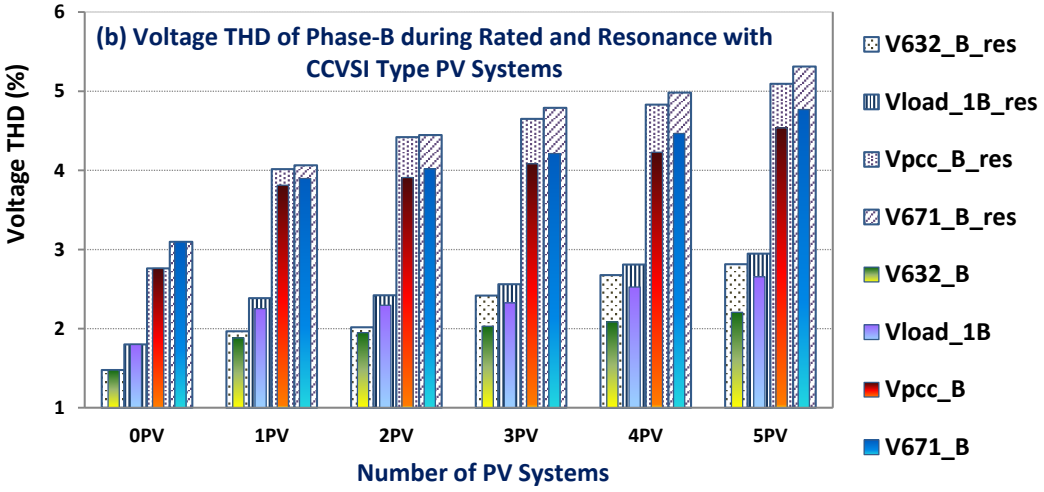

Figure 6.9. Percentage of Voltage THDs at Various Nodes for Phases A and B with CCVSI.

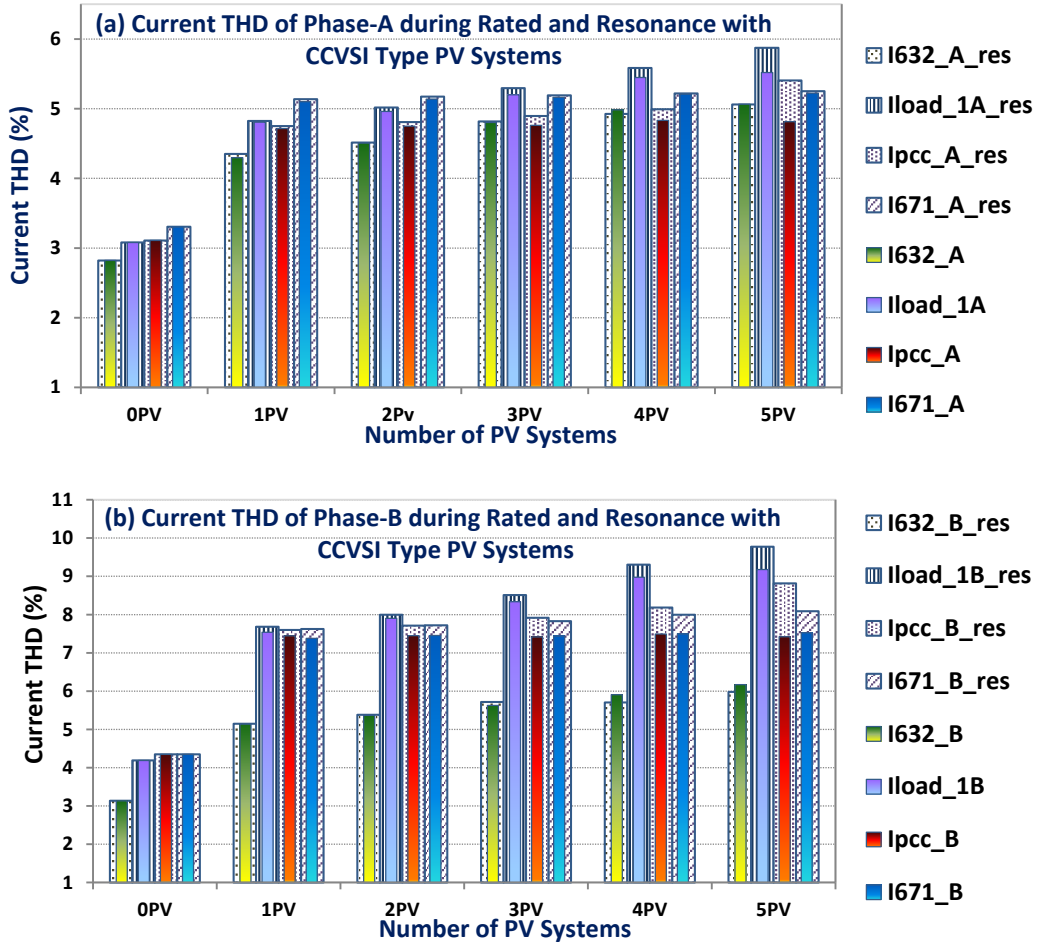

Figure 6.10. Percentage of Current THDs at Various Nodes for Phases A and B with CCVSI.

The current reference for each inverter is produced independently and is updated by the MPPT controller. The change in the inverter current reference due to solar irradiation variations is utilized in the current controller loop as shown in Figure 6.3, which can introduce a resonance condition in a few fundamental cycles. In addition, this type of PV inverter uses grid voltages

as a reference source for synchronization. Therefore, the variation in grid voltage harmonics also affects the inverter current controller performance. Hence, the dynamic operation of the current controller due to transient disturbances has increased the oscillations and ripples at the output of the PV inverter. As a result, the PV inverter injected high harmonic components into the network and was unable to be adequately suppressed by filters. These harmonic currents from the PV systems combining with network background harmonics result in amplification of voltage distortion at the PCC. The increase in voltage distortion depends on both the system impedance variation and the aggregate of harmonic currents injected by the PV system. Excessive voltage distortions can reduce the lifetime of the equipment connected to the network and increases the losses.

The system equivalent impedance will be different for the penetration of different PV inverter technologies. Similar to the previous case study, to verify the system impedance variation with the PV system integration, frequency scan analysis has been conducted. The frequency versus positive and zero sequence impedances are plotted in Figure 6.11 in the case of with and without 5PV systems integration. It is to be observed that the system with nonlinear loads has increased the system impedance and also affected the system resonance frequency points. The system impedance has both series and parallel resonance frequencies as in the previous case. In comparison, the lower peak resonance frequency of positive sequence impedance has been shifted from the 24th (refer Figure 6.8) to almost the 22nd harmonic due to the presence of nonlinear loads. However, the peak impedance has a resonance frequency close to 480Hz (8th), which remains the same. Moreover, the zero sequence peak and lower impedance resonant frequency points were not altered, which have frequencies at the 4th and 18th orders respectively.

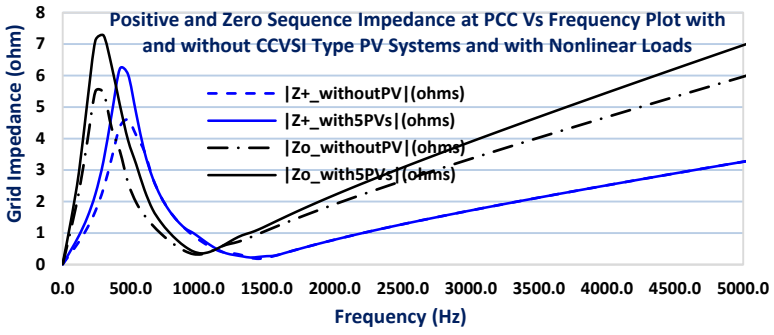

Figure 6.11. Impedance versus Frequency Scan with and without CCVSI PV Systems at PCC.

In addition, PV systems penetration at the PCC causes the sequence impedances to increase their magnitude at the peak resonant points and a frequency shift has also occurred. It can be seen that the peak resonance frequency is close to 7th order i.e., a shift in the frequency from 480Hz to 420Hz. In addition, the zero sequence impedance moves the peak resonance frequency to 300Hz. It is observed that these frequencies are close to the harmonic frequencies injected by both PV systems and nonlinear loads, which lead to higher voltage distortion in the network, achieving a parallel resonance condition.

6.4.2. Analysis of Harmonic Measurements at The University of Queensland PV Site

The UQ St Lucia campus has a large power network supplied by an 11kV line from the local distribution utility. The network is highly loaded with a broad range of machine loads, modern electronic devices and air conditioners. The total maximum load demand is about 23MW and has peak power demand between 6am to 6pm. The network is employed with nearly 40 substations to step-down the voltage from 11kV to 415V as mentioned in the previous chapter. The university has an installed solar PV system of 1.5 MW which is distributed across nine buildings to feed the peak demand. To evaluate the PV inverters interaction in the real distribution network, the harmonic study has been carried out at substation 11. At which, the PV array of 340kW capacity is installed individually on car parks 98A and 98B. Special three-phase grid-tied PV inverters are used to synchronize the PV output with the grid voltage and frequency. Substation 11 has two transformers of 750kVA, 11kV/415V as shown in Figure 5.13 (refer Chapter 5). It is important to note that the university network does not contain shunt capacitor banks; however, it has underground cables that can cause mutual capacitance between phases and ground.

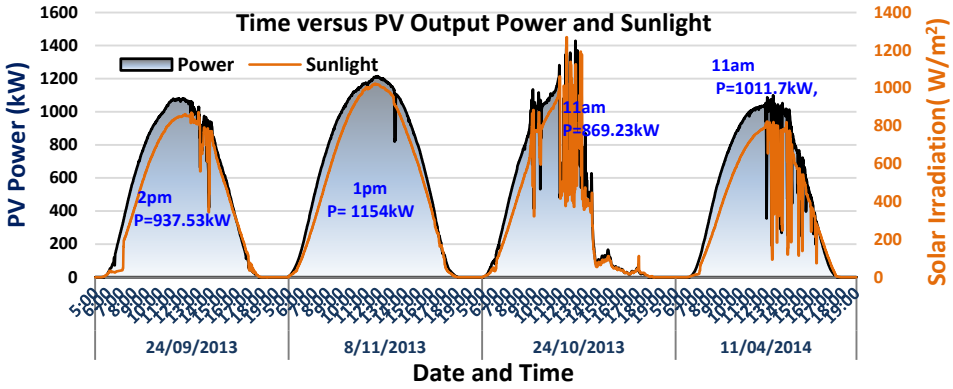

Figure 6.12. Time versus PV Output Power and Sunlight.

For the analysis, the harmonic field measurement data of 1-year was been collected through various power quality (PQ) meters connected at high voltage (HV) and low voltage (LV) levels of the network. These PQ meters recorded the data for every 5ms time resolution and then the data aggregation system recorded the data on an hourly basis. Figure 6.12 shows the time versus PV output power and sunlight for sunny and cloudy days, which were obtained using weather sensors.

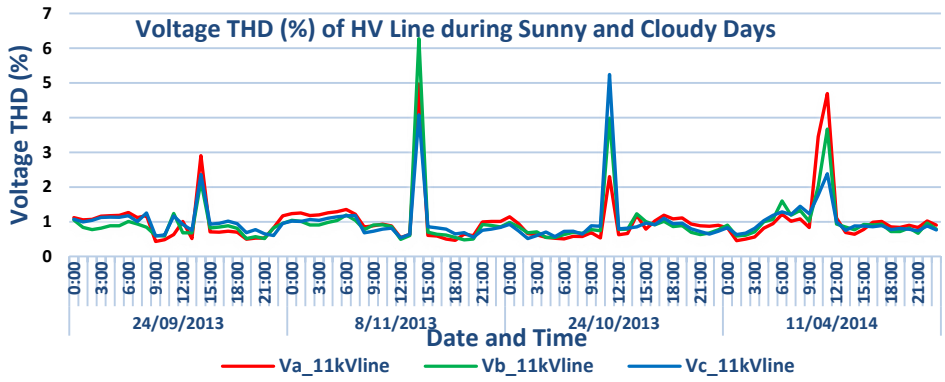

Figure 6.13. Percentage of Voltage THD at HV Side for Parallel Resonance Condition.

The high penetration PV systems and their associated operational behaviours affect the grid harmonic levels, which may excite resonance conditions in the network as discussed in section 6.2. In this study, the network resonance conditions are identified and analysed through amplification factors of voltage and current THDs. During the selected days, the corresponding voltage THDs of the HV line are plotted in Figure 6.13. Results indicate that significant peak voltage distortions are found on the HV side. It is noticed that the variation in PV output power due to fluctuations in solar irradiation has a considerable impact on network harmonic levels at different time intervals. The results show that the voltage THD is notably increased to about 6.25% during PV operation, which is violating the 5% limit as per EEE 519 standards. It can be seen that the voltage THD is more prominent in the network and might appear to be realizing a parallel resonance phenomenon similar to the simulation case study. The exact time and the corresponding PV power are indicated in Figure 6.12 at which the harmonic resonance has been noticed. Besides, the network THD levels other than these time periods are below 1.5%.

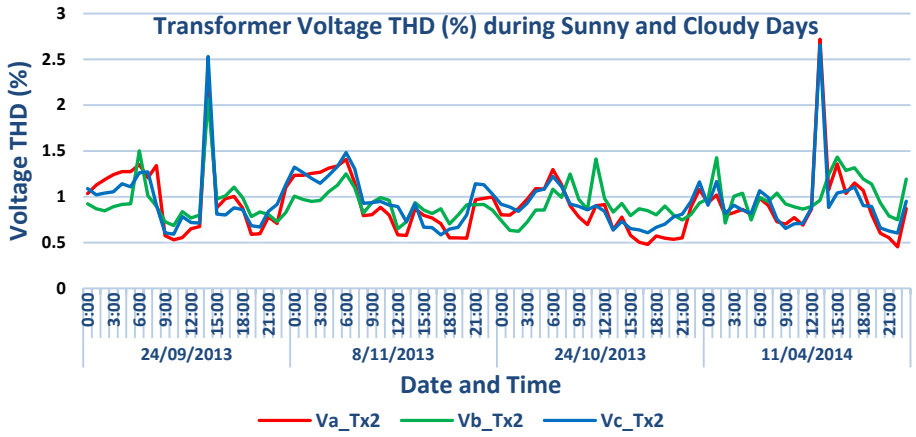

Figure 6.14. Percentage of Voltage THD at the Distribution Transformer TX2 for Parallel Resonance Condition.

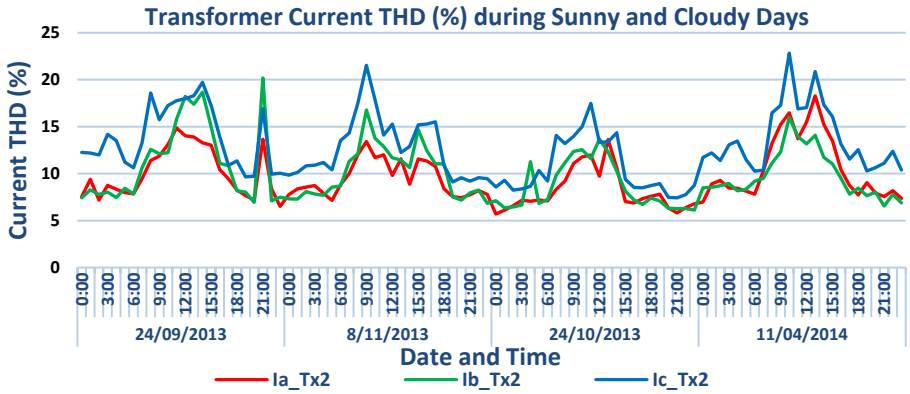

Figure 6.15. Percentage of Current THD at the Distribution Transformer TX2 for Parallel Resonance Condition.

In addition, the voltage and current THDs at one of the transformers (LV side TX2) were collected for the corresponding days as shown in Figures 6.14 and 6.15 respectively. It can be seen that the voltage distortion has peak values during resonance, which lies between 2.5% to 2.8%. It is essential to specify that the university has already been equipped with a capacitive voltage transformer which eliminates the high harmonic components. As a result, the harmonic levels are shown to be damped and are well within the limits. However, these distortions could probably be higher in the network without filtering equipment. Further, the current THDs are increased from 8% to 20% due to an increase in PV power injection, which are over the limits as specified by the standards.

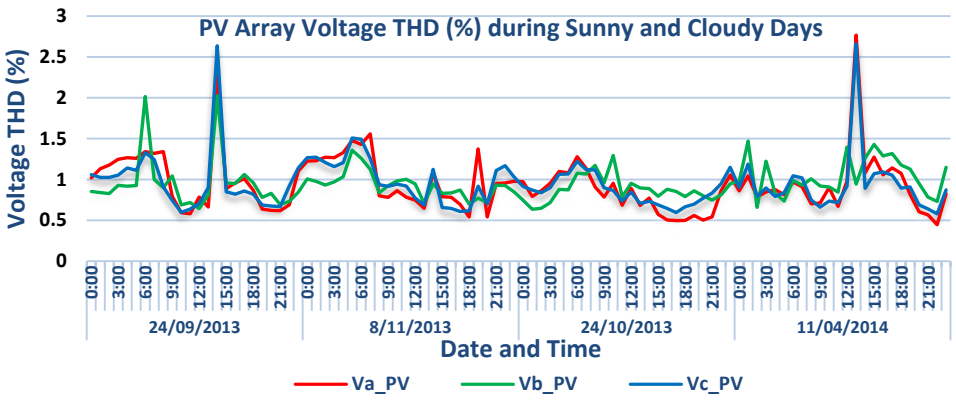

Figure 6.16. Percentage of Voltage THD at the PV Array Output for Parallel Resonance Condition.

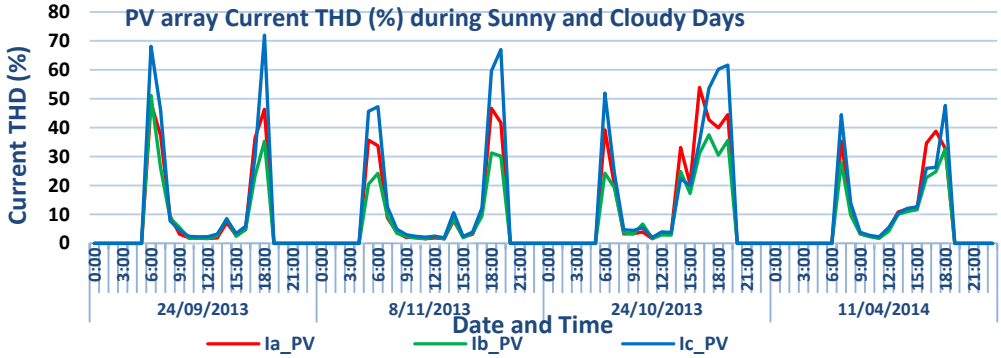

Figure 6.17. Percentage of Current THD at the PV Array Output for Parallel Resonance Condition.

Moreover, the measured voltage and current THDs at car park 98A PV array are plotted as shown in Figures 6.16 and 6.17 respectively. This PV system utilizes grid voltages as a reference source similar to the CCVSI type system. Although the PV system controller was initially designed to avoid resonance frequency during installations, the PV system switching and filter components can cause negative interactions with the grid. Due to instant variation in solar irradiation the PV inverter current controller can be caused to malfunction, which can inject distorted current into the grid. The injection of harmonic currents from several parallel connected PV inverters and their interaction can cause the PCC voltage to distort, which can lead to triggering of the resonance condition. Figure 6.17 shows the current THD is measured with respect to the actual current magnitude. It is observed that the current THD has an inverse correlation with the solar irradiation [9]. Results show that the voltage THDs at the PV array system integration node are more noticeable and have values nearly 2.8% during resonance.

Consequently, the network can also be subjected to series resonance. Therefore, to verify the harmonic interaction issues related to the PV inverter system performance on the network,

the PQ data has been analysed. The time versus PV output power and solar irradiation for the selected days, of sunny and average cloudy days, are plotted in Figure 6.18.

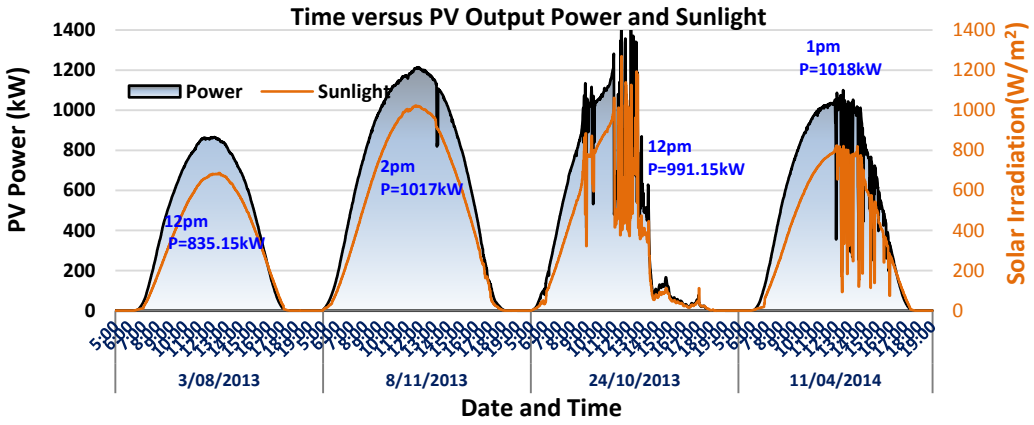

Figure 6.18. Time versus PV Output Power and Sunlight.

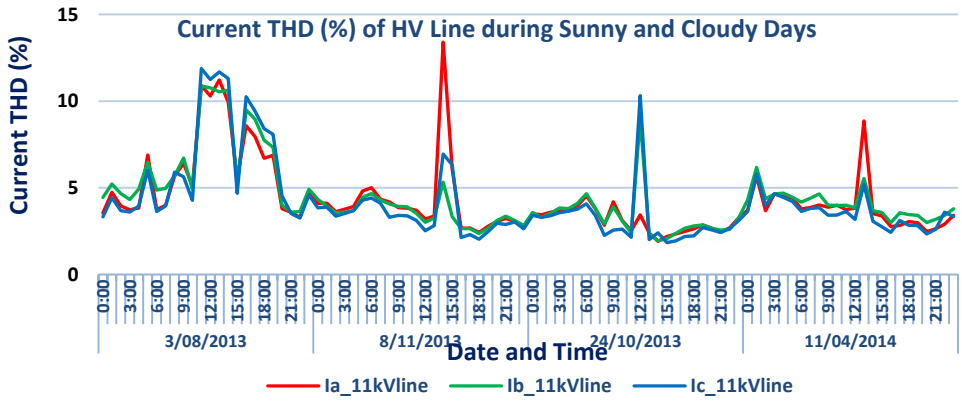

Figure 6.19. Percentage of Current THD at HV Side for Series Resonance Condition.

In the same way, the harmonic measurement data has been collected at both the HV and LV side of the network for the respective days. The current THD of the HV line for the corresponding sunny and cloudy days is plotted in Figure 6.19. Due to unbalance present in the network, each phase possessed different THD values. It can be seen that the harmonic levels are shown to be increased due to PV power injection. Remarkably, it can be observed that the current THDs were significantly raised to high values of about 12-13% for sunny days and around 9-11% in case of cloudy days, which are violating IEEE 519 standard limits.

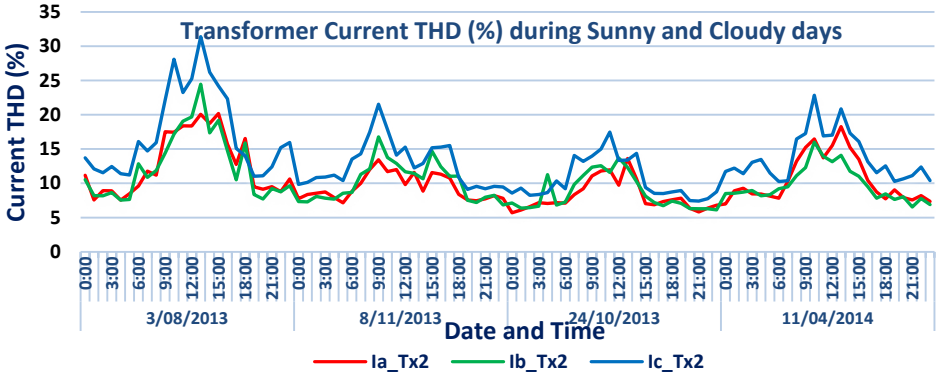

Figure 6.20. Percentage of Current THD at the Distribution Transformer for Series Resonance Condition.

In addition, the corresponding measured current and voltage THDs for both days at the distribution transformer TX2 are plotted as shown in Figures 6.20 and 6.21 respectively to analyse the impact of PV systems. It is noticed that the current THD is increasing from morning to noon time following the PV power trend. During the resonance periods, the current THD has values in the range of 20-32%, which are over the limits as per IEEE 519 standards. However, a small variation is observed in voltage THD during the resonance and are within the limits.

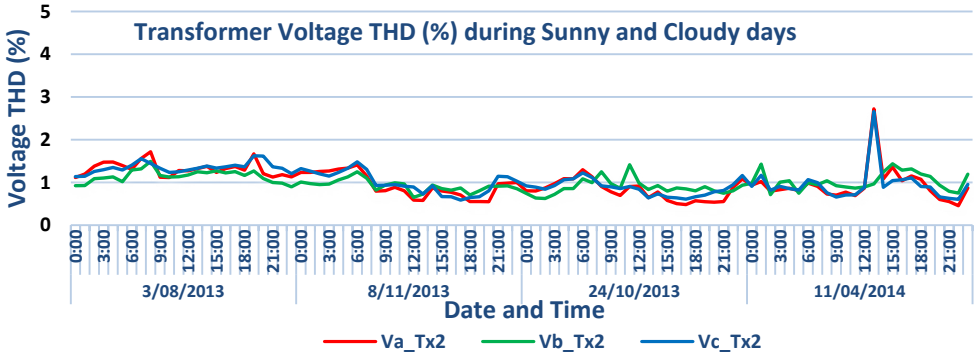

Figure 6.21. Percentage of Voltage THD at the Distribution Transformer for Series Resonance Condition.

Likewise, the PV output voltage and current harmonics have followed similar patterns during the selected days as shown in Figures 6.16 and 6.17 respectively. The current harmonics generation from the PV inverter mainly relies on the type of inverter, control topology and filter. The negative interactions in PV current controllers increase the oscillations and ripples at the output of the PV inverter and are dependent on the controller gains. The oscillations tend to be more severe with an increase in PV system penetration, which in turn affects the grid inductance and shifts the low impedance resonance point. It is noted that the harmonics from several parallel PV inverters connected at the PCC are probably increased the oscillations in

the voltage waveform. In turn, the oscillations in the grid reference voltage affect the current controller performance. The cumulative effect of PV inverter harmonics and the harmonics present in the network due to loads can cause the occurrence of a series resonance condition. Frequent occurrences of harmonic resonances can possess serious power quality issues in the distribution grid such as damaging equipment, transformer heating and mal-operation of protection devices.

6.5. Summary

This chapter has examined an important issue of harmonic resonance phenomena associated with PV system dynamic operations and their penetrations on the distribution network. The analysis was performed on an IEEE 13 bus unbalanced distribution network in two different case studies, specifically with and without background harmonic distortions in the supply system. In the simulation case studies, the dynamic operations of two different PV inverter systems and the solar irradiation variations were taken into account to study the impacts on the grid harmonic resonance incidence. In addition, a frequency versus impedance scan was presented with respect to each resonance condition. Moreover, to verify and validate the simulation results in the case of a real distribution network, the harmonic measurement data of 1-year collected from the UQ PV system were analysed. The measurements at both LV and HV sides of the network were obtained for analysis. Simulation results show that the harmonic resonance occurrence is not only reliant on the type of inverter control topology, filters, and number of PV inverter systems but also on the network configuration and type of customers load. Even though the PV inverters individually satisfy the harmonic limits during rated conditions, these PV systems are negatively interacting for variation in solar irradiation levels. As a result, the PV inverter controller dynamic operation due to transient disturbances injected high harmonic components into the grid, which excited the resonance conditions in the network. During the resonance, the amplification of voltage and current harmonics exceeded the IEEE 519 standard limits. Measurement results indicate that significant peak voltage and current distortions are found on the HV and LV side of the UQ network and are comparable to the simulation results. The following chapter presents a new potential solution to mitigate these power quality impacts on the distribution network with high PV penetration.

CHAPTER 7

SOLAR-DSTATCOM: A NEW SOLUTION TO POOR POWER QUALITY

7.1. Introduction[1]

This chapter proposes a new solution to overcome the power quality challenges influenced by PV system integration in an unbalanced distribution network. In this regard, a novel conception of operating a PV inverter as a virtual DSTATCOM, which is one of the custom power devices, named as Solar-DSTATCOM has been proposed. To mitigate power quality issues in the case of both balanced and unbalanced network conditions, a new control algorithm is proposed for the Solar-DSTATCOM.

[1]This chapter is organised with the following references:

Partially incorporated in Section 7.3 and 7.4:
Annapoorna Chidurala, T. K. Saha, and N. Mithulananthan, "Power quality enhancement in unbalanced distribution network using Solar-DSTATCOM," in Power Engineering Conference (AUPEC), 2013 Australasian Universities, Hobart, TAS, Sept. 29-Oct. 3, 2013, pp. 1-6.

Partially incorporated in Section 7.4:
Annapoorna Chidurala, T. K. Saha, N. Mithulananthan, and R. C. Bansal, "Harmonic emissions in grid connected PV systems: A case study on a large scale rooftop PV site," in *PES General Meeting Conference & Exposition, 2014 IEEE*, National Harbor, MD, 27-31 July 2014, pp. 1-5.

Incorporated as Section 7.5:
Annapoorna Chidurala, T. K. Saha, and N. Mithulananthan, "Real-Time Controller Hardware-in-the-Loop Simulations of Solar-DSTATCOM," in preparation, to be submitted to Elsevier Electric Power Systems Research Journal by September 2016.

The main objective of the Solar-DSTATCOM control strategy is to provide individual phase voltage regulation, harmonic and reactive power compensation at the integration point. Solar-DSTATCOM has the ability to provide dynamic reactive power support during the whole 24 hour period along with real power generation during the daytime. In the first part of this research, the proposed Solar-DSTATCOM controller has been verified in the PSCAD simulation environment. Subsequently, the assessment has been performed on the IEEE-13 bus unbalanced distribution network to compensate voltage rise, voltage unbalance and sag/swell issues. Also, the harmonic emission characteristics for varying solar irradiation conditions has been presented. Furthermore, the Solar-DSTATCOM controller has been verified in a real-time Hardware-in-the-Loop simulation platform, which combines the Real-Time Digital Simulator (RTDS) and dSPACE hardware board.

The following section presents the motivation of this research work. The proposed control scheme of Solar-DSTATCOM is explained in Section 7.3. The power quality investigation performed through PSCAD simulation on the IEEE-13 bus unbalanced distribution network using Solar-DSTATCOM in different case studies is presented in Section 7.4. In Section 7.5, the proposed Solar-DSTATCOM control system has been tested in a Controller Hardware-in-the-Loop simulation environment by considering various realistic case studies. Finally, the summary of this chapter is presented in Section 7.6.

7.2. Motivation

Traditionally, a solar PV system is considered as a real power source which generates active power during the daytime and remains inactive overnight. Also, the peak power generation period is during the midday and over the remaining period, the inverter operates at lower than rated condition due to low solar irradiation levels. Consequently, the inverter capacity and the investment of this equipment is unutilised most of the time. The injection of only active power into the grid at near to the load could cause a reduction in power factor and increase the reactive power requirement. Hence, grid operators have the advantage of putting obligations on the PV power output, those limitations can be a cost for the PV owners. In addition, PV system owners may incur further charges for reactive power purchase from the utility.

On the other hand, traditional distribution networks contain fixed/on-load tap changing transformers at low voltage (e.g. 11 kV in Queensland State of Australia), step voltage regulators and switched capacitors for providing voltage regulation with respect to the load variations [126]. However, PV systems are sensitive to the solar irradiation variations. Frequent

variation in solar irradiation due to cloud cover can cause significant voltage fluctuations [27, 127], which can lead to an increase in the number of operations of regulatory devices and therefore reduce equipment lifetime [23]. Also, sometimes the response of the equipment may be slower than the cloud passage. Consequently, it is necessary to upgrade the regulatory equipment, which would be relatively expensive for the utility.

To overcome these issues, devices with advanced design and faster control functionalities are necessary. Traditionally, standard droop control strategies are installed in distribution networks at centralised, decentralised and localised levels for the voltage quality management. These control schemes follow four droop-settings which include fixed power factor, fixed reactive power, reactive power control dependent on the voltage Q-V control and power factor control dependent on the active power injection PF (P). In the recent past, the concept of implementing Volt-VAr control schemes in PV inverters are adopted to achieve localised control. Nowadays, PV systems with smart inverter technology are commercially available, which have the capability of injecting/absorbing fixed reactive power to address voltage quality issues to some point [91, 92].

According to the previous standards IEEE 1547 [105] and IEEE 929-2000 [106], the PV inverters are not allowed to provide voltage regulation and are required to operate at unity power factor. Nevertheless, recent AS 4777.2-2015 standard [108] proposed that the PV inverter is allowed to provide constant reactive power with a fixed power factor not exceeding 0.95 leading/lagging. The standard also stated that if the PV inverter is capable of operating in reactive power mode, the maximum ratio of reactive power to rated apparent power should be up to 100% leading or lagging. In addition, PV inverters have versatile capabilities similar to the DSTATCOM by modifying a few functionalities to the inverter controller. In order to utilize the PV inverter system as a Solar-DSTATCOM, an appropriate control strategy should be put in place. Numerous types of control methods have been proposed in the literature [87, 88, 93] to produce compensation currents. All these control methods are well suited for steady state, sinusoidal and balanced conditions of the supply voltage. However, in the case of an unbalanced supply and nonlinear unbalanced load conditions these control techniques are unsuccessful. In order to compensate unbalanced network voltages, the active and reactive power injection from PV systems in each phase has to be individually controlled. Therefore, this chapter proposes a new control scheme, which independently compensates each of the three phases to correct any voltage anomalies.

Establishing this type of inverter can address several integration issues and therefore can accommodate more PV systems into the network. These PV inverter capabilities eliminate the buying costs incurred for reactive power needs and by supplying reactive power to the grid during the night-time can also offer additional profits for the PV owner.

7.3. Solar-DSTATCOM Control Strategy

The novel application of the PV inverter as a Solar-DSTATCOM provides grid voltage regulation and reactive power support during the daytime and night-time. Figure 7.1 illustrates the functional block diagram of the grid connected three-phase novel solar PV system configuration. The proposed new control scheme includes different control blocks to achieve the desired control aspects.

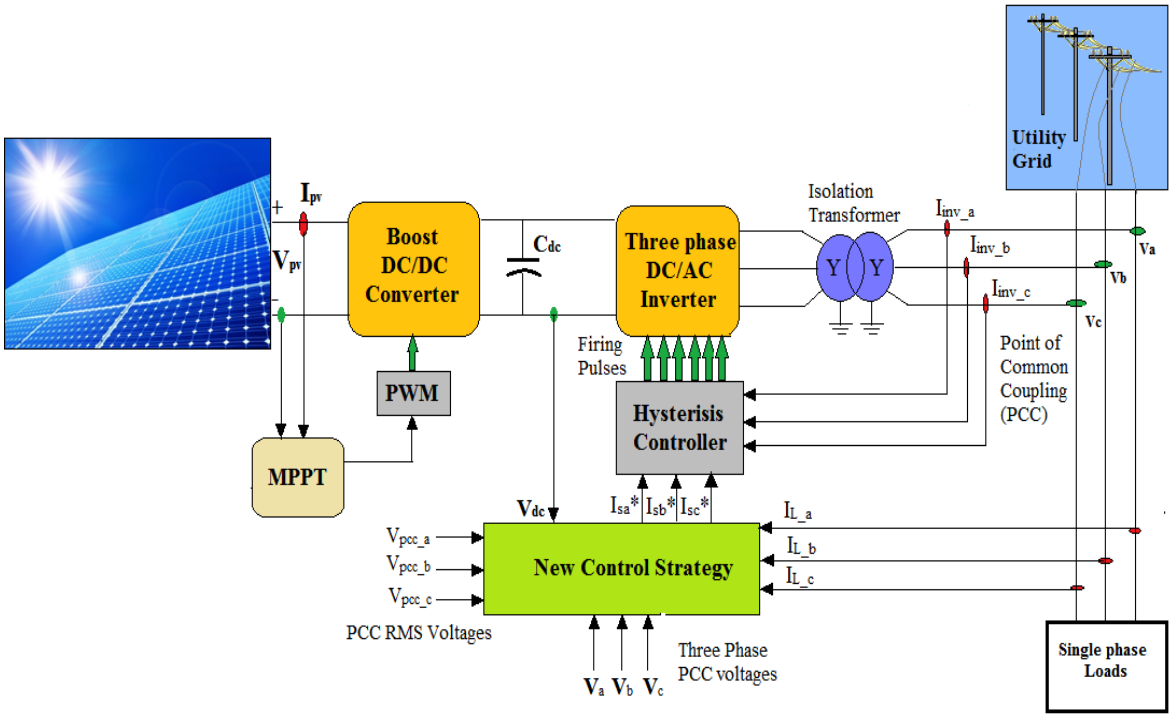

Figure 7.1. Block Diagram of Three-phase Grid Connected Solar-DSTATCOM System.

7.3.1. DC Voltage Controller

Figure 7.2 shows the control block used to regulate the dc bus voltage consisting of a proportional-integral (PI) controller, which is a generic feedback controller widely used in industrial applications. Usually, the DC bus capacitor is charged by solar power during the daytime. However, during low power times (early morning and evening) and at night-time, as there is lower or no power generation, the DC bus voltage regulation is applied to provide a self-supporting DC link voltage. The DC bus voltage controller consumes a small amount of

active power from the grid and charges the DC capacitor in few cycles to retain the preferred reference voltage level. The input to this controller is the difference between the PV reference (V_{pv_ref}) and the measured voltage across the DC capacitor. The difference is given to the proportional-integral (PI) regulator by selecting the appropriate proportional gain and integral time constant to generate the reference active current I_{d_dc} required to maintain the DC-bus voltage constant. This current represents the losses due to inverter switching devices.

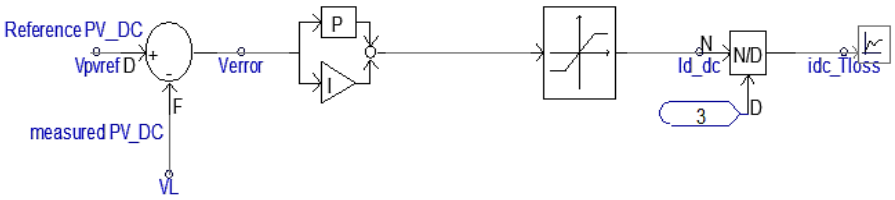

Figure 7.2. PSCAD Model of DC Bus Voltage Regulation Block.

7.3.2. PCC Voltage Controller

This block as shown in Figure 7.3 provides the voltage regulation for each phase at the point of common coupling (PCC). This new control block uses three individual regulators that will compare the sensed three-phase grid voltages with the reference voltages of 1p.u. The errors are processed through PI controllers and generate the reference quadrature currents (I_{pcc_a}, I_{pcc_b}, and I_{pcc_c}), which will be used to regulate the PCC voltages independently.

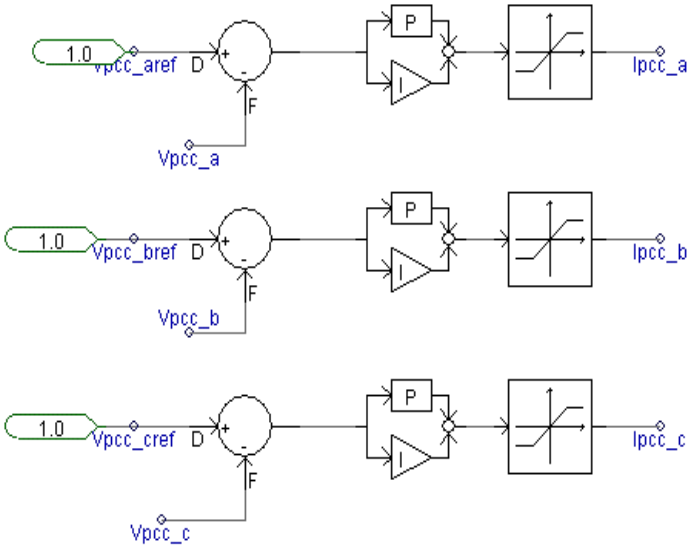

Figure 7.3. PSCAD Model of PCC Voltage Regulation Block.

7.3.3. Load Reactive Power and Current Harmonic Compensation Controller

The block diagram of reactive power and the current harmonic compensation controller is shown in Figure 7.4. A single-phase synchronous reference frame (SRF) based algorithm [128]

is applied to provide reactive power compensation for each individual phase. This controller utilizes the individual measured three-phase load currents (I_{L_a}, I_{L_b}, and I_{L_c}) at the PCC which are treated as the α-axis currents. The application of delay of π/2 radians in each of the currents produces the quadrature β-axis currents of the imaginary two-phase stationary reference frame (αβ-frame). Therefore, the equations for three phases in αβ-frame can be expressed as given in (7.1).

$$\begin{bmatrix} I_{L\_\alpha\_a} \\ I_{L\_\beta\_a} \end{bmatrix} = \begin{bmatrix} I_{L\_a}(\omega t) \\ I_{L\_a}(\omega t - \pi/2) \end{bmatrix}$$
$$\begin{bmatrix} I_{L\_\alpha\_b} \\ I_{L\_\beta\_b} \end{bmatrix} = \begin{bmatrix} I_{L\_b}(\omega t) \\ I_{L\_b}(\omega t - \pi/2) \end{bmatrix} \quad (7.1)$$
$$\begin{bmatrix} I_{L\_\alpha\_c} \\ I_{L\_\beta\_c} \end{bmatrix} = \begin{bmatrix} I_{L\_c}(\omega t) \\ I_{L\_c}(\omega t - \pi/2) \end{bmatrix}$$

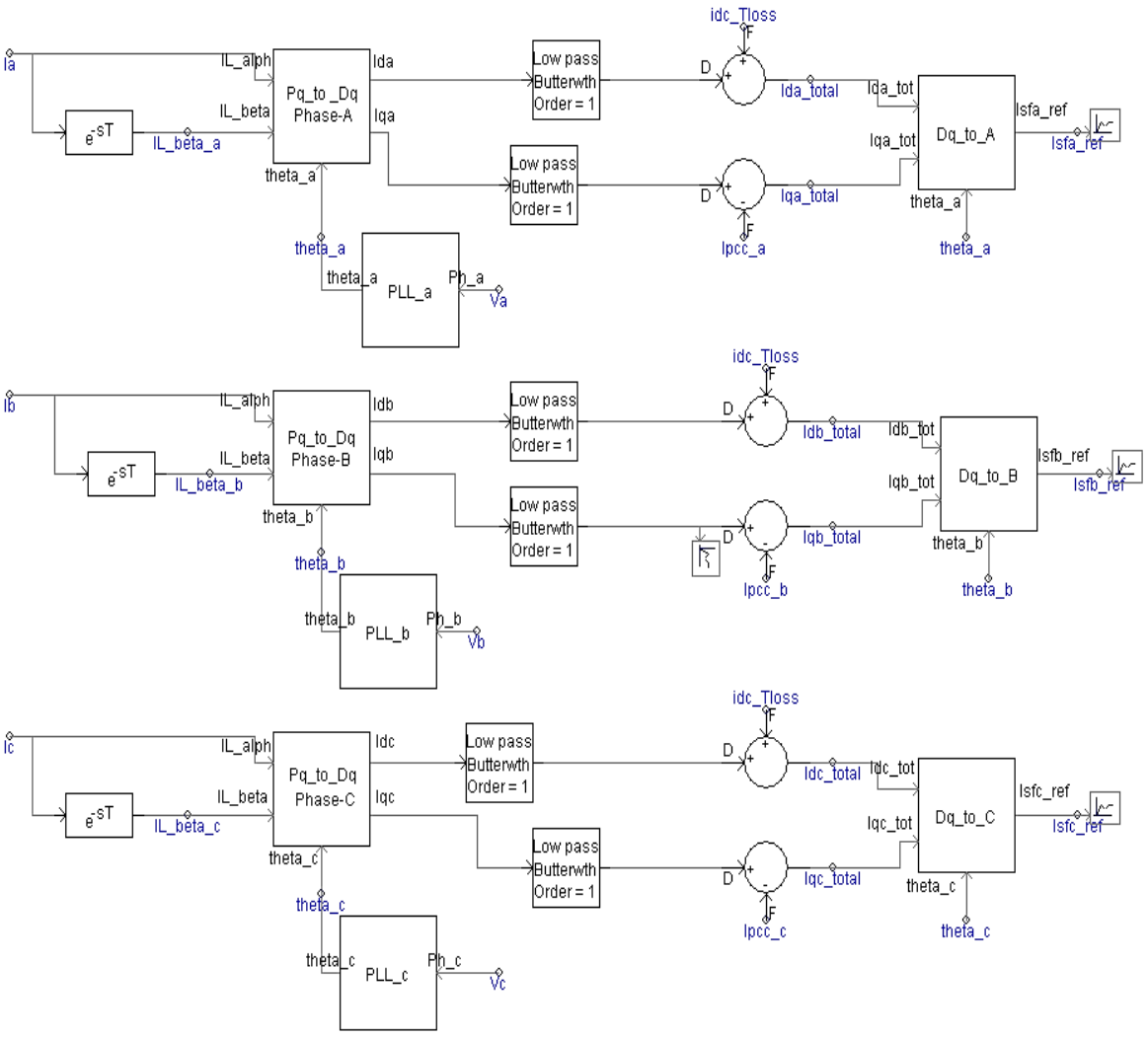

Figure 7.4. PSCAD Model of Reactive Power and Current Harmonic Compensation Controller.

After that, the load current transformations from αβ frame to the dq synchronous reference frame are attained through a transformation matrix as expressed in equation (7.2). In the equation, θ_a, θ_b, and θ_c represent the utility phase angles, which are obtained from three single phase locked loops (PLL). The description of the single-phase PLL circuit is provided in the following subsection.

$$\begin{bmatrix} I_{da} \\ I_{qa} \end{bmatrix} = \begin{bmatrix} \cos\theta_a & \sin\theta_a \\ -\sin\theta_a & \cos\theta_a \end{bmatrix} \begin{bmatrix} I_{L\_\alpha\_a} \\ I_{L\_\beta\_a} \end{bmatrix}$$
$$\begin{bmatrix} I_{db} \\ I_{qb} \end{bmatrix} = \begin{bmatrix} \cos\theta_b & \sin\theta_b \\ -\sin\theta_b & \cos\theta_b \end{bmatrix} \begin{bmatrix} I_{L\_\alpha\_b} \\ I_{L\_\beta\_b} \end{bmatrix} \quad (7.2)$$
$$\begin{bmatrix} I_{dc} \\ I_{qc} \end{bmatrix} = \begin{bmatrix} \cos\theta_c & \sin\theta_c \\ -\sin\theta_c & \cos\theta_c \end{bmatrix} \begin{bmatrix} I_{L\_\alpha\_c} \\ I_{L\_\beta\_c} \end{bmatrix}$$

Accordingly, for each phase the fundamental active and reactive components of load currents are extracted by using Low Pass Filters (LPF), symbolized as $\overline{I_d}$ and $\overline{I_q}$ respectively. At this instant, the filter eradicates the load higher harmonic current components from the dq currents. Subsequently, the total direct current component I_{d_total} is calculated by adding the generated current from the DC voltage controller to the filtered direct current component $\overline{I_d}$. This I_{d_total} current is used to compensate the losses correlated with Solar-DSTATCOM operation in each phase. Similarly, the subtraction of the PCC controller output quadrature currents from the filtered quadrature current $\overline{I_q}$ produces the total quadrature current I_{q_total}, which refers to the total reactive component of the injected reference current used for voltage regulation at the PCC.

Then by using the inverse dq transformations the controllers will generate the reference compensation currents for each individual phase which are equivalent to the PCC currents. This is expressed in the following equation (7.3). In the case of an unbalanced system, the controller will generate the unbalanced reference currents for compensation. Hence, the PV inverter currents are produced from the reference currents. In this case, the summation of the three phase currents cannot be zero, due to the presence of zero sequence components.

$$
\begin{aligned}
I^{*}_{sfa\_ref} &= \begin{bmatrix}\cos\theta_a & -\sin\theta_a\end{bmatrix}\begin{bmatrix}\overline{I_{da}} + I_{dc\_loss} \\ \overline{I_{qa}} - \overline{I_{pcc\_a}}\end{bmatrix} \\
I^{*}_{sfb\_ref} &= \begin{bmatrix}\cos\theta_b & -\sin\theta_b\end{bmatrix}\begin{bmatrix}\overline{I_{db}} + I_{dc\_loss} \\ \overline{I_{qb}} - \overline{I_{pcc\_b}}\end{bmatrix} \\
I^{*}_{sfc\_ref} &= \begin{bmatrix}\cos\theta_c & -\sin\theta_b\end{bmatrix}\begin{bmatrix}\overline{I_{dc}} + I_{dc\_loss} \\ \overline{I_{qc}} - \overline{I_{pcc\_c}}\end{bmatrix}
\end{aligned} \tag{7.3}
$$

a. Single-phase PLL Block

The single-phase PLL structure shown in Figure 7.5 comprises phase detector (PD), filter and voltage controlled oscillator (VCO). This block is used for synchronizing the injected current with the voltages of each individual phase at the PCC. A few methods to create the orthogonal components are presented in [129]. Here, the delay with a quarter of the fundamental period is chosen for implementation. The PD tracks the phase angle error of the relevant PCC voltage by comparing the estimated angle (θ) by PLL irrespective of the other phases. The error is then given to the loop filter and it generates the estimated frequency (ω) by adding it to grid frequency (ω_{ff}). The integral of ω is the estimated angle (θ) and is fed back to the PD. In the case of three-phase grid converters, three such PLL structures are needed. Each PLL circuit closely tracks the phase variation of its corresponding voltage disregarding the other two grid voltages. Any fault results in an unbalanced phase angle leading to produce an unbalanced current reference for the synchronisation. Therefore, the injected currents will synchronize to the respective grid voltages in terms of phase angle and frequency.

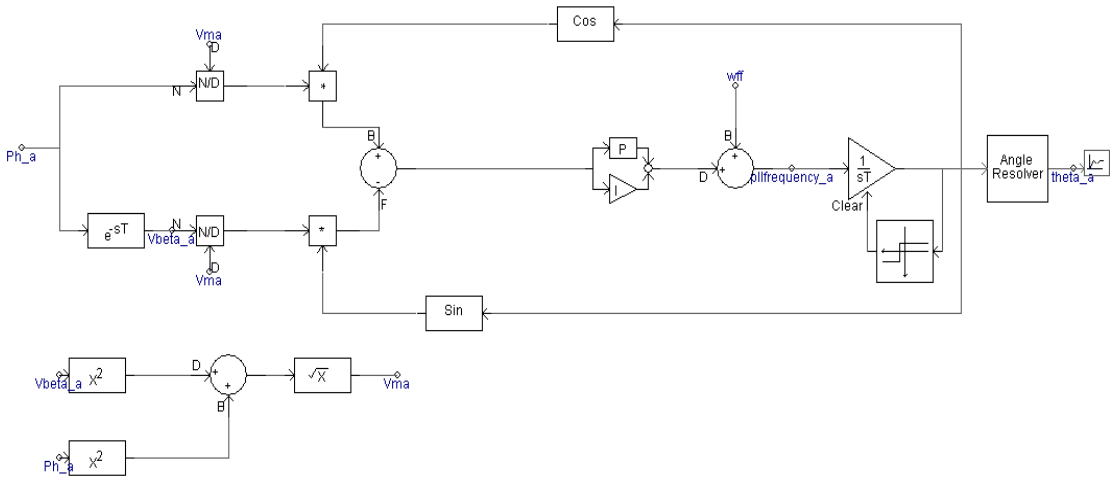

Figure 7.5. Single-phase PLL Structure.

7.3.4. Hysteresis Controller

This controller shown in Figure 7.6 consists of three hysteresis controllers, one for each phase. The inputs to these controllers are the differences between the reference currents and the actual sensed PV inverter currents (I_{inv_a}, I_{inv_b}, and I_{inv_c}). When the difference surpasses the hysteresis band limit, the controller will generate gating signals for the inverter. For example, a switching instant is given to switch T1 and an opposite signal is applied to switch T4 in order to avoid a short circuit for the solar farm inverter.

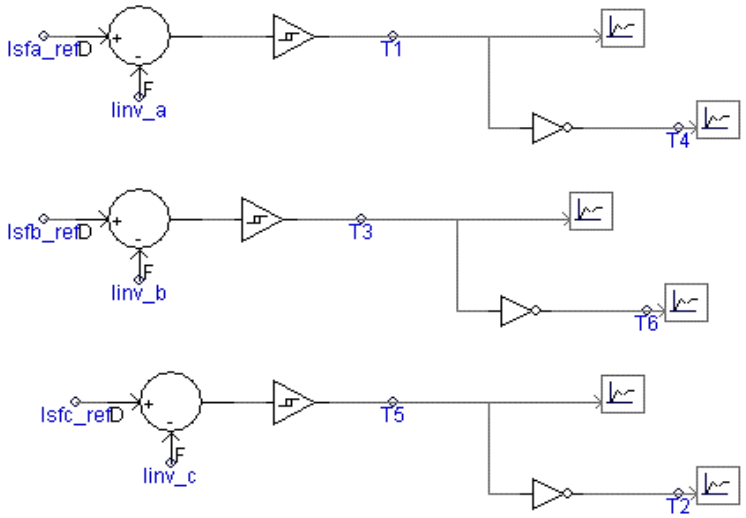

Figure 7.6. PSCAD Model of Hysteresis Controller.

7.4. Power Quality Enhancement in IEEE-13 Bus Unbalanced Network using Solar-DSTATCOM

The proposed Solar-DSTATCOM has been examined in order to overcome the power quality issues associated with conventional PV system penetration on the unbalanced distribution network as presented in Chapter 4, Section 4.2. Similar to the work presented in Chapter 4, the IEEE-13 bus unbalanced distribution network has been considered as a test system. For this study, the Solar-DSTATCOM has been developed with a dynamic PV source to reflect daytime and night-time operation. In the test system, the Solar-DSTATCOM has been integrated at bus 632. The rating of the PV inverter is 950 kVA, with 900 kWp PV power. The complete system is developed in PSCAD/EMTDC software. Simulations have been performed for three different case studies to verify the reliability and robustness of the new control strategy. In this investigation, the initial two case studies emphasize the compensation of voltage quality issues, specifically voltage rise, voltage unbalance and sag/swells, raised by PV

systems penetration. In addition to that, in the final case study the harmonic emission characteristics of Solar-DSTATCOM are captured during daytime and night-time operations.

7.4.1. Case Study-I: Voltage Rise and Voltage Unbalance Assessment

In this case, simulations have been carried out to study the impact of Solar-DSTATCOM performance on the test network during the daytime and night-time operations. A typical static solar irradiation pattern is applied on the Solar-DSTATCOM as shown in Figure 7.7.

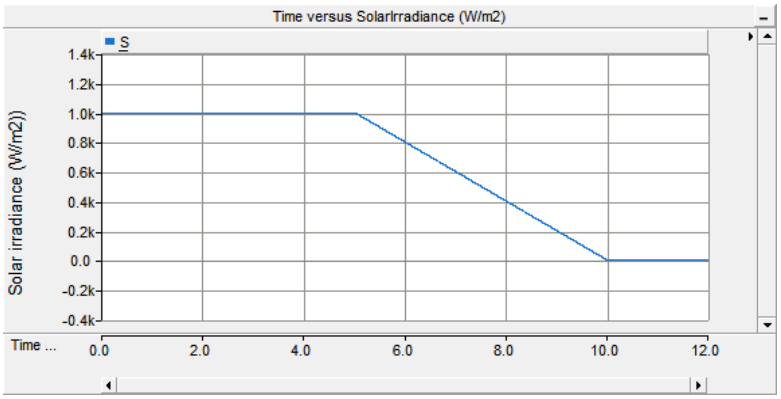

Figure 7.7. Static Solar Irradiation Pattern.

The corresponding Solar-DSTATCOM output active power and reactive power with respect to time is shown in Figure 7.8. Characteristically, the PV active power generation is reliant on the solar irradiation and has a linear relationship with it. For a unity P.F inverter, the generated reactive power remains at zero for the whole period. However, to enable the reactive power capability of the PV inverter, the size of the PV system has been increased by 5% so that around 33% of total capacity is available for reactive power production. It can be observed that during the daytime, the Solar-DSTATCOM has generated reactive power of nearly 285kVAr as can be seen in Figure 7.8. The proposed solar-DSTATCOM operates as DSTATCOM during low PV power levels and at night-time it has provided reactive power support to the grid.

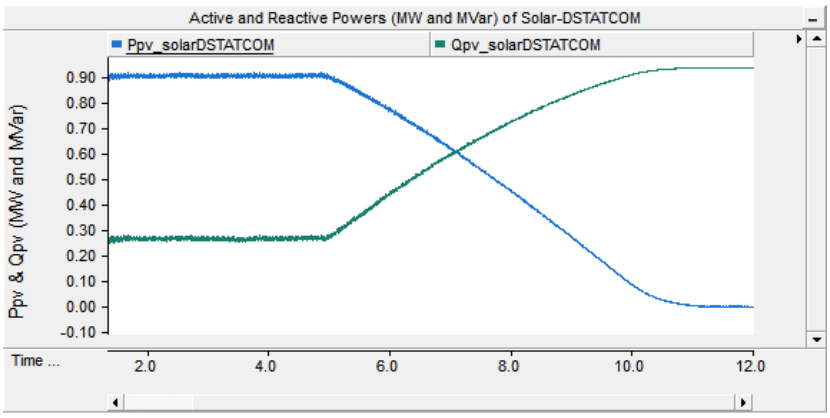

Figure 7.8. Active and Reactive Powers of a 900kW Solar-DSTATCOM.

Subsequently, the measured p.u RMS voltage magnitudes at various buses of the IEEE -13 bus distribution network with Solar-DSTATCOM during daytime and night-time are presented in Table 7.1. In the table, at time t= 4 sec the radiation is 1000 W/m2 (assumed as daytime) and at t=10 sec the radiation is 0 W/m2 (night-time operation). It can be seen that voltage variation differences (ΔV) are very small due to the controller operation and reactive power exchange and the voltage magnitudes are within the preferred operating limits [-2% to +6%] according to AS/NZS 61000.3.100 [96]. It can also be noticed the voltage rise magnitudes due to the PV power injection are lower when compared to the magnitudes with conventional PV system penetration as presented in Chapter 4, Tables 4.1 to 4.3. It is observed that the Solar-DSTATCOM has regulated the PCC and thereby the adjacent bus voltages to be within the limit by applying the PCC voltage controller.

Table 7.1 Voltage Variations during Daytime and Night-time with Solar-DSTATCOM

Bus No.	**Phase-A RMS Voltage (p.u)**			**Phase-B RMS Voltage (p.u)**			**Phase-C RMS Voltage (p.u)**		
	T=4 sec	**T=10 sec**	**ΔV_A**	**T= 4 sec**	**T= 10 sec**	**ΔV_B**	**T= 4 sec**	**T= 10 sec**	**ΔV_C**
V_{632}	1.01890	1.01851	**0.00039**	1.03429	1.03057	**0.0037**	1.02708	1.02440	**0.0026**
V_{633}	1.01601	1.01550	**0.00039**	1.03239	1.02863	**0.0037**	1.02448	1.02185	**0.0026**
V_{634}	0.99189	0.99163	**0.00026**	1.01382	1.01009	**0.0037**	1.00576	1.00299	**0.0027**
V_{645}	-	-	-	1.02506	1.02137	**0.0036**	1.02510	1.02235	**0.0027**
V_{646}	-	-	-	1.02333	1.01952	**0.0038**	1.02303	1.02029	**0.0027**
V_{671}	0.98776	0.98731	**0.00045**	1.04510	1.04123	**0.0038**	0.98772	0.98488	**0.0028**
V_{675}	0.98125	0.98076	**0.00049**	1.0475	1.04355	**0.0039**	0.98584	0.98294	**0.0029**
V_{684}	0.98583	0.98536	**0.00047**	-	-	-	0.98570	0.98281	**0.0028**

Furthermore, simulations have been performed to verify the voltage unbalance (VU) level with Solar-DSTATCOM and compared it with conventional PV inverter operation as shown in Figure 7.9. Results show that the percentage of VU with Solar-DSTATCOM during the daytime and night-time are much lower compared to the VU with a conventional PV system, which is less than the 4% limit according to AS/NZS 61000.4.30 [16] standard. The high PV penetration and conventional PV inverter operation (unity P.F) has increased the VU as presented in Chapter 4, Section 4.2.1. It can also be noticed that PV system integration into the distribution grid has increased the VU at the PCC and has a high value at the end of the feeder. The voltage unbalance with Solar-DSTATCOM followed a similar trend as with conventional PV operation.

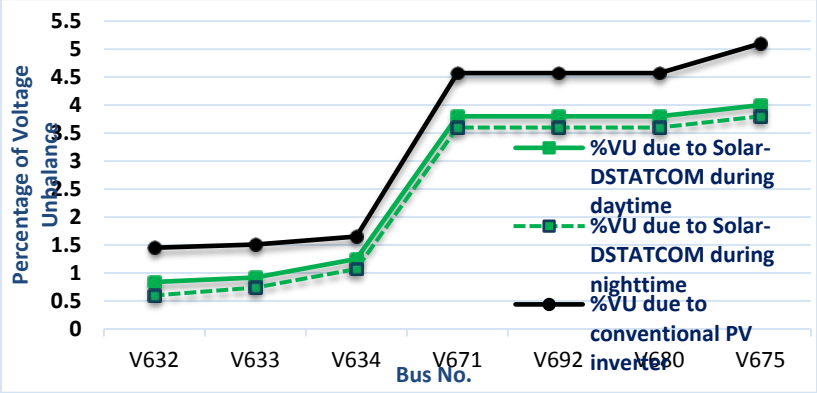

Figure 7.9. %Voltage Unbalance Analysis at Various Buses.

7.4.2. Case Study-II: Voltage Sag/Swell Assessment by Fault Conditions

In this case study, simulations have been performed on a test system to verify the effectiveness of the Solar-DSTATCOM operations in each of the three types of faults. In each case the fault is initiated at time t = 4.5 sec and the duration of the fault is 100ms. In the figures below V_a, V_b, and V_c represent the three phase RMS bus voltages at before fault and V_{af}, V_{bf}, and V_{cf} denote the voltage magnitudes during the fault. Also, LB (0.94p.u) and UB (1.06p.u) indicate the lower and upper operating band limits from the relevant Australian Standard.

7.4.2.1. Single Line to Ground Fault (SLG):

SLG fault is considered to occur on phase A of bus 633. During the fault, the PV source is isolated before the inverter operates as a Solar-DSTATCOM. In order to conquer the unbalanced voltage sags and swells, the Solar-DSTATCOM injects the unbalanced currents shown in Figure 7.10 (a) based on grid reactive power demand. Respectively, the PCC voltage regulators measure the RMS voltages of each phase for the control. Here, the phase B voltage controller operated in inductive mode (absorbed the reactive power) to decrease the voltage at the PCC. On the other hand, phase A and phase C individual controllers operated in capacitive mode to alleviate the voltage sag at the PCC. Figure 7.10 (b) depicts the compensated PCC voltages.

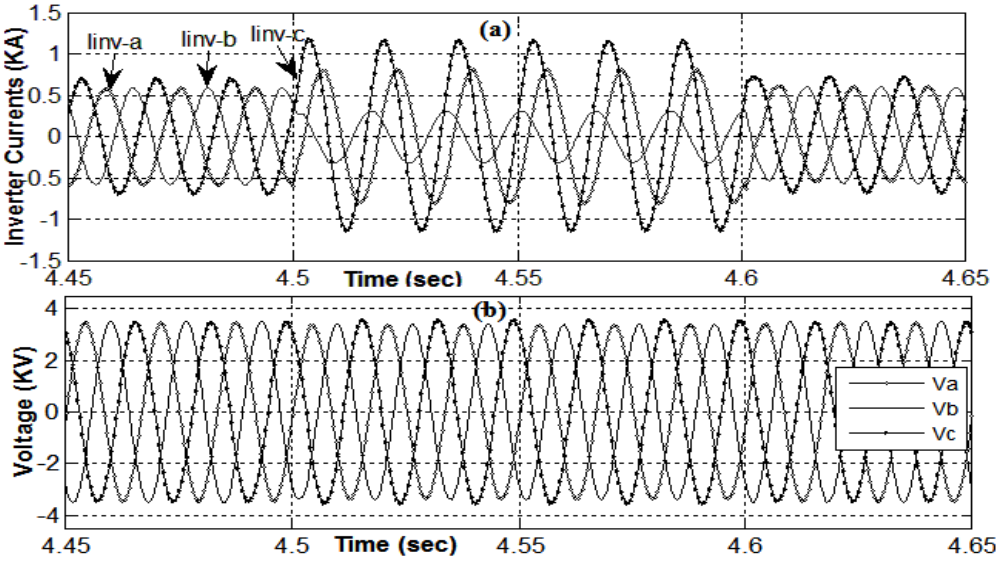

Figure 7.10. Solar-DSTATCOM (a) Inverter Currents and (b) Compensated PCC Voltages during SLG Fault.

The RMS voltage magnitudes at different buses before and during the fault are shown in Figure 7.11. Results show that the magnitude of sag on phase A and phase B have only declined to about 2% and the swell on phase C was about 2%. Therefore, the Solar-DSTATCOM with novel control strategy has significantly improved the system voltages to be within the acceptable limits.

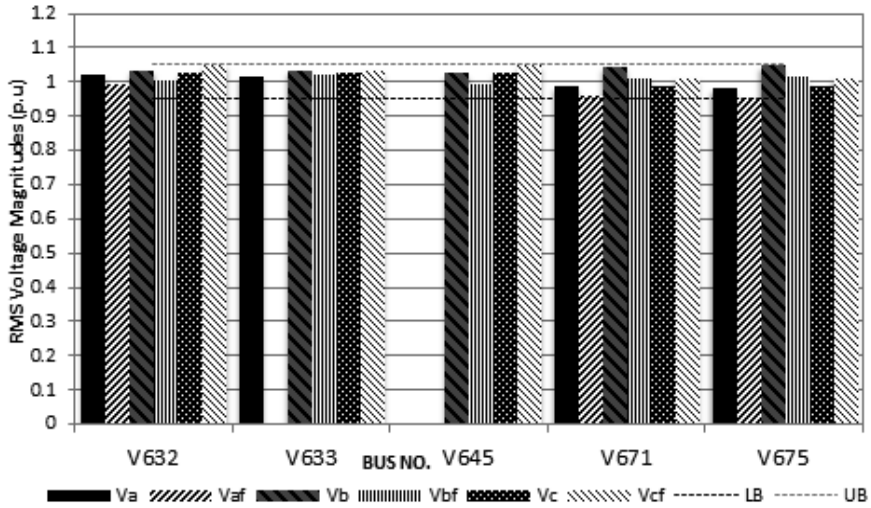

Figure 7.11. The RMS Voltages at Prefault and during SLG Fault with Solar-DSTATCOM.

7.4.2.2. Double Line to Ground Fault (DLG):

In the same way, an unsymmetrical DLG fault is applied on phases A and B of bus 633. Due to the DLG fault, all the bus voltages resulted in very small sag in all three phases. In contrast, with the conventional PV inverter operation shown in Figure 4.4 (refer Chapter 4), the voltage

magnitudes of only phases A and B resulted in a sag condition during the fault. However, in this scenario, the Solar-DSTATCOM controller injected the unbalance reference currents into the grid to counterbalance the reactive power as shown in Figure 7.12 (a). Consequently, the compensated PCC voltages during the fault are shown in Figure 7.12 (b). Similarly, the mitigated RMS voltages for specific buses were shown in Figure 7.13. As regards to the fault, the proposed control scheme has mitigated the voltage sags and swells remarkably.

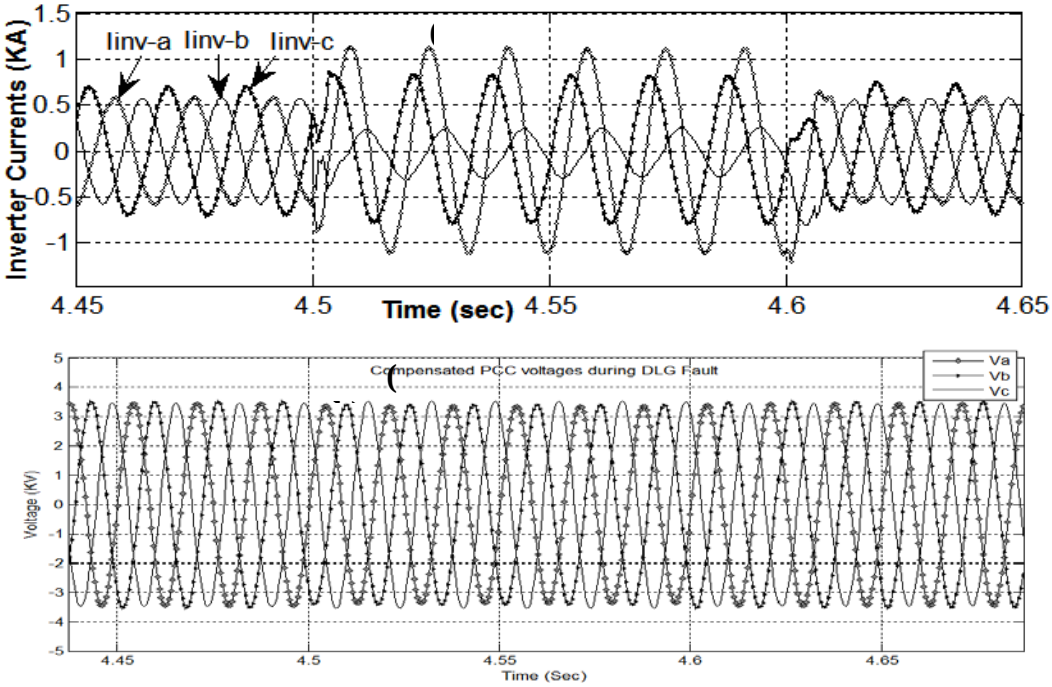

Figure 7.12. Solar-DSTATCOM (a) Inverter Currents (b) Compensated PCC Voltages during DLG Fault.

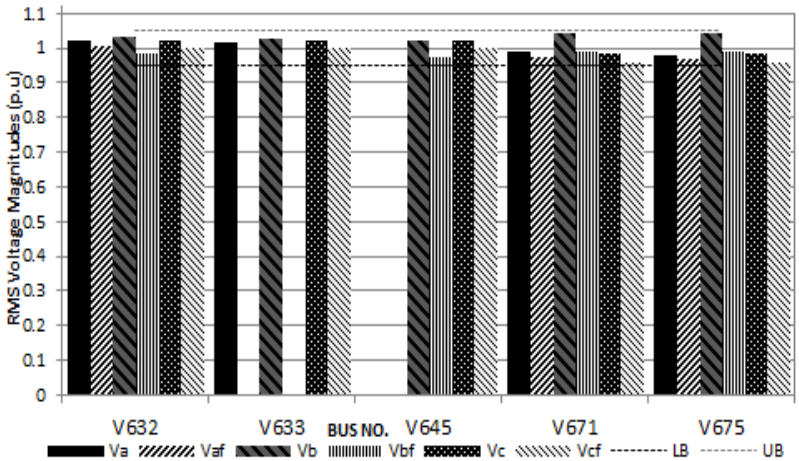

Figure 7.13. The RMS Voltages at Prefault and during DLG Fault with Solar-DSTATCOM.

7.4.2.3. Three-phase Symmetrical Fault (TPG):

Simulations were carried out for the TPG fault which is often seen as the worst case, this was at bus 633. During the fault, the Solar-DSTATCOM injects the appropriate currents for improving the voltage sags. The injected inverter currents, three phase PCC voltages and the simulated RMS voltage levels at various buses before and during the fault are shown in Figures 7.14 and 7.15 respectively. Here the magnitudes of injected currents are followed by the grid reactive power demand. It can be observed that the voltage sag in phase A was nearly 4% and the voltage magnitudes at phases B and C were improved significantly to have only 3% drop.

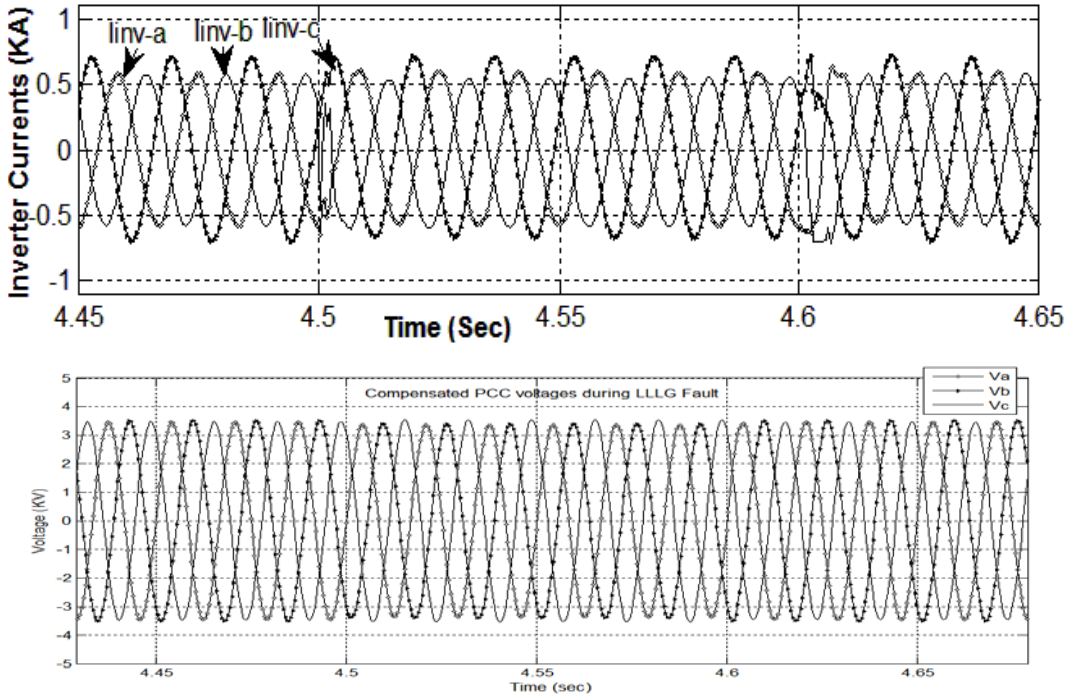

Figure 7.14. Solar-DSTATCOM (a) Inverter Currents (b) Compensated PCC Voltages during TPG Fault.

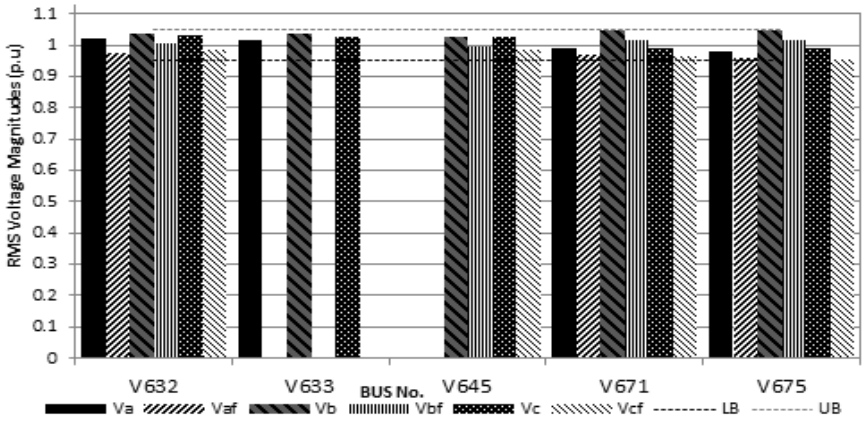

Figure 7.15. The RMS Voltages at Prefault and during TPG Fault with Solar-DSTATCOM.

7.4.3. Case Study-III: Harmonic Distortion Analysis

Finally, the harmonic analysis was carried out using Fast Fourier Transformation (FFT) to obtain harmonic distortions. A similar solar irradiation pattern as shown in Figure 7.7 is applied to verify the effectiveness of the control scheme in eliminating harmonics generation at the PV inverter output. The simulated results for the PV inverter current and voltage harmonic distortions are shown in Figures 7.16 and 7.17 respectively. Figure 7.18 shows the corresponding individual harmonic spectrums of Solar-DSTATCOM inverter currents and PCC voltages during the rated condition. According to IEEE 519-2014 [53], the maximum individual voltage distortion should be less than 5% of the fundamental component and the total harmonic distortion (THD) should be less than 5% at the PCC. As per IEEE 929-2000 [106], the current THD should not exceed a 5% limit. The injected PV currents should have low harmonic distortion levels at the PCC to meet the standards.

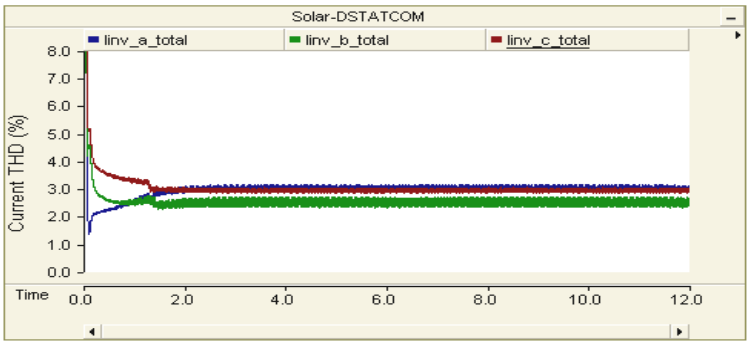

Figure 7.16. Percentage of THDs of Solar-DSTATCOM Output Currents.

Results show that the proposed harmonic compensation controller has eliminated the harmonic distortion during the whole period. It can be seen that THD of the Solar-DSTATCOM current is below 3%, which is lower than the limit prescribed by the standards. This limit maintained constant even for variable solar irradiation conditions. Similarly, the THD of voltage is almost below 0.9%.

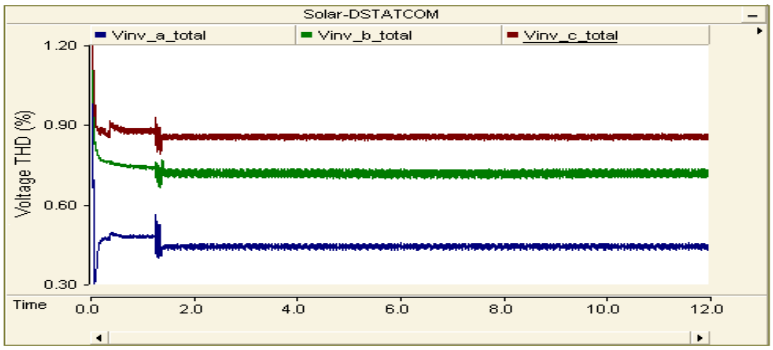

Figure 7.17. Percentage of THDs of Solar-DSTATCOM Output Voltages.

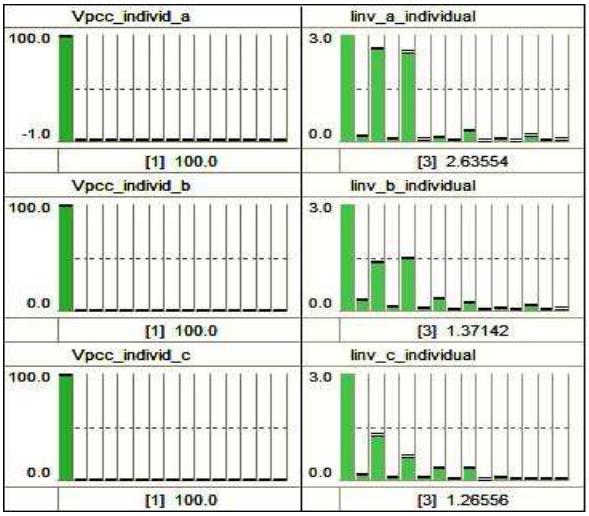

Figure 7.18. Individual Harmonic Distortions of Solar-DSTATCOM Output Currents and PCC Voltages.

Furthermore, the performance of Solar-DSTATCOM has been investigated and verified comprehensively in a real-time hardware environment, which is presented in the following section.

7.5. Real-Time Controller Hardware-in-the-Loop Simulations of Solar-DSTATCOM

The objective of this study is to test and evaluate the Solar-DSTATCOM controller unique capabilities in the real-time Hardware-in-the-loop simulation environment. Generally, any new product in industry will be developed through different designing, testing and implementation phases. In the early phases of a design, initial offline simulations are useful to analyse different component responses. Nonetheless, these offline simulations are not able to replicate the runtime behaviour and real-time events of the electrical network, which may not provide the high fidelity results particularly when designing the control systems and its interfaces. Further, the amount of real-time required to solve the mathematical equations and control functions during a given time-step may be smaller or longer than the simulation time step, which may not influence the accuracy of the results [130]. The solving speed usually depends on the computational power of the PC and the system complexity. Therefore, potential design errors will not be identified, which need to be critically investigated in a real-time simulation environment in addition to the hardware.

Importantly, controller hardware-in-the-loop (HIL) simulations require several considerations due to the involvement of real hardware and software, which need to take care.

Since the control system is developed in software and implemented on hardware, which depends on the execution time, discreteness, errors due to fixed time steps, nonlinearities and communication delay are essential to be considered. The dynamic performance evaluation and testing of digital controller prototypes and its corresponding power electronic equipment are highly recommended before the physical implementation of the product. This real-time HIL testing can be advantageous to conduct various systematic and random tests under normal and worst case operating conditions, which can eliminate potential hazards and the required equipment costs [131]. In references [132-134], the feasibility and effectiveness of the proposed controllers for grid connected PV inverters and wind energy conversion system were evaluated in real-time controller HIL simulations, which utilize the integrated platform of RTDS and dSPACE board. In [135], a unified controller for multiple DG inverter systems and its interaction with a microgrid system has been verified in real-time hardware simulations.

Therefore, in this research real-time controller HIL simulations have been performed to test and validate the potential of a Solar-DSTATCOM controller in achieving the preferred control concepts. This real-time digital simulation involves industry standard simulation tools, RTDS [118, 119], dSPACE DS1103 hardware control board [120] and MATLAB/Simulink software [136]. The assessment has been carried out to verify the performance of the Solar-DSTATCOM controller during the daytime for different solar irradiation profiles and also during the night-time. Conversely, the load profile variation interactions on the Solar-DSTATCOM operation, which is operating at various power levels have been evaluated. Finally, the harmonic analysis of Solar-DSTATCOM has been performed through Fast Fourier Transform.

The following Section 7.5.1 presents the concept of controller hardware-in-the-loop simulation environment. Section 7.5.2 provides the design of the Solar-DSTATCOM controller and test system setup. The results of the various case studies and discussions are presented in Section 7.5.3.

7.5.1. Controller Hardware-in-the-loop Simulation Environment

Controller hardware-in-the-loop simulation is a technique used for testing the digital controllers, which combines real-time hardware with software simulations [135]. This experimental setup consists of dSPACE and RTDS simulators, which are controlled by the software ControlDesk and RSCAD respectively. The block diagram of the experimental setup of hardware-in-the-loop using RTDS and the dSPACE control board is shown in Figure 7.19.

Initial tests have been conducted to realize the time delay and noise content between inputs and outputs of the RSCAD/RTDS and dSPACE hardware system. The issue of signal latency has been resolved with the use of a suitable solver in MATLAB/Simulink and with the optimum simulation time step.

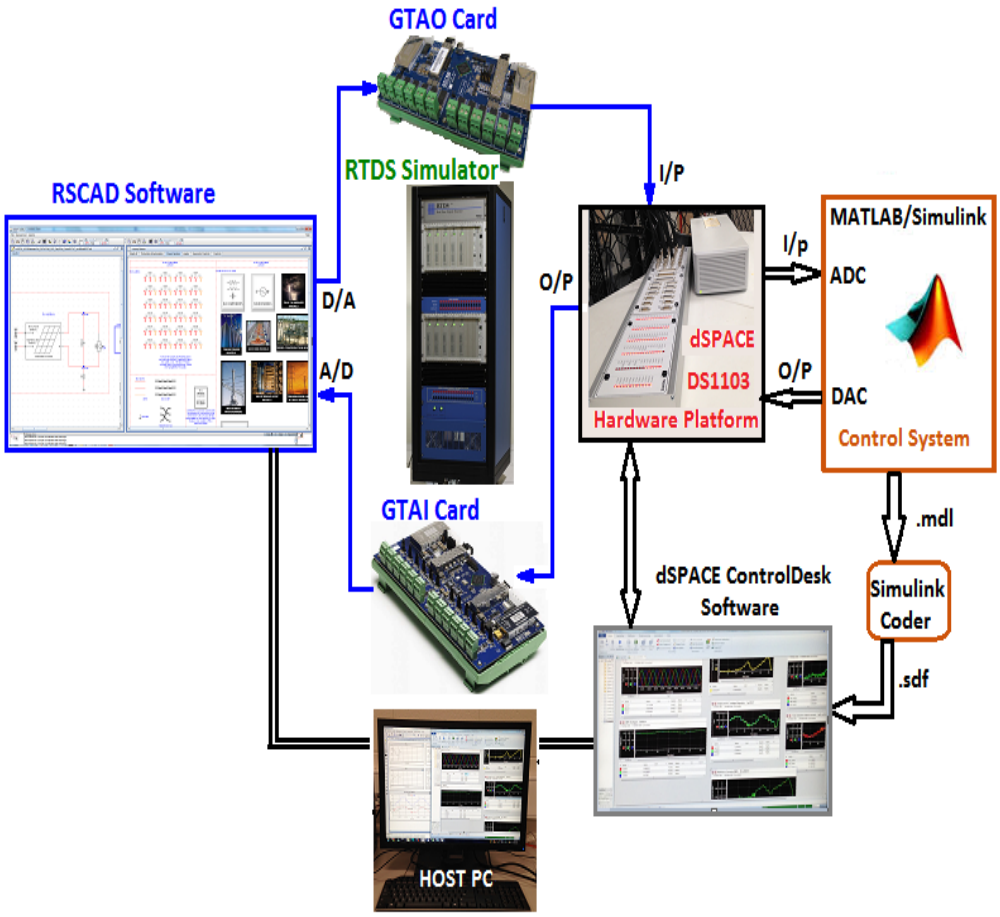

Figure 7.19. Experimental Setup of Hardware-in-the-Loop using RTDS and dSPACE Control Board.

7.5.2. Test System and Solar-DSTATCOM Controller Setup in HIL Platform

In this research, to test and validate the Solar-DSTATCOM controller, a test system with a dynamic load has been considered. The PV system is integrated near to the load referred to as a point of common coupling (PCC). Figure 7.20 shows the complete design of the test system and the Solar-DSTATCOM inverter system in RSCAD software. The test system is developed in a large time step of 50µs simulations, and the PV inverter system is developed in a small time step of less than 2µs simulations. The test system contains a three phase 11kV line-to-line supply and a distribution transformer to step down the voltage to 400V. The capacity of the dynamic load can be varied in runtime using a scheduler or slider component. Depending on

the requirement, various load profile settings have been considered, which will be explained in the results section.

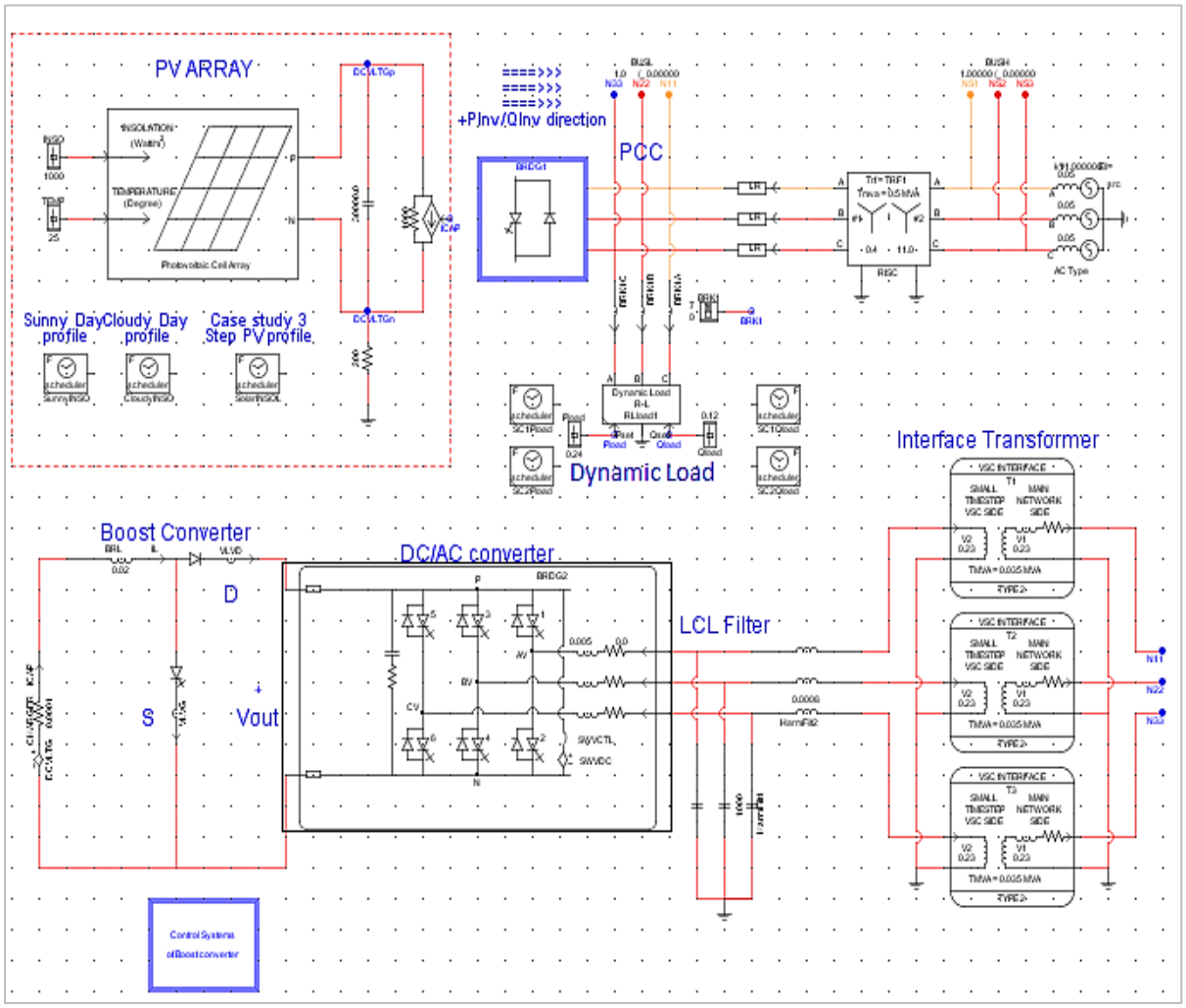

Figure 7.20. Test System and Solar-DSTATCOM Modelling in RSCAD Environment.

The PV system consists of PV panels connected as arrays, a boost converter and a DC/AC inverter with an interfacing LCL filter. Also, to integrate a small time step circuit with a large time step network, an interfacing transformer has been connected. The input solar irradiation to the PV array can be varied by using slider/scheduler components in the simulations to perform several tests. The PV output voltage has been given to the boost converter to get the preferred DC voltage for conversion. The boost converter is operated with a Maximum Power Point Tracking (MPPT) system, which generates a duty cycle for the gate switch. An incremental conductance based MPPT algorithm has been utilized to get the maximum power. The controller for the boost converter is developed in RSCAD software. The control system for the DC/AC inverter is developed in Simulink software for controller testing.

7.5.2.1 Solar-DSTATCOM Control Setup in MATLAB/Simulink:

The concept of utilizing the PV system as a virtual DSTATCOM can eliminate several power quality issues. The detailed description of the Solar-DSTATCOM controller can be found in Section 7.3. The proposed new control consists of a DC bus voltage controller, PCC voltage controller, load reactive power and harmonic compensation controller and hysteresis controller as mentioned earlier. These controllers require a measured DC bus voltage, PCC voltages, load currents and the inverter output currents. The inputs from RSCAD are transferred to dSPACE hardware using GTAO card, which converts the digital signals into analog signals and are scaled down with a scaling factor to produce lower voltage levels below +/-10V. By using BNC cables, the inputs from the GTAI card are connected to the CLP1103 connector panel. To simplify the analog scaling, the signals are converted to per unit values. A scaling factor of 5 is applied for the DC voltages of 0.75p.u (or 0.75kV) to get 0.75V at the output channels of the GTAI card. Similarly, a scaling factor of 5 is selected for the PCC per unit voltages to obtain a 1V peak sinusoidal waveform. A scaling factor of 300 is applied to the load currents, which are in Amps.

The block diagram of the Solar-DSTATCOM controller in the MATLAB software environment with Simulink/dSPACE block sets is shown in Figures. 7.21 and 7.22. The DC bus voltage controller is used to regulate the DC voltage constant across the DC link capacitor. In the circuit, two ADC channels are used to convert analog signals to digital and by default, the signals need to be multiplied by a factor of 10. Then, the signals are scaled up by a scaling factor to get them back to the DC bus voltage range.

Figure 7.21(b) shows the PCC voltage controller, which is used to maintain the PCC voltages within the steady state limits. The sensed PCC voltage signals are obtained through MUXADC channel. In the figure, I_{pc_A}, I_{pc_B} and I_{pc_C} indicate the generated reference quadrature currents for independent phase voltage regulation.

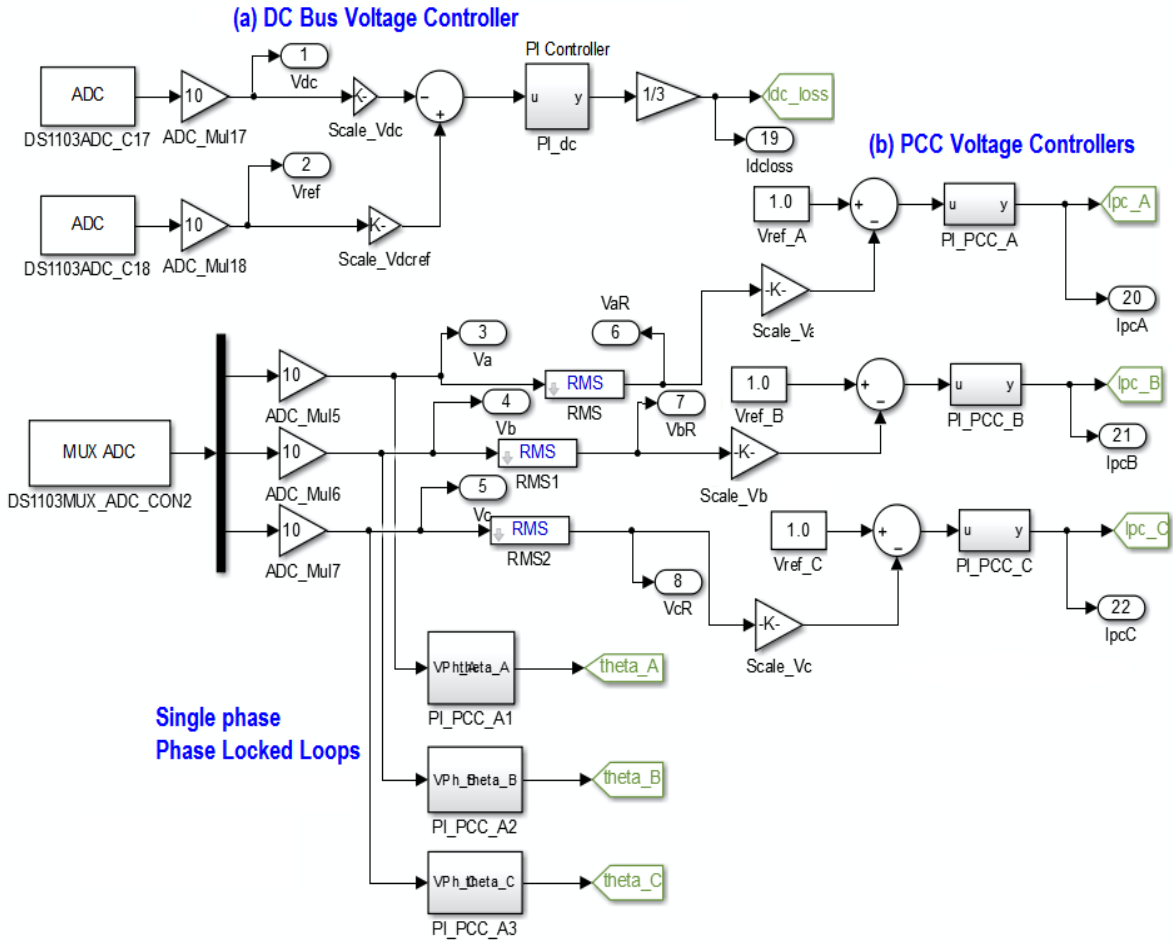

Figure 7.21. (a) DC Bus Voltage Controller and (b) PCC Voltage Controllers.

The block diagram for load reactive power and current harmonic compensation is shown in Figure 7.22. These controllers require measured three-phase load currents, which will be obtained using the MUXADC channel. As mentioned earlier, the currents will be scaled up to the actual current magnitudes. Finally, the reference currents will be scaled down to achieve a low power range and then converted to analog signals by using 3 DAC channels. Note that before the DAC block, the signal is divided by a factor of 10 by default. Further, the analog output signals from the CLP1103 connector panel are connected to the GTAI card with the help of BNC cables. Further, the GTAI card converts the analog signals to digital as indicated in Figure 7.19.

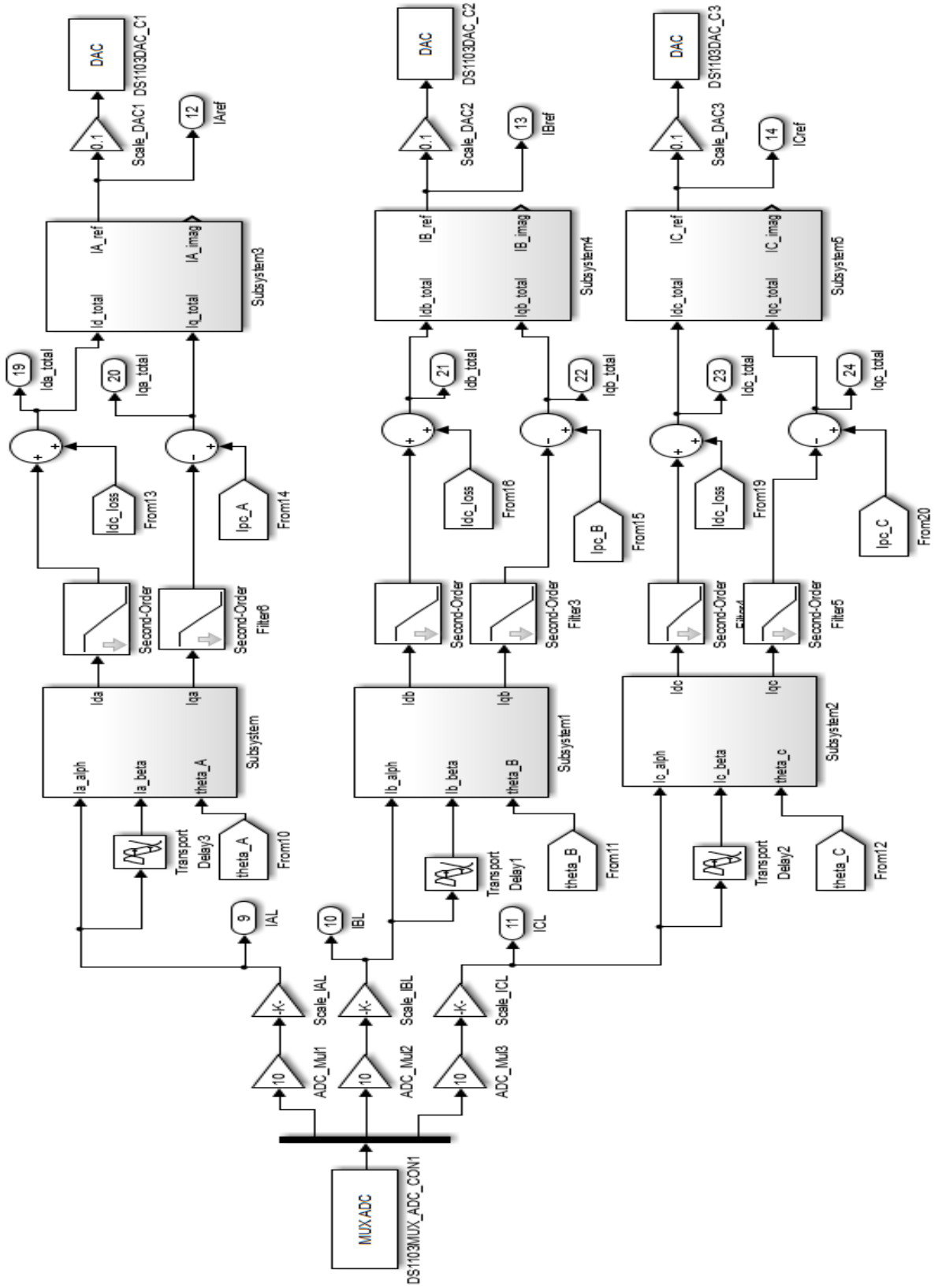

Figure 7.22. Load Reactive Power and Current Harmonic Compensation Block.

The developed control system is converted to custom C code and is loaded into ControlDesk software for the real-time simulation. Finally, the reference currents are compared with the

inverter output currents, the differences are given to the hysteresis controllers to obtain the firing pulses for the inverter switching. The total height of the hysteresis band is chosen to be 5% of the actual PV current. From RSCAD software library, the inverter with a built-in hysteresis current controller functionality has been considered for the simulation.

7.5.3. Results and Discussions

The performance of the Solar-DSTATCOM controller has been investigated in three different case studies with regards to both PV profile and load profile variations. For this, a 100kWp PV inverter system has been considered for the simulation. To enable the reactive power capability, the size of the PV systems has been increased by 5% so that around 33% of the reactive power can be produced during rated conditions. The analysis of results from real-time HIL simulations in both RSCAD/RTDS and dSPACE controlDesk are presented.

7.5.3.1. Case study – I: Performance of Solar-DSTATCOM for Various Daytime PV Profile Variations

The assessment has been performed for a clear sunny day and a typical cloudy day. The real-time solar irradiation data from weather sensors with a resolution of 1min have been collected and are assumed as seconds' data. For daytime operation, the measured solar irradiation levels from 6am to 6pm have been considered and are further reduced to get a total of 360s data points. By using a scheduler component in RTDS, the real-time simulation has been automated for a continuous 360s time. For every second, the input to the PV array changes and produces new output values. It is to be noted that the load on the test system is fixed and is operated at 0.24MW with 0.9 P.F (lagging).

A Sunny Day Operation:

Figure 7.23 shows the time versus solar irradiation profile of a sunny day. Simulations have been performed and the corresponding measured active (P) and reactive (Q) powers at the Solar-DSTATCOM output and grid interconnection point are captured as shown in Figure 7.24. It can be seen that solar irradiation has a linear relationship with the PV output power and has an inverse relationship with the reactive power. With the PV power injection, a reduction in the grid supply P and Q trends can be observed. During the rated condition, the Solar-DSTATCOM has produced an active power (P_{Inv}) of 100kW, reactive power (Q_{Inv}) of 33kVAr which corresponds to a P.F of 0.95. During low solar irradiation levels, the generated P_{Inv} has a decreased trend. In contrast, the Q_{Inv} is increased to its maximum and reached a value of about 94kVAr.

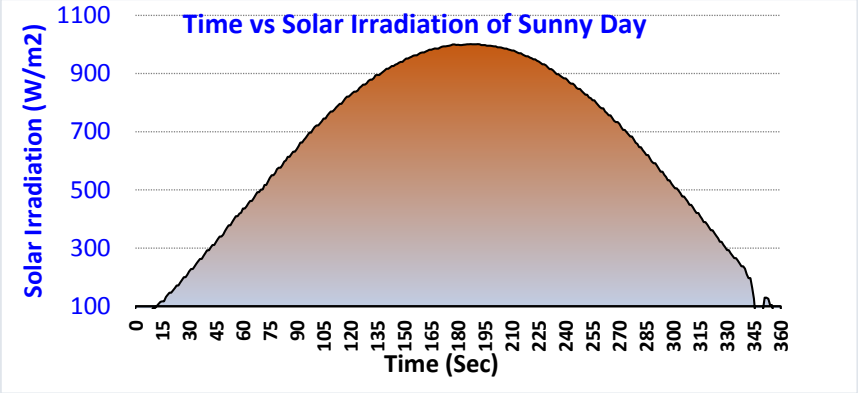

Figure 7.23. Time versus Solar Irradiation of a Sunny Day.

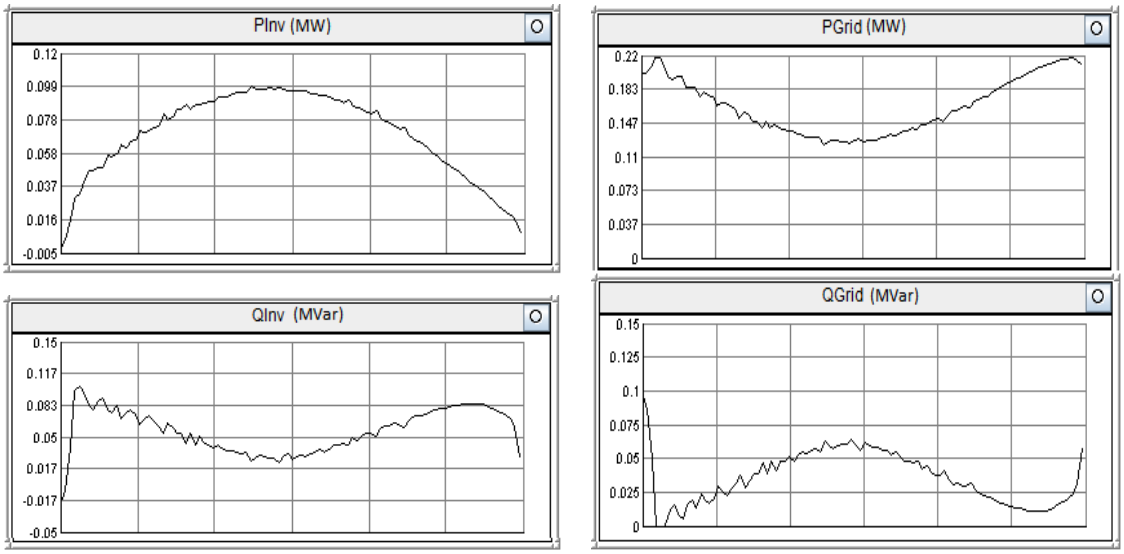

Figure 7.24. Measured Active and Reactive Power Profiles at Solar-DSTATCOM Output and Grid Supply during a Sunny Day.

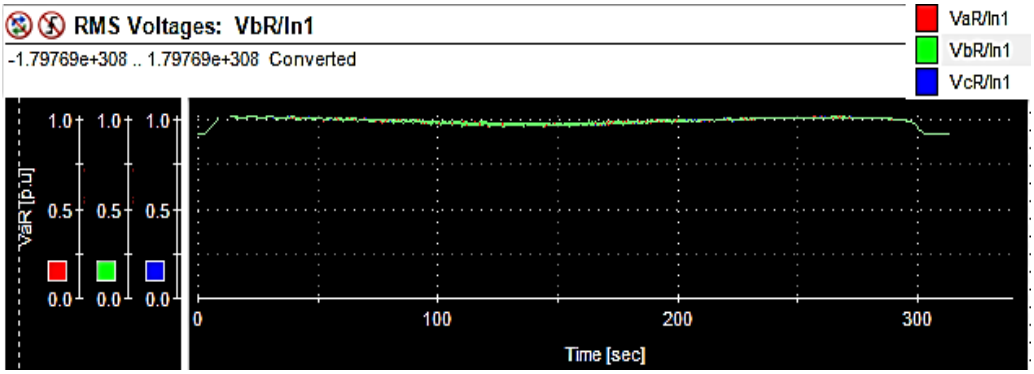

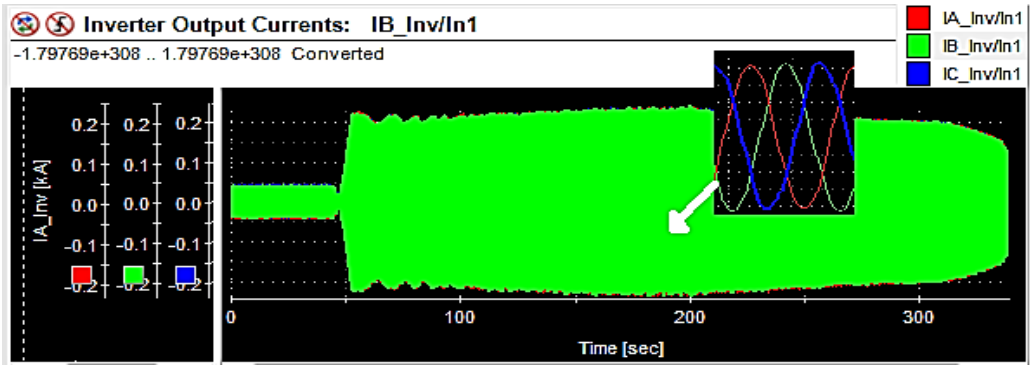

Figure 7.25. Measured PCC RMS Voltages and Solar-DSTATCOM Output Currents during a Sunny Day.

Due to the plot data point limitations in RSCAD software, the waveforms of the Solar-DSTATCOM inverter output currents and PCC voltages were recorded in dSPACE ControlDesk software, which are illustrated in Figure 7.25. It is to be noticed that the PV system capacity is completely utilized for the whole time period and it injected rated current into the grid. The PV inverter acts as a DSTATCOM and has compensated the load reactive power requirement and enhanced the voltage magnitudes at the PCC node. It is to be seen that with reactive power injection, the voltage magnitudes are increased from 0.9p.u to 1.01p.u, which are within the limits specified by the ANSI standard [94]. However, the voltage rise due to PV power injection is observed to be minimal during midday due to the operation of the PCC voltage controller.

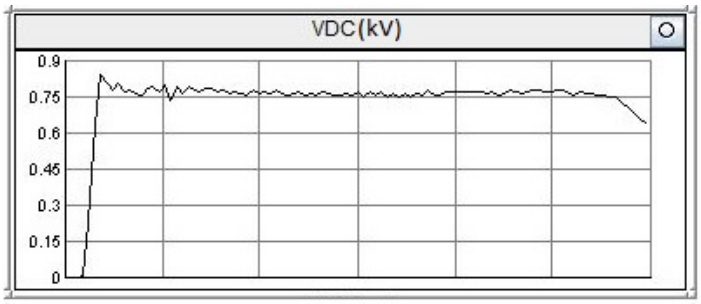

Figure 7.26. DC Bus Voltage Profile during a Sunny Day.

The measured DC bus voltage is shown in Figure 7.26. It can be seen that the DC bus voltage is almost constant and dropped due to solar irradiation levels below 100W/m2. During early morning and evening periods, the DC bus voltage controller has been applied to maintain the DC voltage constant.

Furthermore, due to the involvement of hardware and several signal conversions, the controller inputs/outputs might be influenced by noise and the execution speed, which can

affect the results of simulations. To verify the controller operations, the output of various controller blocks have been captured for 360sec time using the dSPACE ControlDesk software. Figure 7.27 shows the controller trends during a sunny day operation.

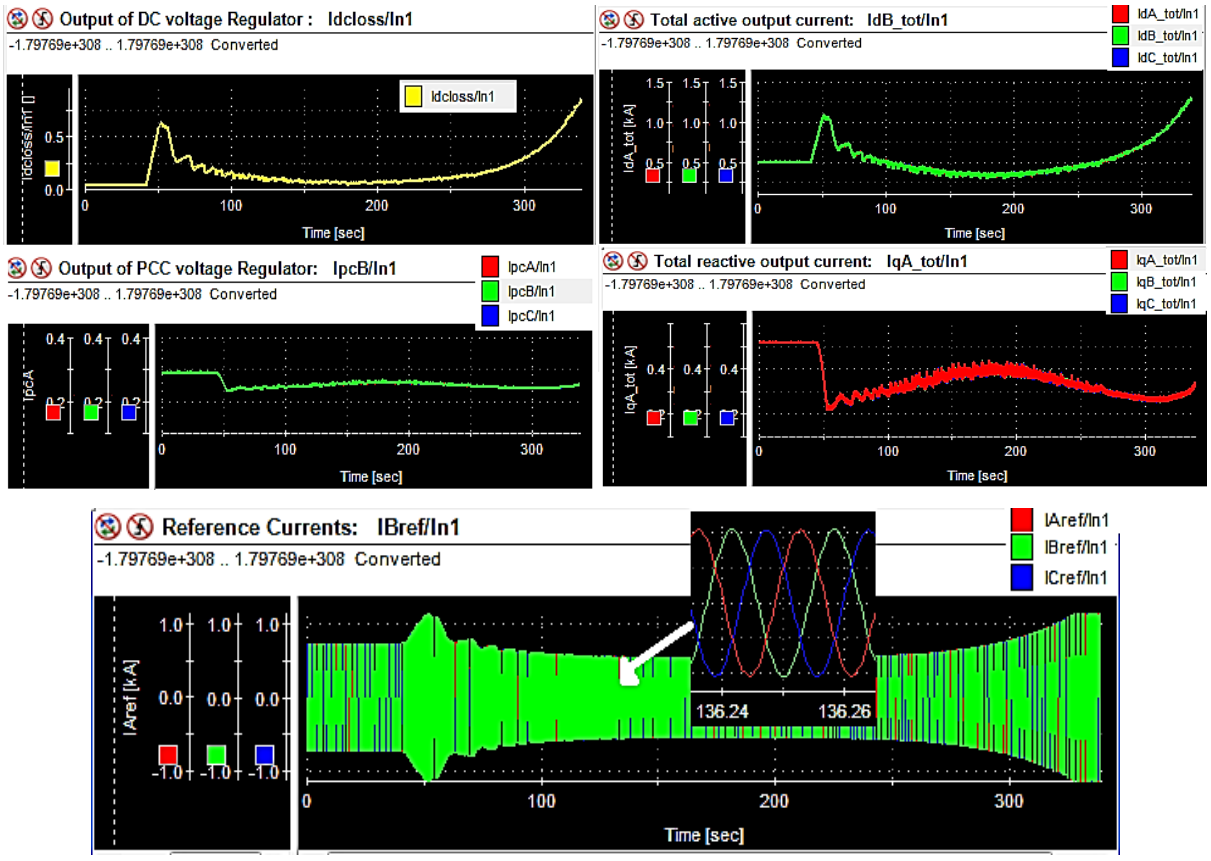

Figure 7.27. Solar-DSTATCOM Controller Various Output Parameters during a Sunny Day Operation.

Note that the PV inverter breaker was closed a few seconds after the RSCAD simulation started. Immediately, the data recording process in dSPACE has been started, this delay can be seen in the waveforms. In the figure, I_{dc_loss} represents the loss current required to maintain the DC bus voltage constant. Then, the PCC voltage regulators generate the currents required to regulate the PCC voltages to be within the limits. The currents I_{dA_total} and I_{qA_total} denote the total real and reactive components of injected inverter currents. These generated signals are following the input dynamic trends and are noise free. It is noticed that the generated reference currents are changed with respect to the load currents.

B Cloudy Day Operation:

Similarly, a typical cloudy day solar irradiation profile has been considered. Figure 7.28 shows the corresponding time versus solar irradiation plot. It can be seen that the solar

irradiation pattern contains high, average and low spikes, which could represent a worst case condition. The Solar-DSTATCOM output and grid supply active and reactive power profiles are illustrated in Figure 7.29. It can be seen that the response of Solar-DSTATCOM is faster for sudden variations in the solar irradiation due to cloud transients. The trends of measured PV and grid powers have a similar tendency as with the above scenario.

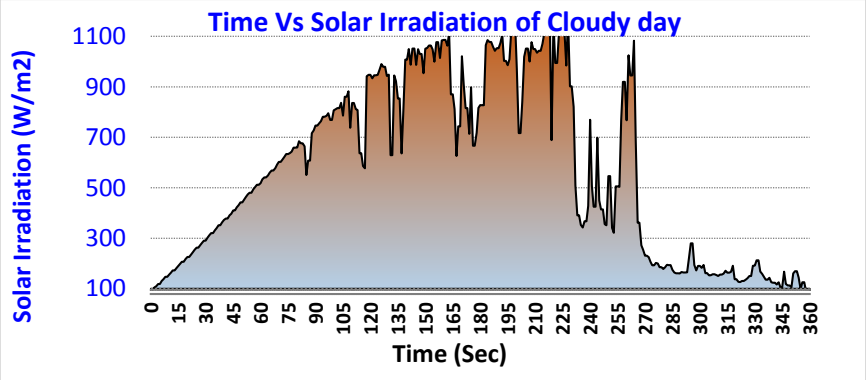

Figure 7.28. Time versus Solar Irradiation of a Cloudy Day.

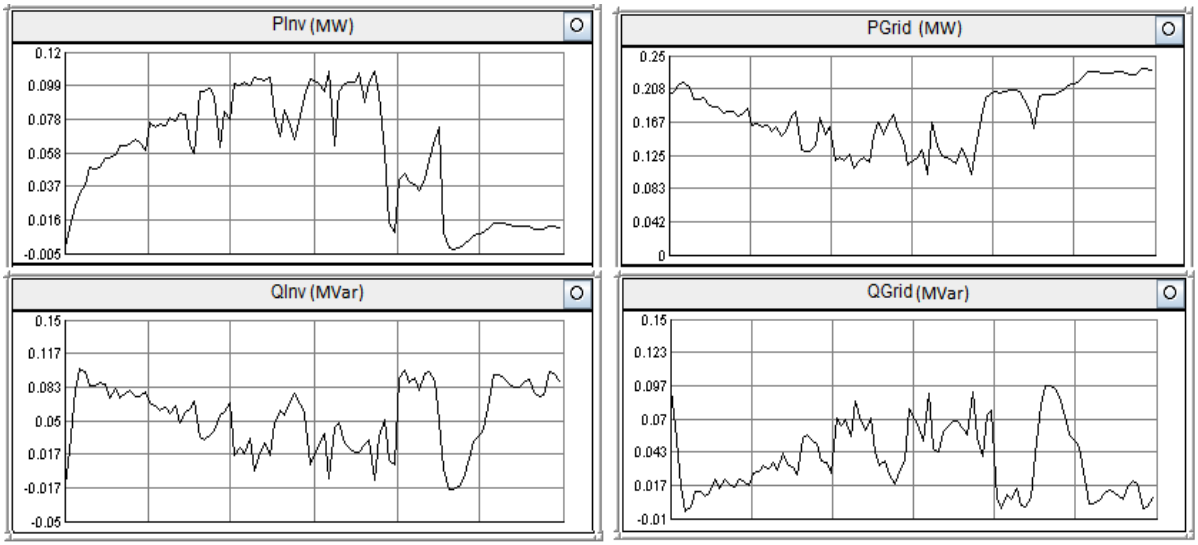

Figure 7.29. Measured Active and Reactive Power Profiles at Solar-DSTATCOM Output and Grid Supply during a Cloudy Day.

Figure 7.30 shows the measured PCC voltage and Solar-DSTATCOM output currents. It can be seen that the voltage fluctuations due to cloud transients are appeared to be lower. The voltage magnitudes are observed to be between 0.98 and 1.0p.u, which are within the steady state voltage limits.

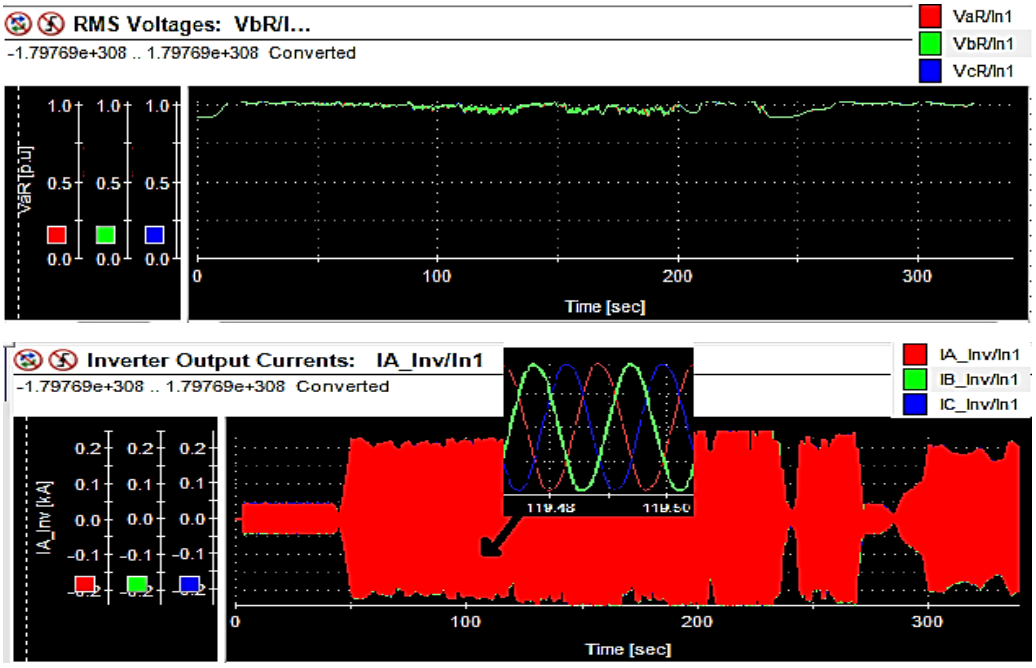

Figure 7.30. Measured PCC RMS Voltages and Solar-DSTATCOM Output Currents during a Cloudy Day.

Accordingly, the measured voltage across the DC link capacitor is shown in Figure 7.31. It can be observed that the reduction in voltage is due to maximum PV power drop by heavy cloud transients. At this period, the DC bus voltage controller extracts a small amount of active power from the grid and charges the DC capacitor in few cycles to retain the preferred operating voltage as can be seen in Figure 7.31. It is noticed that the Solar-DSTATCOM output currents are following the same trend as the DC bus voltage.

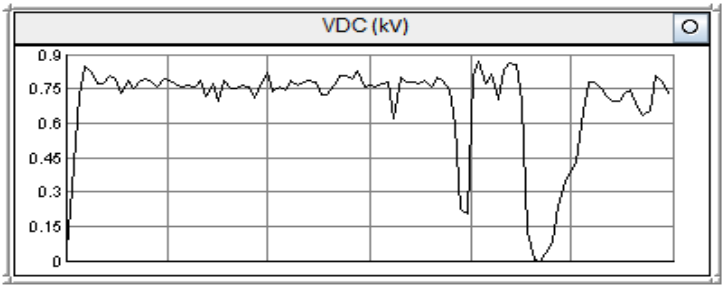

Figure 7.31. DC bus Voltage Profile during a Cloudy Day.

Similarly, the performance of the Solar-DSTATCOM controller with regards to input variations has been investigated. The resultant controller output currents are captured and illustrated in Figure 7.32. It can be seen that the dynamic response of inverter controllers during cloud transient periods are faster and ripple free to perform the preferred control action.

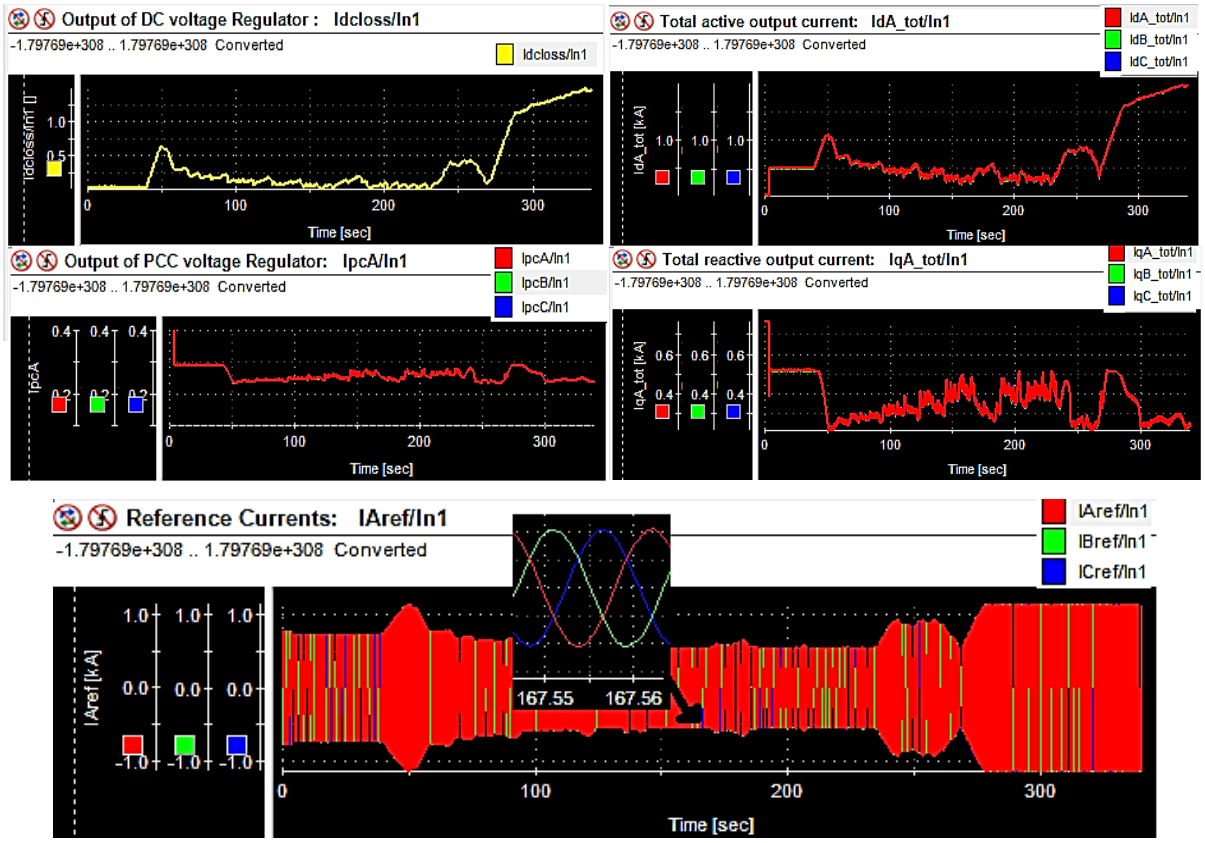

Figure 7.32. Solar-DSTATCOM Controller Various Output Parameters during a Cloudy Day Operation.

7.5.3.2. Case study – II: Performance of Solar-DSTATCOM during Night-time Operation

In addition, the operation of the Solar-DSTATCOM controller is demonstrated during the night-time. Similar to the first case study, the load on the test system is considered constant and it draws 0.24MW power with 0.9 P.F (lagging). It is noted that the proposed Solar-DSTATCOM operates as a DSTATCOM during the night-time, and provides reactive power support to the grid. Figure 7.33 shows the various output parameters of the Solar-DSTATCOM and the results of grid active and reactive power variations. As explained above, when there is no solar power the solar-DSTATCOM consumes a small amount of active power to regulate the DC bus voltage. It is observed that when the transient period is over, the DC link voltage is reached 0.75kV. As a result, the grid real power injection has been increased to 0.2462 MW to compensate for the inverter losses. At this time, the Solar-DSTATCOM controller has injected a reactive power of about 93.3kVAr. Hence, the power factor of the grid has improved and maintained close to unity. It is confirmed that the proposed Solar-DSTATCOM controller could be of benefit to both PV customers and utilities.

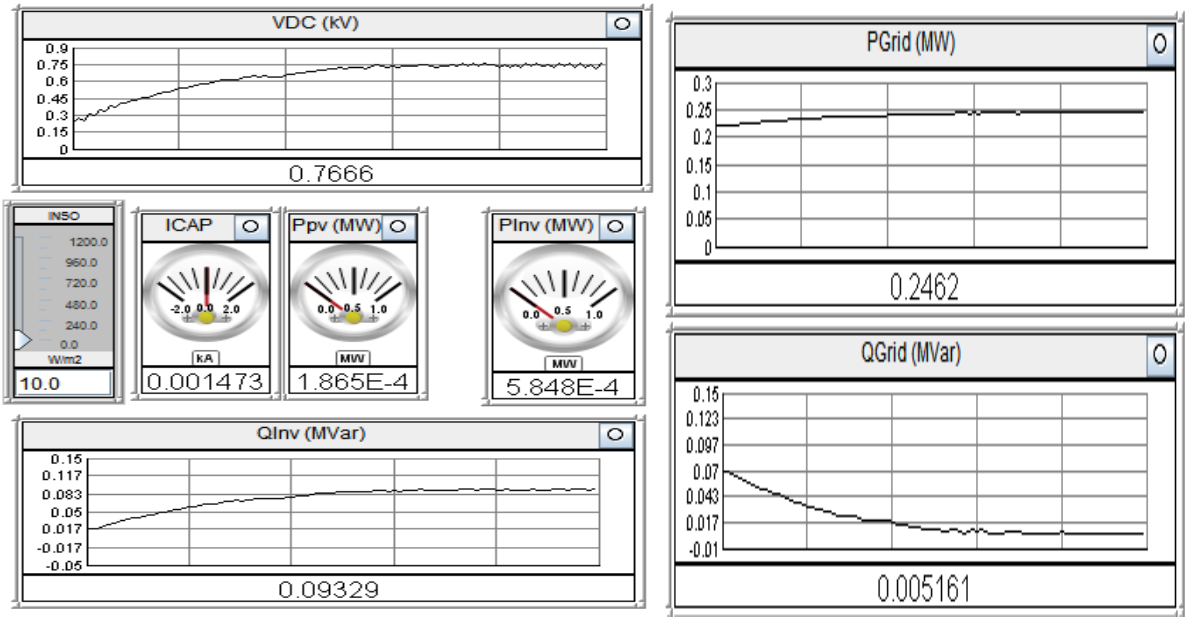

Figure 7.33. Various Operating Parameters of the Solar-DSTATCOM and Grid during the Night-time.

7.5.3.3. Case Study - III: Performance of Solar-DSTATCOM at Various PV Power Levels and Load Profile Variations

In this case study, the influence of load active and reactive power variations on the operation of the Solar-DSTATCOM controller has been verified with controller HIL simulation. The study has been carried out for two load scenarios by changing the active and reactive power demands on the grid to obtain various P.F levels. Also, the variation in power output from the Solar-DSTATCOM is considered for a comprehensive assessment.

A. PV Operational Impact during Various Grid P.F's- If Only Q_{load} Changes:

In the first scenario, the study was performed with variable load reactive power and fixed active power. Consequently, the grid P.F's are varied from 0.7 to 0.9 in steps to achieve realistic conditions. In real time, this condition generally occurs while the large induction machines start up, which increases the reactive power requirement. Moreover, the Solar-DSTATCOM output powers are considered to be changing. The dynamic load scenarios are created for a total of 74sec, in which the load reactive power and PV power/solar irradiation magnitudes are varied for every 3sec and 15sec respectively. Figure 7.34 shows the active and reactive power inputs to the test system, which are scheduled in the RTDS software using scheduler components.

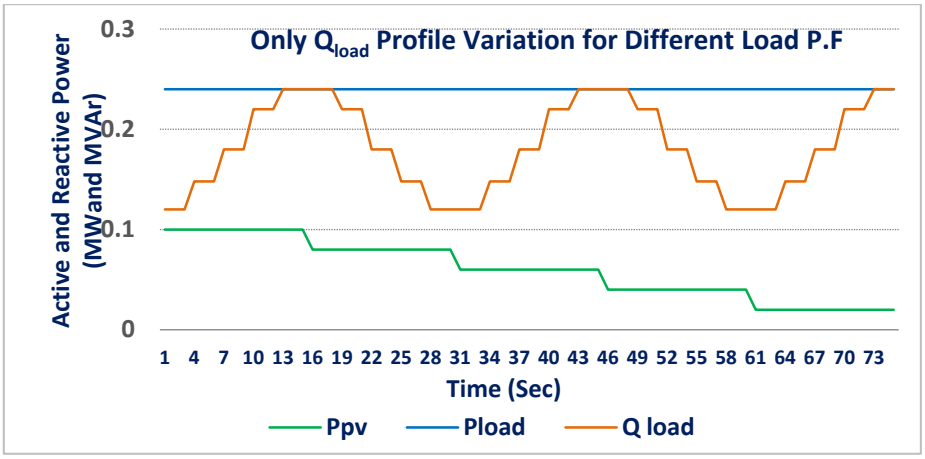

Figure 7.34. Load Active and Reactive Power and PV Power Input Profiles for First Scenario.

A simulation was performed and the active and reactive powers at the Solar-DSTATCOM output, grid supply and load were measured and are as shown in Figure 7.35. The corresponding calculated P.Fs of PV systems, grid and load are indicated in Figure 7.36. It is noticed that when the load reactive power demand increased, in particular when grid P.F decreased from 0.9 to 0.7, the Solar-DSTATCOM controller was operated in P.F correction mode to regulate the grid P.F. It can be seen that during rated conditions, the PV system has sacrificed only 5% of the active power to compensate the grid reactive power demand. Hence, at worst condition, the grid P.F has been increased from 0.7 to 0.92. Further, during low PV power periods, the inverter has supplied maximum reactive power and the P.F was close to 1. Figure 7.37 shows the measured grid voltage at the PCC node. It is noticed that when the reactive power demand increases the system voltage will decreases and vice versa. In low P.F periods, the PCC voltage is regulated to lie above 0.96p.u, and during 0.9 P.F periods the voltage is regulated to be about 1.01p.u, these are within the limits specified by the relevant ANSI standard.

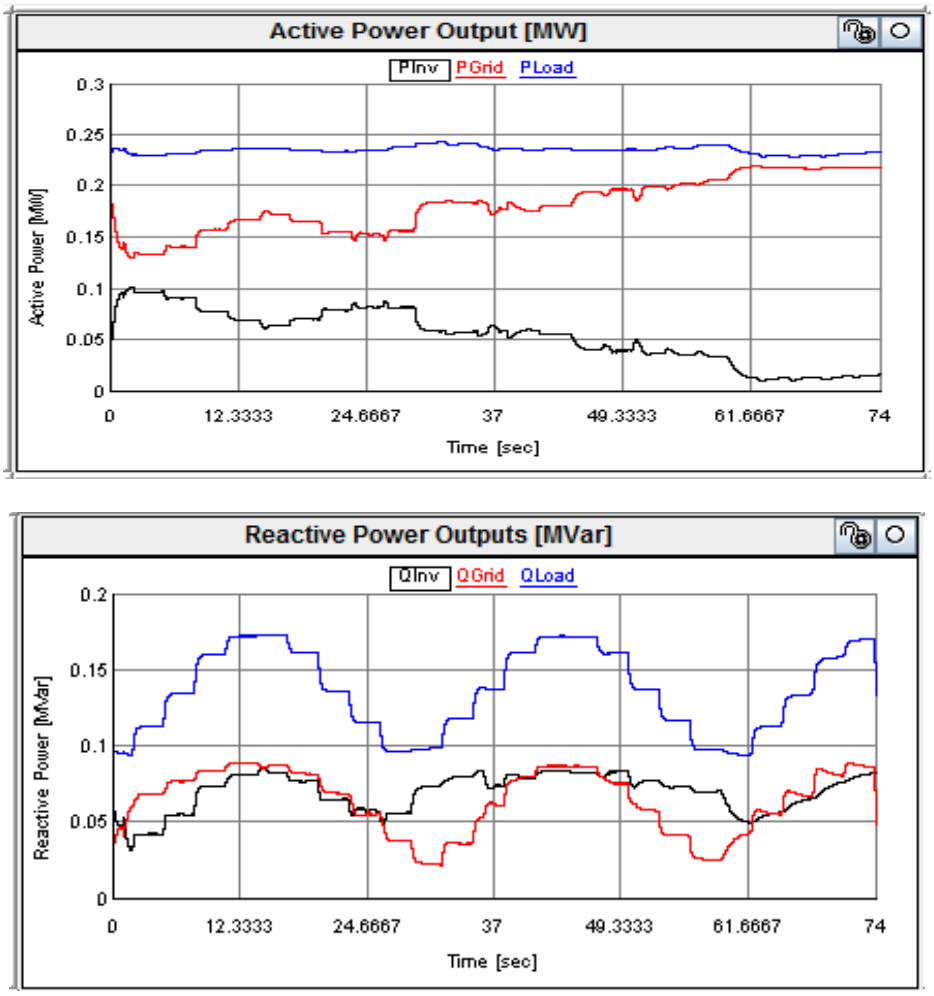

Figure 7.35. Active and Reactive Powers at Solar-DSTATCOM Output, Grid and Load during the First Load Scenario.

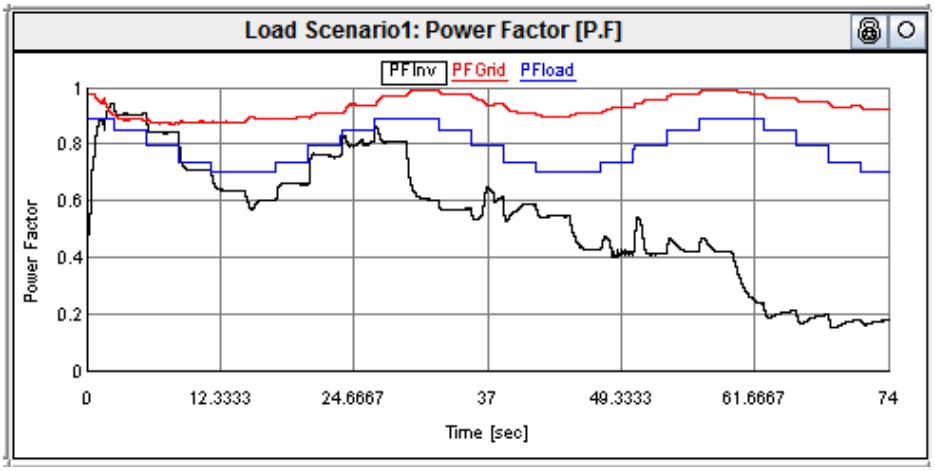

Figure 7.36. Calculated P.F of Solar-DSTATCOM, Grid, and Load.

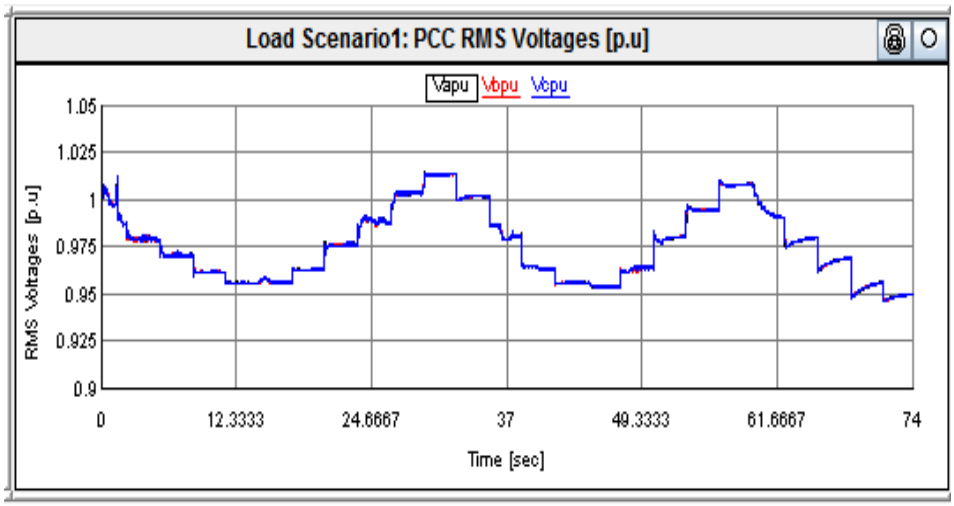

Figure 7.37. Measured PCC RMS Voltages during the First Load Scenario.

It is observed that during the reduced PV power levels and at various load reactive power levels, the Solar-DSTATCOM is operated as a DSTATCOM and injected both real and reactive powers to achieve grid operational necessities. The network operating in lower P.F may result in increased maintenance costs for the utilities, therefore these costs will usually be transferred to the customers in the form of higher tariff charges. To overcome such problems, the Solar-DSTATCOM can be a potential solution for both PV owners and utilities.

Similar to the previous case study, to verify the impact of load variations on the Solar-DSTATCOM controller operation, various outputs of the controller blocks are captured using RTDS and dSPACE software. Figure 7.38 illustrates the DC bus voltage, three-phase inverter output currents and various controller output parameters. It can be seen that the trend of total reactive current I_{qA_total} has an inverse relationship with the load reactive power variations for compensation. The output of the PCC regulator currents are increased during low P.F periods to improve the grid voltage and are decreased at high P.F periods to compensate for the voltage rise issue. It can be seen that the dynamics of controllers for rapid load changes are stable and provided a quick response.

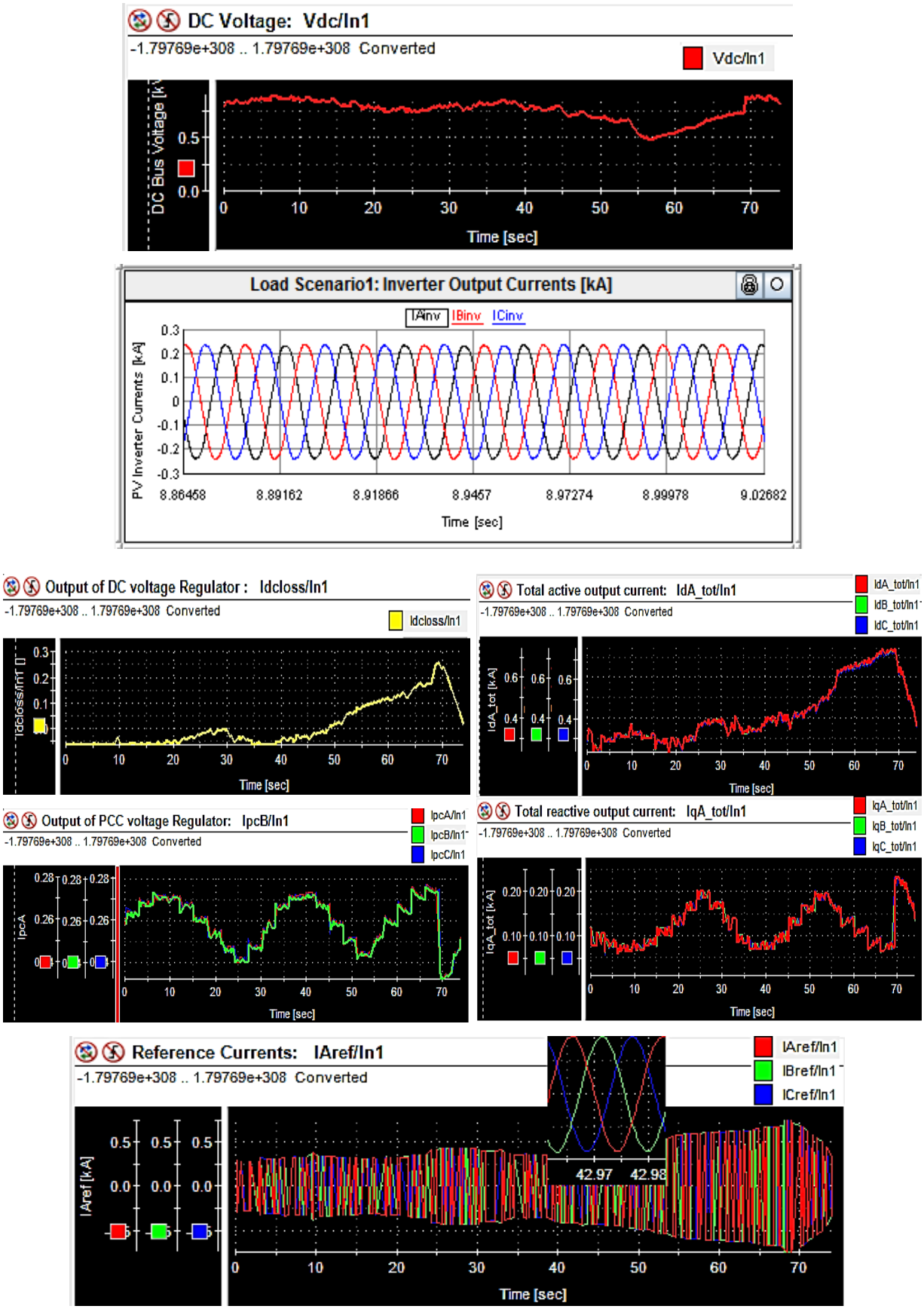

Figure 7.38. Solar-DSTATCOM Controller Various Output Parameters during the First Load Scenario.

B. PV Operational Impact during Various Grid P.F's- If Both P_{load} and Q_{load} Changes:

In this scenario, the evaluation was carried out for both load active and reactive power variation impacts on the Solar-DSTATCOM controller performance. The active and reactive powers were varied such that the load P.F on the network varied between 0.7 and 0.9. Similar to the previous scenario, the simulation scenarios were created for 74sec time and also considered the variations in the PV output powers as displayed in Figure 7.39.

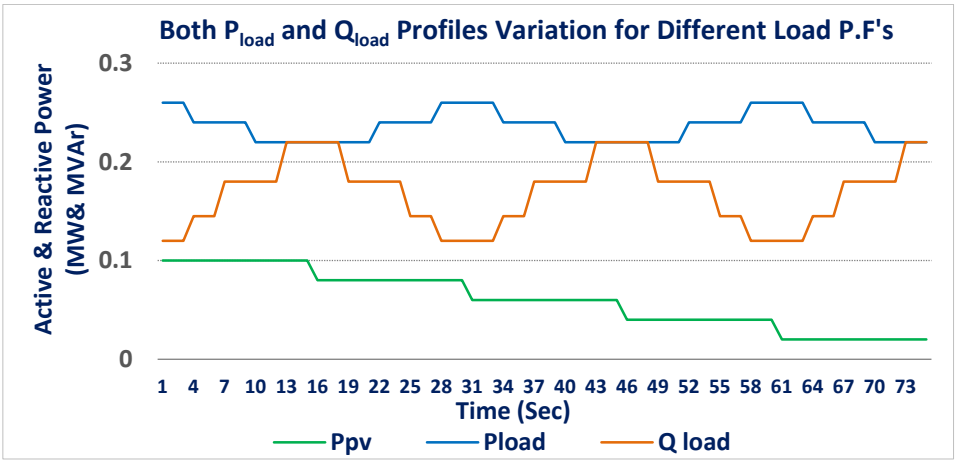

Figure 7.39. Load Active and Reactive Power and PV Power Input Profiles for Second Scenario.

Similar to the first scenario, real-time simulations were performed and the active and reactive powers at Solar-DSTATCOM, grid and load are presented in Figure 7.40. Also, the corresponding calculated P.F's are plotted in Figure 7.41. In comparison with the above scenario, the Solar-DSTATCOM has not reduced its active power injection to the grid during the worst case conditions. However, the controller supplied real and reactive powers in proportion during rated conditions to maintain the grid P.F over 0.82. This kind of control functionality enabled the priority for active power injection, which will be the primary concern of PV system owners. Besides, the PV inverter operates at below its maximum rated current capacity over 95% of the time due to the unavailability of peak solar irradiation. During these times, the excess PV inverter capacity has been utilized for reactive power compensation, which eventually is profitable for the utilities. Further, the grid P.F has been improved for reduced PV output power periods, which is due to the reactive power support from the Solar-DSTATCOM. The grid P.F during this period lies between 0.92 and unity.

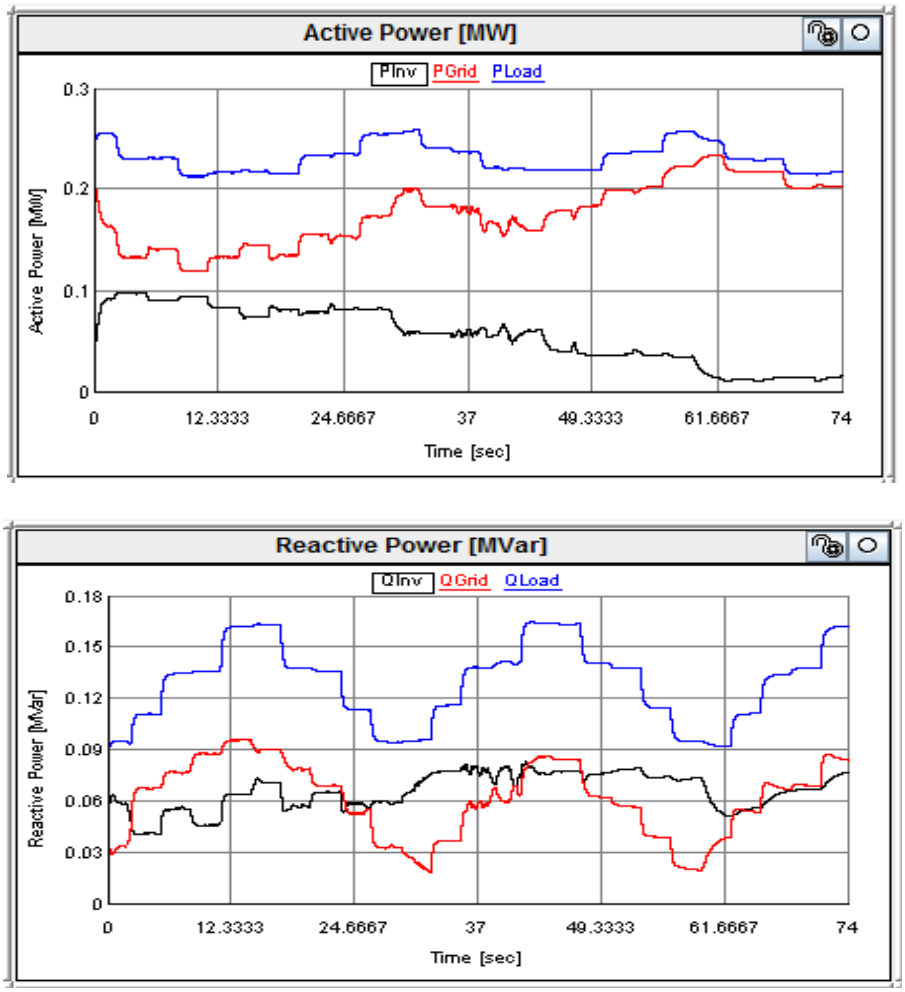

Figure 7.40. Active and Reactive Powers at Solar-DSTATCOM Output, Grid and Load during the Second Load Scenario.

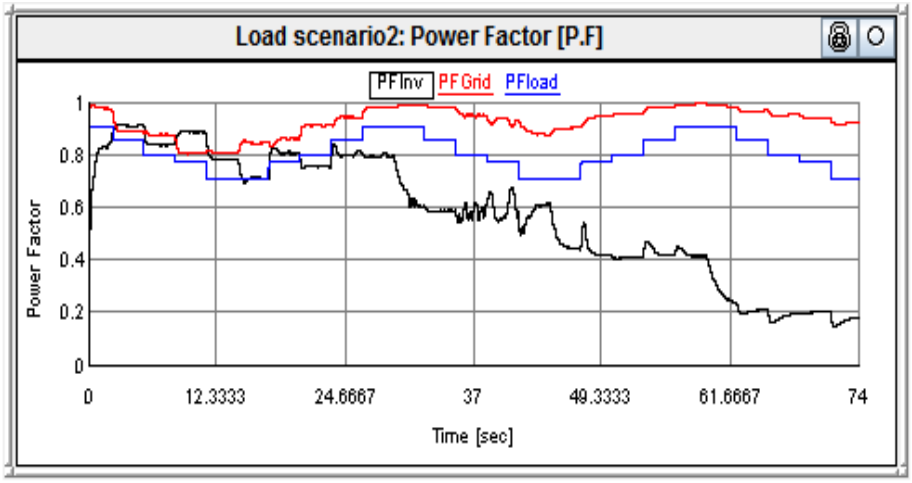

Figure 7.41. Calculated P.F of Solar-DSTATCOM, Grid, and Load.

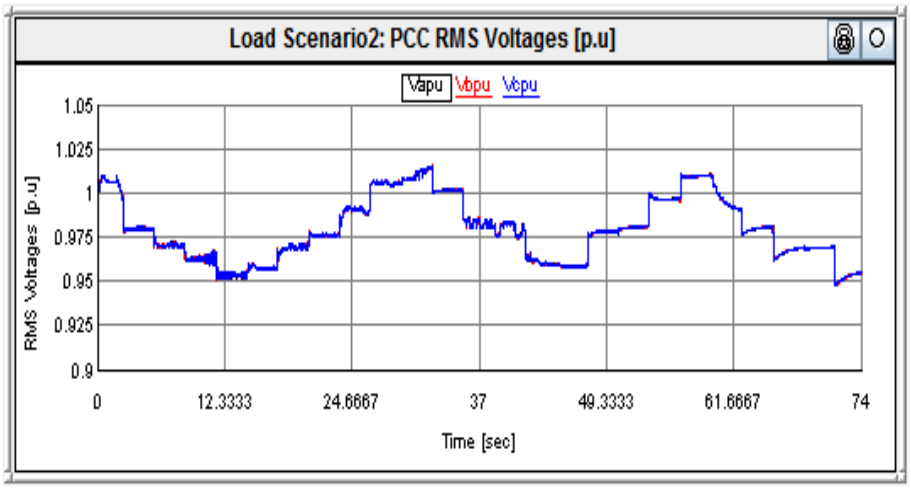

Figure 7.42. Measured PCC RMS Voltages during the Second Load Scenario.

Moreover, the grid PCC voltages are captured and presented in Figure 7.42. It is observed that the voltage magnitudes due to load active and reactive power variations are within the 1.015p.u to 0.96p.u range. The Solar-DSTATCOM voltage controller is applied to improve the voltage to above 0.96p.u in peak load reactive power demand periods. Subsequently, various parameters of the Solar-DSTATCOM controllers are plotted in Figure 7.43 for analysis. Similar to the first scenario, the controller dynamics subjected to input load and PV power variations are faster in response and stable.

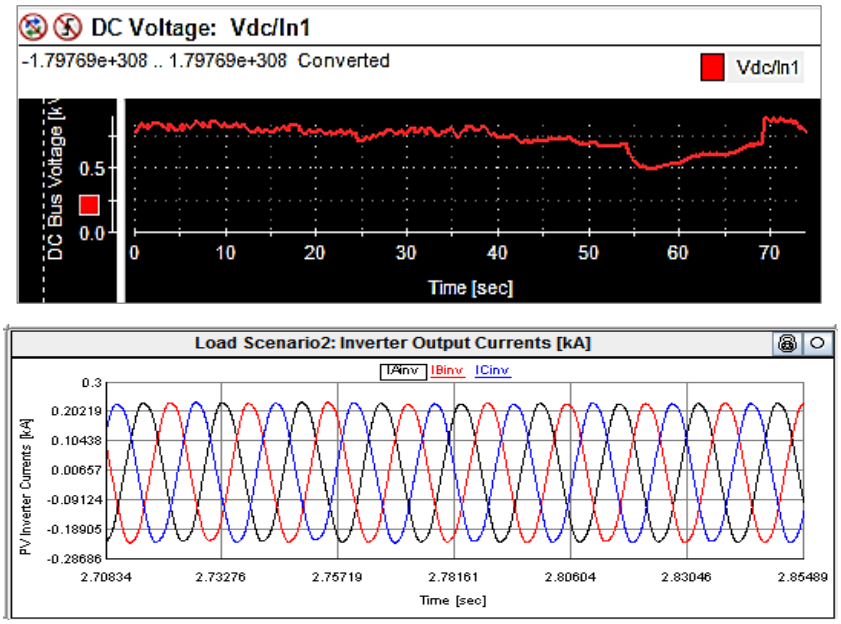

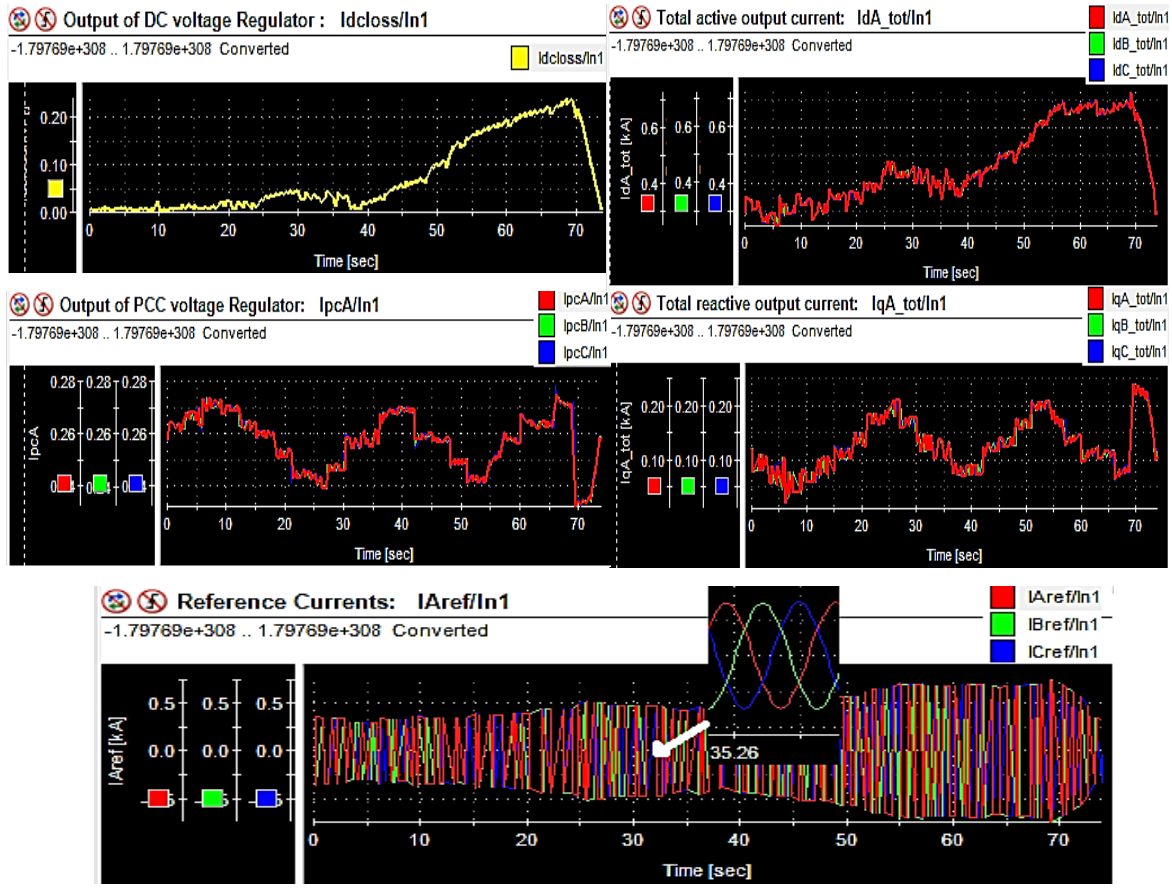

Figure 7.43. Solar-DSTATCOM Controller Various Output Parameters during the Second Load Scenario.

7.5.3.4. Case Study-IV: Harmonic Distortion Analysis

In addition, Harmonic analysis has been done using Fast Fourier Transformation (FFT) to obtain harmonic distortions. The inverter current total harmonic distortion (THD) is measured to be very low about 1.7% and voltage THD is about 0.73% as indicated in Figure 7.44, which are satisfying the limits specified by IEEE 929 [106] and IEEE 519 [53] PV interconnection standards. Moreover, the measured percentage of individual harmonic distortions of voltage and current with respect to their fundamental during rated conditions are shown Figure 7.45. Results show that 5th order harmonic is intensified both in voltage and current, which is satisfying the individual harmonic limits. The next prominent current harmonic is 3rd order, which fluctuated between 0.4 and 1.1%. It is observed that the current magnitudes of 7th order harmonic is below 0.4% and the harmonic orders from 9th to 31st order harmonics laid lower than 0.3%, which are very low according to the IEEE standards. Correspondingly, individual voltage harmonic orders have a similar tendency with the current harmonic orders. Results show that the measured harmonic orders from 3rd to 31st are lower than 0.28% and are satisfying the IEEE limits. Furthermore, for the reduced power levels the Solar-DSTATCOM can produce

a constant THD profile similar to the PSCAD simulation results as indicated in Figures 7.16 and 7.17.

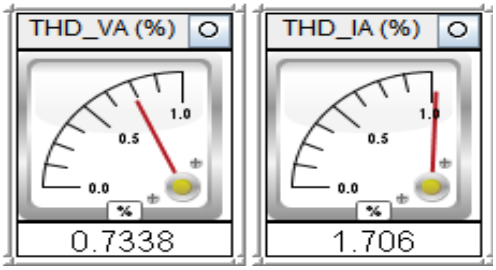

Figure 7.44. Voltage and Current THDs of Solar-DSTATCOM.

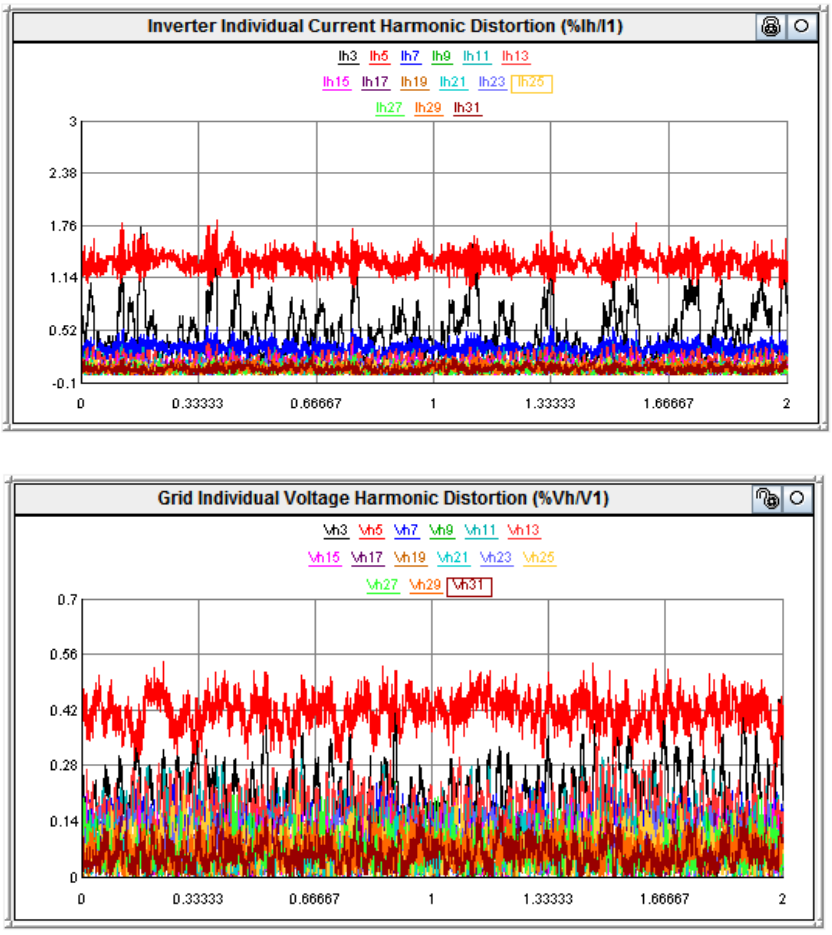

Figure 7.45. Solar-DSTATCOM Individual Harmonic Distortion of Voltage and Current.

7.6. Summary

This chapter presented a novel solution to the poor power qualities caused by PV systems penetration in the distribution network. Regarding that, a new concept of utilizing the PV inverter as a DSTATCOM, which is a custom power device was proposed. A new control strategy to alleviate problems in the unbalanced distribution network, which provides

unbalanced voltage regulation, reactive power and harmonic compensations was introduced and is known as Solar-DSTATCOM. In this chapter, the operation and modelling of the Solar-DSTATCOM control strategy in PSCAD software environment was first presented. Primary assessment was performed on the IEEE bus unbalanced distribution network. The power quality analysis was presented in three case studies. In the first two case studies, the voltage quality issues such as voltage rise, unbalance and sag/swell discussed in Chapter 4 were compensated for with the Solar-DSTATCOM operation. The voltage quality impact of Solar-DSTATCOM daytime and night-time operations were also presented. Finally, the harmonic analysis was performed and the voltage and current harmonic distortion trends were captured for various solar irradiation conditions.

Furthermore in this research, to test and validate the Solar-DSTATCOM controller performance in a real-time environment, controller Hardware-in-the-loop simulations were performed. The controller HIL platform consists of various hardware and software tools which involve RSCAD/RTDS, dSPACE DS1103 control hardware along with associated ControlDesk and MATLAB/Simulink software. The implementation of the proposed Solar-DSTATCOM control algorithm in MATLAB/Simulink with dSPACE RTI library components was presented. The input/output signals from/to RSCAD were converted and transferred through GTAI and GTAO cards. Also, the test system along with a dynamic load considered for this study was modelled in RSCAD. In this research, a comprehensive testing of Solar-DSTATCOM was performed in four different case studies with various realistic grid and PV operating scenarios. The dynamic performance of the Solar-DSTATCOM controller during sunny and cloudy days was investigated. In addition, the night-time operation of the Solar-DSTATCOM was verified. Moreover, various load profile variation interactions on the Solar-DSTATCOM performance was presented. This analysis also considered the Solar-DSTATCOM influence at various output power levels. The trends of various controller outputs and grid operating parameters were captured.

Results from both studies show that the Solar-DSTATCOM performance in unbalanced and balanced network condition has enhanced the grid power quality. Finally, the harmonic emission analysis during rated conditions was presented. The following chapter provides the summary, conclusions and contributions of this thesis.

CHAPTER 8

CONCLUSIONS AND FUTURE WORKS

8.1. Conclusions

Solar PV systems are believed to be one of the most reliable alternative resources to produce electrical energy as it relies on one of the earth natural resources, sunlight. With the proliferation of distributed solar PV systems penetration in existing low voltage (LV) distribution networks, power quality becomes a major area of interest. Although PV systems can have positive impacts on the distribution network to meet local energy demand, they could also have negative impacts. Solar PV systems are sensitive to variations in solar irradiation, which can cause potential challenges in the LV distribution networks. The literature review provided in Chapter 2 revealed that these PV systems could initiate a new set of power quality concerns in terms of voltage quality and harmonics. In addition, traditional distribution networks are unbalanced in nature due to unbalanced loading and line configurations. Consequently, it is very important and interesting to examine the penetration impacts of PV systems in unbalanced network conditions. Therefore, this research has been focussed on the comprehensive investigation of various power quality issues influenced by high PV penetration and also proposes a new compensation method for their mitigation.

In the first part of the thesis, various voltage quality issues such as voltage rise, unbalance, sag/swell and voltage fluctuation/flicker emissions were thoroughly investigated in the unbalanced distribution network with PV systems penetration. Secondly, harmonic emission

issues from PV inverter technologies and their impact on the distribution network were systematically analysed. Furthermore, excitation of harmonic resonance issues associated with PV system dynamic operations were emphasized. After exploring the potential issues, a novel solution was proposed to overcome these power quality issues in the perspective of high level of localised PV penetrations.

In order to study the power quality impacts of PV systems, it is essential that accurate simulation models of PV systems, various kinds of load units and distribution networks are required for accomplishing the dedicated studies, which were presented in Chapter 3. This chapter also provided the background theory of each component of the grid connected PV systems and their models in PSCAD software. In addition, software and hardware tools used throughout this research were presented. The contributions of the thesis along with the main conclusions drawn from individual research works [5-11, 137] are highlighted as below.

In Chapter 4, the assessment of voltage quality issues with PV penetration were provided. Firstly, the investigation was performed through PSCAD simulations on an IEEE-13 bus unbalanced distribution network. For this analysis, a developed dynamic model of a PV system was considered to reflect a realistic PV operating scenario. The analysis was carried out in two case studies to investigate the severity of voltage quality issues.

- In the first case study, simulations were performed to assess voltage rise and unbalance in three scenarios, which included lumped PV penetration at the beginning of the feeder, dispersed PV penetration at multiple buses close to the loads, and with increased penetration by single phase PV systems respectively. In the first two scenarios, the network was considered to have 25% PV penetration and this penetration is increased by 5% in the third scenario. Results show that the voltage rise due to distributed PV integration is higher than compared to the lumped PV penetration at the beginning of the feeder. This impact is even higher with increased PV penetration as in the third scenario. Results also demonstrate that the PV power injection provided the voltage support in the highly loaded phases. Furthermore, the rise in voltages even with the three-phase PV systems are different in each phase due to unbalanced loading and has higher values on the lightly loaded phase. In contrast, voltage unbalance factor is higher in the case of the first scenario as compared to the second scenario. Furthermore, this voltage unbalance has increased in the third scenario with random distributed single-phase PV systems integration.

- In the second case study, fault analysis was carried out to estimate the influence of PV presence and absence in the network during three types of faults. Results showed that during the fault condition, the unbalanced voltage sags are slightly compensated by the contribution of PV power. However, the voltage swell is attained higher values compared to without PV scenario.

Furthermore in Chapter 4, to analyse the voltage quality issues caused by PV system penetration in a real-time distribution network, field measurement based investigations were performed on the University of Queensland (UQ), St Lucia and Gatton Campus PV sites. The PV power generation strongly depends on the solar irradiation and temperature, which impacts the grid voltages. In this research, rapid variation in solar irradiation levels were considered to determine the effect on voltage variation issues.

- Firstly, the investigation was performed on the UQ St Lucia PV site, which had a grid connected PV system with an installed capacity of 1.5 MW. Field measurements were conducted through the installation of Fluke Power Quality Analysers at one of the UQ buildings, which had a 339 kW PV system. For the analysis, the power quality measurements at the PV inverter output level, low voltage and high voltage (HV) sides of the corresponding distribution feeder were recorded for various operating days. Results show that the network voltage magnitudes are increased with respect to the PV power injection. In the UQ St Lucia network, the voltage rise at the integration point is actually compensated by the voltage drop caused by loads and the voltage levels are well within the limits. Furthermore, the voltage fluctuations and flicker caused by variations in solar irradiation were analysed. Results show that during the measurement period, the voltage flickers were lower and satisfied the AS/NZS standard. Nevertheless, the severity of voltage flickers may vary depending on the ramp rate of cloud transients and the connected PV systems size. For this reason, the measurement data of 1-year at the LV and HV sides of the PCC was analysed. Measurements of some typical days exhibited higher flicker emission levels. In order to quantify the probability of the flicker levels in a year, a data clustering technique was applied for further assessment. It is confirmed that the voltage flickers are insignificant in the UQ 339kW PV site and are well within the limits according to the AS/NZS standard.
- Secondly, the measurement based investigation was performed on a large scale of a 3.3MW PV system, which is located at the UQ Gatton campus. Note that this distribution network had a Step Voltage Regulator (SVR) for voltage regulation, which was connected

at the 11kV side. The power quality measurements were recorded at the PV inverter output and the grid interconnection point of the 11kV side for a three months' period with 1 second resolution. Similar voltage variation trends with respect to PV power generation are observed and the voltage magnitudes are within the limits specified by the AS/NZS standard and the Energex agreement. However, the voltage rise impact on the 11kV network with PV Power injection is slightly reduced by the SVR operation. However, the voltage fluctuations are higher and exceeded the limits most of the time, which might be due to the false operation of the SVR. In addition, these voltage fluctuations are increased during heavy cloud periods. Furthermore, results of the flicker emissions at the 11kV side of the PCC through clustering technique showed that the voltage flickers are appeared to be under control for 70% of the time and satisfying the AS/NZS standard limits. From the results, it is perceived that the flicker levels are more noticeable in the 3.3MW PV system as compared with the 1.5MW PV system, which depend on the size, location of the PV system and connected network operating condition.

In Chapter 5, the harmonic emission issues from PV systems and their penetration impacts on the distribution network were analysed. In this chapter, firstly the characterisation of harmonics and their interaction issues associated with multiple PV systems interconnection was studied with simulations and compared with field measurements. This analysis considered the variations in solar irradiation conditions. The simulation assessment was supplemented with simulations in two case studies, which reveals the PV system operation in the case of with and without the presence of background harmonic distortions in the supply network. To inject harmonic distortions into the network, developed detailed power electronic based nonlinear load models were connected to the IEEE-13 bus network. Moreover, a validation study was performed through field investigations conducted at the UQ 1.5 MW PV site. The measurement data for various operating days at the inverter level were recorded through Fluke power quality analysers.

- Measurement results indicate that the characteristics of harmonics have identical trends with simulations. The individual voltage harmonics had a linear relationship with the solar power generation. The percentage of voltage distortion is increased due to the increased voltage amplitude with the addition of PV inverters and also the influence of augmentation of individual voltage harmonic magnitudes. The individual voltage and current harmonics during rated power levels are within the limits prescribed by the IEEE and AS/NZ standards. However, the current THD has increased due to lower fundamental component

of current during low power levels. Nonetheless, the standards only provide limiting values of the harmonic limits during rated conditions. Besides, in the case of multiple PV integrations the current harmonic levels appeared to be minimized due to increase in fundament current, however the individual harmonic magnitudes increased with every parallel PV penetration.

Moreover in Chapter 5, the impact of increased harmonic distortion levels with high PV penetration on a LV distribution network was assessed. A thorough harmonic behaviour analysis was first performed on the IEEE-13 bus network with high PV penetration. Furthermore, an evaluation study was conducted at the UQ, St Lucia PV network to validate simulation results.

- In the simulation study, to simulate a real-time network scenario, several types of probabilistic nonlinear loads were incorporated in the network for harmonics injection. In addition, to consider the effect of a PV inverter control scheme on the network harmonic levels, two types of PV inverter models were considered. The investigation was carried out in three different case studies, namely PV systems integration at a single node in particular with and without background harmonic distortions in the supply and finally PV penetration at multiple nodes with supply distortions. Simulation results show that the harmonics generated from PV systems are multiplied in nature due to an increase in individual voltage magnitudes. These magnitudes are also dependent on the concentration of harmonics from nonlinear loads. The voltage THDs are higher at the PCC and after the PCC node or end feeder node. Results confirmed that the distortion levels increased with multiple installations at the same node compared to dispersed integration.
- The current harmonic distortions are higher at upstream nodes of the network because of PV power injection causing a supply current reduction. However, the current THDs are exceeding the IEEE limit at the PCC node and the nodes after PCC with increased PV penetration, where the magnitude of network fundamental current is same. Further, even though three-phase PV systems inject balanced currents into the IEEE 13 bus network, the harmonic distortion levels are different in each phase due to an unbalanced customer loading level. Furthermore, depending on the type of control strategy, the harmonic generations from PV systems and their interaction impacts in the network are dissimilar.
- In addition, the harmonic field measurements were taken by PQ analysers at the LV and HV sides of the UQ network for different operating conditions. Measured results show that

the THD trends follow similar trends as with simulation results. The THD of voltage and currents increases with PV power injection. The levels of current harmonics are significantly increased at the distribution transformer during rated PV power output and full load condition. The corresponding k-factor measurements show the effect of excessive harmonic flow in the transformer, which could lead to overloading and heating.

- The harmonic effect is shown to be under control, however increased PV system penetration in the distribution network can cause adverse effects. The capacity of the existing feeder lines and the transformers are not able to withstand such conditions. So, the utilities are required to pay attention to preventive measures.

In addition, the analysis of harmonic resonances accompanied with the PV inverter systems was presented in Chapter 6. Harmonic analysis was carried out through simulations on the IEEE-13 bus unbalanced distribution network in two different case studies, namely with and without harmonic distortions in the supply network. In each case study, the dynamic operations of two PV inverter control topologies for variations in solar irradiation were considered to characterise the harmonic resonance modes in the network. Also, a frequency versus impedance scan has been presented with respect to each resonance condition. Furthermore, a validation study has been carried out with the field measurement data obtained at the University of Queensland PV system.

- Simulation results show that the harmonic resonance occurrence is not only reliant on the type of inverter control topology, filters and the number of PV inverter systems but also on the network configuration and type of load. The integration of PV systems in the distribution network modified the magnitude of grid impedance and shifted its resonance frequency. Analysis revealed that the generated harmonics PV systems during rated condition have satisfied the standard limits. However, the dynamic controller operation of PV systems due to cloud transients injected high harmonic components into the network, which may have excited the resonance conditions in the network. The amplification of voltage and current distortions during harmonic resonance exceeded the limits according to the IEEE 519 standards.
- Moreover, to verify and validate the simulation results in the case of a real distribution network, the harmonic measurement data of 1-year collected from the UQ PV system has been analysed. Results show that the probability of harmonic resonance events are higher in the real network and possess severe voltage and current THDs on the 11kV line and are

confirming the simulation results. At present, during rated PV output power levels, the distortions in the network are found to be under control. However, the regular incidence of resonance conditions can lead to malfunction of sensitive devices, overheating and premature ageing of the distribution transformer. Therefore, the utilities are required to take measures of harmonic compensation devices to overcome these issues.

In Chapter 7, to address these power quality issues a new approach of adopting the PV inverter as a Solar-DSTATCOM with the help of a new control strategy was proposed. The proposed control topology can independently regulate the phase voltage and provide harmonic and reactive power compensation in each phase during the whole day. At first, the investigation was performed through PSCAD simulations and further testing and a validation study was performed in the real-time controller Hardware-in-the-loop platform.

- For the simulation study, an IEEE-13 bus unbalanced distribution network was considered. In this work, a static variation of solar insolation condition was applied to verify the effectiveness and robustness of the proposed control scheme in improving power quality of the unbalanced distribution network. This study emphasized the compensation of various power quality issues, namely voltage rise, unbalance, sag/swell and harmonics. Regarding this, simulations were performed for three different case studies. Simulation results showed that the voltage rise and voltage unbalance levels due to PV power injection were compensated. Also, results from fault analysis demonstrated that the unbalanced voltage sags and swells during unsymmetrical and symmetrical grid faults were greatly ameliorated. Results from the harmonic analysis showed that individual voltage and current harmonics were lower and were well within the Australian/New Zealand and IEEE standards. The current THD has possessed a constant profile for varied solar irradiation levels from daytime to night-time operation. Therefore, this proposed novel control topology enabled independent phase reactive power compensation and voltage regulation at the PCC and showed superior performance in an unbalanced system.
- In addition, this chapter presented a real-time controller Hardware-in-the-loop simulation of the proposed Solar-DSTATCOM using RSCAD/RTDS, dSPACE DS1103 control hardware and the MATLAB/Simulink software platform. For this, a test system along with PV inverter systems were modelled in RSCAD and the proposed controller was implemented in Simulink using dSPACE RTI library components. A comprehensive testing of the Solar-DSTATCOM controller was performed in various case studies with various realistic operating scenarios. The impacts of solar irradiation variations of sunny

and cloudy days on the Solar-DSTATCOM daytime operation were investigated. Also, the night-time operation of Solar-DSTATCOM has been presented. Furthermore, the Solar-DSTATCOM performance has been verified for the load profile variations. The trends of various controller outputs and grid operating parameters were captured. Results indicated that the Solar-DSTATCOM has provided the reactive power support during both day and night-time along with active power injection during the daytime. Moreover, the Solar-DSTATCOM has improved grid performance during load operations by providing reactive power compensation thereby improving the grid power factor and PCC voltage regulation similar to the DSTATCOM. The controller responses with respect to the rapid input variations are faster. The harmonics emissions are very low and satisfy the IEEE standard limits.

Implementing this type of advanced functionality in the PV inverter systems will enable additional revenue for PV owners and grid operators in addition to the feed-in-tariffs for active power generation. Multiple installations of this type of PV inverter will better manage the LV network by controlling the grid in a distributed manner and the response would be faster compared to a single point control.

8.2. Summary of Contributions

This research has investigated power quality challenges associated with high penetration of PV systems in LV distribution network and proposed a practical solution to overcome these issues. The main contributions of this thesis are summarised as follows:

Investigation of Voltage Quality Impacts:

- Various voltage quality issues in a LV unbalanced distribution network with high PV penetration were investigated thoroughly in PSCAD simulations.
- For that purpose, a comprehensive dynamic PV source, different PV inverter models and IEEE-13 bus test systems was developed.
- Practical field investigation of voltage quality challenges in the real grid connected PV sites located at the University of Queensland St. Lucia and Gatton Campuses, were performed.
- The impact of short-term solar irradiation variations on voltage flicker emissions were evaluated.
- Using the actual measurement data of several months, the probability of voltage flicker severity was estimated.

Assessment of Harmonic Impact of PV Systems:

- The harmonic emission characteristics of PV systems and their aggregation issues during real operating conditions were assessed through PSCAD simulations and validated with actual measurements obtained through practical connection of power quality analysers.
- Harmonic impact of high penetration PV systems on the unbalanced distribution network was comprehensively analysed through PSCAD simulations and validated with field measurements.
- For the simulation study, IEEE-13 bus network with comprehensive linear, nonlinear harmonic producing load models and different PV inverter systems were developed to demonstrate real network operating scenarios.
- Developed online JAVA programs to extract the real-time harmonic measurements at various voltage levels of UQ PV site.
- The phenomenon of harmonic resonance on the distribution network with PV system penetrations and their dynamic operational interactions were also analysed through simulations and compared with the actual harmonic measurements.

Practical Solution to Mitigate Power Quality Issues:

- A novel practical solution of adopting PV inverter as a virtual DSTATCOM was proposed named as Solar-DSTATCOM.
- A new control algorithm for Solar-DSTATCOM to compensate power quality issues in unbalanced and balanced distribution networks was designed and implemented.
- The performance of developed new control algorithm was verified initially in PSCAD software environment and detailed investigations were performed on IEEE-13 bus unbalanced network to compensate poor power quality issues during the daytime and night-time.
- Comprehensive testing and validation of Solar-DSTATCOM controller was performed in Real-time Hardware-in-the-Loop simulation platform. This practical setup combines Real-time Digital simulator and dSPACE control hardware board.
- Various studies were conducted to demonstrate the performance of Solar-DSTATCOM controller for daytime, night-time and dynamic load demand scenarios.

8.3. Future Works

Recommendations for future research are as follows.

- Further research to investigate the Solar-DSTATCOM operation in mitigating the voltage quality issues in various scenarios through RSCAD real-time simulations is recommended.
- Analysis of field measurement data monitoring at the distribution transformer levels are required to better manage the LV network and to maximize PV penetration.
- More research is required to understand and mitigate the harmonic resonance issues accompanied with PV systems penetration.
- In future, Energy storage systems will play a vital role in the LV networks. The collective impact of PV and energy storage technology need to be studied. Also, the proposals like community energy storage and distributed energy storage systems installation in the network could be interesting.

REFERENCES:

[1] "IEA World Energy Outlook," International Energy Agency, 2015.

[2] "Renewables 2015 Global Status Report, [Online] Available on http://www.ren21.net/status-of-renewables/global-status-report/http://www.ren21.net/wp-content/uploads/2015/07/GSR2015_KeyFindings_lowres.pdf," 2015.

[3] "EPIA: Global Market Outlook- For Photovoltaics 2014-2018," Eur. Photovolt. Ind. Assoc, 2014.

[4] "AEMO 2012b rooftop PV information; available online at http://www.aemo.com.au/Electricity/~/.../Rooftop_PV_Information_Paper.ashx."

[5] A. Chidurala, T. K. Saha, and N. Mithulananthan, "Harmonic characterization of grid connected PV systems and validation with field measurements," in *Power & Energy Society General Meeting, 2015 IEEE*, Denver, CO, USA, 2015, pp. 1-5.

[6] A. Chidurala, T. Saha, and N. Mithulananthan, "Field investigation of voltage quality issues in distribution network with PV penetration," in *Power and Energy Engineering Conference (APPEEC), 2015 IEEE PES Asia-Pacific*, 2015, pp. 1-5, Brisbane, Australia.

[7] A. Chidurala, T. K. Saha, and N. Mithulananthan, "Power quality enhancement in unbalanced distribution network using Solar-DSTATCOM," in *Power Engineering Conference (AUPEC), 2013 Australasian Universities*, 2013, pp. 1-6, Hobart, Tasmania.

[8] A. Chidurala, T. K. Saha, and N. Mithulananthan, "Harmonic impact of high penetration photovoltaic system on unbalanced distribution networks – learning from an urban photovoltaic network," 'Harmonic impact of high penetration photovoltaic system on unbalanced distribution networks – learning from an urban photovoltaic network', IET Renewable Power Generation, Volume 10, Issue 4, April 2016, pp. 485 – 494 DOI: 10.1049/iet-rpg.2015.0188.

[9] A. Chidurala, T. K. Saha, N. Mithulananthan, and R. C. Bansal, "Harmonic emissions in grid connected PV systems: A case study on a large scale rooftop PV site," in *PES General Meeting | Conference & Exposition, 2014 IEEE*, 2014, pp. 1-5, National Harbor, MD, USA.

[10] A. Chidurala, Tapan Kumar Saha, and Mithulananthan N., "Real-Time Controller Hardware-in-the-Loop Simulations of Solar-DSTATCOM," *Submitted to IEEE transaction on Industrial Electronics*, Submitted on 15 March, 2016.

[11] A. Chidurala, Tapan Kumar Saha, and Mithulananthan N., "Harmonic Resonance on the Distribution Network with PV Penetration and Field Measurements Validation," *Elsevier International Journal of Electrical Power & Energy Systems journal*, Submitted on 3 July 2015.

[12] M. Munsell. (2016) U.S. Solar Market Insight: Q3 2015 available on www.greentechmedia.com/research/subscription/u.s.-solar-market-insight.

[13] T. Buckley, "India's Electricity-Sector Transformation: available online on http://ieefa.org/wp-content/uploads/2015/08/IEEFA-Indian-Electricity-Sector-Transformation-August-2015.pdf," Institute for Energy Economics and Financial Analysis (IEEFA), August 2015.

[14] "The Renewable Energy Target (RET) scheme | Department of the Environment: available online on https://www.environment.gov.au/climate-change/renewable-energy-target-scheme," Accessed on Feb 2016.

[15] *Australian PV Institute live report on market analyses, available online at http://pv-map.apvi.org.au/analyses.*

[16] "Energex Distribution Annual Planning Report," August 2015.

[17] R. Tonkoski, D. Turcotte, and T. H. M. El-Fouly, "Impact of High PV Penetration on Voltage Profiles in Residential Neighborhoods," *Sustainable Energy, IEEE Transactions on,* vol. 3, pp. 518-527, 2012.

[18] "PVupscale. Publication review on the impacts of PV Distributed Generation and Electricity networks [cited 03/11/2011]: available from http://www.pvupscale.org/IMG/pdf/D41_final.pdf," 2007.

[19] G. M. Comfort. R, Mansoor. A, Barker. P, Short. T, Sundaram. A, "Power Quality Impact of Distributed Generation Effect on Steady State Voltage Regulation," PQA conference, 2001.

[20] M. E. Baran, H. Hooshyar, Z. Shen, J. Gajda, and K. M. M. Huq, "Impact of high penetration residential PV systems on distribution systems," in *Power and Energy Society General Meeting, 2011 IEEE,* 2011, pp. 1-5, San Diego, CA.

[21] Y. Ruifeng and T. K. Saha, "Voltage Variation Sensitivity Analysis for Unbalanced Distribution Networks Due to Photovoltaic Power Fluctuations," *Power Systems, IEEE Transactions on,* vol. 27, pp. 1078-1089, 2012.

[22] "Addressing Grid interconnection issues with variable renewable energy sources," Asia Pacific Economic corporation, IT Power Australia, http://www.itpau.com.au/wp-content/uploads/2012/08/ITP-APEC-Web-Summary.pdfDec 2010 2010.

[23] M. S. ElNozahy and M. M. A. Salama, "Technical impacts of grid-connected photovoltaic systems on electrical networks—A review," *Journal of Renewable and Sustainable Energy,* vol. 5, p. 032702, 2013.

[24] Patsalides, M., Evagorou, D., Makrides, G., Achillides, Z., Georghiou, G.E., Stavrou, A., Efthymiou, V., Zinsser, B., Schmitt, W. and Werner, J.H. (2007) The effect of solar irradiance on the power quality behaviour of grid connected photovoltaic systems. In, International Conference on Renewable energies and Power Quality, ICREPQ, La Coruña, ES, 25 - 27 Mar 2007.

[25] Y. Ruifeng and T. K. Saha, "Investigation of voltage sensitivities to photovoltaic power fluctuations in unbalanced distribution networks," in *Power and Energy Society General Meeting, 2012 IEEE*, 2012, pp. 1-7, San Diego, CA.

[26] Y. Ruifeng and T. K. Saha, "Investigation of voltage variations in unbalanced distribution systems due to high photovoltaic penetrations," in *Power and Energy Society General Meeting, 2011 IEEE*, 2011, pp. 1-8, San Diego, CA.

[27] A. Woyte, V. Van Thong, R. Belmans, and J. Nijs, "Voltage fluctuations on distribution level introduced by photovoltaic systems," *Energy Conversion, IEEE Transactions on*, vol. 21, pp. 202-209, 2006.

[28] J. Marcos, L. Marroyo, E. Lorenzo, D. Alvira, and E. Izco, "Power output fluctuations in large scale pv plants: One year observations with one second resolution and a derived analytic model," *Progress in Photovoltaics: Research and Applications*, vol. 19, pp. 218-227, 2011.

[29] E. M. Stewart, T. P. Aukai, S. D. J. MacPherson, B. P. Quach, D. Nakafuji, and R. Davis, "A realistic irradiance-based voltage flicker analysis of PV applied to Hawaii distribution feeders," in *Power and Energy Society General Meeting, 2012 IEEE*, 2012, pp. 1-7, San Diego, CA.

[30] F. Shahnia, A. Ghosh, G. Ledwich, and F. Zare, "Voltage Unbalance reduction in low voltage distribution networks with rooftop PVs," in *Universities Power Engineering Conference (AUPEC), 2010 20th Australasian*, 2010, pp. 1-5, Christchurch.

[31] F. Shahnia, Majumder, R., Ghosh, A.,Ledwich, G., Zare, F., "Voltage unbalance analysis in residential low voltage distribution networks with rooftop PVs," *ELECTRIC POWER SYSTEMS RESEARCH*, vol. 81, pp. 1805-1814, 2011.

[32] A. von Jouanne and B. Banerjee, "Assessment of voltage unbalance," *Power Delivery, IEEE Transactions on*, vol. 16, pp. 782-790, 2001.

[33] A. Guinane, G. M. Shafiullah, A. M. T. Oo, and B. E. Harvey, "Voltage fluctuations in PV penetration on SWER networks -A case study for regional Australia," in *Power and Energy Society General Meeting, 2012 IEEE*, 2012, pp. 1-6, San Diego, CA.

[34] J. D. Mondol, Y. Yohanis, M. Smyth, and B. Norton, "Long term performance analysis of a grid connected photovoltaic system in Northern Ireland," *Energy Conversion and Management*, vol. 47, pp. 2925-2947, 11// 2006.

[35] D. L. Garrett and S. M. Jeter, "A photovoltaic voltage regulation impact investigation technique. I. Model development," *Energy Conversion, IEEE Transactions on*, vol. 4, pp. 47-53, 1989.

[36] "IEEE Std 1250-1995: IEEE guide for service to equipment sensitive to momentary voltage disturbances," ed, 1995.

[37] M. I. A. Bakar, "Assessments for the impact of harmonic current distortion of non linear load in power system harmonics," in *Transmission and Distribution Conference and Exposition: Latin America, 2008 IEEE/PES*, 2008, pp. 1-6.

[38] S. S. T. R.Kameswara Rao, "Harmonic modelling of residential and commercial loads with unified power quality conditioner," *International Journal of Scientific and Engineering Research*, pp. 770-743, 2012.

[39] Y. Jing, C. Liang, and C. Shuangyan, "Modeling of Home Appliances for Power Distribution System Harmonic Analysis," *Power Delivery, IEEE Transactions on*, vol. 25, pp. 3147-3155, 2010.

[40] M. G. Villalva, J. R. Gazoli, and E. R. Filho, "Comprehensive Approach to Modeling and Simulation of Photovoltaic Arrays," *Power Electronics, IEEE Transactions on*, vol. 24, pp. 1198-1208, 2009.

[41] T. Esram and P. L. Chapman, "Comparison of Photovoltaic Array Maximum Power Point Tracking Techniques," *Energy Conversion, IEEE Transactions on*, vol. 22, pp. 439-449, 2007.

[42] J. Schlabbach, "Harmonic current emission of photovoltaic installations under system conditions," in *Electricity Market, 2008. EEM 2008. 5th International Conference on European*, 2008, pp. 1-5, Lisboa.

[43] G. Chicco, J. Schlabbach, and F. Spertino, "Experimental assessment of the waveform distortion in grid-connected photovoltaic installations," *Solar Energy*, vol. 83, pp. 1026-1039, 7// 2009.

[44] M. Sidrach-de-Cardona and J. Carretero, "Analysis of the current total harmonic distortion for different single-phase inverters for grid-connected pv-systems," *Solar Energy Materials and Solar Cells*, vol. 87, pp. 529-540, 5// 2005.

[45] J. H. R. Enslin and P. J. M. Heskes, "Harmonic interaction between a large number of distributed power inverters and the distribution network," *Power Electronics, IEEE Transactions on*, vol. 19, pp. 1586-1593, 2004.

[46] A. Bhowmik, A. Maitra, S. M. Halpin, and J. E. Schatz, "Determination of allowable penetration levels of distributed generation resources based on harmonic limit considerations," *Power Delivery, IEEE Transactions on*, vol. 18, pp. 619-624, 2003.

[47] F. J. F.J. Ruiz-Rodriguez *Modeling of photovoltaic generator as a random variable*: Nova Publisher, 2014 in blue, : 'Photovoltaics: synthesis, applications and emerging technologies' (Nova Publisher, 2014), pp. 91–120.

[48] F.-J. Ruiz-Rodriguez, Hernandez, J.-C., Jurado, F., "Harmonic modelling of PV systems for probabilistic harmonic load flow studies," *Int. J. Circuit Theory Application*, pp. 1541–1565 2015.

[49] R. Torquato, F. C. L. Trindade, and W. Freitas, "Analysis of the harmonic distortion impact of photovoltaic generation in Brazilian residential networks," in *Harmonics and Quality of Power (ICHQP), 2014 IEEE 16th International Conference on*, 2014, pp. 239-243, Bucharest.

[50] A. A. Latheef, "Harmonic impact of photovoltaic inverter systems on low and medium voltage distribution systems," MEng, University of Wollongong, 2006.

[51] H. Farooq, Z. Chengke, M. E. Farrag, and M. Ejaz, "Investigating the Impacts of Distributed Generation on an Electrical Distribution System Already Stressed by Non-Linear Domestic Loads," in *Power and Energy Engineering Conference (APPEEC), 2012 Asia-Pacific*, 2012, pp. 1-4, Shanghai.

[52] "IEEE 519-1995: IEEE recommended practices and requirements for harmonic control in electrical power system," ed IEEE, 1995.

[53] "IEEE Standard 519-2014: *EEE recommended practices and requirements for harmonic control in electrical power systems*," ed: IEEE, 2014.

[54] A. Elmoudi, M. Lehtonen, and H. Nordman, "Effect of harmonics on transformers loss of life," in *Electrical Insulation, 2006. Conference Record of the 2006 IEEE International Symposium on*, 2006, pp. 408-411, toronto, Ont.

[55] D. Martin, S. Goodwin, O. Krause, and T. Saha, "The effect of PV on transformer ageing: University of Queensland's experience," in *Power Engineering Conference (AUPEC), 2014 Australasian Universities*, 2014, pp. 1-6, Perth, WA, Australia.

[56] J. Desmet, C. Debruyne, J. Vanalme, and L. Vandevelde, "Power injection by distributed generation and the influence of harmonic load conditions," in *Power and Energy Society General Meeting, 2010 IEEE*, 2010, pp. 1-6, Minneapolis, MN.

[57] *Modeling and Control of Sustainable Power Systems*. Springer: Green Energy and Technology, 2012.

[58] S. J. Lewis, "Analysis and management of the impacts of a high penetration of photovoltaic systems in an electricity distribution network," in *Innovative Smart Grid Technologies Asia (ISGT), 2011 IEEE PES*, 2011, pp. 1-7, Perth, WA, Australia.

[59] T. F. o. H. M. a. Simulation, "Modelling and simulation of the propagation of harmonics in electric power networks. I. concepts, models, and simulation techniques," *IEEE Trans. Power Deliv.ery*, vol. 11, pp. 452–465 1996.

[60] S. A. Ali, "Impact of Personal Computers and Compact Fluorescent Lamps on the Power Quality," *American Academic & Scholarly Research Journal*, vol. 5, March 2013.

[61] J. T. E. Caamano, H. D. Moor, et al., "State-of-the-art on dispersed PV power generation: Publications review on the impacts of PV distributed generation and electricity networks," EIE/05/171/SI2.420208 23rd June 2007.

[62] B. G. S. Cobben, and H. Laukamp, "WP4 – Deliverable 4.3 - Impact of Photovoltaic Generation on Power Quality in Urban Areas with High PV Population," EIE/05/171/SI2.4202082008.

[63] N. R. W. Jos Arrillaga, *Power Systems harmonics*: John Wiley & Sons Ltd, 2003.

[64] J. H. R. Enslin, W. T. J. Hulshorst, A. M. S. Atmadji, P. J. M. Heskes, A. Kotsopoulos, J. F. G. Cobben, *et al.*, "Harmonic interaction between large numbers of photovoltaic inverters and the distribution network," in *Power Tech Conference Proceedings, 2003 IEEE Bologna*, 23-26 June 2003, pp 6, Vol.3.

[65] Z. H. Y. C. Y. Wang, G. Sinha, and X. M. Yuan, "Output filter design for a grid connected three-phase filter," in *34th IEEE Annual Power Electron. Spec. Conf. (PESC'03)*, 15-19 June 2003, pp. 779-784.

[66] X. Wilsun, H. Zhenyu, C. Yu, and W. Haizhen, "Harmonic resonance mode analysis," *Power Delivery, IEEE Transactions on,* vol. 20, pp. 1182-1190, 2005.

[67] M. F. M. R. C. Dugan, S. Santoso, H. W. Beaty, *Electrical Power Systems Quality*, Second Edition ed.

[68] V. Smith, "Small Scale Domestic Rooftop Solar Photovoltaic Systems," Endeavour Energy Power Quality & Reliability Centre, University of Wollongong: NSW, Australia2011.

[69] A. Al-Sabounchi, J. Gow, M. Al-Akaidi, and H. Al-Thani, "Minimizing line energy loss of radial distribution feeder with a PV Distributed Generation unit avoiding reverse power flow," in *Electric Power and Energy Conversion Systems (EPECS), 2011 2nd International Conference on*, 2011, pp. 1-6, Sharjah.

[70] A. Saidian, M. Heidari, and D. Mirabbasi, "Improvement of voltage unbalance and voltage sag in radial distribution systems using DG," in *Industrial Electronics and Applications (ICIEA), 2010 the 5th IEEE Conference on*, 2010, pp. 835-839, Taichung.

[71] C. Gonzalez, J. Geuns, S. Weckx, T. Wijnhoven, P. Vingerhoets, T. De Rybel, *et al.*, "LV distribution network feeders in Belgium and power quality issues due to increasing PV penetration levels," in *Innovative Smart Grid Technologies (ISGT Europe), 2012 3rd IEEE PES International Conference and Exhibition on*, 2012, pp. 1-8, Berlin.

[72] K. Turitsyn, x030C, P. ulc, S. Backhaus, and M. Chertkov, "Distributed control of reactive power flow in a radial distribution circuit with high photovoltaic penetration," in *Power and Energy Society General Meeting, 2010 IEEE*, 2010, pp. 1-6, Minneapolis, MN.

[73] R. Yan and T. K. Saha, "Voltage Variation Sensitivity Analysis for Unbalanced Distribution Networks Due to Photovoltaic Power Fluctuations," *IEEE Transactions on Power Systems*, vol. 27, pp. 1078-1089, 2012.

[74] C. L. Masters, "Voltage rise: the big issue when connecting embedded generation to long 11kV overhead lines," *Power Engineering Journal*, vol. 16, pp. 5-12, 2002.

[75] A. B. a. V. L. C. Oates, "Tap changer for distributed power," presented at the European Conference on Power Electronics and Apllications, Aalborg, 2007.

[76] M. J. E. Alam, K. M. Muttaqi, and D. Sutanto, "Distributed energy storage for mitigation of voltage-rise impact caused by rooftop solar PV," in *Power and Energy Society General Meeting, 2012 IEEE*, 2012, pp. 1-8, San Diego, CA.

[77] K. H. Chua, L. Yun Seng, P. Taylor, S. Morris, and W. Jianhui, "Energy Storage System for Mitigating Voltage Unbalance on Low-Voltage Networks With Photovoltaic Systems," *Power Delivery, IEEE Transactions on*, vol. 27, pp. 1783-1790, 2012.

[78] K. H. Chua, J. Wong, Y. S. Lim, P. Taylor, E. Morris, and S. Morris, "Mitigation of Voltage Unbalance in Low Voltage Distribution Network with High Level of Photovoltaic System," *Energy Procedia,* vol. 12, pp. 495-501, // 2011.

[79] L. Xiaohu, A. Aichhorn, L. Liming, and L. Hui, "Coordinated Control of Distributed Energy Storage System With Tap Changer Transformers for Voltage Rise Mitigation Under High Photovoltaic Penetration," *Smart Grid, IEEE Transactions on,* vol. 3, pp. 897-906, 2012.

[80] F. Shahnia, A. Ghosh, G. Ledwich, and F. Zare, "Voltage correction in low voltage distribution networks with rooftop PVs using custom power devices," in *IECON 2011 - 37th Annual Conference on IEEE Industrial Electronics Society*, 2011, pp. 991-996.

[81] G. R. F. Q. Mafra, W. Uturbey, and B. J. C. Filho, "Analysis of the operation of a D-STATCOM in unbalanced distribution systems under voltage disturbances," in *Transmission and Distribution Conference and Exposition: Latin America (T&D-LA), 2010 IEEE/PES*, 2010, pp. 629-634, Sao Paulo.

[82] A. R. V. B. S.Siva Kesava Reddy, S. Suman, K.Divya Manasa, ", International Journal of Engineering Research and Applications (IJERA) ISSN: 2248-9622, 2011., "Reactive Power Compensation Using DSTATCOM," *International Journal of Engineering Research and Applications (IJERA)* 2011.

[83] P. D. R. K. K.Madhale, "Design And Simulation Studies of D-STATCOM For Voltage Sag, Swell Mitigation," *International Journal of Power System Operation and Energy Management,* vol. 2, 2008.

[84] D. N. S.F. Torabi, Y. Shayestehfard, "Compensation of Sags And Swells Voltage Using Dynamic Voltage Restorer (DVR) During Single Line to Ground and Three-Phase Faults," *International Journal on Technical and Physical Problems of Engineering (IJTPE),* vol. 4, pp. 126-132, Sep 2012 2012.

[85] Y. Hen-Geul, D. F. Gayme, and S. H. Low, "Adaptive VAR Control for Distribution Circuits With Photovoltaic Generators," *Power Systems, IEEE Transactions on,* vol. 27, pp. 1656-1663, 2012.

[86] P. J. a. D. C. Aliprantis, "Distributed Volt/Var control by PV inverters," *IEEE Transaction on Power System,* vol. 28, pp. 3429-3439, 2013.

[87] J. W. Smith, W. Sunderman, R. Dugan, and B. Seal, "Smart inverter volt/var control functions for high penetration of PV on distribution systems," in *Power Systems Conference and Exposition (PSCE), 2011 IEEE/PES*, 2011, pp. 1-6, Phoenix, AZ.

[88] R. K. Varma, S. A. Rahman, and T. Vanderheide, "New Control of PV Solar Farm as STATCOM (PV-STATCOM) for Increasing Grid Power Transmission Limits During Night and Day," *Power Delivery, IEEE Transactions on,* vol. 30, pp. 755-763, 2015.

[89] R. K. Varma, V. Khadkikar, and R. Seethapathy, "Nighttime Application of PV Solar Farm as STATCOM to Regulate Grid Voltage," *Energy Conversion, IEEE Transactions on,* vol. 24, pp. 983-985, 2009.

[90] R. K. Varma, B. Das, I. Axente, and T. Vanderheide, "Optimal 24-hr utilization of a PV solar system as STATCOM (PV-STATCOM) in a distribution network," in *Power and Energy Society General Meeting, 2011 IEEE*, 2011, pp. 1-8, San Diego, CA.

[91] "Australia report on smart inverters: Good news for utilities. http://ecogeneration.com.au/news/smart_inverters_good_news_for_utilities/55950."

[92] NREL, "Advanced inverter functions to support high levels of distributed solar- policy and regulatory considerations. http://www.nrel.gov/docs/fy15osti/62612.pdf", NREL/BR-6A20-62612, November 2014.

[93] S. K. B. Ambarnath Banerji , Bhim Singh, "DSTATCOM Control Algorithms: A Review," *International Journal of Power Electronics and Drive System (IJPEDS)*, vol. 2, pp. 285-296, September 2012 2012.

[94] A. N. S. Institute, "ANSI C84.1-2006, 2006," in *American National Standard for Electric Power Systems and Equipment- Voltage Ratings (60Hertz)*, ed: National Electrical Manufacturers Association (NEMA).

[95] " AS 60038-2000: Australian Standard voltages," ed, 2000.

[96] "Australian Standard AS/NZS 61000.3.100:2011, Electromagnetic compatibility (EMC) – Limits – Steady state voltage limits in public electricity systems," ed, 2011.

[97] "IEEE Std 1159-2009 (Revision of IEEE Std 1159-1995): IEEE Recommended Practice for Monitoring Electric Power Quality," ed, 2009, pp. 1-81.

[98] "Australian Standard AS/NZS 61000.4.30:2012, Electromagnetic compatibility (EMC) – Testing and measurement techniques-Power quality measurement methods (IEC61000-4-30:Ed.2.0(2008))," ed, 2012.

[99] A. Singh, G. Singh, and R. Mitra, "Some Observations on Definitions of Voltage Unbalance," in *Power Symposium, 2007. NAPS '07. 39th North American*, 2007, pp. 473-479, Las Cruces, NM.

[100] G. C. Cornfield, "Definition and measurement of voltage flicker [in lighting]," in *Electronics in Power Systems Measurement, IEE Colloquium on*, 1988, pp. 4/1-4/4, London.

[101] "Australian Standards, AS/NZS 4377:1996, Flicker meter – Evaluation of flicker severity," ed, 1996.

[102] "IEEE Std 1453-2004: IEEE Recommended Practice for Measurement and Limits of Voltage Fluctuations and Associated Light Flicker on AC Power Systems," *(Adoption of CEI/IEC 61000-4-15:1997+A1:2003)*, pp. 1-0, 2005.

[103] "AS/NZS 61000.3.3:2012, Electromagnetic compatibility (EMC) - Limits - Limitation of voltage changes, voltage fluctuations and flicker in public low-voltage supply systems, for equipment with rated current =16 A per phase and not subject to conditional connection," ed, 2012.

[104] "AS/NZS 61000.3.7:2001, Electromagnetic compatibility (EMC) Part 3.7: Limits - Assessment of emission limits for fluctuating loads in MV and HV power systems," ed, 2001.

[105] "IEEE Std 1547-2003: IEEE Standard for Interconnecting Distributed Resources with Electric Power Systems," ed, 2003.

[106] "IEEE 929-2000: IEEE recommended practice for utility interface of residential and intermediate photovoltaic systems," in *IEEE Stand. Coordinating Committee 21, Photovoltaic*, ed, 2000.

[107] "Australian Standard AS4777.2, Grid connection of energy systems via inverters - Inverter requirements.," 2005.

[108] "AS/NZS 4777.2:2015, Grid connection of energy systems via inverters Part 2: Inverter requirements ", ed, 2015.

[109] "IEC 61000-3-2: Electromagnetic compatibility (EMC) Part 3-2: Limits for harmonic current emission. (equipment input current < 16 A per phase)," ed: International Electrotechnical Commission (IEC), 2012.

[110] S. J. B. Ong and C. Yeong Jia, "An overview of international harmonics standards and guidelines (IEEE, IEC, EN, ER and STC) for low voltage system," in *Power Engineering Conference, 2007. IPEC 2007. International*, 2007, pp. 602-607, Singapore.

[111] K. H. Matter, "Comparison for Maximum Power Point Tracing Algorithms for Photovoltaic System in Purpose of Developing an Efficient System," Master of Engineering, Faculty of Graduate Studies Department of Electrical Engineering The Islamic University of Gaza, 2014.

[112] B. Subudhi and R. Pradhan, "A Comparative Study on Maximum Power Point Tracking Techniques for Photovoltaic Power Systems," *IEEE Transactions on Sustainable Energy*, vol. 4, pp. 89-98, 2013.

[113] I. V. Banu and M. Istrate, "Modeling of maximum power point tracking algorithm for photovoltaic systems," in *Electrical and Power Engineering (EPE), 2012 International Conference and Exposition on*, 2012, pp. 953-957, Iasi.

[114] M. S. E. Muljadi, and V. Gevorgian, "PSCAD Modules Representing PV Generator," NREL/TP-5500-5818, August 2013.

[115] "IEEE 13 Node Test Feeder," ed: IEEE Power Engineering Society, 2009.

[116] A. Hughes, *Electric Motors and Drives: Fundamentals, Types and Applications*, 2005.

[117] *Power Systems Computer Aided Design (PSCAD/EMTDC) online available at https://hvdc.ca/pscad/, Acessed in 2016.*

[118] "RTDS Technologies, RTDS Manual Set, accessed in 2015.."

[119] RTDS Technologies website: *https:*//www.rtds.com/applications/control-systems-testing/*, accessed in 2015.*

[120] dSPACE DS1103 PPC control hardware board manual*: https://www.dspace.com/en/inc/home/products/hw/singbord/ppcconbo.cfm,* accessed in 2015.

[121] "AS/NZS 61000. 4.15: 2012, Electromagnetic compatibility (EMC) - Part 4.15: Testing and measurement techniques – Flicker meter - Functional and design specifications," ed, 2012.

[122] Fluke Power Analyzer 434 data sheet, available online a*t http://www.transcat.com/media/pdf/Fluke_434.pdf.*

[123] Fluke Power Analyzer 1735 data sheet, available online at *http://www.electrorent.com/products/search/pdf/FLU-1735.pdf.*

[124] "IEEE C57.110–1998: IEEE recommended practice for establishing transformer capability when supplying non-sinusoidal load currents," ed, 1986.

[125] C. N. M. Ho, V. S. P. Cheung, and H. S. H. Chung, "Constant-frequency hysteresis current control of grid-connected VSI without bandwidth control," in *Energy Conversion Congress and Exposition, 2009. ECCE 2009. IEEE*, 2009, pp. 2949-2956, San Jose, CA.

[126] S. Civanlar and J. J. Grainger, "Volt/Var Control on Distribution Systems with Lateral Branches Using Shunt Capacitors and Voltage Regulators Part II: The Solution Method," *Power Apparatus and Systems, IEEE Transactions on,* vol. PAS-104, pp. 3284-3290, 1985.

[127] M. L. J. Marcos, Lorenzo E, Garcia M, , "Power output fluctuations in large-scale PV plants," in *Proceedings of International conference on renewable energies and power quality*, Spain, 2012.

[128] V. Khadkikar and A. Chandra, "Control of single-phase UPQC in synchronous d-q reference frame," in *Harmonics and Quality of Power (ICHQP), 2012 IEEE 15th International Conference on*, 2012, pp. 378-383, Hong Kong.

[129] A. V. Timbus, R. Teodorescu, F. Blaabjerg, M. Liserre, and A. Dell'Aquila, "Independent synchronization and control of three phase grid converters," in *Power Electronics, Electrical Drives, Automation and Motion, 2006. SPEEDAM 2006. International Symposium on,* 2006, pp. 1246-1251, Taormina.

[130] J. Mahseredjian, V. Dinavahi, and J. A. Martinez, "Simulation Tools for Electromagnetic Transients in Power Systems: Overview and Challenges," *Power Delivery, IEEE Transactions on,* vol. 24, pp. 1657-1669, 2009.

[131] B. Lu, X. Wu, H. Figueroa, and A. Monti, "A Low-Cost Real-Time Hardware-in-the-Loop Testing Approach of Power Electronics Controls," *IEEE Transactions on Industrial Electronics,* vol. 54, pp. 919-931, 2007.

[132] Z. Qing, Y. N. , W. K. , F. L. , L. G. , and C. K. , "Hardware-in-the-loop Simulation Platform of Photovoltaic Grid-Connected System " *TELKOMNIKA Indonesian Journal of Electrical Engineering* vol. 12, pp. 2465 - 2473 April 2014.

[133] S. Yang, " Novel sensorless generator control and grid fault ride-through strategies for variable-speed wind turbines and implementation on a new real-time simulation platform," Graduate Theses and Dissertations, 2010.

[134] H. Li, M. Steurer, K. L. Shi, S. Woodruff, and D. Zhang, "Development of a Unified Design, Test, and Research Platform for Wind Energy Systems Based on Hardware-in-the-Loop Real-Time Simulation," *IEEE Transactions on Industrial Electronics,* vol. 53, pp. 1144-1151, 2006.

[135] L. Yunwei, D. M. Vilathgamuwa, and L. Poh Chiang, "Design, analysis, and real-time testing of a controller for multibus microgrid system," *Power Electronics, IEEE Transactions on,* vol. 19, pp. 1195-1204, 2004.

[136] MATLAB/Simulink*:http://au.mathworks.com/products/simulink,* accessed in 2015.

[137] J. E. Alam, R. Yan, T. K. Saha, Annapoorna Chidurala, D Eghbal, "Learning from a 3.275 MW Utility Scale PV Plant Project," in *CIGRE*, 21, rue d'Artois, F-75008 PARIS 2016.

APPENDIX A: IEEE-13 Bus Test System Configuration Data

The IEEE 13 Bus distribution network data sheet can be obtained from [115]. The test system has seven line configurations which are provided in Table A.1 and A.2. The corresponding impedance matrices are presented Table A.3. Also, the line length information is presented in Table A.4.

Table A.1 Overhead Line Configuration Data

Config.	Phasing	Phase	Neutral	Spacing
		ACSR	ACSR	ID
601	B A C N	556,500 26/7	4/0 6/1	500
602	C A B N	4/0 6/1	4/0 6/1	500
603	C B N	1/0	1/0	505
604	A C N	1/0	1/0	505
605	C N	1/0	1/0	510

Table A.2 Underground Line Configuration Data

Config.	Phasing	Cable	Neutral	Space ID
606	A B C N	250,000 AA, CN	None	515
607	A N	1/0 AA, TS	1/0 Cu	520

Table A.3 Line Impedance Matrices

Config.	Impedance Z (R +jX) (ohm/mile)	B in micro Siemens per mile
601	$\begin{bmatrix} 0.3465 + j1.0179 & 0.1560 + j0.5017 & 0.1580 + j0.4236 \\ & 0.3375 + j\,1.0478 & 0.1535 + j0.3849 \\ & & 0.3414 + j1.0348 \end{bmatrix}$	$j\begin{bmatrix} 6.2998 & -1.9958 & -1.2595 \\ & 5.9597 & -0.7417 \\ & & 5.6386 \end{bmatrix}$
602	$\begin{bmatrix} 0.7526 + j1.1814 & 0.1580 + j0.4236 & 0.1560 + j0.5017 \\ & 0.7475 + j1.1983 & 0.1535 + j0.3849 \\ & & 0.7436 + j1.2112 \end{bmatrix}$	$j\begin{bmatrix} 5.6990 & -1.0817 & -1.6905 \\ & 5.1795 & -0.6588 \\ & & 5.4246 \end{bmatrix}$
603	$\begin{bmatrix} 0.0000 + j0.0000 & 0.0000 + j0.0000 & 0.0000 + j0.0000 \\ & 1.3294 + j1.3471 & 0.2066 + j0.4591 \\ & & 1.3238 + j1.3569 \end{bmatrix}$	$j\begin{bmatrix} 0.0000 & 0.0000 & 0.0000 \\ & 4.7097 & -0.8999 \\ & & 4.6658 \end{bmatrix}$
604	$\begin{bmatrix} 1.3238 + j1.3569 & 0.0000 + j0.0000 & 0.2066 + j0.4591 \\ & 0.0000 + j0.0000 & 0.0000 + j0.0000 \\ & & 1.3294 + j1.3471 \end{bmatrix}$	$j\begin{bmatrix} 4.6658 & 0.0000 & -0.8999 \\ & 0.0000 & 0.0000 \\ & & 4.7097 \end{bmatrix}$
605	$\begin{bmatrix} 0.0000 + j0.0000 & 0.0000 + j0.0000 & 0.0000 + j0.0000 \\ & 0.0000 + j0.0000 & 0.0000 + j0.0000 \\ & & 1.3292 + j1.3475 \end{bmatrix}$	$j\begin{bmatrix} 0.0000 & 0.0000 & 0.0000 \\ & 0.0000 & 0.0000 \\ & & 4.5193 \end{bmatrix}$

606	$\begin{bmatrix} 0.7982 + j0.4463 & 0.3192 + j0.0328 & 0.2849 - j0.0143 \\ & 0.7891 + j0.4041 & 0.3192 + j0.0328 \\ & & 0.7982 + j0.4463 \end{bmatrix}$	$j\begin{bmatrix} 96.8897 & 0.0000 & 0.0000 \\ & 96.8897 & 0.0000 \\ & & 96.8897 \end{bmatrix}$
607	$\begin{bmatrix} 1.3425 + j0.5124 & 0.0000 + j0.0000 & 0.0000 + j0.0000 \\ & 0.0000 + j0.0000 & 0.0000 + j0.0000 \\ & & 0.0000 + j0.0000 \end{bmatrix}$	$j\begin{bmatrix} 88.9912 & 0.0000 & 0.0000 \\ & 0.0000 & 0.0000 \\ & & 0..0000 \end{bmatrix}$

Table A.4 Line Segment Data

Node A	Node B	Length(ft.)	Config.
632	645	500	603
632	633	500	602
633	634	0	XFM-1
645	646	300	603
650	632	2000	601
684	652	800	607
632	671	2000	601
671	684	300	604
671	680	1000	601
671	692	0	Switch
684	611	300	605
692	675	500	606

The following Table A.5 provides the transformer data. The capacitor bank information and single phase voltage regulator data are presented in the Tables A.6 and A.7 respectively. The data of different load types at various nodes are presented in Tables A.8 and A.9.

Table A.5 Transformer Data

	kVA	kV-high	kV-low	R - %	X - %
Substation:	5,000	115 - D	4.16 Gr. Y	1	8
XFM -1	500	4.16 – Gr.W	0.48 – Gr.W	1.1	2

Table A.6 Capacitor Bank Data

Node	Ph-A	Ph-B	Ph-C
	kVAr	kVAr	kVAr
675	200	200	200
611			100
Total	200	200	300

Table A.7 Regulator Data

Regulator ID:	1		
Line Segment:	650 - 632		
Location:	50		
Phases:	A - B -C		
Connection:	3-Ph,LG		
Monitoring Phase:	A-B-C		
Bandwidth:	2.0 volts		
PT Ratio:	20		
Primary CT Rating:	700		
Compensator Settings:	Ph-A	Ph-B	Ph-C
R - Setting:	3	3	3
X - Setting:	9	9	9
Voltage Level:	122	122	122

Table A.8 Spot Load Data

Node	Load	Ph-1	Ph-1	Ph-2	Ph-2	Ph-3	Ph-3
	Model	kW	kVAr	kW	kVAr	kW	kVAr
634	Y-PQ	160	110	120	90	120	90
645	Y-PQ	0	0	170	125	0	0
646	D-Z	0	0	230	132	0	0
652	Y-Z	128	86	0	0	0	0
671	D-PQ	385	220	385	220	385	220
675	Y-PQ	485	190	68	60	290	212
692	D-I	0	0	0	0	170	151
611	Y-I	0	0	0	0	170	80
	TOTAL	1158	606	973	627	1135	753

Table A.9 Distributed Load Data

Node A	Node B	Load	Ph-1	Ph-1	Ph-2	Ph-2	Ph-3	Ph-3
		Model	kW	kVAr	kW	kVAr	kW	kVAr
632	671	Y-PQ	17	10	66	38	117	68